Exploring the Capabilities of Landsat Soil Reflectance Composites for Soil Organic Carbon Estimation and Monitoring of Topsoil Croplands in Bavaria, Germany

Dissertation zur Erlangung des Doktorgrades
an der Fakultät für Geowissenschaften
der Ludwig-Maximilians-Universität
München

vorgelegt von
Simone Zepp

Herrsching a. Ammersee, 01. Dezember 2022

Erstgutachter: Prof. Dr. Ralf Ludwig, Department of Geography, Ludwig-Maximilians Universität München, Germany

Zweitgutachter: Prof. Dr. Bas van Wesemael, Earth and Life Institute, Université Catholique de Louvain, Belgium

Tag der mündlichen Prüfung: 21. Juni 2023

Acknowledgement

After a very exciting time, this thesis finally comes to an end. The work was carried out at the German Remote Sensing Data Center (DFD) at the German Aerospace Center (DLR) in Oberpfaffenhofen. My sometimes hard and frustrating, but positively challenging and mostly very enjoyable doctoral time would not have been possible without the support of numerous people. With the next lines, I want to express my sincere gratitude to specific people.

First, I would like to thank Prof. Dr. Ralf Ludwig in particular, who has been present alongside my studies since my early days at the University also supervising my Bachelor and Master Theses. Thank you for supporting and encouraging me from student-level on, and for giving me the opportunity to freely choose this PhD topic in cooperation with my employer, the DLR.

Additionally, I would like to express my deepest gratitude to Prof. Dr. Bas van Wesemael, my second supervisor, whose reliable motivation, ideas and support on the soil topics are invaluable. He often gave me broader understanding of soil related topics. I always appreciated his valuable review and his open, friendly and direct mind.

This study could not have been achieved without the background of the Soil-DE project. The financial funding of Soil-DE by the German ministry of Ernährung und Landwirtschaft (BMEL) is gratefully acknowledged.

I would like to express my deepest appreciation to Dr. Uta Heiden, my DLR supervisor, for the several thoughtful supervise and inspiring discussions during sparkling conversations, reflective emails and several Skype calls. Her valuable expertise and connections to the scientific soil community has greatly enriched my work.

In this particular pandemic situation, I am very fortunate to have several great mentors to keep me on track with the research. I would like to thank Dr. Martin Bachmann for his guidance and valuable methodological suggestions. My thank also goes to Dr. Michael Steininger, Dr. Markus Möller and Dr. Marianne Jilge for their valuable discussions and technical support.

Further, I would like to thank Prof. Dr. Claudia Künzer and all my colleagues of the department of Land Surface Dynamics at DFD for enabling a nice and fruitful working environment. Here, I want to especially mention my former colleague and office mate Dr. Chaonan Ji for her constant support and encouragement during all stages of the doctoral period, and all colleagues of the Team Agricultural and Forest Ecosystems under the team management of Dr. Ursula Geßner. It is a pleasure to work with your passion and warm support.

I would also like to thank my family and friends for their support and motivation. Finally, I especially want to thank Chris for his support, love and for always being there for me over the past years.

Zusammenfassung

Mit dem Start des Satelliten Landsat-4 TM am 16. Juli 1982 wurde der Beginn einer langen Ära der Erhebung optischer Satellitenbildinformationen eingeläutet. Die bis heute regelmäßig ergänzte U.S. amerikanische Landsat Satellitenfamilie stellt insbesondere durch die Archivöffnung der Bilddaten im Jahr 2008 ein bisher konkurrenzloses Erdbeobachtungsprogramm für retrospektive, wiederkehrende sowie aktuelle Analysen der globalen Erdoberfläche dar. Unvergleichlich sind dabei die hohe räumliche und zeitliche Abdeckung der zur Verfügung stehenden Daten. In vielen Umweltdisziplinen zur Erforschung von Ökosystemen oder forstwirtschaftlicher, landwirtschaftlicher und urbaner Flächen kommen die Daten der Satelliten seit Jahrzehnten erfolgreich zum Einsatz. Auch in der Geologie und der Bodenkunde sind die gemessenen Spektralinformationen ein zentrales Analyseelement, um beispielsweise Folgen von Erosion, Klimawandel oder Landnutzungsänderungen zu erfassen und zu quantifizieren.

Vor allem die Ressource Boden charakterisiert für viele Lebensräume eine wichtige Grundlage. Durch Ökosystemleistungen ermöglicht diese Leben und Überleben auf der Erde. Die Tatsache, dass Böden den größten terrestrischen Kohlenstoffspeicher darstellen, verdeutlicht dabei die Relevanz der Geosphäre. Beispielsweise kann durch aktive Kohlenstoffbindung in landwirtschaftlichen Böden eine Minderung der Treibhausgasemissionen erreicht werden, um somit einen wertvollen Beitrag zum Klimaschutz zu leisten. In den vergangenen Jahren gab es zahlreiche nationale und internationale Bestrebungen und Aktivitäten, die Bedeutung des Bodens hervorzuheben und eine nachhaltige Nutzung der Ressource zu realisieren. Aktuell wird in den von den Vereinten Nationen definierten Sustainable Development Goals (SDG) explizit der Schutz sowie der nachhaltige Umgang mit Böden adressiert. Vor allem der organische Kohlenstoffgehalt (C_{org}) in landwirtschaftlichen Flächen stellt einen wesentlichen Parameter zur Beurteilung gesunder, nachhaltig genutzter Böden dar. Kenntnisse über den C_{org}-Gehalt sind höchst relevant und lassen unter anderem Aussagen über Ernteerträge oder die Erosionsanfälligkeit zu. Ein ausreichend hoher C_{org}-Gehalt ist deshalb Kernelement diverser politischer Reglementierungen. Um den zahlreichen (politischen) Anforderungen gerecht zu werden, bedarf es hochaufgelöster und flächenscharfer Informationen, die auch ein (rückblickendes) Verständnis von Bodenparametern ermöglichen. Aktuelle Bodenkarten und Datenbanken sind allerdings zeitlich und räumlich zu limitiert, um eine nachhaltige Nutzung der Ressource Boden zu dokumentieren und den formulierten Zielen gerecht zu werden. Traditionelle Methoden zur Bodenkartierung sind mit einem hohen zeitlichen und finanziellen Aufwand verbunden.

Die optische Erdbeobachtung liefert Techniken und Auswertungsverfahren, diesen zeitlichen und räumlichen Limitierungen zu begegnen. Als sog. Mapping Mission, ermöglichen die Landsat Satelliten mit deren seit mehr als 40 Jahren erhobenen Daten dabei großflächige und wiederkehrende Beobachtungen und Analysen. Zudem sind durch die hohe Pixelauflösung (30 m) Analysen auf Schlagebene möglich. Die Bilddaten bieten so die Möglichkeit der Erfassung und des Monitorings von Oberböden landwirtschaftlicher Flächen und können helfen, die zeitliche und

räumliche Dimensionen bestehender Datenbanken zu optimieren. Für verschiedene Regionen konnten bereits diverse Bodenparameter erfolgreich mit validen Genauigkeiten modelliert werden. Auch die Anwendung von Landsat Daten zur Abschätzung von C_{org}-Gehalten wurde gezeigt. Eine Limitierung der Anwendung optischer Erdbeobachtungsdaten stellt die Tatsache dar, dass ausschließlich Böden, die bei einem Überflug unbedeckt und vegetationslos sind, analysiert werden können. In Deutschland sind dies hauptsächlich ackerbaulich genutzte Flächen. Um die Satellitenbilddaten in Wert setzen zu können, müssen zunächst unbedeckte Böden ermittelt und von anderen Landbedeckungsarten separiert werden. Der Zeitraum, in dem ein Schlag unbedeckt ist, kann allerdings durch die regionale Fruchtfolge variieren und teilweise sehr kurz sein. Sog. Kompositttechniken multispektraler Bilddaten stellen eine Alternative zur Nutzung singulärer Aufnahmen dar und bieten die Möglichkeit, die Limitierung durch Vegetationsbedeckung zu überbrücken. Erste Studien haben bereits die Anwendbarkeit einer derart optimierten Datenquelle in Hinblick auf die Ableitung von Bodenparametern gezeigt. Sog. Bodenreflektanzkomposite (engl. surface reflectance composite, SRC), welche mittels der Kompositttechniken generiert werden, werden dabei mit Feldproben verknüpft, um Aussagen über Oberbodenparameter zu treffen. Allerdings sind zahlreiche Fragen bezüglich einer Verwendung solcher auf Landsat-Daten basierten SRCs zur Erfassung von Bodenparametern und vor allem zur Analyse von (rückblickenden) Veränderungen derzeit noch unbeantwortet.

Diese Dissertation umfasst Aktivitäten zur Exploration der Möglichkeiten zur Ableitung und des (retrospektiven) Monitorings von Oberbodeninformationen ackerbaulich genutzter Flächen aus SRCs, generiert mittels langjähriger Landsat-Daten. Zur Abschätzung des Potentials wurde das Bundesland Bayern in Deutschland als Testgebiet gewählt, da hier neben Expertenwissen eine umfangreiche Bodendatenbank zur Verfügung steht. Der Fokus liegt auf der Ableitung des C_{org}-Gehalts. Verwendet werden mehrjährige SRCs, die mittels des sog. Soil Composite Mapping Processors (SCMaP) generiert wurden.

Zu Beginn wurde die Notwendigkeit der Überarbeitung des Schwellwertverfahrens, welches einen essentiellen Teil der SCMaP Methodik darstellt und der Ableitung unbedeckter Böden dient, identifiziert. Vor allem für überregionale Analysen ist ein standardisiertes Verfahren, welches hier auf dem Verhalten verschiedener Landbedeckungsklassen beruht, essentiell für eine erfolgreiche Separierung unbedeckter Böden von anderen Oberflächen. Die Ableitung der Grenzwerte basierend auf überregionalen bio-geographischen Räumen zeigte sich dabei als der beste Ansatz. Auch eine Validierung der räumlichen und zeitlichen Verteilung unbedeckter Böden wurde durchgeführt, um das Verständnis der Datengrundlage für aufbauende Bodenparametermodellierungen zu maximieren.

Bei einer anschließenden Studie zur Beurteilung der Anwendbarkeit eines 30-jährigen SRCs zur Ableitung von C_{org}-Gehalten von Ackeroberböden in Bayern wurde dieses mit zahlreichen Feldproben verknüpft. Algorithmen des maschinellen Lernens (Multiple Linear Regression, Partial Least Square Regression und Random Forest Regression) wurden dabei miteinander verglichen, wobei sich der Einsatz des Random Forests als am besten geeignet herausstellte. Vor allem die Verschneidung von Bodenpunktdaten mit Fernerkundungspixeln, welche mehrere Meter Kantenlänge (Landsat: 30 m) besitzen, bedingen zahlreiche Quellen für Ungenauigkeiten. Hier wurde ein räumlicher/spektraler Filteransatz, welcher auf spektralen Beziehungen des Probenpixels und dessen Nachbarpixeln beruht, entwickelt, um heterogene Pixelcluster von der C_{org} Modellierung auszuschließen. Zudem bestätigte eine zusätzlich durchgeführte Validierung basierend auf einem externen unabhängigen Datensatz die hohe Genauigkeit des Modellierungsansatzes.

Da für eine Erfassung von Änderungen von C_{org} im Oberboden ein 30-jähriger Kompositzeitraum eine zu lange Zeitspanne darstellen kann, wurden die im zweiten Teil gewonnenen Erkenntnisse durch weitere Analysen vertieft, inwieweit dieser Zeitraum minimiert werden kann. Obwohl nachgewiesen werden konnte, dass längere Zeiträume (10/15 Jahre) höhere Modellierungskapazitäten bieten, zeigte bereits ein fünf-jähriger Zeitraum ausreichend hohe Modellgenauigkeiten im Untersuchungsgebiet für wiederkehrende Analysen. Die Erstellung der SRCs basiert auf einem spektralen Vegetationsindex. Die Resultate dieser Arbeit zeigen, dass Indices im Vergleich zu einer saisonalen Vorauswahl an Szenen, welche in das SRC integriert werden, eine untergeordnete Rolle bezüglich der Modellierungskapazitäten von C_{org} spielen. Einen weiteren zentralen Aspekt stellt ein Vergleich der zeitlichen Auswahl unbedeckter Böden mit Daten, an denen das beobachtete Feld (wahrscheinlich) unbedeckt ist dar. Ein Vergleich der extrahierten Daten unbedeckter Böden mit Feldbeobachtungen und phänologischen Informationen aus dem regionalen Feldfruchtkalender zeigte, dass der Großteil der ermittelten unbedeckten Böden in Zeiträumen lag, in denen der betrachtete Schlag vegetationslos und vom Satelliten sichtbar war. Auf Basis dieser Informationen wird eine Vorauswahl der Szenen basierend auf den phänologischen Informationen der im jeweiligen Gebiet angebauten Feldfrüchte geraten.

Zusammenfassend konnten im Rahmen dieser Dissertation zahlreiche Erkenntnisse für die Modellierungen des C_{org}-Gehalts in Ackeroberböden auf Basis multispektraler SRCs der Landsat Satellitenfamilie gewonnen werden. Die Ergebnisse liefern einen entscheidenden Beitrag zum Verständnis der großflächigen Anwendbarkeit satellitengestützter Erdbeobachtungsdaten zur Überwindung der räumlichen und zeitlichen Limitierungen herkömmlicher Bodenkartierungen und eines (retrospektiven) Monitorings von C_{org}.

Summary

The launch of Landsat-4 TM satellite on July 16, 1982, marked the beginning of a long era of optical satellite imagery. The U.S. Landsat family, which has been regularly expanded, represents an unrivaled Earth Observation program for retrospective, recurrent and recent analyses of the Earth's surface, especially due to the opening of the image data archive in 2008. The high spatial and temporal coverage of the freely accessible data is incomparable. For decades, Landsat data have been successfully used in many environmental disciplines to study ecosystems or forestry, agriculture and urban surfaces. Measured spectral information is a central element of analyses in geology and soil science, e.g., to detect and quantify soil erosion, impacts of climate change or land cover changes.

Soils are an essential resource for human subsidence, as they carry out a number of ecosystem services. The fact that soils represent the largest terrestrial carbon pool illustrates the relevance of the geosphere. Active carbon sequestration in agricultural soils can reduce greenhouse gas emissions and thus make a valuable contribution to climate protection. In recent years, there have been numerous national and international efforts and activities to highlight the importance of soils and to realize a sustainable use of the resource. Currently, the Sustainable Development Goals (SDG), defined by the United Nations, explicitly address the protection and sustainable use of soils. Above all, soil organic carbon (SOC) in croplands represents an essential parameter for assessing healthy sustainable used soils. Knowledge about SOC contents is highly relevant and allows conclusions about crop yields or erosion vulnerability. Therefore, sufficiently high SOC contents are a core element of various political regulations. In order to fulfil the numerous (political) requirements, high-resolution information is needed that also enables to capture the temporal development of soil parameters. However, current soil maps and databases are temporally and spatially limited to capture a sustainable use of the resource and to achieve the formulated goals. Traditional methods for soil mapping are associated with a high temporal and financial effort.

Optical Earth Observation (EO) is a valuable data source for area-wide soil mapping and monitoring purposes to distinguish patterns between or even within fields and to overcome the temporal and spatial limitations. As a long-term mapping mission, Landsat enables recurring observations and analyses. In addition, the high pixel resolution (30 m) supports analyses at field level. The image data thus offer the possibility of acquisition and monitoring of topsoil croplands and can help to optimize the temporal and spatial dimensions of existing databases. Various soil parameters have already been successfully modeled with valid accuracies for different regions (i.e., different climatic conditions, crop cycles, land management). The use of Landsat data to estimate SOC was also demonstrated. A limitation of the application of optical EO data is the fact that only soils which are exposed during the satellite overpass can be analyzed. In Germany, these are mainly cropland areas. In order to use the satellite imagery, uncovered soils must first be identified and separated from all other land cover types. However, the period during which a field is uncovered can vary due to regional crop rotation and can be limited to a short window of time. Soil compositing techniques of multispectral image data provide an alternative to the use of single

scenes and offer the possibility to bridge the limitation due to vegetation cover. First studies have demonstrated the applicability of such an optimized data source for soil parameter estimation. Soil reflectance composites (SRC), which are generated by these compositing techniques, are linked with field samples to predict topsoil parameter information. However, numerous questions regarding the use of such Landsat based SRCs for the estimation of soil parameters and especially for analyzing (retrospective) changes are still unanswered.

The efforts in this dissertation comprise activities to explore the capabilities of deriving and (retrospectively) monitoring topsoil cropland SOC information from SRCs, generated with long-term Landsat data. To assess the potential, the Federal state of Bavaria in Germany was chosen as a test area, since an extensive soil database is available here in addition to expert knowledge. The focus is on the derivation of SOC contents. Therefore, multi-year SRCs, generated by the Soil Composite Mapping Processor (SCMaP) are used.

At first, the need to revise the index thresholding, which is an essential part of the SCMaP methodology as it is the baseline to separate soils from all other land cover classes, was identified. Especially for area-wide analyses, a standardized procedure, which in this case is based on the behavior of different land cover classes, is essential for successful separation of exposed soils from other surfaces. The derivation of thresholds based on bio-geographically classified regions was shown to be the best approach. Validation of the spatial and temporal distribution of exposed soils was also performed to maximize the understanding of the SCMaP data basis for building soil parameter models.

In a consecutive study the applicability of a 30-year SRC to derive topsoil SOC contents of croplands in Bavaria was tested. The SRC was linked to numerous legacy field samples and different machine learning algorithms (Multiple Linear Regression, Partial Least Square Regression, and Random Forest Regression) were compared. The use of the Random Forest algorithm was determined to be the most suitable. Especially the intersection of point soil samples with remote sensing pixel, which have several meters resolution (Landsat: 30 m), can be a source of inaccuracies. Here, a spatial/spectral filtering approach based on spectral relationships of the sample pixel and its eight neighboring pixels was developed to exclude heterogenous pixel clusters. Furthermore, an additional validation based on an external independent data set confirmed the high accuracy of the modeling approach.

Considering that a 30-year composite period could be too long for detecting topsoil SOC changes, the results obtained in the second part of this thesis were further analyzed to minimize the compositing period. Although it has been demonstrated that longer compositing lengths (10/15 years) provide higher model performances, a five-year period already showed sufficiently high modeling accuracies in the study area. The SRC processing is based on a spectral vegetation index. The results of this work showed that different spectral indices for SRC generation have a minor impact on SOC modeling compared to a seasonal pre-selection of scenes, integrated into the SRC. Another key aspect of this thesis represents a comparison of the temporal selection of exposed soils with dates when the observed field is likely to be bare. A comparison of the extracted exposed soil dates with field observation and phenological information based on the regional crop calendar showed that the majority of the identified exposed soils are located in periods when the observed field is vegetation-free and visible from the satellite. Based on these findings, a pre-selection of scenes, derived from regional phenological information of crops, should be considered for SRC generation and SOC estimation.

In summary, this dissertation contains numerous insights for modeling SOC in topsoil croplands based on multispectral Landsat SRCs. The results provide a crucial contribution to the understanding of large-scale applicability of spaceborne EO data to minimize the spatial and temporal limitations of traditional soil mapping and (retrospective) monitoring of SOC.

Table of Contents

List of Figures

List of Tables

1. Introduction

Annually on December 5th the World Soil Day, organized by the United Nations (UN), is celebrated in order to raise awareness of the critical role of soils and to advocate for the sustainable management of soil resources (Bouma 2019). Soil is a complex system as a mixture of minerals, organic materials, air, and water and is the upper part of our earth's crust with a thickness of a few centimeters up to several tens of meters (Blume et al. 2010). In terms of the earth radius of 6,370 km, soils form the thin and vulnerable skin of the earth (Blume et al. 2010). Nevertheless, this thin skin is essential for human existence as it carries out a number of ecosystem services throughout soil functions (Blounin et al. 2013, Adhikari and Hartemnik 2016). One of the most recognized service of soil is its support for food production. Nearly 95% of the food is (in-)directly produced on soils (FAO 2015). In this context, soil health is defined as "the continued capacity of soil to function as a vital living ecosystem that sustains plants, animals and humans" (EJP SOIL 2022) and is amongst others an indicator for food productivity (Lehmann et al. 2020). As an important component of solid soils (Lal 2018) Soil Organic Carbon (SOC) is a key soil property for several ecosystem services (Adhikari and Hartemnik 2016). SOC directly impacts a huge variety of services as water regulation and filtering, nutrient conservation or climate and gas regulation of weathering or soil formation (Adhikari and Hartemnik 2016). Additionally, SOC is a principle determinant of soil health (Lal 2014) for ensuring food security and agricultural sustainability (Ren et al. 2020). Especially, SOC in cropland soils is of particular relevance and is becoming increasingly important.

1.1. Relevance of SOC for croplands

Soils are the largest terrestrial carbon (C) pool, where more C is stored than in the biosphere and the atmosphere combined (Jobbagy and Jackson 2000, Todd-Brown et al. 2013). The soil C stocks are comprised of two different C types, the soil inorganic C (SIC) and the soil organic C (SOC) fractions (Lorenz and Lal 2016). For the organic carbon portion, the primary source consists of materials from various biological origins (Kumar et al. 2006) and includes plant, animal and microbial residues in all stages of decomposition (Post and Kwon 2000). Croplands account for 10% of the global SOC with an estimated amount of 128-165 Pg C (Ren et al. 2020, Watson et al. 2000). Cropland soils with balanced and sufficient high SOC contents are less prone to soil degradation and can serve as a fundamental basis for food production (Lorenz and Lal 2016). A threshold level of approximately 2% SOC in the root zone is essential and indicates healthy soils (Lal 2014, Loveland and Webb 2003, Schjonning et al. 2010, Musinguzi et al. 2013, Lal 2016, Panagos et al. 2013). Below this concentration, the productivity is about to reduce notably (McBratney et al. 2014). However, in depleted soils, an increase of SOC concentration due to adequate management practices can contribute to raising crop yields (Lal 2006, Seremesic et al. 2011, Seitz et al. 2022). This can also be achieved, for example, by the use of cover crops between two crop cycles (Seitz et al. 2022). During the last decades, decreasing SOC stocks have been detected in many European croplands (e.g., Sleutel et al. 2006, Lal et al. 2007, Ciasis et al. 2010,

Wiesmeier et al. 2016, Guillaume et al. 2020), which in addition to crop yield decreases have also negative implications for climate change (Lal 2004). Since, as described at the beginning, organic carbon stocks in soils represent one of the largest reservoirs in the global carbon cycle (Jobbgay et al. 2000, Scharlemann et al. 2014).

The rising concern about soil health has been answered with several global or European-wide soil policies and regulations, aiming for a more detailed information gain on SOC contents for soil management and soil protection (Chabrillat et al. 2019). E.g., in the framework of the 17 Sustainable Development Goals (SDGs), defined by the United Nations, SOC is listed as one of the most relevant soil properties with regard to climatic regulations (Toth et al. 2018). In this context, carbon stocks, with SOC as the initial metric, are one of the three sub-indicators for SDG 15.3.1 (proportion of land that is degraded over total land) (Lorenz et al. 2019, Sims et al. 2019). SOC contents are treated here as a proxy for land degradation (Giuliani et al. 2020). The European Commission considered the decline of SOC as one of the eight threats for soil degradation in the European Union Thematic Strategy for Soil Protection back in 2006 (COM 2006) and updated this recently (Panagos and Montanarella 2018). Therefore, the goal of maintaining and improving SOC levels is included in the European Commission's Roadmap for a resource efficient Europe (EC 2011, Panagos et al. 2013). Recently, the importance of SOC was re-stated in the Soil Thematic Strategy 2030 (Panagos and Montanarella 2018, Panagos et al. 2022). Within the Paris Agreement at the 21st Conference of Parties (COP21) of the United Nations Framework Convention on Climate Change (UNFCCC) a limiting of global warming well below 2 °C was stated (Soussana et al. 2019). In preparation for the COP21, amongst others, the voluntary action plan, '4 per 1000 initiative: Soils for Food Security and Climate' was launched by the French Ministry of Agriculture in 2015 (Poulton et al. 2017). The initiative is supported by 39 countries and is striving for SOC stock increase at a rate of 0.4% (4 per 1000) per year for agricultural soils (Francaviglia et al. 2019, Soussana et al. 2019). The targeted annual increase is supposed to compensate a high percentage of human-induced carbon emissions (Wiesmeier et al. 2016, van Groeningen et al. 2017). In the context of the European Green Deal (EGD), which addresses Europe's goal to become the world's first climatic-neutral continent by 2050, a sustainable soil management is explicitly addressed (Montanarella and Panagos 2021). As a measure for sustainably managed and thus healthy soils, relevant factors include appropriate SOC contents in agricultural soils (Montanarella and Panagos 2021). The political programs mentioned represent only a small selection of aspirations to emphasize the importance of soil and the relevance of SOC.

To capture, quantify and monitor SOC contents, especially in croplands, for efficient and sustainable land use, and in order to control the implementation of policy objectives, SOC estimations with high spatiotemporal resolution on a national to global scale are urgently required. For instance, progress toward achieving the SOC-related SDGs is hampered by the lack of basic soil data and reliable monitoring systems for several countries (Lorenz et al. 2017). Hence, there is an urgent need of adequate soil data to achieve the SDGs (Toth et al. 2018). As McBratney (2014) pointed out: "SOC varies in space and time, modelling approaches are needed to predict SOC dynamics in both dimensions". However, as Heuvelink et al. (2021) indicated, there are only a few studies on modelling SOC variations in time. Most of the existing studies and databases are temporally and spatially limited. Changes in topsoil SOC contents are often related to (local or regional) land-use decisions and/or agricultural management adaptions (Meersmans et al. 2016) and may require more frequent observations (Collier et al. 2021). Especially for this purpose, retrospective estimation of cropland SOC is of high importance. In many European countries,

monitoring networks are existing, using only a limited number of sites per country (Panagos et al. 2013). However, global soil monitoring programs are still immature (Jandl et al. 2014).

For applications with a large geographical extent (nation to European-wide) maps are mostly available with an insufficient spatial (i.e., 250 m to 1 km) and a low temporal resolution of more than ten years. E.g., the European Soil Data Center (ESDAC) provides several pan-European SOC maps. Both soil datasets, the OCTOP: Topsoil Organic Carbon Contents for Europe (Jones et al. 2005) and the Topsoil Soil Organic Carbon Map based on the LUCAS (Land Use and Coverage Area frame Survey) for EU25 (de Brogniez et al. 2015) are generated in coarse 1 km raster format. Distributed and coordinated by the Food and Agriculture Organization (FAO) of the United Nations the Global Soil Organic Carbon Map (GSOCmap) was released in 2018 in support of the SDG 15.3.1. The generic map is based on a consultative and participatory process involving contributions of member countries and is available on a 1 km raster format (FAO and ITIPS 2018). The International Soil Reference and Information Center's (ISRIC) SoilGrids250m provides global information about SOC in the upper 30 cm with a spatial resolution of 250 m (Hengel et al. 2017). Supplied by the Joint Research Center (JRC), the Harmonized World Soil Database (HSWD) is also a well-known map, containing the spatial distribution of SOC contents (Nachtergaele et al. 2010, Hiederer and Köchy 2011). Although the latter three are available worldwide, small-scale analyses at field level are not feasible. In addition to the limitation of the spatial resolution, most maps have in common that they represent only one temporal snapshot, for which conceivably a long period of time is summarized. The applicability of the vast majority of the maps for recurring field-scale analysis is limited as the spatial and temporal resolution is insufficient. Currently, "the methods, data needs and models for the assessment of SOC changes at a spatial resolution relevant for decision-making in land-use are not yet sufficiently elaborated" (Jandl et al. 2014). Also, Popleau et al. (2020) defined especially for Germany the essential need for centralized and accurate monitoring of SOC dynamics to cope with the rising management of climate-driven alterations of SOC.

To fulfill the growing demand for high spatiotemporal SOC analyses, traditional soil mapping involves intense soil sampling effort (in time and financial constraints) and laboratory analysis (Stevens et al. 2013, Ward et al. 2020). Often, the high financial efforts of field sampling and laboratory analysis restrict the monitoring of soil properties at large scale (Conant et al. 2011). However, as elaborated, there is a growing demand for alternative soil mapping and monitoring approaches applicable for an area-wide mapping which enables recurring analyses (Chabrillat et al. 2019, Castaldi et al. 2019). Earth Observation techniques and model approaches provide an alternative to traditional soil mapping because of the ability to overcome the spatial and temporal limitation of existing maps and databases.

1.2. Earth Observation for soil analysis

Earth Observation (EO) is a valuable data source for area-wide soil mapping and monitoring purposes to distinguish patterns between or even within fields. Hyperspectral airborne data (e.g., Ben-Dor et al. 2009, Bartholomeus et al. 2011, Bayer et al. 2016, Chabrillat et al. 2019) or (simulated) data of the Italian PRISMA (Hyperspectral Precursor and Application Mission - Loizzo et al. 2019; Mzid et al. 2022) and the German EnMAP (Environmental Mapping and Analysis Program - Guanter et al. 2015; Ward et al. 2020) satellites, as well as multispectral spaceborne datasets (e.g., Castaldi et al. 2019, Vaudour et al. 2019, Wang et al. 2020, Gholizadeh et al. 2018) have been intensively studied during the past years for soil analysis to derive cropland SOC

contents. Especially the spaceborne multispectral mapping missions (i.e., Landsat and Sentinel-2) are suitable for SOC topsoil estimation purposes due to their high spatial and multitemporal resolution, global coverage and recurring acquisitions. Mapping approaches based on spaceborne multispectral sensors can provide a temporal and spatial information increase to existing maps and databases (section 1.1). For monitoring purposes and to understand changes due to management adoptions, special emphasis must be given to the long history of Landsat data (> 40 years with global coverage), as Sentinel-2 does not yet provide such a long data history (Sentinel-2A: launched in 2015, Sentinel-2B: launched in 2017, Phiri et al. 2020).

For SOC estimation, soil reflectance values acquired by the EO instrument are correlated with field soil point information based on spectral and/or digital soil modeling techniques. Machine learning is a widely applied and effective approach to generate successful soil property prediction models. Commonly techniques such as random forests (RF), partial least-square regressions (PLSR), support vector machines (SVM) or convolutional neural networks (CNN) are widely applied for soil property estimation and mapping (Tziolas et al. 2021). For the use of optical sensors, which are only able to detect the upper nanometers of the observed surface, first bare soil pixels have to be selected and separated from all other land cover classes. Due to temporal or permanent surface vegetation cover, mapping of bare, uncovered and undisturbed soils for SOC prediction is challenging (Dematte et al. 2018). The area of exposed soil in temperate areas is usually spatially limited, distributed differently throughout the year, and often restricted to a short time period in the crop cycle. E.g., at the beginning of the crop cycle, i.e. after tilling, when the field is in seedbed conditions, the possibility of enhancing soil property prediction of exposed soils exists. However, this is related to the regional crop phenology of the observed field and varies in time (e.g., winter and summer crops). Temporal compositing techniques of multispectral satellite images can provide an alternative in contrast to the use of single data takes and are widely applied in the literature to get a comprehensive understanding of the Earth's surface including soils (e.g., Hansen et al. 2011, White et al. 2014, Hermosilla et al. 2015, Diek et al. 2017, Dematte et al. 2018, Griffiths et al. 2019, Loiseau et al. 2019, Adams et al. 2020, Safanelli et al. 2020, Vaudour et al. 2021). In general, the compositing technique, initially introduced by Holben (1986), strives for a reduction of a range of difficulties, as e.g., cloud contamination, different atmospheric compositions, and view or illumination geometry by incorporating information from several overpasses for the same pixel (Flood 2013). In addition to these aspects, a compositing approach for soil analyses enables to overcome the limitation of temporal vegetation cover of croplands during the overpass of one satellite. All bare soil occurrences of all input scenes are combined pixel wise to create soil reflectance composites (SRC). The SRC represents mostly the averaged situation (sometimes also the barest situation) of all exposed soil occurrences in the observed time period. This implies, that the spectra of the spatially enhanced data source are relatively independent of seasonal differences in soil moisture and other soil surface conditions (e.g., occurring during rain events or longer drought periods) as only permanent spatial soil moisture differences or texture characteristics remain, at least for an SRC where multiple scenes are averaged over time. Temporal and spatial averaging of exposed soil occurrences in an observed area allows the processing of a spatially enhanced data source (i.e., SRC) for soil parameter estimation. Based on multispectral spaceborne EO images (mainly Landsat and Sentinel-2) several bare soil compositing techniques were developed and applied for soil analysis (e.g., Diek et al. 2017, Rogge et al. 2018, Dematte et al. 2020, Castaldi et al. 2021, Sorenson et al. 2021, Vaudour et al. 2021).

Dematte et al. (2018) developed the first operational SRC processor (Geospatial Soil Sensing System (GEOS3)) based on Landsat data for large scale soil mapping. Safanelli et al. (2020) applied the GEOS3 derived bare soil composite, called Synthetic Soil Images (SYSI), for large scale soil analysis over Europe and estimated SOC contents amongst other soil parameters. The Soil Composite Mapping Processor (SCMaP; Rogge et al. 2018, see chapter 1.3), established at the German Aerospace Center (DLR), is an alternative valuable tool to build area-wide SRCs. A unique characteristic of SCMaP is its independence of external data sources for exposed soil identification. Besides these two area-wide compositing methods, several studies have created small scale optimized SRC approaches for different geographically regions in terms of soil parameter modeling using multispectral Landsat and/or Sentinel-2 data (e.g., Diek et al. 2017, Zizala et al. 2019, Dvorakova et al. 2021, Mzid et al. 2021, Sorenson et al. 2021, Zepp et al. 2021 b, Möller et al. 2022). Some approaches are extended by the use of ancillary data to pre-select scenes for compositing. Common are SAR (synthetic aperture radar) and Sentinel-3 data (e.g., Lin et al. 2020, Tziolas et al. 2020, Vaudor et al. 2021) or the pre-selection of input scenes (e.g., crop calendar, minimal surface roughness, and minimal soil moisture) to improve the exposed soil selection based on expert-knowledge (e.g., Castaldi et al. 2019, Dvorakova et al. 2021, Mzid et al. 2021, Vaudour et al. 2019). However, most of these approaches are developed and applied at the local level for a small spatial extent (0.09 to 10,000 km^2).

When comparing available bare soil compositing techniques, the spectral index and index threshold derivation, responsible for exposed soil selection, is of particular importance for almost all compositing techniques. The well-known normalized difference vegetation index (NDVI) is used by a wide range of approaches individually (Vaudour et al. 2019, Loiseau et al. 2019) in combination with other indices (Diek et al. 2016, Dematte et al. 2018, Sorenson et al. 2021, Urbina Salazar et al. 2021) or is slightly modified (Rogge et al. 2018, Heiden et al. 2022). In addition to the NDVI the majority of authors used the Normalized Burn Ratio II (NBR2) (e.g., Dematte et al. 2018, Gallo et al. 2018, Dvorakova et al. 2021, Urbina-Salazar et al. 2021, Castaldi et al. 2021) and/or the Bare Soil Index (BSI) (e.g. Diek et al. 2017, Mzid et al. 2021) separately or in combination for bare soil selection. In general, each approach requires one or more thresholds to separate exposed soils from other land cover classes. These thresholds are either set empirically or by an expansion integrating LUCAS (Land Use and Coverage Area frame Survey, Origazzi et al. 2018) topsoil spectral measurements into the framework specified for local or site-specific conditions. The selection of the thresholds mainly determines the quality of the composites and requires therefore special emphasis. However, these methods have in common, that there is no standardized systematic selection of the thresholds and the determination is mainly focused on regional characteristics. A data-driven standardized and systematic index thresholding approach can enable area-wide mapping of exposed soils and an operational use of the technique without ancillary data.

Beside the index and the index thresholding, responsible for exposed soil selection, the compositing length (i.e., how many years and a seasonal composition integrated into the compositing process) is of particular importance for SRC generation. This is a crucial point especially for SOC monitoring purposes claimed by the political requirements. So far, only a small number of studies investigated and compared different compositing lengths (Castaldi et al. 2021) for long-term SOC estimation and monitoring purposes. However, only by answering this question a concept for recurrent (retrospective) analyses can be designed. By using the long-term Landsat archive, the SCMaP approach enables such recurrent and retrospective SOC predictions to detect changes.

1.3. Bare Soil Information (SCMaP)

The operational SCMaP chain has been developed by Rogge et al. (2018) for the use of Landsat imagery. It is a multitemporal compositing approach, which enables an automated extraction of exposed soil pixels and the generation of area-wide cloud-free SRCs for an individually defined period of time (Figure 1.1). This section provides a brief summary of the methodology, which is described in detail by Rogge et al. (2018).

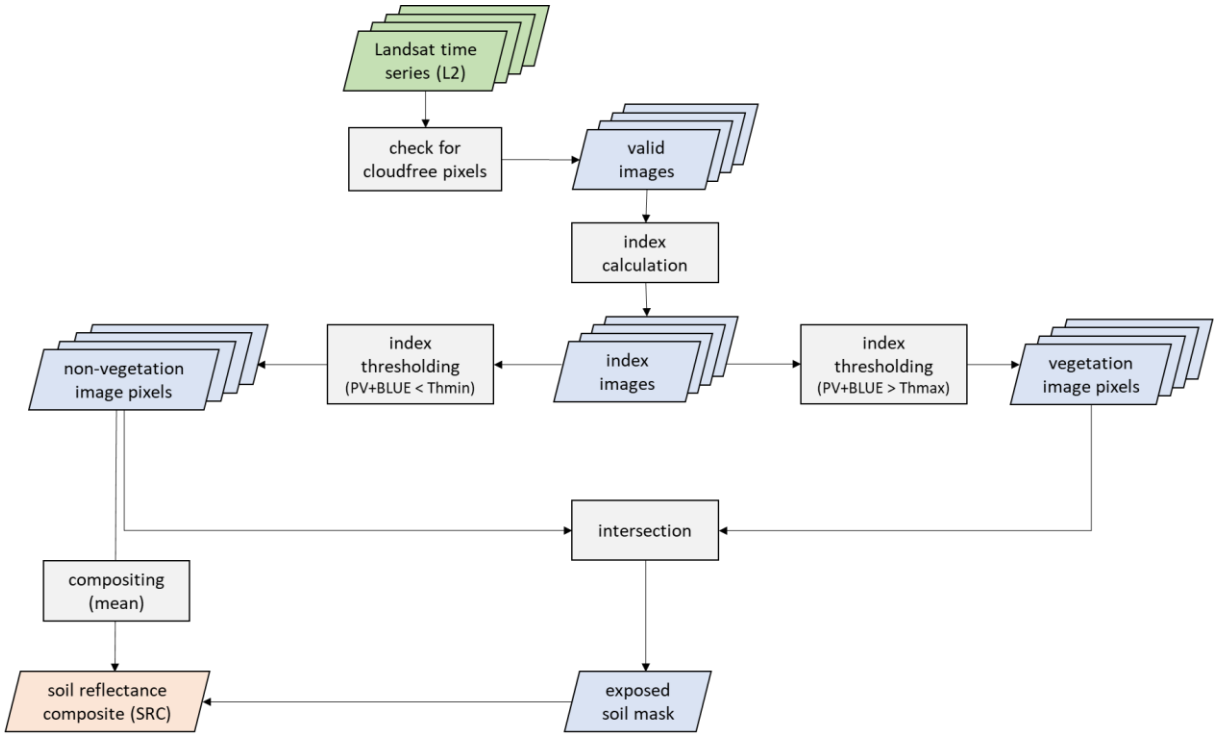

Figure 1.1: Summary of the SCMaP processing chain including index calculation, index threshold determination and SRC generation.

To separate soils from photosynthetic active (PV) areas, a spectral vegetation Index (PV+BLUE, Equation 1) based on the NDVI (Rouse et al. 1974) is used:

$$PV + BLUE = \frac{\rho_{NIR}-\rho_{Red}}{\rho_{NIR}+\rho_{Red}} + \frac{\rho_{NIR}-\rho_{Blue}}{\rho_{NIR}+\rho_{Blue}} \quad (1)$$

where ρ is the reflectance [%] of the Red, Blue, and NIR (near infrared) spectral regions (Landsat-4 TM, Landsat-5 ETM, Landsat-7 ETM+: Blue = Band (B) 1, Red = B3, NIR = B4, Landsat-8 OLI: Blue = B2, Red = B4, NIR = B5). The PV+BLUE index is based on the NDVI for effectively separating photosynthetic active vegetation from most other materials. However, the index alone provides no possibility to separate soils from other not photosynthetically active land cover types. To overcome this limitation in the SCMaP methodology two thresholds are set, that can be used combined to extract exposed soil pixels. The addition of the second normalized difference index, using the blue reflectance information of Landsat, is chosen to minimize increased reflectance in the blue channel caused by thin haze which is not filtered during pre-processing.

SCMaP has been developed for temperate and continental climates. Here, exposed soils occur mainly in agricultural areas not permanently covered by vegetation (i.e., grasslands). Croplands in this climatic region are characterized by a transition from bareness after field tillage (e.g., seedbed preparation) to vegetation cover during the vegetative active phase. Therefore, the thresholding is optimized to select pixels with a change from vegetation cover to bare conditions.

To extract the exposed soil pixels, two temporal composites containing the minimum PV+BLUE index (PV_{min}) and the maximum PV+BLUE index (PV_{max}) per pixel and observed compositing period are derived. Based on the spatial and temporal behavior of the $PV_{min/max}$ index composites, two thresholds (TH) are determined, built on specific land cover (LC) classes (urban, deciduous trees, and croplands), to distinguish between exposed soils and other LC classes. Exposed soils and urban surfaces show the lowest PV_{min} composite values but are also intermixed with non-photosynthetic active vegetation (e.g., crop residues after harvesting) or dry grassland. When soils are covered with vegetation, they show an overlap with forests and grasslands in the PV_{max} composite. Here, soils can be easily separated from urban surfaces and areas showing permanent low vegetation indices (i.e., water or mining sites). Therefore, TH_{min} is set to separate urban surfaces and exposed soils from LC classes with active vegetation cover. The TH_{max} is set to distinguish soils temporally covered by vegetation from classes never covered by vegetation, as urban materials or water. By applying $TH_{min/max}$ to the $PV_{min/max}$ composites, two masks are generated, one containing permanent non-vegetation pixels, while the other mask contains permanent vegetated pixels. The intersection of these masks allows the determination of the exposed soil mask containing all pixels with an alternating vegetation cover. These pixels are showing at least one exposed soil occurrence in the observed time period. The SRC is calculated at each pixel as the average reflectance per band of all exposed soils in the image data stack, where the index value is lower than TH_{min} and the pixel is spatially within the soil mask (Figure 1.1).

Non-photosynthetic active vegetation (NPV, Daughtry et al. 2006) such as crop residues, grassland (dry condition) or leaf-off condition of deciduous forests show a spectral similarity with soils. A clear separation of NPV and exposed soils is hampered by the limited spectral resolution of multispectral images, especially in the short-wave infrared (SWIR) region (Asner and Heidebrecht 2002, Okin 2007, Malec et al. 2015). For the differentiation of NPV from exposed soils, these LC classes have to be considered with specific emphasis in the threshold derivation method. The data-driven SCMaP index thresholding focuses on a clearer separation from grassland and leaf-off conditions of deciduous forests applicable for an area-wide mapping. A majority of other small-scale compositing approaches focus on empirically selected and locally limited thresholds. Also, ancillary data such as urban or water masks are often used for a selection of exposed soils. There is a need for a data-driven definition of two spectral index-based thresholds to overcome an empirical derivation of the thresholds and to avoid the implementation of ancillary data masks. For SCMaP the determination of the thresholds is originally based on manually selected LC data which show no change over the entire investigation time. The approach is applicable for area-wide mappings of exposed soils. However, it is time consuming and prone to user errors, why a revision to a data-driven automated, standardized approach was identified and developed in this thesis.

SCMaP is requiring a multispectral Level 2 database. Landsat collection data (Dwyer e al. 2018, Landsat-4 TM, Landsat-5 ETM, Landsat-7 ETM+, and Landsat-8 OLI) between 1984 and 2019 were used for SRC generation. To avoid external effects, the same pre-processing steps (i.e., atmospheric correction (ATCOR – Atmospheric / Topographic Correction software, Richter and Schläpfer 2013) and cloud masking (FMask algorithm, Zhu et al. 2015)) were applied to all scenes

to prepare a consistent database. SCMaP can be applied to different compositing lengths. However, for Landsat due to the temporal coverage and the resulting number of cloudless scenes at least five years should be integrated in the compositing approach (Rogge et al. 2018).

1.4. Overall goal of the thesis

As discussed in the last chapters, currently available soil maps and monitoring approaches demonstrate a spatial and/or temporal limitation for achieving the policy objectives and for creating an information gain on SOC contents for the various soil management and soil protection aspirations for croplands. These spatiotemporal gaps can be bridged by the use of multispectral EO data. Especially the long-term archive of Landsat imagery is a valuable data source for various (retrospective) soil analysis. Landsat, as a mapping mission, provides the opportunity for area-wide mapping approaches supported by a high spatial resolution (30 m) enabling analysis on field scale, and it is the only optical mission on a global scale for the past 40 years. Despite the high potential, the Landsat data have barely been used for (retrospective) soil analyses and monitoring purposes to overcome the spatial and/or temporal limitation of current mapping approaches. However, more research is needed to capture the potential use and the applicability of Landsat data for (retrospective) soil analyses integrated to a soil compositing approach for bare soil extraction. This paves the ground for increasing the physical and chemical understanding on soil developments and their impacts on e.g. climatic processes, yield capacities or erosion resilience.

To address the numerous demands for an area-wide mapping and (retrospective) monitoring of SOC contents in non-permanently covered cropland topsoils the overall goal of the thesis was defined to explore the capabilities of the long-term Landsat based SCMaP SRCs for SOC prediction and monitoring. The analyses were conducted for a subset of Germany, the Federal State of Bavaria. In addition to in-depth expert knowledge, extensive validation data were available here. In order to answer the overall goal, several analyses were conducted to fill some identified scientific gaps (chapter 2). The emerged research gaps and the conducted analyses are presented and discussed in detail in the following chapter.

2. Research Objectives and Framework of the Thesis

This work is a synthesis of the research done over the past years and is published in three scientific international journals. In order to explore SOC monitoring capabilities, different research gaps and challenges were identified, and were also highlighted in the previous chapters. A majority of them were addressed in this thesis by several analyses. Therefore, three research objectives (RO) were established to focus on the different demands for exploring a monitoring concept (Figure 2.1). Each RO is treated in a scientific publication and defines the overall goal of the analyses conducted per publication in order to address the overall scope of the thesis (chapter 1.4). The ROs are linked with and built on each other and are (partly) based on findings of the previous objective. It must be emphasized, that there is a strong connection between the analyses. The interaction and the combination of results of the three ROs gives a comprehensive analysis addressing the different requirements and aspects needed for exposed soil retrieval and the subsequent SOC estimation for monitoring purposes based on Earth Observation Landsat timeseries data.

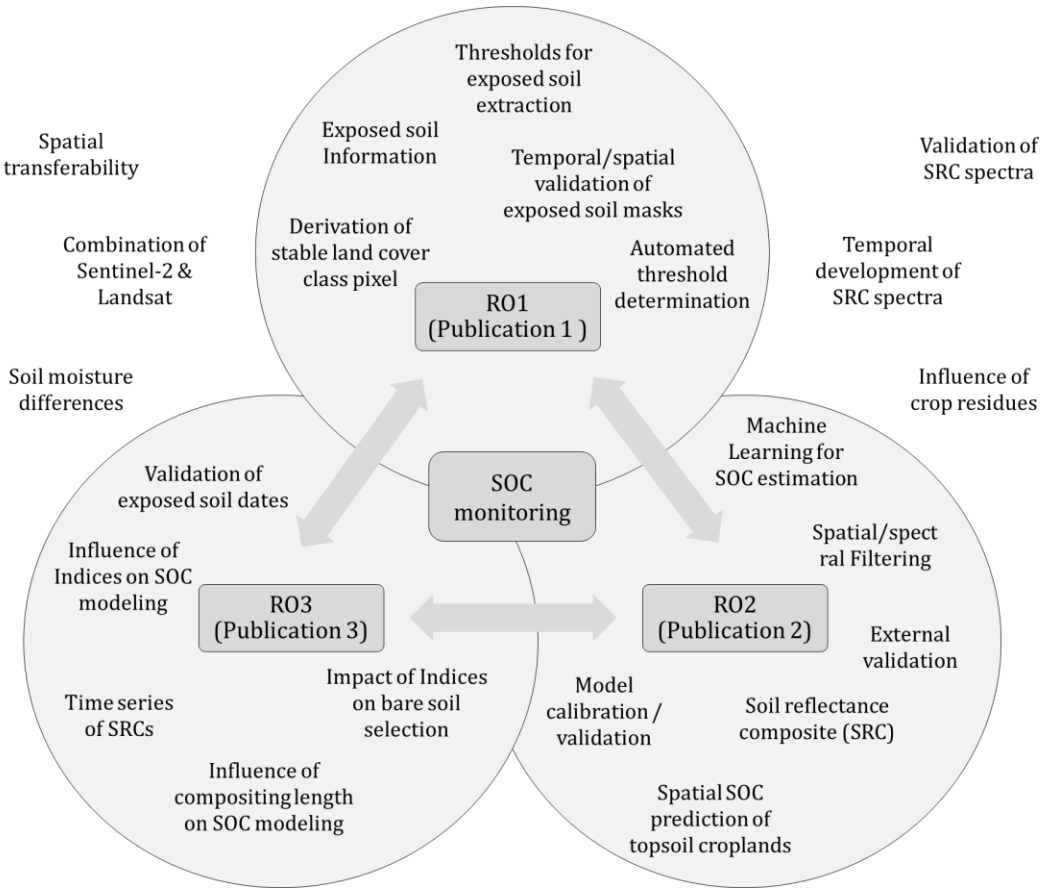

Figure 2.1: Framework of this thesis - aspects for SOC monitoring addressed by the three defined research objectives (RO) and answered within the related scientific publication.

RO 1: Derivation and validation of masks that contain exposed soil pixels from multi-year Landsat data stacks for Germany from 1984 to 2019.

EO exposed soil information is essential for SOC estimation and monitoring purposes. In this context, the SCMaP methodology in combination with Landsat data for bare soil selection was used. Currently, only few approaches use the area-wide (retrospective) mapping potential of Landsat images. In contrast to other compositing approaches, the extraction of bare soil information based on the SCMaP methodology can benefit area-wide mapping purposes (e.g., country-wide, continental) with a high spatial resolution. However, for an area-wide application of the approach, critical methodological constraints of the existing thresholding method were recognized. The need of a systematic and standardized threshold determination was identified. A re-definition of the thresholding also contributes to the uniqueness of the process, as most of the existing comparable composite approaches use empirically determined thresholds and are thus mainly applicable for a regional use. The aim was to create a data-driven concept, where no auxiliary data was needed. Furthermore, the resulting exposed soil areas identified for 5-year periods between 1984 and 2019 can be of great value for statistical analysis due to land cover changes or the localization and monitoring of extensively used cropland areas over time. Regarding the data-driven approach for threshold determination and the potential applicability of the spatial and temporal exposed soil information for statistical purposes, special emphasis was also dedicated to a comprehensive validation concept. Based on the manual thresholding approach, there was no validation of the spatial and temporal distribution of exposed soil pixels conducted so far.

Both, the need of a standardized threshold derivation concept to go beyond existing approaches and the lack of a spatial and temporal validation of exposed soil pixels using the SCMaP methodology resulted in RO1. It gives the methodological baseline (processor optimization and output validation) in order to create an operational approach, which is independent of auxiliary or empirical threshold fitting to prepare soil products for SOC estimation. The first technical focus is set on the impact and the optimization of a training sampling strategy to automatically and randomly select land cover (LC) pixels from CORINE Land Cover (CLC) data. The spectral-temporal behavior of these LC classes is then used for the determination of two thresholds required for the derivation of exposed soil information. The aim is the development of the originally manual selection of land cover pixels for threshold determination in the SCMaP chain by Rogge et al. (2018) towards an automatically standardized approach for an operational use which is not limited to a local application. A manual sampling is not robust enough, time-consuming and might not represent the spectral variability of the required LC classes. For the selection of LC pixels, a data-driven random sampling approach was chosen, using CLC data sets that do not change in the observed time period. Further, it was tested, if the threshold definition rule is still applicable or has to be adjusted due to the automated LC pixel selection process. The second focus of RO1 is to validate the resulting masks of exposed soil pixels covering Germany for all time periods in order to enhance the understanding of the spatial and temporal extraction. For this purpose, the resulting exposed soil masks are correlated with two independent reference datasets (surveys from the Federal Statistical Office (DESTATIS) and the CLC inventories) available for different time steps containing information about the coverage of croplands in Germany. Both data sets contain the spatial distribution of croplands for several time steps since 1990.

RO2: Estimating the potential of the SCMaP SRC generated from Landsat images covering 30 years to derive a high-resolution map of SOC contents in Bavarian croplands.

Shown by the good validation results given in the first publication, the methodological revisions of the SCMaP chain were successful. This allows the question, if the soil reflectance composites (SRC), which are generated on behalf of the exposed soil masks, can be used for SOC estimation of topsoil croplands. So far, the SCMaP SRCs have not been used for SOC prediction for larger areas. However, the SCMaP SRCs, generated with multitemporal Landsat data can serve as a spatially enhanced data source for EO based SOC estimation and modeling. Additionally, they can benefit the temporal and spatial limitation of current approaches. The applicability of Landsat SCMaP SRC for topsoil SOC predictions of croplands has to be estimated. For this purpose, methodological constraints for SOC modeling have to be analyzed and in this context several components were identified (Figure 2.1). Beside a pre-processing of the soil sample database an appropriate machine learning algorithm for spatial SOC prediction has to be selected. Further, several publications show the successful implementation of additional spectral indices for modeling purposes. Existing studies usually do not contain an external validation using an independent dataset that goes beyond the model validation. However, such an additional validation is a central aspect to enhance the understanding of SOC estimation. All the formulated requirements led to RO2.

In order to answer RO2, the second publication addresses the applicability of the SCMaP SRC, for SOC estimation of not permanently covered topsoil croplands. The focus of RO2 was on a regional feasibility study to use Landsat SCMaP SRC for SOC predictions covering large parts of Bavaria (Germany) and adjacent regions. The SRC was generated for a time-period of 30-years (1984-2014) as no changes in cropland SOC contents are expected in the investigation area. Furthermore, the cooperation with two Bavarian environmental agencies enabled the use of a unique soil database containing numerous field samples (n > 1,000) between 1986 and 2016. The available legacy SOC data were intersected with the SRC and the resulting database was used to build spectral models. For the preparation of a modeling framework, special focus was put on several aspects. Firstly, the intersection of point soil samples with EO pixels can be a potential source of inaccuracies. In this regard, a spatial/spectral filtering technique to prepare the dataset for modeling purpose was developed. Several established Machine Learning approaches (Multiple Linear Regression, Partial Least Square Regression, and Random Forest Regression) for SOC prediction were compared. Furthermore, the influence of spectral indices as additional covariates in combination with the reflectance composite pixel features on the model performances were evaluated. The prediction quality was assessed by established performance and accuracy measures (R^2, root mean squared error - RMSE, ratio of performance to deviation - RPD) and compared with existing approaches, to better understand the advantages / disadvantages of the developed model setup and database. In order to answer RO2, special emphasis was also given to an independent external validation, based on a dataset not integrated within the model calibration and validation. From the authors point of view, an additional external validation offers a new perspective to the understanding of the applicability of SCMaP SRCs for SOC modeling.

RO3: Optimization of parameters for SRC generation for recurrent assessments of SOC contents using Landsat data, considering the reliability of the selection of exposed soil dates.

The results of RO2 showed a reliable applicability of the SCMaP SRC for SOC prediction of topsoil croplands in Bavaria and adjacent regions. However, a 30-year compositing length can be too long, especially for monitoring purposes in areas, where changes are expected within a shorter period of time or to capture retrospective SOC developments. Other studies barely give insights into the impacts of different compositing lengths for SOC determination, even though Landsat offers a high (retrospective) monitoring potential due to its long lifetime. This led to thoughts about the role of the compositing length in general. Also, the influence of other processing parameters (e.g., a pre-selection of scenes, different spectral indices) for bare soil selection are relevant issues in order to understand their implications on SRC generation and thus on SOC estimation. Closing this research gaps forms an integral part of RO3. In view of maximizing the understanding of the SRC generation process, the reliability of the bare soil dates identified by the SCMaP approach have not been evaluated yet. The question, if the index (-combination) used, correctly extracts the acquisition dates, i.e., fields which are bare, smooth and show dry soils was not addressed yet. In addition to this, a clear separation of NPV and exposed soils by the index thresholding is an essential part of bare soil compositing approaches. The validation aims to improve the understanding of bare soil selection, the separation between NPV and bare soils and forms the second focus of RO3.

All analyses addressing RO3 are presented in the third scientific publication and are based on the findings of the first (index thresholding) and second publication (SOC prediction methodology). Again, the analyses were conducted for the Federal State of Bavaria and adjacent regions, even though no high temporal SOC changes are expected. The valuable, comprehensive database and the expert knowledge available were the decisive factors for the decision here. First, bare soil dates determined by the approach are validated against field observations and information from the local crop calendar, when the fields are likely to be bare and visible from the satellite. In this context also, the influence of different spectral indices for bare soil selection were discussed. Furthermore, the impacts of SRCs composed of these spectral indices for topsoil SOC determination were analyzed in the test area. Conclusively, the publication indicates which compositing length and seasonal composition allows the most accurate derivation of SOC contents in terms of (retrospective) monitoring purposes.

Based on the topics addressed by the three scientific publications, a comprehensive analysis was conducted to explore the potential of the novel soil compositing approach SCMaP for long-term SOC monitoring using Landsat data. In the following chapter, the findings of the analyses addressing the different ROs are presented and discussed in more detail.

3. Publications

This cumulative thesis comprises three peer-reviewed scientific publications in international journals. Each publication is dedicated to a RO given in chapter 2 in order to answer the scope of the thesis. Two of the three publications have been published, the third is submitted and currently under review. The scientific publications are presented in chronological order as this follows the framework of the thesis. For all papers, the SCMaP approach is the methodological baseline for the extraction of exposed soil information. In order to answer the scope of the thesis, a revision of the SCMaP methodology (Paper I), a regional feasibility study of the applicability of SCMaP exposed soil information for SOC estimation (Paper II) followed by a comprehensive validation of identified bare soil dates and an analysis regarding an optimization of the parameters for SRC generation and SOC modeling using Landsat data (Paper III) was conducted.

In the following subsections, the findings of the analysis related to the scientific publications are presented in detail. Each is introduced by a concise overview page, where information about the journal, the impact factor of the selected journal, the status of the paper, and the contribution of the author and co-authors are given.

In addition to the three publications, the author has contributed to research as co-author in the following articles, which are (partly) built on findings of the scientific publications:

Möller, M., S. Zepp, M. Wiesmeier, H. Gerighausen, U. Heiden, 2022. Scale-Specific Prediction of Topsoil Organic Carbon Contents Using Terrain Attributes and SCMaP Soil Reflectance Composites. Remote Sensing, 14, 2295.

Heiden, U., P. d'Angelo, P. Schwind, P. Karlshöfer, R. Müller, S. Zepp, M. Wiesmeier, P. Reinartz, 2022. Soil Reflectance Composites – Improved Thresholding and Performance Evaluation. Remote Sensing, 14, 4526.

3.1. Scientific Publication I: The Influence of Vegetation Index Thresholding on EO-based Assessments of Exposed Soil Masks in Germany between 1984 and 2019

Reference: Zepp, S., M. Jilge, A. Metz-Marconcini, U. Heiden, 2021. The influence of vegetation index thresholding on EO-based assessments of exposed soil masks in Germany between 1984 and 2019. ISPRS Journal of Photogrammetry and Remote Sensing, 178 (2021), 366-381.

https://doi.org/10.1016/j.isprs.2021.06.015

Status: published

Author`s contribution: **SZ**: Conceptualization, Methodology, Software, Data curation, Writing – Original Draft, Visualization, Project administration. **MJ**: Methodology, Software, Data curation, Writing – Review & Editing. **A.M.-M.**: Software, Writing – Review & Editing. **UH**: Conceptualization, Writing – Review & Editing, Supervision, Funding acquisition.

Scope of the journal: The ISPRS Journal of Photogrammetry and Remote Sensing (P&RS) is the official journal of the International Society for Photogrammetry and Remote Sensing (ISPRS). The Journal provides a channel of communication for scientists and professionals in all countries working in the many disciplines that employ photogrammetry, remote sensing, spatial information systems, computer vision, and related fields. The Journal is designed to serve as a source reference and archive of advancements in these disciplines.

5-year impact factor: 11.774 (2021)

Article

The Influence of Vegetation Index Thresholding on EO-based Assessments of exposed Soil Masks in Germany between 1984 and 2019

Simone Zepp [a,*], Marianne Jilge [a], Annekatrin Metz-Marconcini [a], Uta Heiden [b]

[a] German Aerospace Center (DLR), German Remote Sensing Data Center (DFD), Muenchener Str. 20, 82234 Wessling, Germany

[b] German Aerospace Center (DLR), Remote Sensing Technology Institute (IMF), Muenchener Str. 20, 82234 Wessling, Germany

[*] Corresponding author at: German Aerospace Center (DLR), Muenchener Str. 20, 82234 Weßling, Germany

Received: 14 December 2020; Accepted: 17 June 2021

Abstract: Knowledge about the spatial and temporal distribution of exposed soils is necessary for e.g., soil erosion mitigation. Earth Observation (EO) is a valuable data source for detecting exposed soils on a large scale. In the last couple of years, the multitemporal compositing technique has been used for the generation of so-called exposed soil composites that overcome the limitation of temporarily coverage of the soils with vegetation as it is occurring at agricultural sites. The selection of exposed soil pixels from the stack of multispectral images is mainly done using spectral reflectance indices such as NDVI, NBR2 and others calculated on a per-pixel basis. The definition of the thresholds that are applicable to large areas such as regions, countries or continents is still a challenge and requires a reliable and robust sampling data base. In this study, the Soil Composite Mapping Processor (SCMaP) is used to build exposed soil masks containing all pixels in a given time period showing at least once exposed soil. For this purpose, a modified vegetation index (PV) based on the NDVI is used to separate the soils from other land cover (LC) classes by two PV thresholds. The overall goal of this study is to derive and validate exposed soil masks from multi-year Landsat data stacks for Germany from 1984 to 2019. The first focus is set on the impact of a newly developed sampling approach of LC classes such as urban areas, deciduous forests and agricultural fields that are automatically derived from Corine Land Cover (CLC) data. The spectral-temporal behavior of these LC classes in $PV_{min/max}$ index composites show larger variability of the PV values compared to a manual sampling for selective LC classes such as urban areas. It reveals that the threshold definition method previously developed by Rogge et al. (2018) is not robust enough and the percentile rule used to define the T_{max} threshold had to be adapted from 0.995 to 0.900. On the other hand, the sampling data base has proven to be robust across time and region. The second focus of the paper is to validate all generated exposed soil masks covering Germany for seven time periods from 1984 to 2019. A linear correlation analysis was performed comparing the SCMaP data with surveys from the Federal Statistical Office (Destatis) and the CLC inventories. The comparison with both datasets showed high regression coefficients (R2 = 0.79 to 0.90) with small regional deviations for areas in the Northern part of Germany. Strong correlation was found for time periods based on a higher number of cloud free Landsat images such as from 2000 to 2009. This demonstrates the high potential of SCMaP's to generate exposed soil masks based on an automated sampling and a robust threshold derivation. To contribute to soil erosion studies that need information about where and when soils are bare, accurate exposed soil masks in suitable time periods can be of great value.

Keywords: Soil exposure, Soil reflectance composites, Landsat, Multispectral, Thresholding

1. Introduction

Soils provide numerous ecosystem services that are essential for human life on Earth (Adhikari and Hartemink, 2016). Knowledge about the spatial and temporal distribution of exposed soils is very informative for assessing ecosystem processes and statistical analyses and can serve as a basis for further soil-related assessments (Lavelle et al., 2014). Natural or anthropogenically induced soil degradation and erosion affects the quality of ecosystem services (Demattè et al., 2018). In particular, exposed soils that are not covered by vegetation are prone to erosion (Virto et al., 2015), resulting in a notable amount of soil loss each year (Borelli et al., 2017; Borelli et al., 2018; Steinhoff-Knopp and Burkhard, 2018). In addition to the location and exposition of uncovered soils (Panagos et al., 2014a; Panagos et al., 2015), the duration of exposure indicates the vulnerability of an area (Cerdan et al., 2010; Panagos et al., 2014b) to different geofactors, such as wind (Borelli et al., 2015; Schmidt et al., 2017) or water (Gobin et al., 2004; Steinhoff-Knopp and Burkhard, 2018). Thus, information on the spatial and temporal distribution of exposed soils enables estimations of the vulnerability of a region (Cerdan et al., 2010; Panagos et al., 2015a) and can support the assessment of the future availability of soil-derived ecosystem services (Baude et al., 2019).

Earth Observation (EO) is a valuable data source for detecting exposed soils. Merging information from multiple images have been developed as suitable technique for many purposes such as cloud-freeimages (Hermosilla et al., 2015), crop and land cover (LC) detection (White et al., 2014; Griffiths et al., 2019; Hansen et al., 2011) and for analyzing forests (Adams et al., 2020). In the last couple of years, the compositing technique has also been used for the generation of images containing reflectance values of exposed soils (Rogge et al., 2018; Dematt`e et al., 2018; Diek et al., 2017; Vaudour et al., 2021). This is an important step towards subsequent large-scale soil analyses that overcomes the temporarily coverage of soils by vegetation. The selection of exposed soil pixels from the multitemporal time stack is still a challenge and there are different solutions tested by previous studies. Loiseau et al. (2019) empirically defined a threshold based on the Normalized Difference Vegetation Index (NDVI) to select exposed soil pixels. Demattè et al. (2018) used field soil samples spectrally measured in the laboratory to define a suitable threshold based on the NDVI and the Normalized Burn Ratio 2 (NBR) for exposed soil compositing. The methodology was developed for an area-wide automated processing to retrieve soil spectral reflectances (Geospatial Soil Sensing System (GEOS3)). Diek et al. (2017) used the Bare Soil Index (BSI) to build a bare Soil Composite for topsoil characterization of the agricultural areas in Switzerland. Different indices (NDVI, NBR2, BSI and Soil Surface Moisture Index (S2WI)), thresholds and regulations for creating composites were tested and compared by Vaudour et al. (2021) for two test sites in France. In all these cases, exposed soils can be successfully separated from photosynthetic active vegetation. Spectral index thresholds are used due to their simplicity and applicability.

A lot of emphasis has been put to cope with the spectral similarity of soils with non-photosynthetic active vegetation (NPV; Daughtry et al., 2006) such as grasslands (dry condition) or deciduous forests (leaf-off condition). But also crop residuals can have an impact on the soil pixel purity. The clear spectral separation of NPV and exposed soils is hampered by the limited spectral resolution of multispectral images in the SWIR region (Asner and Heidebrecht, 2002; Okin, 2007; Dematt`e et al., 2018; Malec et al., 2015). However, studies from Demattè et al. (2018) and Rogge et al. (2018) have shown that this influence can be minimized. Demattè et al. (2018) have tested different NBR2 values in order to minimize the influence of NPV in the soils spectra that especially are traced back to stubbles and crop residuals. They concluded that the results can be improved, if longer time ranges are considered that allows for a stricter threshold and thus, purer bare soil pixels in the soil mask. Rogge et al. (2018) developments have focused on a clearer separation from grasslands and leaf-off conditions of deciduous forests. The developed technique

uses the change of agricultural fields from soil exposure to vegetation coverage to derive two spectral index-based thresholds. The definition of these thresholds is based on LC classes derived from CORINE Land Cover (CLC) data sets that do not change in the observation period. Thus, the spectral-temporal behavior of urban areas, deciduous trees and agricultural fields are analyzed to set the thresholds. These thresholds are applied to first, separate exposed soils from permanently photosynthetic active vegetation and second, to distinguish between exposed soils and permanently non-vegetated areas such as urban areas, water and mine sites. In the result, areas with a changing cover and an index value lower than a previously defined threshold are selected as exposed soils (exposed soil mask) and averaged (mean) into a soil reflectance composite. The advantage of this technique is that no further ancillary data is necessary to separate exposed soils from other LC classes such as forests and urban areas (e.g. Diek et al., 2017).

CLC are selected for the derivation of thresholds because it is European-wide available and thus, has the potential to derive thresholds suitable for continental processing. However, sampling of CLC pixels in Rogge et al. (2018) has been done manually, which is very time consuming and a pixel selection might not represent the spectral and spatial variability of the LC. For country-wide and continental mappings of exposed soils, automated sampling strategies are needed that first, can help to handle regional differences of LC dynamics (Ying et al., 2017) represented in multispectral satellite data and second, allows for repeated derivation of thresholds in order to analyze their stability across time. The influence of these parameters is not yet fully understood or analyzed. For operational processors such as SCMaP and GEOS3, it is important to know the effect of different threshold settings to optimize operational processors and find the best solution for the regions of interest.

The overall goal of this study is to derive and validate masks that contain exposed soil pixels from multi-year Landsat data stacks for Germany from 1984 to 2019. For the exposed soil masks, it is important to clearly separate grasslands in dry conditions and deciduous trees as examples for NPV from exposed soils. The first focus is set on the impact of the sampling strategy to derive spectral index thresholds. We use SCMaP for the detection of exposed soils that require two spectral index thresholds and we also used the concept of threshold definition based on percentile rules. For the definition of the threshold, this paper presents a new and fully automated sampling strategy. In order to analyze the impact of the sampling scheme, we compared the results of the automated sampling with the manual sampling (Rogge et al., 2018) by comparing the spatial-temporal behavior of the LC classes. Further, selection criteria such as the number of samples and the repeatability of the results are analyzed. We also tested, if the threshold definition rule that is used in Rogge et al. (2018) is still applicable. Therefore, the impact of the new sampling data base on the resulting exposed soil masks is analyzed. We select the best approach for deriving seven exposed soil masks for entire Germany for different time periods ranging between 1984 and 2019.

The second focus of the paper is to validate all exposed soil masks covering Germany for all time periods. For this objective, the selection of suitable and independent data sets that contain country-wide repeated statistics is essential. In Germany and regions with similar climate conditions, exposed soils are rare and occur predominantly in agricultural areas. The pixels that SCMaP is collecting for the exposed soil masks are characterized by a change from vegetated to non-vegetated condition. The majority of these pixels are occurring on agricultural sites. All other permanently vegetated and permanently non-vegetated areas are neglected. Therefore, we used two independent data sets that contain information on the coverage of agricultural areas at different time steps. The Federal Statistical Office (Destatis) collects statistical data regarding agricultural areas and crop types in Germany on a regular basis (Destatis, 2017). However, determining the methods used for the data collection is in the responsibility of each federal state and might result in regional differences. For that purpose and for future continental processing,

we additionally used the agricultural classes of the CLC surveys for the validation of exposed soil masks. Both data sets have their pros and cons and validation results are shown.

2. Study area

Germany stretches over an area of 357,095 km2, of which 47% is used for agricultural purposes (Destatis, 2020a). These areas are split into permanent grassland (14%) and cropland (33%). In order to discuss the regional differences of the developments in this study, a brief introduction to the characteristics of the federal states of Germany is necessary. Intensively used arable land is the dominant land use in the federal states of Schleswig-Holstein (41%), Lower Saxony (39%), North Rhine Westphalia (31%), Brandenburg (35%), Mecklenburg-Western Pomerania (47%), Saxony (39%), Saxony-Anhalt (49%) and Thuringia (38%) (Destatis, 2020a; Destatis, 2020b). The federal states of Schleswig Holstein (22%), Lower Saxony (15%), Bremen (17%) and Saarland (16%) show a higher portion of permanent grasslands compared to the areas in the state. In particular, northern Germany is primarily covered by permanent grasslands.

The investigation area of Germany is covered by three bio-geographical regions (EEA, 2016). These bio-geographical regions were developed by the European Environmental Agency (EEA) and represent similar biodiversity and biological structures based on comparable vegetation and climatic conditions (EEA, 2016). All of Europe consists of eleven regions, which are defined geographical reference units for characterizing the habitat types and species present in different countries (EEA, 2020). Germany is mainly covered by the continental bio-geographical region (Fig. 3.1.1). Small portions in northwestern Germany are associated with the atlantic bio geographical region, whereas the high mountainous areas in southern Germany are classified as an alpine bio-geographical region (EEA, 2016).

Multiple analyses on the influence of thresholding on the derivation of the exposed soil masks shown in this study are performed for five subportions of the study area (Fig. 3.1.1). The test areas were selected to cover all three bio-geographical regions and land cover/land use types in Germany.

3. Methods and data

3.1 Using SCMaP for mapping soil exposure

SCMaP is used to build exposed soil masks containing all pixels in a given time period showing at least once exposed soil. For this purpose, a modified vegetation index (PV) (Rogge et al., 2018), based on the NDVI (Rouse et al., 1974), is used to separate the soils from other LC classes: PV = ((NIR - RED)/(NIR + RED)/((NIR - BLUE)/(NIR + BLUE)). Although authors have tested different indices for detecting bare soils such as BSI (e.g. Diek et al., 2017), combinations of NDVI and NBR2 (Demattè et al., 2018; Demat`t`e et al., 2020), NBR2 and soil moisture indices (Vaudour et al., 2021) or NDVI and Normalized Difference Builtup Index (NDBI) (Ying et al., 2017), we retain the PV index for this study in order to compare the results of the manual sampling with the automated sampling strategy. It is further important to remark that for the purpose of this study, the focus is not on selecting the purest soil pixels, but on creating an exposed soil mask that correspond to agricultural areas with changing covers and excludes all grasslands and deciduous forests.

To extract the exposed soil pixels, two composites containing the minimum (PV_{min}) and the maximum PV index (PV_{max}) per pixel are generated for a given time frame. Using the spatial and temporal behavior of the PV index values, two thresholds (T_{min} and T_{max}) are defined to distinguish

the exposed soil areas from all other LC classes (Fig. 3.1.2) to build the exposed soil mask. The determination of the thresholds is based on different LC classes (Fig. 3.1.2a). Exposed soils (referred to as fields) and urban surfaces show the lowest PV values in the PV_{min} composite but also overlap with non-photosynthetic active vegetation (e.g., stubble on fields), dry grassland and deciduous forests. In the PV_{max} composite, soils are covered with vegetation, showing an overlap with forests and grasslands, and can be clearly separated from urban surfaces and areas showing permanent low vegetation indices, such as water. Therefore, the minimum threshold (T_{min}) is to separate urban surfaces and exposed soils from grassland, deciduous forests coniferous forests and water. The maximum threshold (T_{max}) is set to distinguish the soils covered by vegetation from urban materials and water. By applying T_{min} and T_{max} thresholds to the PV_{min} and PV_{max} composites, two masks are generated. The intersection of the two masks results in the exposed soil mask.

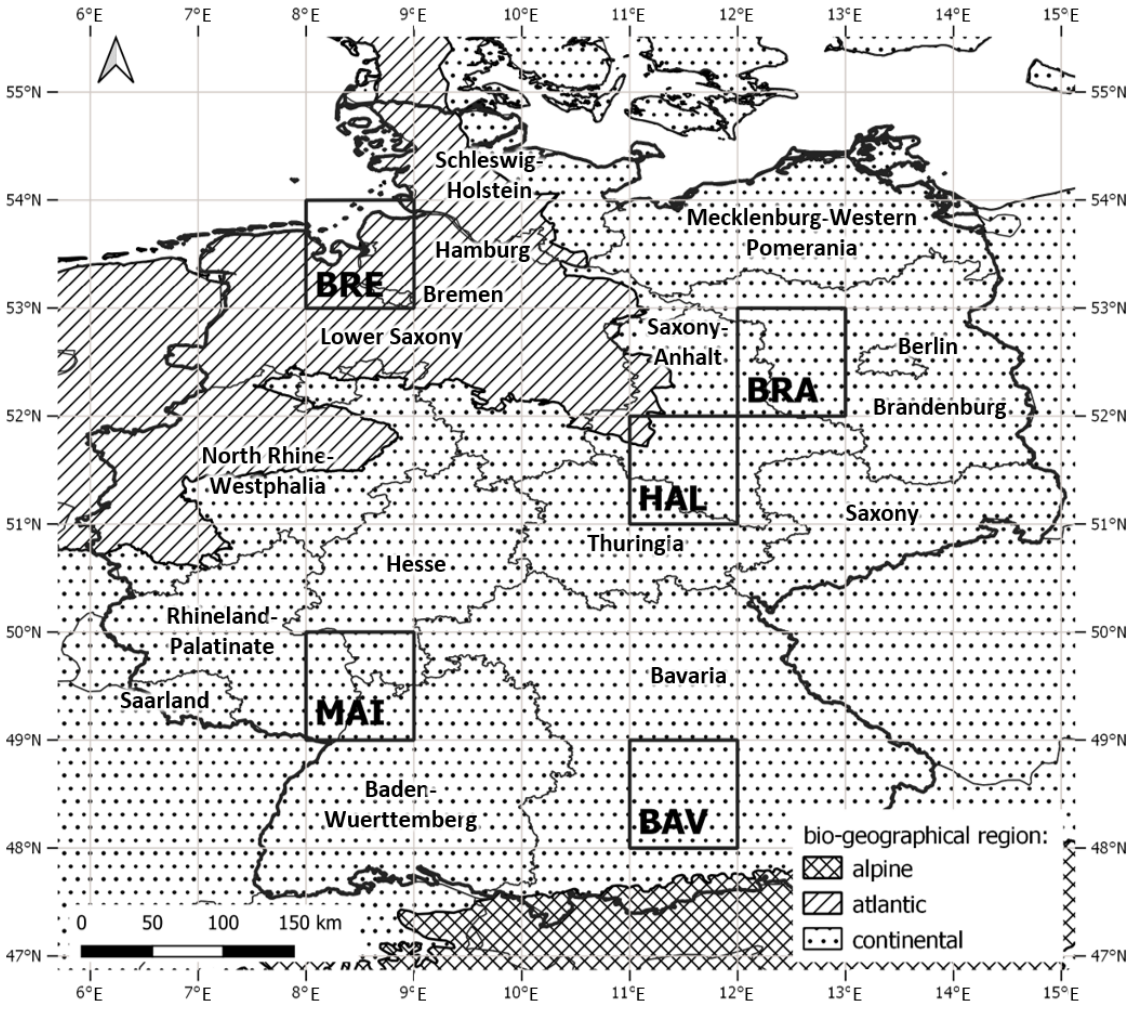

Figure 3.1.1: Coverage of the three bio-geographical regions in Germany and the location of the five test areas (BRE - Bremen, BRA - Brandenburg, HAL - Halle, MAI - Mainz, BAV - Bavaria).

As Rogge et al. (2018) demonstrated in detail, the lower 0.005 percentile of the deciduous forests defining T_{min} (Fig. 3.1.2b) and the upper 0.995 percentile of the class urban are used to separate soils from all other LC classes (Fig. 3.1.2c). These points are selected to avoid as many false positives as possible.

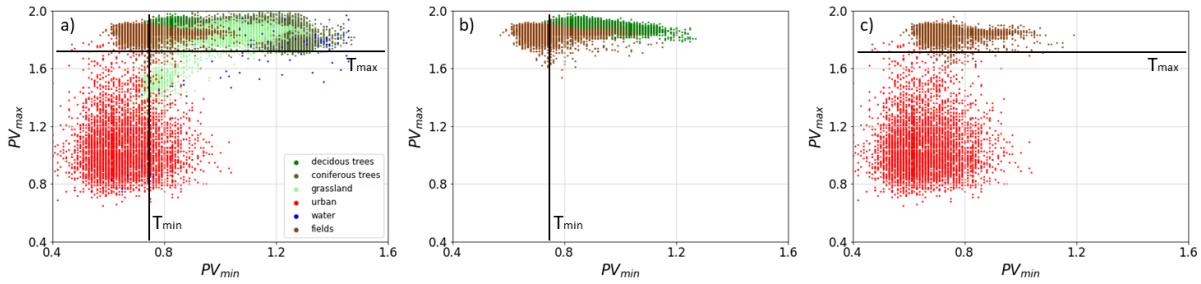

Figure 3.1.2: PV_{min} and PV_{max} characteristics of a) six LC types for the study area, b) the behavior of exposed soils (referred to as LC vlass fields) and LC class deciduous trees to define T_{min} and c) the behavior of fields and urban areas to define T_{max}.

3.2 Data preparation

3.2.1 Landsat data base preparation

The Landsat database used in this study is built from reprocessed Landsat-4 TM, Landsat ETM 5, Landsat-7 ETM+, and Landsat-8 OLI collection data sets provided by the USGS (Dwyer e al. 2018) for all path/row combinations covering Germany (paths 192 to 197, rows 22 to 27) between 1984 and 2019. The images were downloaded from the Google Archive in 2018 and 2019. All scenes available in the Level-1C processing state flagged with the highest correction level L1TP (calibration and orthorectification based on ground control points and digital elevation model data to correct for relief displacements (USGS, 2020)) were downloaded. A total of 17,852 pre-processed Landsat images are used in this study (Table 3.1.1). SCMaP is applied to seven time periods from 1984 to 2019 each making use of five years of data. However, the first time period contains six years (1984–89).

For the seven composite periods, all available scenes per time period of the different sensors are combined. The merging of Landsat-4 TM, -5 ETM and -7 ETM+ images is a well-established method (Claverie et al., n2015; Kovalskyy and Roy, 2013; Teillet et al., 2001). For the time period of 2015–19, scenes from Landsat-7 ETM+ and -8 OLI were combined, even though the equivalent bands for the calculation of the PV index of the two sensors contained slightly different wavelength ranges (Chastain et al., 2019). However, several studies have shown a minor to negligible influence resulting from merging the different wavelength ranges of Landsat-7 ETM+ and -8 OLI bands (Langford, 2015;Xu and Guo 2014; Zhu et al., 2016; Roy et al., 2016; Holden and Woodcock 2016; Flood 2014). Based on these findings, the Landsat-7 ETM+ and Landsat-8 OLI data were merged as input to the SCMaP processing chain and were not separated for the generation of the 2015–19 composite.

For this study, Landsat collection data were used instead of the former Landsat pre-collection data, as the Landsat re-processed data sets provided a higher data quality (Li et al., 2018; Wulder et al., 2019) and showed fewer artifacts in direct comparison.

Several pre-processing steps were applied to the Landsat path/row scenes. The FMask algorithm (Zhu and Woodcock 2012; Zhu et al., 2015)detected and removed clouds, cloud shadows and pixels that were covered by snow. An atmospheric correction was applied to all scenes using Atmospheric Topographic Correction (ATCOR) software for satellite imagery (Richter and Schläpfer, 2014; Richter 2010; Richter et al., 2006). Saturated pixels in urban areas and water bodies were identified and eliminated. Furthermore, manual filtering was performed to identify large-scale data artifacts as detector striping effects. The manually flagged path/row scenes (approximately 330 scenes) were excluded from the database. In particular, large artifacts

covering a whole scene can substantially affect the SCMaP output, as the processor occasionally includes affected pixels in the exposed soil mask. Finally, the database was reorganized in 1◦ by 1◦ geographical tiles. For this purpose, lists of all intersecting path/row scenes per tile were generated and used by SCMaP for achieving efficient data handling and processing benefits.

Table 3.1.1: Overview of the number of pre-processed Landsat scenes available for all five-year time periods in the investigation area between 1984 and 2019.

time period	Landsat-4 TM	Landsat-5 ETM	Landsat-7 ETM+	Landsat-8 OLI	total
1984-89	85	1,772	-	-	1,857
1990-94	143	2,030	-	-	2,173
1995-99	-	1,986	211	-	2,197
2000-04	-	1,612	1,421	-	3,033
2005-09	-	1,946	1,154	-	3,100
2010-14	-	644	1,547	460	2,681
2015-19	-	-	1,319	1,982	3,301
1984-2019	228	9,990	5,652	2,472	18,342

3.2.2 Data preparation for automated sampling

Threshold determination requires the identification of known regions with no LC change over the observed time frame. For this purpose, temporarily stable LC areas without transition to other LC classes, preferably for the total investigation period (since 1984), are needed. The CORINE Land Cover (CLC) data set (EEA, 2007) is a European data set containing repeated LC surveys that is provided by the EEA. To identify the stable areas, all available CLC layers and CLC change layers in vector format were downloaded (https://land.copernicus.eu/pan-european/corine-land-cover) and underwent several pre-processing steps (Fig. 3.1.3b).

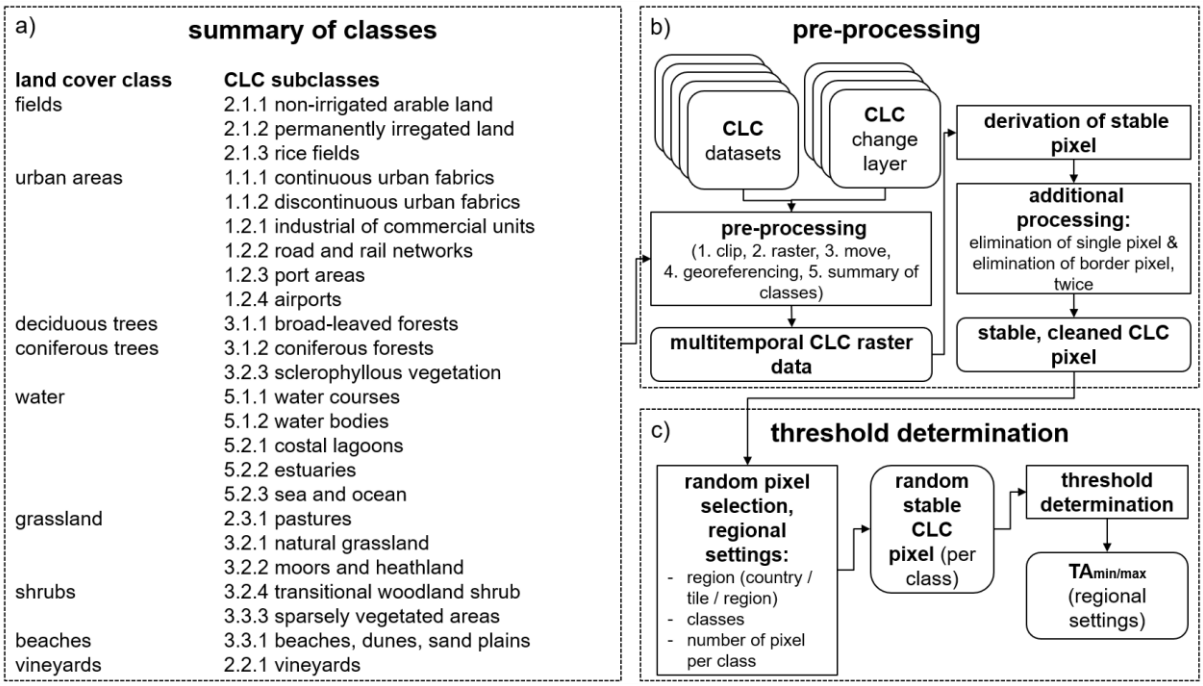

Figure 3.1.3: Workflow for preparation of the LC data for the required threshold determination for SCMaP: a) summarized CLC classes used to build the nine LC classes for the automated selection of stable LC pixels; b) deviation of randomly selected stable CLC pixels; and c) subsequent threshold determination using regional settings per processing area (described in Section 3.3).

In a first step, the CLC classes that also contain land use components are reorganized and generalized to ensure that the resulting areas can be clearly assigned to a specific LC. The CLC data set consist of classes with different levels of detail. Fig. 3.1.3a shows the summarized CLC subclasses for the subsequent threshold derivation (Section 3.3). In addition, the CLC change layers containing the information regarding the transition of one LC class to another between two classification periods was subtracted from the data set. The reclassified and cleaned data sets were rasterized to the Landsat spatial resolution of 30 m. The removal of single pixels as well as a reduction of direct border pixels of individual class clusters was performed twice in order to exclude edge effects. To remove them, a three by three pixel moving window was used to analyze the relationships in a pixel neighborhood following von Neumann criteria (Toffoli and Margolous, 1987). Finally, the resulting stable and cleaned data set contains LC pixels that did not change between 1990 and 2018 and are therefore called stable.

The threshold determination is built on randomly selected, automatically extracted stable CLC pixels based on different regional settings (Fig. 3.1.3c), and is described in Section 3.3.

3.2.3 Validation data sets

For the validation of the exposed soil masks for Germany generated by SCMaP, a country-wide data set is needed that can be assigned to exposed soils. Following the philosophy of SCMaP that is only extracting those exposed soil pixels that additionally show a change to vegetated condition in the observation time, a data set containing agricultural areas is needed. For Germany, the statistical federal agency Destatis provides several surveys containing, for instance, the spatial size of agricultural areas in Germany per federal state and per county. These data sets are available for the years 1999, 2001, 2003, 2007, 2005, 2010 and 2016 (Destatis, 2020a; Destatis, 2020b). The general agricultural structure survey and agricultural census data sets were downloaded from the regional statistical database provided online by Destatis (https://www.regionalstatistik.de/genesis/online/logon). The surveys contain the number of farms and combined of agricultural area of common crop types, including grasslands in Germany per federal state and county. Because SCMaP is applied to an optical multispectral remote sensing database itis not possible to detect soils underneath permanent vegetation, the proportion of grasslands was excluded from the Destatis agriculture statistical analysis. All spatial information was converted to the percent coverage of agricultural area per federal state and per county using the size of each state and county provided by Destatis (2018). As the SCMaP time periods of 2000–04 and 2005–09 contain two Destatis data sets each, the two respective statistics were averaged. For the states Berlin, Bremen, Hamburg and Mecklenburg Western Pomerania (Fig. 3.1.1), no statistical data were available for any given time step. For the federal state of Saxony, data for a subset of the administrative districts were available.

The second validation data set used was the CLC inventories of 1990, 2000, 2006, 2012 and 2018 provided by the EEA (EEA, 2007). The data sets were downloaded as vector files for Europe (https://land.copernicus.eu/pan-european/corine-land-cover), clipped to the extent of Germany, re-projected, resampled to the spatial resolution of the soil mask (30 m by 30 m) and saved as raster files. For validating the spatial distribution of the exposed soil masks in Germany extracted by SCMaP, the agricultural classes were of interest. The LC classes non-irrigated arable land (2.1.1) and permanently irrigated land (2.1.2) were extracted from the whole data set and summarized as the input for validation. For better comparability of the validation results to the Destatis survey, the percent coverage of the agricultural areas in the CLC data sets was also calculated per county and federal state.

3.3 Automated sampling and threshold derivation

Thresholds are necessary to separate exposed soils from all other LC classes. The objective is to derive thresholds that are applicable to the entire area of Germany. Therefore, a training data set that can be derived from the CLC mapping is needed, as described in Section 3.2.2. For this purpose, a new technique was developed that randomly selects CLC pixels that are stable over a long time period (Section 3.2.2) and then applied to the Landsat database (Section 3.2.1).

Originally, the threshold determination was based on the behavior of PV_{min} and PV_{max} of the manually selected LC pixels for the five test areas covering the spatial differences across Germany (see Rogge et al., 2018). The manual selection of LC pixels is a time-consuming step, which needs to be repeated for every processed region. Furthermore, the manual selection process can be influenced by the user. To overcome these limitations, an automated and random selection of LC pixels based on stable CLC pixels was developed. The stability of the new approach was tested via an in-depth comparison with the manual determination approach, and an analysis of the influence of the randomized selection procedure on the derivation of the thresholds was performed.

Due to the automated nature of the pixel selection procedure, several settings were tested to assess the performance of the new technique (Fig. 3.1.3c). In this method, the area (tiles, countries, geographic regions, etc.), the LC classes (different amounts and composition of LC classes), the time steps, and the number of pixels per class can be selected individually, and enabling the assessment of the influence of these settings on the thresholds and the resulting exposed soil masks. To compare the random selection method with the manual selection method, the same regional settings were chosen. For this purpose, pixels were selected from the same five tiles covering Germany (Fig. 3.1.1). A total of 5,000 stable CLC pixels per class and tile were selected using a random selection approach to avoid biased manual selection and a clustered distribution to ensure that all expressions of a land use class were recorded per region.

To determine the influence of the random selection approach on the thresholds, the temporal behavior of the LC classes needed to be analyzed in the first step. Therefore, the randomly selected $PV_{min/max}$ pixel values for the LC classes urban, deciduous trees and fields (presumably exposed soils), which are used to determine the thresholds, are shown in a histogram and compared to the $PV_{min/max}$ values derived from the manual selection approach.

Based on the $PV_{min/max}$ pixel values, the thresholds were defined. The defined thresholds based on manually selected LC pixels are referred to as $TM_{min/max}$ and were compared with the thresholds derived from the random selection approach ($TA_{min/max}$). In the first step, the applicability of the established percentiles for defining $TA_{min/max}$ was investigated. Furthermore, $TA_{min/max}$ were compared to the original sets of $TM_{min/max}$ for all tiles (2000–04; period with the largest overlap of data between Landsat-5 TM and -7 ETM+ and a minimum SCL failure of Landsat-7 ETM+) and all time steps of the Bavarian tile to investigate the spatial and temporal stability of the random selection approach. To estimate the influence of the random selection approach, ten sets of stable pixels per LC class (5,000 per LC class) for all tiles (2000–04) were selected. The influence of the $TA_{min/max}$ on the different sets of randomly selected pixels was investigated. Additionally, the absolute number of random stable pixels per class was altered. The influence of fewer (2,500) and more (10,000) stable pixels per class was investigated. Therefore, the $TA_{min/max}$ of ten sets of different numbers of randomly stable pixels per class for the Bavarian test tile (2000–04) were derived and compared.

3.4 Validation of the exposed soil masks in Germany

The processing of the SCMaP exposed soil masks (Section 3.1) was performed by applying the averaged $TA_{min/max}$ of all five test areas (2000–04) (Section 3.3) to all tiles in Germany for the seven time periods. The validation of the spatial and temporal distribution of the extracted exposed soil masks was performed using the two data sets described in Section 3.2.3. The five prepared Destatis and CLC data sets were compared to the exposed soil masks for the time period containing the year in which each survey was conducted. To compare the validation data set and the mask, the coverage of the exposed soils extracted by SCMaP, expressed as percent, was calculated per federal state and county for each time step. To validate the spatial distribution of the exposed soil masks provided by SCMaP, a linear correlation analysis between the coverages of the exposed soil masks extracted by SCMaP and the agricultural areas provided by the Destatis statistics as well as the CLC data sets was explored for all 16 German federal states and at the county level. The comparison was evaluated by calculating the correlation coefficients (R^2) and root mean squared errors (RMSE) for each comparison to estimate the potential of SCMaP to build exposed soil masks for Germany based on the new thresholding method.

4. Results

4.1 Index thresholding

In Fig. 3.1.4, the frequencies of the summarized $PV_{min/max}$ pixel values for the LC classes urban, fields and deciduous trees from all tiles comparing the manual and random pixel selection approaches are visualized, as these classes are relevant for the derivation of thresholds. For PV_{min}, the distributions are similar, excluding the LC class urban. Here, a clear shift of the maximum and a higher variability of PV_{min} values are visible. However, the shift of the class does not influence the determination of the TA_{min} as the LC class urban is not used to determine TA_{min}. Comparing the PV_{max}, the LC class shows a shifted and diversified distribution of values. The distribution of the LC classes deciduous trees and fields are less extreme and narrower than that of the manually selected pixels. Excluding the LC class urban, the $PV_{min/max}$ of the automated selected pixels shows a higher variance and standard deviation, whereas the median is similar. The shift and differing distribution of the PV_{max} of the LC class urban indicates an adaption of the point at which the TA_{max} has to be set to realize the separation between soils and other LC classes.

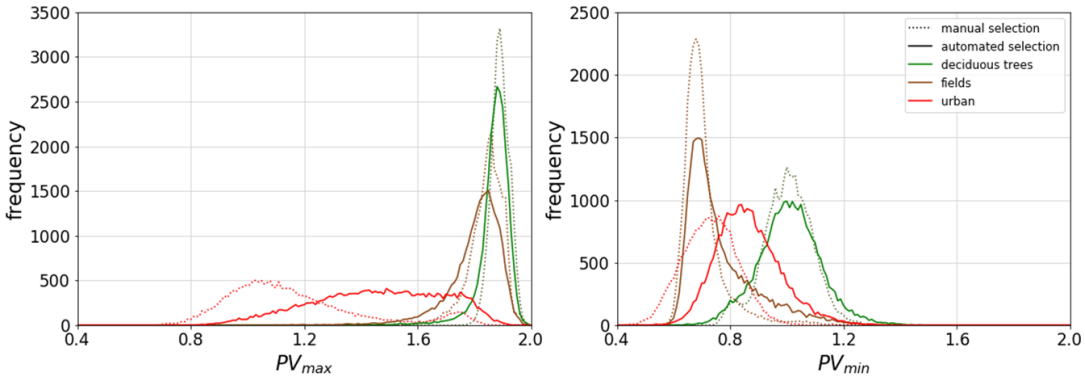

Figure 3.1.4: Histogram of the $PV_{min/max}$ frequencies summarized for all five test tiles comparing manual (dashed line) and random, automated (solid line) selected LC class pixels for the time step 2000-04.

The behavior of the LC classes urban and deciduous trees is used for the determination of $TA_{min/max}$ (Rogge et al., 2018). Comparing the scatterplots of the $PV_{min/max}$ values of the manually (Fig. 3.1.5a) and randomly (Fig. 3.1.5b) selected LC pixels, a lower clustering tendency of the data is visible. Mainly, the randomly selected pixel cluster of the LC class urban is not as selective

compared to the manually selected pixel cluster. As mentioned, originally, the 0.995 percentile of the class urban was used to define the TM_{max}. Applying the 0.995 percentile to the automatically sampled pixels excludes almost half of the data cloud from fields and this, seems to be too high. Fig. 3.1.5b shows that in the resulting exposed soil mask, a significant number of pixels is missing compared to the original exposed soil mask generated based on the manual sampling (Fig. 3.1.5a). Therefore, an adjustment of the percentile to set the TA_{max} is required due to the less clustered distribution and the less selective behavior of the LC class urban (Fig. 3.1.5b). For this purpose, a test has been designed by varying the TA_{max} from 0.995 to 0.89 for the exposed soil mask building.

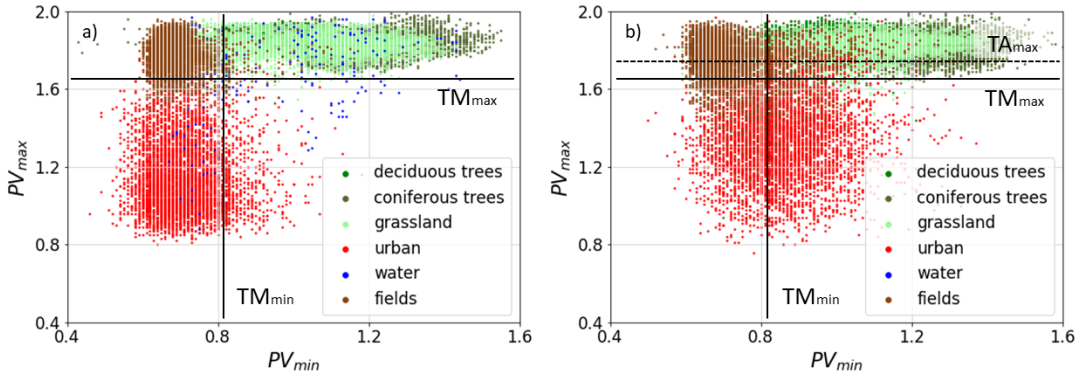

Figure 3.1.5: $PV_{min/max}$ pixel values for different LC classes comparing a) manual and b) randomly selected LC pixels and the derivation of TM_{max} and TA_{max} using the 0.995 percentile of the manually and randomly slected pixels of the LC class urban.

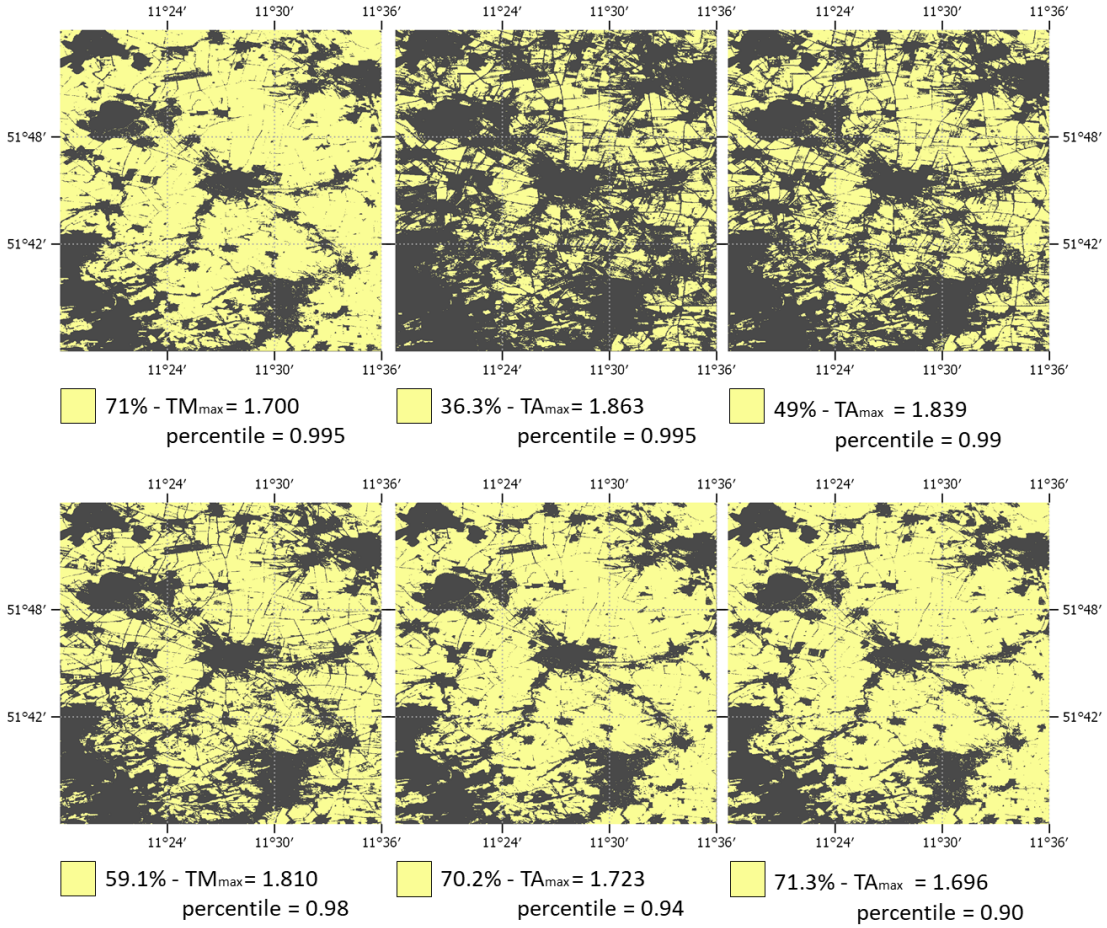

Figure 3.1.6: Influence of different percentiles on TA_{max} and the percentage coverage of exposed soil masks in comparison to TM_{max} shown for the time period 2000-04 for an area near Aschersleben.

Fig. 3.1.6 shows the result of this test for an area surrounding Aschersleben (within the test region HAL) in which different percentiles for the derivation of TA_{max} have been applied to the $PV_{min/max}$ composites (time period 2000–04). Based on CLC, approximately 78% of the land surface is covered by agricultural fields in the selected region. When using the TM_{max} value, 71% of the area is included in the exposed soil mask. Setting the TA_{max} at 0.995 results in a coverage of 36.6% in the same area. Using different TA_{max} values based on varying percentiles, the reduction in the percentiles used for setting the TA_{max} value resulted in an increase in the soil exposure mask saturating at the 0.94 percentile (TA_{max} = 1.723) (Fig. 3.1.7). As Fig. 3.1.6 shows, a percentile of 0.90 for the LC class urban is used to define TA_{max}, and the resulting soil exposure is 71.3%, which is comparable to the soil exposure (71%) defined by TM_{max}.

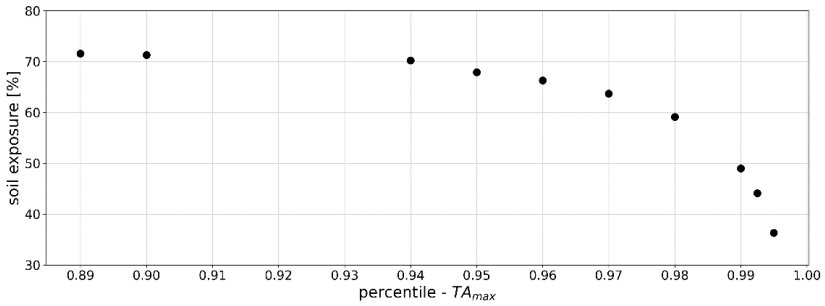

Figure 3.1.7: Varying soil exposure [%] determined for different percentiles to set the TA_{max} for an area around Aschersleben.

Following the selection of the percentile to be used in the definition of $TA_{min/max}$, Table 3.1.2 displays all $TA_{min/max}$ values and comparisons them to the TMmin/max used across the different test areas for the time period of 2000–04 and for all time steps in the Bavarian tile. The $TA_{min/ max}$ values for all areas are similar to the $TM_{min/max}$ values. Additionally, the averaged thresholds across the test areas fall within a similar range. The standard deviations across the test areas of $TA_{min/max}$ in comparison to $TM_{min/max}$ are slightly lower. For the different time steps of the Bavarian tile, the $TA_{min/max}$ values are also similar to the $TM_{min/max}$ values, reporting low standard deviations (STDs).

Table 3.1.2: $TA_{min/max}$ in comparison to $TM_{min/max}$ for all investigation areas (2000-04) and across time (only for Bavaria).

tile (time step)	**TM_{min}**	**TM_{max}**	**TA_{min}**	**TA_{max}**
BRE (2000-04)	0.896	1.831	0.866	1.795
MAI (2000-04)	0.803	1.675	0.823	1.635
HAL (2000-04)	0.836	1.762	0.844	1.666
BRA (2000-04)	0.861	1.467	0.827	1.701
BAV (2000-04)	0.758	1.749	0.744	1.685
average (areas – 2000-04)	**0.831**	**1.697**	**0.821**	**1.696**
STD (areas – 2000-04)	**0.053**	**0.140**	**0.046**	**0.060**
BAV (1984-89)	0.758	1.738	0.762	1.733
BAV (1990-94)	0.722	1.757	0.748	1.724
BAV (1995-99)	0.744	1.741	0.767	1.724
BAV (2005-09)	0.741	1.795	0.779	1.713
BAV (2010-14)	0.794	1.763	0.756	1.702
BAV (2015-19)	0.818	1.741	0.815	1.709
average (BAV – time)	**0.762**	**1.755**	**0.767**	**1.713**
STD (BAV – time)	**0.033**	**0.020**	**0.024**	**0.016**

Additionally, the reliability of the automated random selection of the stable LC pixels was investigated. The influence of the spatial distribution of the 5,000 randomly selected pixels was found to be minor though a comparison of ten sets of derived thresholds based on different sets of random stable pixels across the five test areas (Fig. 3.1.8a and b). The ten sets of thresholds of each test area show few differences, which are evidenced by low standard deviations (0.002 to 0.005).

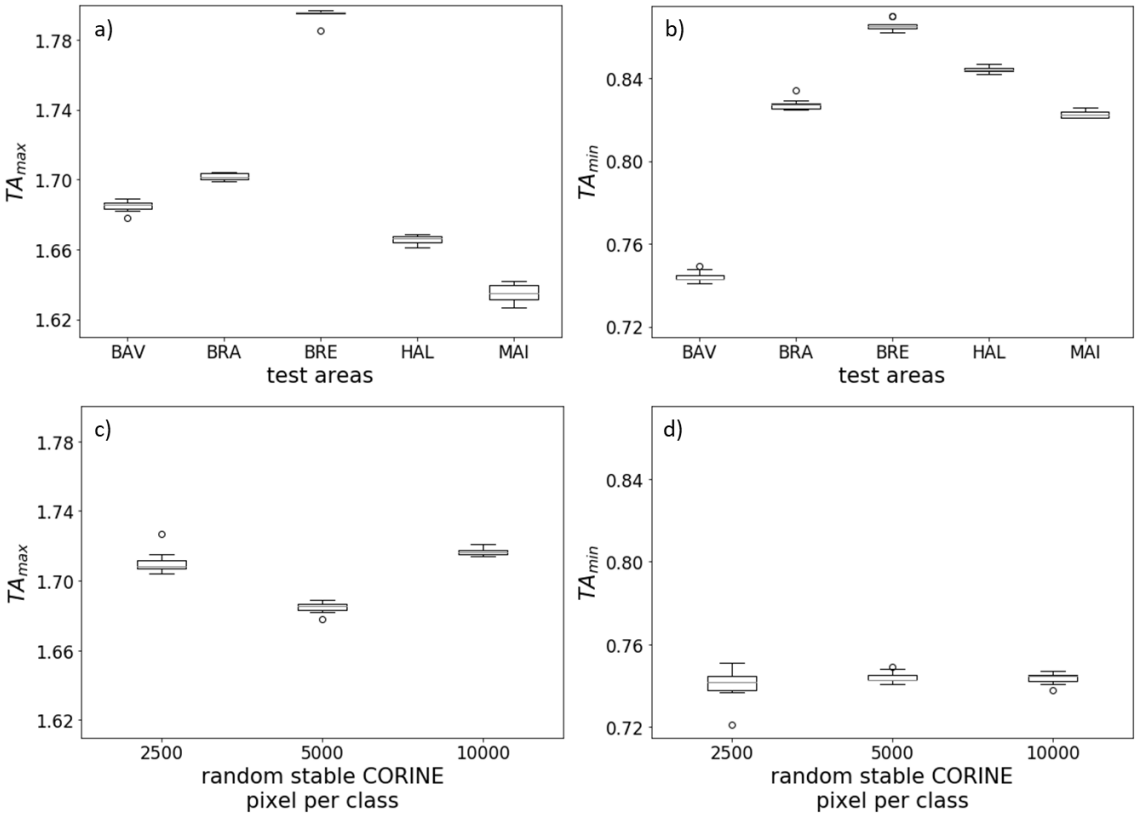

Figure 3.1.8: $TA_{min/max}$ variability across ten sets of randomly selected stable pixels for all test areas (2000-04) (a, b) and based on a different number of randomly selected stable pixels per LC class, extracted for the Bavarian tile (2000-04) (c, d).

In addition to the spatial distribution of the random stable pixels, the influence of the total number of selected pixels on the determination of the thresholds was analyzed. Hence, ten sets of determined thresholds based on 5,000 randomly selected stable pixels per LC class were investigated and further compared to ten sets of 2,500 and 10,000 randomly selected stable pixels in the test area of Bavaria (Fig. 3.1.8c and d). Overall, low standard deviations are observed (0.02 to 0.003), and the determined TA_{max} varies slightly (Fig. 3.1.8c).

Due to the temporal and spatial stability of the defined thresholds and the statistically significant small influence of the location and number of random stable pixels, the presented derivation of the thresholds was found to be suitable for further processing steps.

4.2 Application of new thresholds

The five sets of thresholds derived for the five test areas are averaged to one set of global thresholds, resulting in a TA_{min} of 0.831 and a TA_{max} of 1.697. Both thresholds were applied to all tiles in Germany to produce the exposed soil masks for all seven time periods.

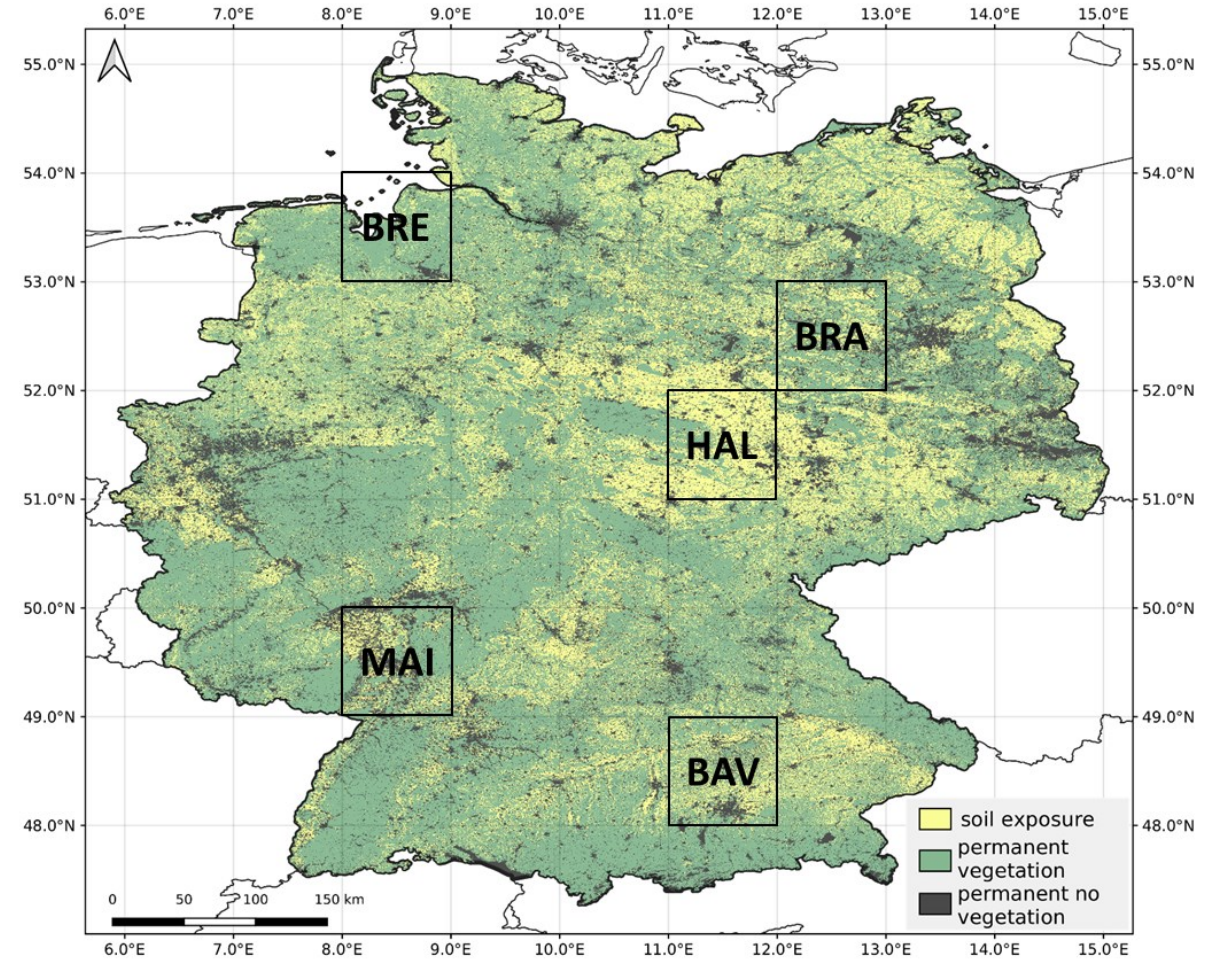

Figure 3.1.9: Generic LC classification for the study area showing pixels with soil exposure (yellow), permanent vegetation (green) and permanent no vegetation (gray) derived from 2000-04. The five test areas are marked. (For interpretation of the references to color in this figure legend, the reader is referred to the web version of this article.)

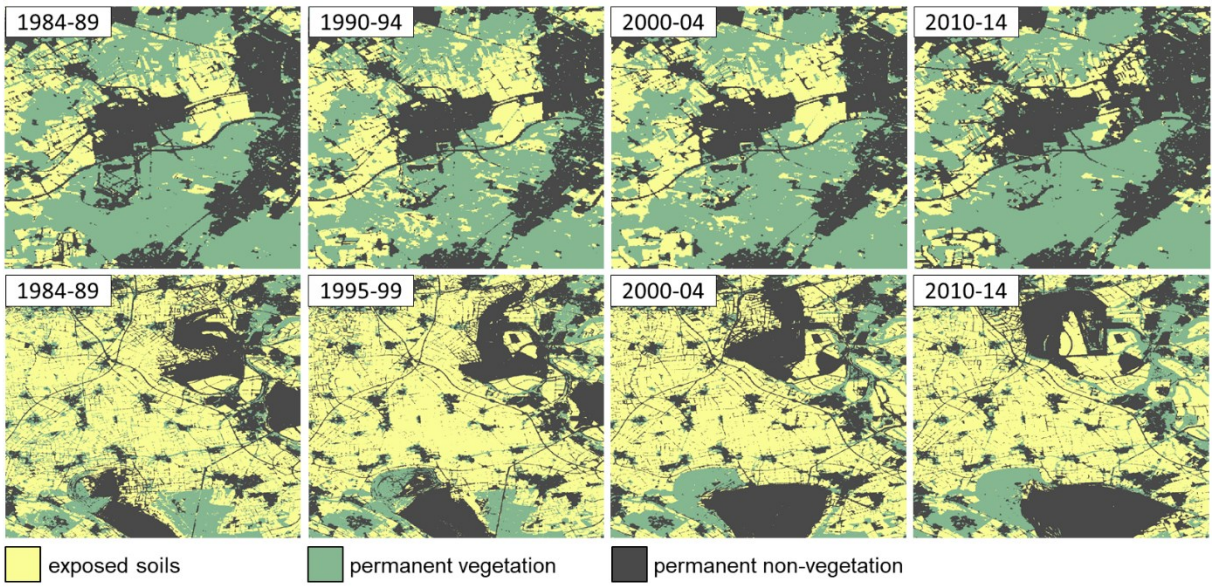

Figure 3.1.10: Detail of the generic land use classification showing the temporal development between 1984 and 2014 of a mainly urbanized area in the west of the city of Munich within BAV (upper row) and the temporal development of two mining areas (Etzweiler and Garzweiler) near Juelich (bottom row).

These soil exposure masks contain pixels that show at least once exposed soil in the given time period. In addition, SCMaP provides two further binary masks per period containing the areas showing permanently low PV indices, which comprise urban areas, infrastructure, bare rocks and water bodies. In addition, a mask is generated in areas that show permanently high PV indices representing areas with permanent vegetation (e.g., grassland or coniferous trees). The combination of the three masks generates a generic LC classification of the investigation area (Fig. 3.1.9).

Since the soil mask is available for several time steps between 1984 and 2019, changes in the spatial soil cover can be detected. Fig. 3.1.10 (upper row) shows the temporal development of an area in western Munich (within the test region BAV). Here, areas with permanently low vegetation indices, which include the expansion of the city of Munich and the expansion of infrastructure, are increasing. Due to the expansion of Munich, a decrease in the area with exposed soils in the shown region is observed. Most agricultural areas have been transformed into settlement areas. The southern part is dominated by forests, where, in the early 1990s, a thunderstorm event deforested large portions, mainly in the southwest of Munich. The deforestation shows recovery in the subsequent time periods up until 2014. Here, the exposed soil areas gradually fill with permanent vegetation.

The bottom row of Fig. 3.1.10 shows the development of two mining (Etzweiler and Garzweiler) near the city of Juelich in northeastern Germany. A spatial shift in the mining areas to different local regions can be seen. In addition to the spatial shift, a spatial expansion of the mining sites had resulted in a decreasing agricultural area around the sites was found to be suitable for further processing steps.

Table 3.1.3: Correlation coefficients comparing the exposed soil masks determined by SCMaP to the agricultural areas provided by the statistical surveys by Destatis for all 16 Federal States of Germany. However, some states were not included in the statistical survey due to missing data.

Federal state	agricultural area [%]	1995-99/ 1999	2000-04/ 2001/03	2005-09/ 2005/07	2010-14/ 2010	2015-19/ 2019
Baden-Wuerttemberg	22.69	0.85	0.97	0.95	0.94	0.96
Bavaria	30.70	0.93	0.94	0.92	0.88	0.93
Berlin	8.58	-	-	-	-	-
Brandenburg	39.02	0.88	0.95	0.92	0.85	0.95
Bremen	8.62	-	-	-	-	-
Hamburg	6.61	-	-	-	-	-
Hesse	22.78	0.82	0.92	0.92	0.87	0.95
Mecklenburg-Western Pomerania	62.43	-	-	-	-	0.94
Lower Saxony	37.95	0.68	0.78	0.66	0.70	0.59
North Rhine-Westphalia	27.39	0.90	0.95	0.94	0.93	0.92
Rhineland-Palatinate	27.27	0.93	0.94	0.93	0.90	0.91
Saarland	14.30	0.80	0.91	0.86	0.82	0.94
Saxony	49.23	0.81	-	-	-	-
Saxony-Anhalt	60.26	0.84	0.88	0.92	0.91	0.91
Schleswig-Holstein	36.39	0.82	0.86	0.90	0.90	0.94
Thuringia	48.75	0.93	0.93	0.93	0.91	0.94

4.3 Validation of the exposed soil masks determined by SCMaP

The spatial and temporal distribution of exposed soil masks across Germany at several time steps is first validated according to Destatis statistics. The correlation coefficients (R2) of the comparison for all 16 German federal states are shown in Table 3.1.3. Overall, high R2 for all time steps and states can be derived. The lowest R2 values are detected in the Lower Saxony state (0.59 to 0.78). Here, the agricultural area covers 37.95% of the total state. The highest R2 values are reported in the states of Baden-Wuerttemberg (0.85 to 0.97), North Rhine-Westphalia (0.90 to 0.95) and Rhineland-Palatinate (0.90 to 0.94). For the states with a high amount of used agricultural area (Brandenburg, Saxony, Schleswig Holstein and Thuringia), the correlation coefficients are higher than 0.82 (Schleswig Holstein – SCMaP: 1995–99/Destatis: 1999) per time step. As described above, the Destatis survey does not include all federal states as it does for the city states; no data are available for Mecklenburg Western Pomerania and parts of Saxony.

Table 3.1.4: R^2 based on a comparison between the exposed soil masks derived by SCMaP and agricultural areas of the CLC data in comparison to the total amount of agricultural areas per stats.

Federal state	agricultural area [%]	1990-94/ 1990	2000-04/ 2000	2005-09/ 2006	2010-14/ 2012	2015-19/ 2018
Baden-Wuerttemberg	22.69	0.91	0.92	0.91	0.94	0.97
Bavaria	30.70	0.85	0.90	0.86	0.90	0.84
Berlin	8.58	-	-	-	-	-
Brandenburg	39.02	0.80	0.92	0.94	0.91	0.97
Bremen	8.62	-	-	-	-	-
Hamburg	6.61	-	-	-	-	-
Hesse	22.78	0.82	0.95	0.93	0.92	0.97
Mecklenburg-Western Pomerania	62.43	0.91	0.96	0.94	0.92	0.99
Lower Saxony	37.95	0.68	0.86	0.79	0.75	0.61
North Rhine-Westphalia	27.39	0.84	0.92	0.91	0.91	0.90
Rhineland-Palatinate	27.27	0.90	0.95	0.92	0.94	0.93
Saarland	14.30	0.85	0.88	0.90	0.95	0.99
Saxony	49.23	0.90	0.95	0.96	0.93	0.84
Saxony-Anhalt	60.26	0.86	0.95	0.96	0.97	0.95
Schleswig-Holstein	36.39	0.90	0.65	0.94	0.92	0.80
Thuringia	48.75	0.91	0.96	0.96	0.96	0.94

Additionally, the comparison between the exposed soil masks determined by SCMaP and the agricultural areas provided by CLC data sets show high R2 values for each time step (Table 3.1.4). Comparing all federal states, the lowest correlation coefficients are reported for the state of Lower Saxony (0.61 to 0.86), as described for the validation with the Destatis data, whereas the highest correlation coefficients can be found for Baden-Wuerttemberg (0.91 to 0.97), Mecklenburg-Western Pomerania (0.91 to 0.97) and Rhineland-Palatinate (0.90 to 0.95). In contrast to the correlation of the exposed soil masks provided by SCMaP and the Destatis data, the state North Rhine Westphalia shows lower R2 (0.84 to 0.92) comparing SCMaP and CLC. Overall, the states show similar R2 when comparing to the correlation of the SCMaP and Destatis data. For the states with a large amount of agricultural area (i.e., the states of Brandenburg, Mecklenburg-Western Pomerania, Saxony, Schleswig Holstein and Thuringia), the correlation coefficients are higher than 0.80 (Schleswig Holstein – SCMaP: 1995–99/Destatis: 1990) for all compared time steps. The high R2 indicate high potential for the determination of exposed soil masks over time in agricultural areas.

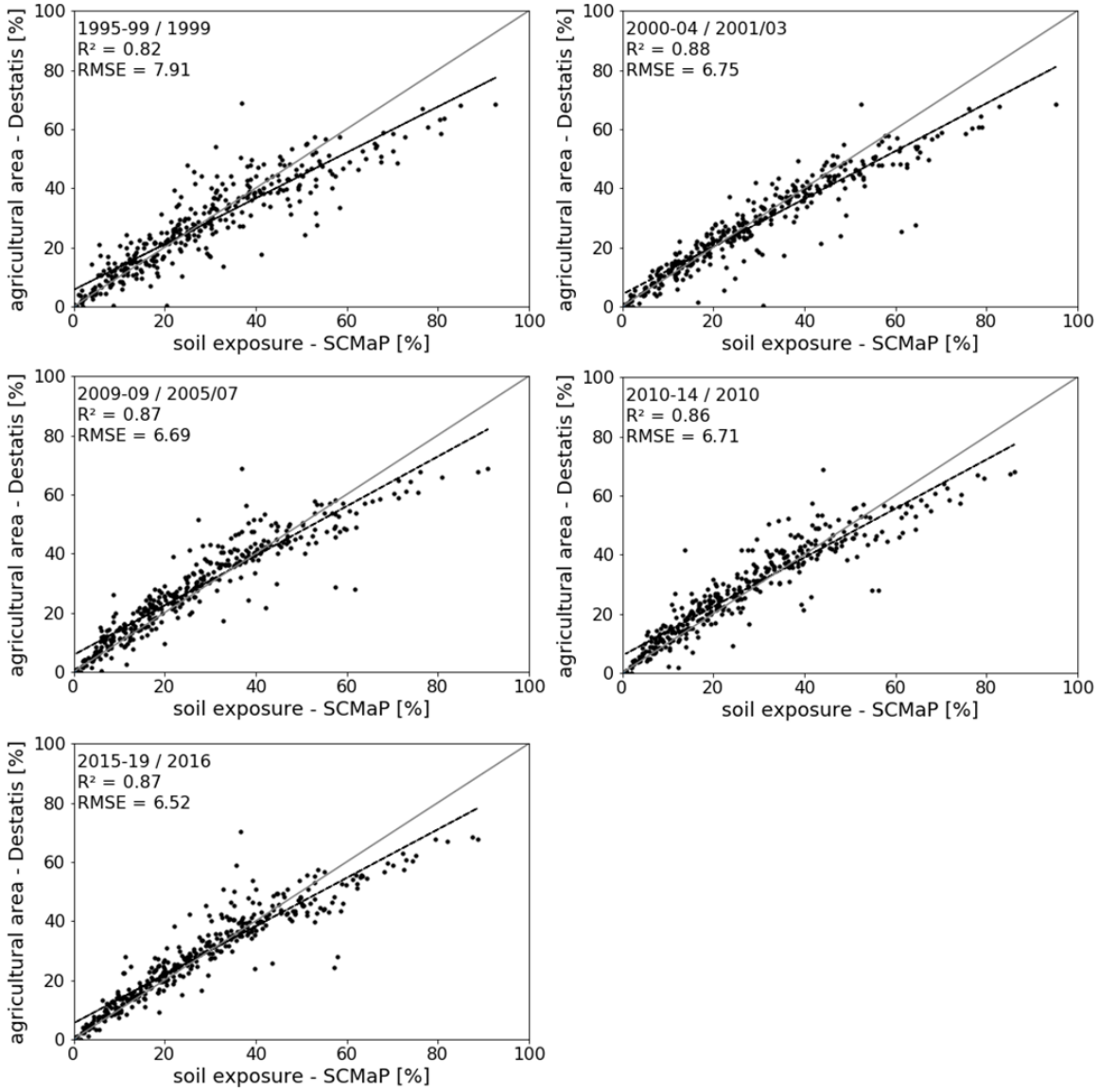

Figure 3.1.11: Regression between exposed soil masks identified by SCMaP and the agricultural areas based on Destatis at the county level for Germany.

In addition to the correlation per federal state, a comparison at the county level was conducted. High R2 values and low RMSE values (Fig. 3.1.11) demonstrate that SCMaP captures the exposed soil masks in Germany well. For all time periods, high correlations between the percentage proportion of SCMaP exposed soil masks and the agricultural areas provided by statistical surveys of Destatis are identified. The highest correlation can be found for the SCMaP time period 2000–04 (R^2 = 0.88) compared to the respective averaged Destatis data sets of 2001/03, whereas the SCMaP time period 1995–99 shows the lowest correlation (R^2 = 0.82) compared to the corresponding Destatis data set from 1999. Although the general correlation is high, there is a minor systematic underestimation of the higher soil exposure values in all analyzed time periods (Fig. 3.1.11).

Moreover, a linear correlation analysis comparing the percentage of exposed soil masks per county derived by SCMaP to the percentage of agricultural areas provided by the CLC data sets was performed. The results show a strong correlation between the tested data sets (Fig. 3.1.12). The highest correlation is reported for the SCMaP periods of 2000–04 and 2005–09 to the CLC data sets of 2000 (R^2 = 0.89) and 2006 (R^2 = 0.88), respectively. The weakest correlation can be

found for the SCMaP time period of 1990–94 when compared with the CLC data set from 1990 (R^2 = 0.80). Overall, low RMSE values are observed.

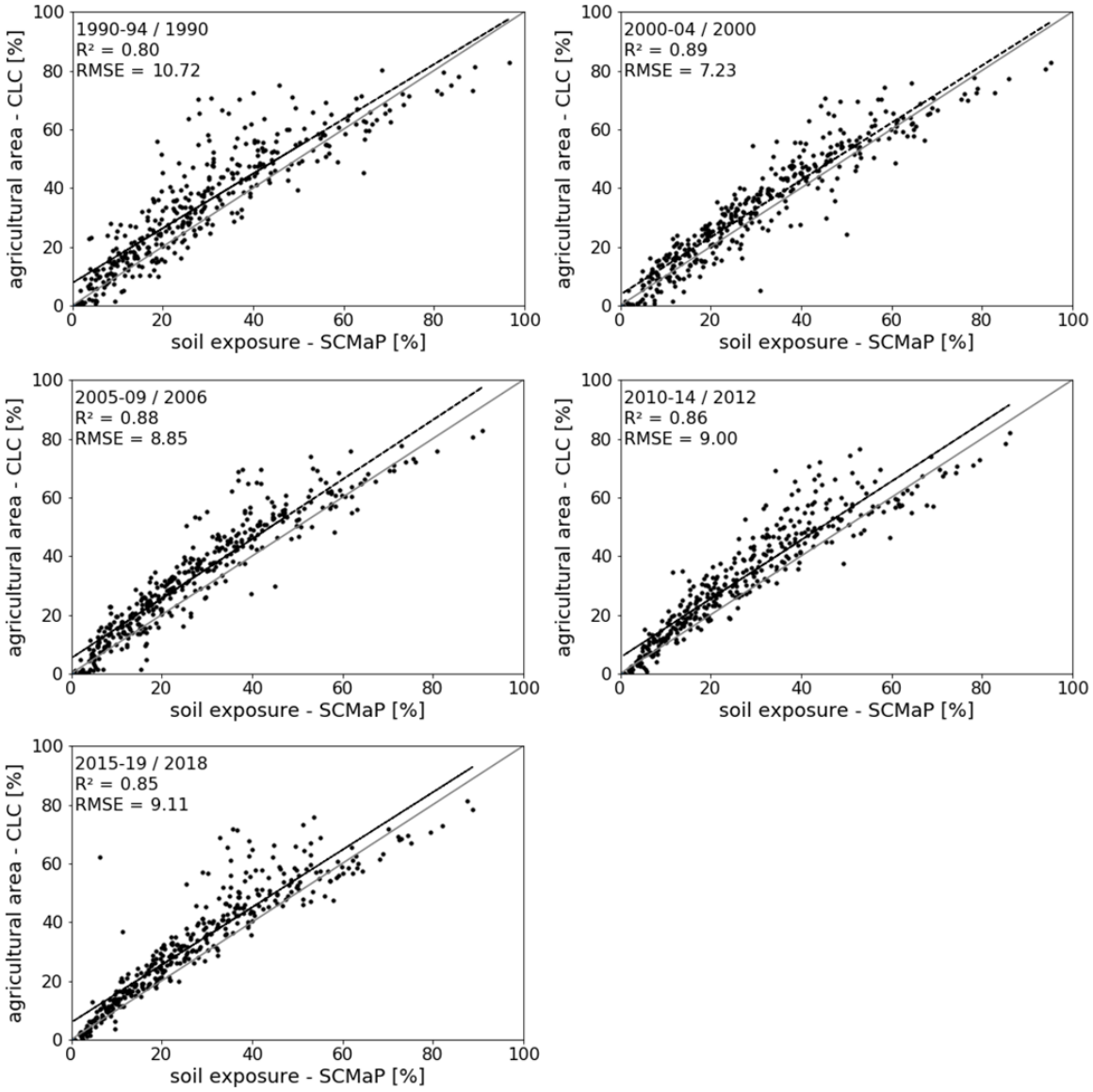

Figure 3.1.12: Regression between exposed soil masks extracted by SCMaP and the agricultural used areas based on CLC data for all counties in Germany.

Fig. 3.1.13 shows the variability between the differences in the percentages of exposed soil masks extracted by SCMaP and the portion of agricultural areas provided by the validation data sets for all counties and compared time steps. Comparing the exposed soil masks extracted by SCMaP to the agricultural areas based on the Destatis surveys, a deviation to the mean, ranging on average between - 1.46% (SCMaP: 2005–09/Destatis: 2007) and +1.43% (SCMaP: 2000–04/Destatis: 2001/03), is detected. However, the range of 50% of the counties varies between ± 5.04% (SCMaP: 2005–09/Destatis: 2007) and ± 7.38% (SCMaP: 1995–99/Destatis: 1999). Excluding the outliers, there is a small absolute difference between the percentage of agricultural areas documented by the Destatis surveys and the exposed soil masks derived by SCMaP. The differences between the percentages of exposed soil masks extracted by SCMaP and the CLC-derived agricultural areas show a slightly stronger underestimation, ranging between - 5.61% (SCMaP: 2005/CLC: 2006) and - 2.90% (SCMaP: 2000–04/CLC: 2000). Excluding the outliers, the

range of 50% of the counties varies between ± 5.63% (SCMaP: 2005–09/CLC: 2006) and ± 3.42% (2000–04/CLC: 2000).

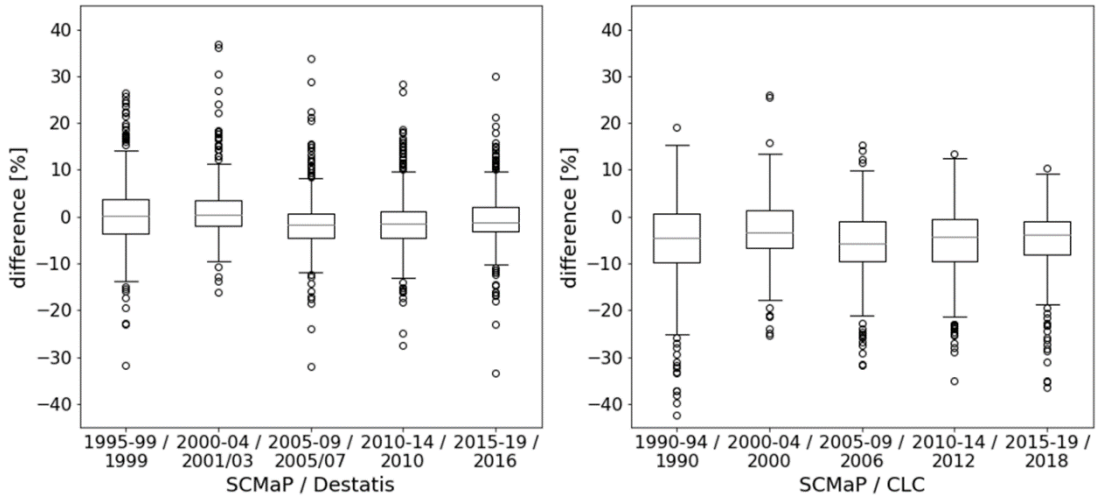

Figure 3.1.13: Variability of the difference in exposed soil masks extracted by SCMaP compared to the validation data sets of Destatis and CLC based on all counties in Germany for all time periods.

Overall, the comparison between both validation data sets indicates a high consistency across all time periods. In particular, the time periods of 2000–04 and 2005–09 show the highest correlation coefficients and lowest RMS errors for both validation data sets compared at the state (Tables 3.1.3 and 3.1.4) and county level (Figs. 3.1.11 and 3.1.12).

5. Discussion

5.1 Sampling and threshold definition

Section 4.1 shows the results of the different settings used to derive the $TA_{min/max}$ thresholds. The random selection of stable CLC pixels demonstrates an overall minor influence on the frequency distribution of LC classes, such as deciduous trees and fields, comparing the $PV_{min/max}$ behaviors in relation to the manually selected LC pixels. The main differences were found for the class urban (Figs. 3.1.4 and 3.1.5). The manual selection of the land cover class urban was concentrated in the downtown areas of metropolitan regions (e.g., central Munich in the Bavarian test tile), the random selection of stable CLC pixels resulted in an even distribution across the complete tile. This better captures the variability associated with urban structures (e.g., densely to less densely populated areas, industry, infrastructure, etc.) and can also include vegetated pixels from parks or trees and lawns along streets. The less clustered selection influences the frequency distribution of the PV indices for the land cover class urban and thus, more pixels have higher PV_{max} values (Fig. 3.1.4).

To account for the differences in the distribution of the LC classes in the PV_{max} composite, an adaptation of the percentile used for the determination of the TA_{max} was necessary. Figs. 3.1.6 and 3.1.7 show the influence of the modified percentile rule depending on the spatial–temporal behavior of the analyzed LC. However, we observed a gradual decrease (TA_{max} = 0.89 – 0.98) followed by a rapid decrease (TA_{max} > 0.99) of the resulting soil exposure. A decrease of the percentile (0.995 to 0.900) for the definition of the TA_{max} enabled the generation of an exposed soil mask (Fig. 3.1.6) comparable to the coverage of agricultural area provided by the reference data set and comparable to the soil exposure mask based on the manual derived TM_{max} for an example area in the Halle test tile.

The adapted percentiles were the basis for further analyses. In this way, thresholds have been derived separately for the five different regions across Germany (Fig. 3.1.8). In particular, the TA_{max} of Bremen is higher than the four other TA_{max} values (Fig. 3.1.8a). Although the $TA_{min/max}$ values of the individual test sites are comparable to the averaged $TM_{min/max}$ of all five areas, the derivation of exposed soil masks could be affected, especially for the region near Bremen. A varying $TA_{min/max}$ value may impact the classification of exposed soil masks, so it might be more feasible to process all of Germany not only using one set of $TA_{min/max}$. A scheme summarizing comparable areas should be established. This could include replacing political borders with larger geographically homogenous units. For this purpose, the bio-geographical regions (Section 2 and Fig. 3.1.1) (EEA, 2016) could provide a valuable baseline for the definition of the thresholds. Germany is covered mainly by the continental bio-geographical region (the test areas Bavaria, Mainz, Brandenburg and Halle), whereas the areas near Bremen, as the northwestern part of Germany, are covered by the atlantic bio-geographical region. Applying SCMaP with $TA_{min/max}$ adapted to the different regions could reduce the local effects on the thresholds and improve the extraction of exposed soil masks.

Finally, we tested the influence of the number of pixels per class selected for the threshold determination and found almost no influence. This suggests that regardless of the number of selected pixels, the thresholds are very stable when they are equally distributed over the area of interest.

In summary, the new automated sampling is a very flexible and robust method to provide the data base for the threshold derivation, whereas the threshold definition based on percentile seemed not as the best method although its simplicity (Lobell et al., 2007; Zhao et al., 2012; Avisse et al., 2017; Thonfeld et al., 2020; Zhuo et al., 2019). In this study, an adaption of the percentile rule was necessary for the changed sample data set and it is very likely that the percentile rule need to be changed again if a different area is explored. Therefore, in the future, alternative methods to extract exposed soil pixels should be tested for instance regression and classification methods such as logistic regression (Kleinbaum et al., 2002), Random Forests (Breiman, 2001) or maximum likelihood classification (Richards, 1993) or any other machine learning approaches. For this study, it was important to use the same methodology as for the manual sampling to obtain the highest possible comparability to the method of Rogge et al. (2018).

Table 3.1.5: Average cloudless scenes per pixel for Germany and R^2 at the county level per time period.

time period	average cloudless scenes per pixel (Germany)	STD (Germany)	maximum cloudless scenes per pixel (Germany)	R^2 (SCMaP – Destatis)	R^2 (SCMaP – CLC)
1984-89	35.0	12.1	112	-	-
1990-94	44.3	15.0	112	-	0.80
1995-99	41.7	14.2	134	0.82	-
2000-04	56.0	18.6	102	0.88	0.89
2005-09	59.0	17.6	140	0.87	0.88
2010-14	41.6	12.3	104	0.86	0.86
2015-19	49.7	19.4	146	0.87	0.85

5.2 Validation of exposed soil masks across Germany

We have chosen TA_{min} of 0.831 and TA_{max} of 1.697 as the best results and used them for the generation of exposed soil masks for several time periods. We validated the extraction of exposed soil masks per selected time periods at the federal state and county level by using the Destatis and CLC data sets (see Section 4.3). The comparison of the soil exposure with both validation datasets

showed overall high correlation results (R2 > 0.80 on county level for) for all time periods (Tables 3.1.3 and 3.1.4, Figs. 3.1.11 and 3.1.12).

In particular the five-year periods of 2000–04 (R^2 = 0.88 for Destatis; R^2 = 0.89 for CLC) and 2005–09 (R^2 = 0.87 for Destatis; R^2 = 0.88 for CLC) show the overall highest R^2, and the periods of 1990–94 (R2 = 0.80 for CLC) and 1995–99 (R^2 = 0.82 for Destatis) show the weakest R^2 comparing the exposed soil masks to the agricultural areas of the validation datasets on county level. These results are similar at the state levels based on both validation datasets. The high R^2 in the periods of 2000–04 and 2005–09 might correlate to the high availability of input data. In 2000–04 and 2005–09; even though the scan line correction failure of Landsat-7 ETM+ appeared in 2002 (Markham et al., 2004), over 3,000 pre-processed input images were available (2000–04: 1946 Landsat-5 TM, 1154 Landsat-7 ETM+; 2005–04: 1946 Landsat-5 TM, 1154 Landsat-7 ETM+). In comparison to the 1990–94 and 1995–99 periods with lower R^2 values, less than 3,000 images per composite were available (1990–94: 1857, 1995–99: 2681 pre-processed scenes). This availability of scenes resulted in a large number of cloudless scenes per pixel (Table 3.1.5). On average, 56.0 ± 18.6 (2000–04) and 59.0 ± 17.6 (2005–09) cloudless scenes per pixel were included in the database for the extraction of exposed soil masks for Germany. In contrast, there were 44.3 ± 15.0 and 41.7 ± 14.2 cloudless scenes that built the database for the time periods of 1990–94 and 1995–99, respectively. For the time periods showing weaker R2 values, fewer cloudless input scenes are available per pixel, which could indicate a higher deviation from the validation data. Here, too few data are available to capture the exposed soil masks with high accuracy compared to the following periods.

The correlation analysis showed an overall high R2 for Germany on the state and county levels (Tables 3.1.3 and 3.1.4, Figs. 3.1.11 and 3.1.12). The federal state of Lower Saxony shows a lower R2 for all time periods for both scenarios compared. An in-depth review of the input data has shown no data artifacts or comparable data quality limitations for the federal state or the entire region in northwestern Germany. A possible source of the low accuracy of the soil mask in Lower Saxony could be the lower number of cloudless scenes per pixel in comparison to all of Germany. The number of maximum cloudless scenes per pixel for the Lower Saxony state is lower than the cloudless scenes available for all of Germany (Section 5.1). In Germany, a maximum number of 102 (2000–04) to 140 (2005–09) are available for the extraction of exposed soil masks. For the state of Lower Saxony, a maximum number of 70 (1984–89) to 110 (1995–99) cloudless scenes are available. This difference could have been driving the deviation in accuracy, as a certain number of scenes should be available for the extraction of exposed soils.

Furthermore, as described in Section 4.2, all of Germany was processed using the averaged $TA_{min/max}$ of the five test tiles. However, as discussed above, the $TA_{min/max}$ value of Bremen, situated in the center of Lower Saxony, varies more relative to the other four sets of TAs. Considering that the different thresholds have an influence on the extraction of the soil pixels, the use of the bio-geographical region as the definition of thresholds in Germany could result in better adjustment to the natural conditions present in the northwestern parts of the country.

However, it should be mentioned that a possible source of inaccuracy could have resulted from the comparison of a multiyear composite with a validation data set collected in one year. In all five-year composites, areas that show at least one exposed soil in the observed time period are included in the exposed soil mask. The selection of the longer time period was performed based on previous experience as it guaranteed the capture of all agricultural exposed soils. As the five-year periods are compared to one reference data set, changes in land use could have had an influence on the accuracy analysis. For instance, if a transition of permanent grassland to exposed soils occurred early within an observed period, the possibility of obtaining a sufficient number of available scenes showing exposed soils is high. SCMaP would then classify these areas correctly

as exposed soils. For validation purposes, a comparison to a data set recorded early in the five-year period would then result in an erroneous identification of the area by SCMaP. As the five-year composites contain two LC types; grassland and exposed soils; however, the classification by SCMaP for exposed soils is correct. A reduction in the time for compositing could enable a decrease in the occurrence of such cases.

For validation purpose of the SCMaP exposed soil masks two different data sets were chosen. The Federal Statistical Office (Destatis) collects statistical data regarding agricultural areas in Germany on a regular basis since 1999. However, determining the methods used for the data collection is in the responsibility of each federal state and might result in regional differences. Additionally, the lowest available spatial resolution is on county level. For that purpose and for future continental processing, we additionally used the agricultural classes of the CLC surveys for the validation of exposed soil masks as the data sets are available since 1990. Although the CLC inventories are derived from a pixel-based classification, the data also shows a lower spatial resolution than the SCMaP exposed soil masks. This demonstrates that both data sets have their advantages and disadvantages for the validation of the exposed soil masks, since both comparisons showed systematic differences with respect to lower correlations of the earlier periods and regarding to lower R2 for the federal state Lower Saxony. However, since both validation results are similar and in the same order of magnitude, we believe that they represent realistic accuracy values. Both datasets seem to be suitable for large scale accuracy analyses, whereas CLC has the potential for a European-wide validation of the detection of exposed soils.

6. Conclusion and Outlook

In this study, we analyzed the influence of the new automated sampling strategy on thresholding and the derivation of exposed soil masks. Further, we provided a Germany-wide validation for several time periods in order to show the accuracy of the resulting exposed soil masks across time. An automatized random sampling of stable CLC pixels required for the determination of two thresholds ($TA_{min/max}$) to separate exposed soils from all other LC classes was developed and implemented in the SCMaP processing chain. The automatization of the thresholding process is necessary for operational processors to ensure the fast and correct adaption of the thresholds to regions of interest and to provide regionalize thresholds for the processing of large areas, such as countries and continents. Our results demonstrated the large dependencies that the vegetation index approach has on environmental conditions. Thus, we suggest regionalizing the parameter setting by using e.g., bio-geographical regions instead of counties or countries. Furthermore, the rules to derive thresholds need to be evaluated depending on the sample database. In this study, we used CLC information; however, we would not suggest applying a fixed percentile rule since it needs to be adapted according to the sampling scheme. A more robust method that accounts for the minimal overlap of spectral similar LC classes would be more suitable. Additionally, the nature of fixed thresholds for large regions are not suggested. A flexible method to derive region-specific thresholds or the use of dynamic thresholds using machine learning techniques or artificial intelligence approaches could be a valuable topic for future developments. The implementation of such approaches in operational processors is important for future studies. For this purpose, the automated and robust sampling such as developed in this study is of high importance.

The validation using two independent reference data sets again shows the need to account for the regional differentiation of the thresholds. For both data sets (CLC and Destatis) we selected agricultural classes that can be assigned to exposed soils. Areas in northwestern Germany have shown a systematic underestimation of exposed soils compared to both reference data. Additionally, there is a difference in R2 based on the number of available input scenes per time

step. We could show that the more scenes per time period are available, the higher the percentage of cloudless scenes and thus, the higher the R2. The implementation of Sentinel-2 data could potentially shorten the recent composite time length of five years. This is also in line with the findings of Demattè et al. (2018). Sentinel-2 delivers data from two twin satellites with a combined revisit time of less than five days (Lacroix et al., 2018; Ienco et al., 2019). The use of Sentinel-2 data could therefore result in an increased accuracy in the building of exposed soil masks and the shortening of the compositing time period. Additionally, the current developed "Harmonized Landsat and Sentinel-2 surface reflectance data set" (Claverie et al., 2018) should be considered. Since both data sets have been pre-processed following the same protocols and methods, thisdata set could be a highly valuable input regarding the large number of available scenes and needs to be analyzed in the future. This could enable monitoring of soil more frequently than every five years.

In summary, the automated and random sampling of LC pixels for the determination of thresholds is a stable and reliable workflow that enables the identification of the spatial and temporal distribution of exposed soils with high accuracy. Thus, it can be a valuable data source for statistical surveys of agricultural areas in Germany. SCMaP is additionally used to generate information about how frequently soils are exposed and how often these areas shift from exposure to vegetation. To contribute to soil erosion studies that need information about where and when soils are bare, accurate exposed soil masks in suitable time period can be of great help for these studies (Pimentel and Burgess, 2013; Labriere et al., 2015; Ayalew et al., 2020). The exposed soil masks derived from SCMaP can additionally offer a new remote sensing database for retrospective erosion and LC analysis.

Funding: This research was funded by the German Federal Ministry of Food and Agriculture (BMEL), grant number 281B301816 as part of the SoilDE Project "Entwicklung von Indikatoren zur Bewertung der Ertragsfahigkeit, Nutzungsintensitat und Vulnerabilitat landwirtschaftlich genutzter Boden ¨ in Deutschland"

Declaration of Competing Interest: The authors declare that they have no known competing financial interests or personal relationships that could have appeared to influence the work reported in this paper.

References

Adams, B., Iverson, L., Matthews, S., Peters, M., Prasadm, A., Hix, D.M., 2020. Mapping Forest Composition with Landsat Time Series: An Evaluation of Seasonal Composites and Harmonic Regression. Remote Sens. 12, 610. https://doi.org/10.3390/ rs12040610.

Adhikari, K., Hartemink, A.E., 2016. Linking soils to ecosystem services – A global review. Geoderma 262 (2016), 101–111. https://doi.org/10.1016/j. geoderma.2015.08.009.

Asner, G.P., Heidebrecht, K.B., 2002. Spectral unmixing of vegetation, soil and dry carbon cover in arid regions: Comparing multispectral and hyperspectral observations. Int. J. Remote Sens. 23 (19), 3939–3958. https://doi.org/10.1080/ 01431160110115960.

Avisse, N., Tilmant, A., Müller, M.F., Zhang, H., 2017. Monitoring small reservoirs' storage with satellite remote sensing in inaccessible areas. Hydrol. Earth Syst. Sci. 21, 644–6459. https://doi.org/10.5194/hess-21-6445-2017.

Ayalew, D.A., Deumilch, D., Sarapatka, B., Doktor, D., 2020. Quantifying the Sensitivity of NDVI Based C Factor Estimation and Potential Soil Erosion Prediction using Spaceborne EarthObservation Data. Remote Sens. 12, 113. https://doi.org/10.3390/rs12071136.

Baude, M., Meyer, B.C., Schindewolf, M., 2019. Land use change in an agricultural landscape causing degradation of soil-based ecosystem services. Sci. Total Environ. 659, 1526–1536. https://doi.org/10.1016/j.scitotenv.2018.12.455.

Borelli, P., Panagos, P., Montanarella, L., 2015. New insights into the Geography and Modelling wind Erosion in the European Agricultural Land. Application of a Spatially Explicit Indicator of Land Susceptibility to Wind Erosion. Sustainability 7, 8823–8836. https://doi.org/10.3390/su7078823.

Borelli, P., Lugato, E., Montanarella, L., Panagos, P., 2017. A new assessment of soil loss due to wind erosion in European agricultural soils using a quantitative spatially distributed modelling approach. Land Degrad. Dev. 28, 335–344. https://doi.org/10.1002/ldr.2588.

Borelli, P., van Oost, K., Meusburger, K., Alewell, C., Lugato, E., Panagos, P., 2018. A step towards a historic assessment of soil degradation in Europe: Coupling on-site erosion with sediment transfer and carbon fluxes. Environ. Res. 161, 291–298. https://doi.org/10.1016/j.envres.2017.11.009.

Breiman, L., 2001. Random Forests. Mach. Learn. 45, 5–32.

Cerdan, O., Govers, G., Le Bissonnaus, X., van Oost, K., Poesen, J., Saby, N., Gobin, A., Vacca, A., Quinton, J., Auerswald, K., Klik, A., Kwaad, F.J.P.M., Raclot, D., Ionita, I., Rejman, J., Rousseva, S., Muxart, T., Roxo, M.J., Dostal, T., 2010. Rates and spatial variations of soil erosion in Europe: A study based on erosion plot area. Geomorphology 12, 167–177. https://doi.org/10.1016/j.geomorph.2010.06.011.

Chastain, R., Housman, I., Goldstein, J., Finco, M., Renneson, K., 2019. Empirical cross sensor comparison of Sentinel-2A and 2B MSI, Landsat-8 OLI and Landsat-7 ETM + top of atmosphere spectral characteristics over the conterminous United States. Remote Sens. Environ. 221, 274–285. https://doi.org/10.1016/j.rse.2018.11.012.

Claverie, M., Vermote, E.F., Franch, B., Masek, J.G., 2015. Evaluation of the Landsat-5 TM and Landsat-7 ETM + surface reflectance products. Remote Sens. Environ. 169, 390–403. https://doi.org/10.1016/j.rse.2015.08.030.

Claverie, M., Ju, J., Maesk, J.G., Dungan, J.L., Vermote, E.F., Roger, J.-C., Skakun, S.V., Justice, C., 2018. The Harmonized Landsat and Sentinel-2 surface reflectance data set. Remote Sens. Environ. 219, 145–161. https://doi.org/10.1016/j.rse.2018.09.002.

Daughtry, C.S.T., Doraiswamy, P.C., Hunt Jr., E.R., Stern, A.J., McMurtrey III, J.E., Prueger, J.H., 2006. Remote Sensing of Crop Residue Cover and Soil Tillage Intensity. Soil Tillage Res. 91 (1–2), 101–108. https://doi.org/10.1016/j.still.2005.11.013.

Dematt`e, J.A.M., Fongaro, C.T., Rizzo, R., Safanelli, J.L., 2018. Geospatial Soil Sensing System (GEOS3): A powerful data mining procedure to retrieve soil spectral reflectance from satellite images. Remote Sens. Environ. 212 (2018), 161–175. https://doi.org/10.1016/j.rse.2018.04.047.

Dematt`e, J.A., Safanelli, J.L., Poppiel, R.R., Rizzo, R., Quinonez Silvero, N.R., de Sousa Mendes, W., Bonfatti, B.R., Dotto, A.C., Urbina Salazar, D.F., de Oliveira Mello, F.A., de Silveira Paiva, A.F., Barros Souza, A., dos Santos, N.V., Nascimento, C.M., de Mello, D.C., Bellinaso, H., Gonzaga Neto, L., Accorsi Amorim, M.T., de Resende, M.E. B., de Souza Vieira, J., de Queiroz, L.G., Gallo, B.C., Sayao, V.M., de Silva Lisboa, C. J., 2020. Bare Earth's Surface Spectra as a Proxy for Soil Resource Monitoring. Sci. Rep. 10, 4461. https://doi.org/10.1038/s41598-020-61408-1.

Statistisches Bundesamt (Destatis), 2017. Land- und Forstwirtschaft, Fischerei. Methodische Grundlagen der Agrarstrukturerhebung 2016. Fachserie 3 Reihe 2. S.5. Published: 05/02/2017; Art.no.: 2032605169004. Statistisches Bundesamt (Destatis), 2018. Data licence Germany – 1111-01-01-4 Gebietsflache ¨ in qkm – Stichtag 31.12. – regionale Tiefe: Kreise und krfr. Stadte ¨ " – Version 2.0 (licence text available at www.govdata.de/dl-de/by-2-0). Online: https://www.regionalstatistik.de/genesis/online/data;sid=720713C799CA2789F6A9C8153B70911.reg1?operation=abruftabelleBearbeiten&levelindex=2&levelid=1583486661043&auswahloperation=abruftabelleAuspraegungAuswaehlen&auswahlverzeichnis=ordnungsstruktur&auswhlziel=werteabruf&selectionname=11111-01-01-4&auswahltext=&werteabruf=Werteabruf (accessed July 2018).

Statistisches Bundesamt (Destatis), 2020a. Data licence Germany – 41120-01-02-4 Blandwirtschaftliche Betriebe & landwirtschaftlich genutzte Fl¨ achen (LF) nach Kulturarten Erhebungsjahr – regionale Ebene" – Version 2.0 (licence text available at www.govdata.de/dl-de/by-2-0). Online: https://www.regionalstatistik.de/genesis/online/data;sid=DBAD6FFC87187C0E7C135DE45A1BA91.reg2?operation=abruftabelleAbrufen&selectionname=41120-01-02-4-B&levelindex=1&levelid=1580825413509&index=2 (accessed January 2020).

Statistisches Bundesamt (Destatis), 2020b. Data licence Germany – 41141-01-01-4-B landwirtschaftliche Betriebe & landwirtschaftlich genutzte Fl¨ ache (LF) nach Kulturarten – Jahr – regionale Ebene" – Version 2.0 (licence text available at www.govdata.de/dl-de/by-2-0). Online: https://www.regionalstatistik.de/genesis/online/data;sid=063CCEEC3A73F6F691D924763E80A785.reg2?operation=abruftabelleAbrufen&selectionname=41141-01-01-4B&levelindex=1&levelid=1580825429023&index=2 (accessed January 2020).

Diek, S., Fornallaz, F., Schaepman, M.E., de Jong, R., 2017. Barest Pixel Composite for Agricultural Areas Using Landsat Time Series. Remote Sens. 2017 (9), 1245. https://doi.org/10.3390/rs9121245.

EEA, 2007. CLC 2006 technical guidelines. In: EEA Technical Report, No. 17/2007, Copenhagen. URL: https://www.eea.europa.eu/publications/technical_report_2007_17 (last access: 20.04.2020).

EEA, 2016. Biogeographic Regions in Europe. European Environment Agency, https://www.eea.europa.eu/data-and-maps/figures/biogeographical-regions-in-europe-2 (last access: 20.04.2020).

EEA, 2020. Europe's biodiversity – biogeographical regions and seas. European Environmental Agency, Report No 1/2002. URL: https://www.eea.europa.eu/publications/report_2002_0524_154909 (last access: 20.04.2020).

Flood, N., 2014. Continuity of Reflectance Data between Landsat-7 ETM+ and Landsat-8 OLI, for Both Top-of-Atmosphere and Surface Reflectance: A Study in the Australian Landscape. Remote Sens. 6, 7952–7970. https://doi.org/10.3390/rs6097952.

Gobin, A., Jones, R., Kirkby, M., Campling, P., Govers, G., Kosmas, C., Gentile, A.R., 2004. Indicators for pan-European assessment and monitoring of soil erosion by water. Environ. Sci. Policy 7, 25–38. https://doi.org/10.1016/j.envsci.2003.09.004.

Griffiths, P., Nendel, C., Hostert, P., 2019. Intra-annual reflectance composites from Sentinel-2 and Landsat for national-scale crop and land cover mapping. Remote Sens. Environ. 220, 135–151. https://doi.org/10.1016/j.rse.2018.10.031.

Hansen, M.C., Egorov, A., Roy, D.P., Potapov, P., Ju, J., Turubanov, S., Kommareddy, I., Loveland, T.R., 2011. Continuous fields of land cover for the conterminous United States using Landsat data: first results from the Web-Enabled Landsat Data (WELD) project. Remote Sens. Lett. 2, 279–288. https://doi.org/10.1080/01431161.2010.519002.

Hermosilla, T., Wulder, M.A., White, J.C., Coops, N.C., Hobart, G.W., 2015. An integrated Landsat time series protocol for change detection and generation of annual gap-free surface reflectance composites. Remote Sens. Environ. 158, 220–234. https://doi.org/10.1016/j.rse.2014.11.005.

Holden, C.E., Woodcock, C.E., 2016. An analysis of Landsat 7 and Landsat 8 underflight data and the implications for time series investigations. Remote Sens. Environ. 185, 16–36. https://doi.org/10.1016/j.rse.2016.02.052.

Ienco, D., Interdonato, R., Gaetano, R., Minh, D.H.T., 2019. Combining Sentinel-1 and Sentinel-2 Satellite Image Time Series for land cover mapping via a multi-source deep learning architecture. ISPRS J. Photogramm. Remote Sens. 158, 11–22. https://doi.org/10.1016/j.isprsjprs.2019.09.016.

Kleinbaum, D., Dietz, D.G., Gail, M., Klein, M., Klein, M., 2002. Logistic regression. Springer-Verlag, New York.

Kovalskyy, V., Roy, D.P., 2013. The global availability of Landsat 5 TM and Landsat 7 ETM+ land surface observations and implifications for global 30 m Landsat data product generation. Remote Sens. Environ. 130, 280–293. https://doi.org/10.1016/j.rse.2012.12.003.

Labriere, N., Locatelli, B., Laumonier, Y., Freycon, V., Bernoux, M., 2015. Soil erosion in the humid tropics: A systematic quantitative review. Agric. Ecosyst. Environ. 203, 127–139. https://doi.org/10.1016/j.agee.2015.01.027.

Lacroix, P., Bievre, G., Pathier, E., Kniess, U., Jongmans, D., 2018. Use of Sentinel-2 images for the detection of precursory motions before landslide failures. Remote Sens. Environ. 215, 507–516. https://doi.org/10.1016/j.rse.2018.03.042.

Langford, R.L., 2015. Temporal merging of remote sensing data to enhance spectral regolith, lithological and alteration patterns for regional mineral exploration. Ore Geol. Rev. 68, 14–29. https://doi.org/10.1016/j.oregeorev.2015.01.005.

Lavelle, P., Rodriguez, N., Arguello, O., Bernal, J., Botero, C., Chaparro, P., Gomez, Y., Guiterrez, A., del Pilar Hurtado, M., Loaiza, S., Pullido, S.X., Rodriguez, E., Sanabria, C., Velasquez, E., Fonte, S.J., 2014. Soil ecosystem services and land use in the rapidly changing Orinoco River Basin of Colombia. Agric. Ecosyst. Environ. 185, 106–117. https://doi.org/10.1016/j.agee.2013.12.020.

Li, S., Wang, W., Ganguly, S., Nemani, R., 2018. Radiometric Characteristics of the Landsat Collection 1 Dataset. Adv. Remote Sens. 7, 203–217. https://doi.org/10.4236/ars.2018.73014.

Lobell, D.B., Ortiz-Monasterio, J.I., Gurrola, F.C., Valenzula, L., 2007. Identification of saline soils with multiyear remote sensing of crop yields. Soil Sci. Soc. Am. J. 7, 777–783. https://doi.org/10.2136/sssaj2006.0306.

Loiseau, T., Chen, S., Mulder, V.L., Roman Dobarco, M., Richer-de-Forges, A.C., Lehmann, S., Bourennane, H., Saby, N.P.A., Martin, M.P., Vaudour, E., Gomez, C., Lagacherie, P., Arrouays, D., 2019. Satellite data integration for soil caly content modelling at a national scale. Int. J. Appl. Earth Obs. Geoinf. 82, 101905 https://doi.org/10.1016/j.jag.2019.101905.

Malec, S., Rogge, D., Heiden, U., Sanchez-Azofeifa, A., Bachmann, M., Wegmann, M., 2015. Capability of spaceborne hyperspectral EnMAP mission for mapping fractional cover for soil modeling. Remote Sens. 7 (9), 11776–11800. https://doi.org/10.3390/rs70911776.

Markham, B.L., Storey, J.C., Williams, D.L., Irons, J.R., 2004. Landsat sensor performance: History and Current Status. IEEE Trans. Geosci. Remote Sens. 42 (12), 2691–2694. https://doi.org/10.1109/TGRS.2004.840720.

Okin, G.S., 2007. Relative spectral mixture analysis – A multitemporal index of total vegetation cover. Remote Sens. Environ. 106, 467–479. https://doi.org/10.1016/j.rse.2006.09.018.

Panagos, P., Borelli, P., Meusburger, K., Alewell, C., Lugato, E., Montanarella, L., 2015a. Estimating the soil erosion cover-management factor at the European scale. Land Use Policy 38–50. https://doi.org/10.1016/j.landusepol.2015.05.021.

Panagos, P., Meusburger, K., van Liedekerke, M., Alewell, C., Hiederer, R., Montanarella, L., 2014a. Assessing soil erosion in Europe based on data collected through a European network. Soil Sci. Plant Nutr. 60 (1), 15–29. https://doi.org/10.1080/00380768.2013.835701.

Panagos, P., Karydas, C., Borelli, P., Ballabio, C., Meusburger, K., 2014b. Advances in soil erosion modelling through remote sensing availability at European scale. In: Proc. SPIE 9229, Second International Conference on Remote Sensing and Geoinformation of the Environment (RSCy2014), p. 92290I. https://doi.org/10.1117/12.2066383.

Panagos, P., Borelli, P., Meusburger, K., 2015. A New European Slope Length and Steepness Factor (LS-Factor) for Mideling Soil Erosion by Water. Geoscience 5, 117–126. https://doi.org/10.3390/geosciences5020117.

Pimentel, D., Burgess, M., 2013. Soil Erosion Threatens Food Production. Agriculture 3, 443–463. https://doi.org/10.3390/agriculture3030443.

Richards, J.A., 1993. Remote Sensing Digital Image Analysis: An Introduction, second ed. Springer-Verlag, Berlin.

Richter, R., Schlapfer, ¨ D., Müller, A., 2006. An automatic atmospheric correction algorithm for visible/NIR imagery. Int. J. Remote Sens. 27 (10), 2077–2085. https://doi.org/10.1080/01431160500486690.

Richter, R., 2010. Atmospheric/topographical correction for airborne imagery. ATCOR4 User Guide. Wessling, Germany.

Richter, R., Schlapfer, ¨ D., 2014. Atmospheric/Topographic Correction for Satellite Imagery (ATCOR-2/3 User Guide, Version 8.3. 1, February 2014). ReSe Applications Schlapfer ¨ Langeggweg 3.

Rogge, D., Bauer, A., Zeidler, J., Müller, A., Esch, T., Heiden, U., 2018. Building an exposed soil composite processor (SCMaP) for mapping spatial and temporal characteristics of soils with Landsat imagery (1984–2017). Remote Sens. Environ. 205, 1–17. https://doi.org/10.1016/j.rse.2017.11.004.

Rouse, J.W., Haas, R.H., Schell, J.A., Deering, D.W., 1974. Monitoring Vegetation Systems in the Great Plains with ERTS Processing. In: Proceedings of the Third Earth Reserves Technology Satellite Symposium, Greenbelt: NASA SP-351, 1974, vol. 30103017.

Roy, D.P., Kovalskyy, V., Zhang, H.K., Vermote, E.F., Yan, L., Kumar, S.S., Egorov, E., 2016. Characterization of Landsat-7 to Landsat-8 reflective wavelength and normalized difference vegetation index continuity. Remote Sens. Environ. 185, 57–70. https://doi.org/10.1016/j.rse.2015.12.024.

Schmidt, S., Meusburger, K., de Figueiredo, T., Alewell, C., 2017. Modelling Hot Spots of Soil Loss by Wind Erosion (SoLo Wind) in Western Saxony, Germany. Land Degrad. Dev. 28, 1100–1112. https://doi.org/10.1002/ldr.2652.

Steinhoff-Knopp, B., Burkhard, B., 2018. Soil erosion by water in Northern Germany: long-term monitoring results from Lower Saxony. Catena 165 (2018), 299–309. https://doi.org/10.1016/j.catena.2018.02.017.

Teillet, P.M., Barker, J.L., Markham, B.L., Irish, R.R., Fedosejevs, G., Storey, J.C., 2001. Radiometric cross-calibration of the Landsat-7 ETM+ and Landsat-5 TM sensors based on tamdem data sets. Remote Sens. Environ. 78, 39–54. https://doi.org/10.1016/S0034-4257(01)00248-6.

Thonfeld, F., Steinebach, S., Muro, J., Kirmi, F., 2020. Long-Term Land Use/Land Cover Change Assessment of the Kilombero Catchment in Tanzania Using Random Forest Classification and Robust Change Vector Analysis. Remote Sensing 12, 1057. https://doi.org/10.3390/rs12071057.

Toffoli, T., Margolous, N., 1987. Cellular Automata Machines: A New Environment for Modeling. MIT Press: Cambridge, MA, USA, 1987; ISBN 0-262-20060-0.

USGS, 2020. Landsat Mission – Landsat Level-1 Processing Details. United States Geological Suvey. URL: https://www.usgs.gov/land-resources/nli/landsat/landsat-level-1-processing-details (last access: 20.04.2020).

Vaudour, E., Gomez, C., Lagacherie, P., Loiseau, T., Baghdadi, N., Urbina-Salazar, D., Loubet, B., Arrouays, D., 2021. Temporal mosaicking approaches of Sentinel-2 images for extending topsoil organic carbon content mapping in croplands. Int. J. Appl. Earth Observ. Geoinform. 96, 102277 https://doi.org/10.1016/j.jag.2020.102277.

Virto, I., Jose, Imaz M., Fernandez-Ugalde, O., Gartzia-Begngoetxea, N., Enrique, A., Bescansa, P., 2015. Soil Degradation and Soil Quality in Western Europe: Current Situation and Future Perspectives. Sustainability 7, 313–365. https://doi.org/10.3390/su7010313.

White, J.C., Wulder, M.A., Hobart, G.W., Luther, J.E., Hermosilla, T., Griffiths, P., Coops, N.C., Hall, R.J., Hostert, P., Dyk, A., Guindon, L., 2014. Pixel-Based Image Compositing for Large-Area Dense Time Series Applications and Science. Can. J. Remote Sens. 40 (3), 192–212. https://doi.org/10.1080/07038992.2014.945827.

Wulder, M.A., Loveland, T.R., Roy, D.P., Crawford, J.C., Masek, J.G., Woodcock, C.E., Allen, R.G., Anderson, M.C., Belward, A.S., Cohen, W.B., Dwyer, J., Erb, A., Gao, F., Griffiths, P., Helder, D., Hermosilla, T., Hipple, J.D., Hostert, P., Hughes, M.J., Huntington, J., Johnson, D.M., Kennedy, R., Kilic, A., Li, Z., Lymburner, L., McCorkel, J., Pahlevan, N., Scambos, T.A., Schaaf, C., Schott, J.R., Sheng, Y., Storey, J., Vermote, E., Vogelmann, J., White, J.C., Wynne, R.H., Zhu, Z., 2019. Current status of Landsat program, science and applications. Remote Sens. Environ. 225, 127–147. https://doi.org/10.1016/j.rse.2019.02.015.

Xu, D., Guo, X., 2014. Compare NDVI extracted from Landsat 8 imagery with that from Landsat 7 imagery. Am. J. Remote Sens. 2 (2), 10–14. https://doi.org/10.11648/j.ajrs.20140202.11.

Ying, Q., Tyukavina, A., Wang, L., Hansen, M.C., Hancher, M., Popatov, P.V., Moore, R., Stehman, S.V., 2017. Global bare ground gain from 2000 to 2012 using Landsat imagery. Remote Sens. Environ. 194, 161–176. https://doi.org/10.1016/j.rse.2017.03.022.

Zhao, D., Jiang, H., Yang, T., Cai, Y., Xu, D., Shuqing, A., 2012. Remote sensing of aquatic vgetation distribution in Taihu Lake using an improved classification tree with modified thresholds. J. Environ. Manage. 95, 98–107. https://doi.org/10.1016/j.jenvman.2011.10.007.

Zhu, Z., Woodcock, C.E., 2012. Object-based cloud and cloud shadow detection in Landsat imagery. Remote Sens. Environ. 118 (15), 89–94. https://doi.org/10.1016/j.rse.2011.10.028.

Zhu, Z., Wang, S., Woodcock, C.E., 2015. Improvement and expansion of the Fmask algorithm: cloud, cloud shadow, and snow detection for Landsats 4–7, 8 and Sentinel-2 images. Remote Sens. Environ. 159, 269–277. https://doi.org/10.1016/j.rse.2014.12.014.

Zhu, Z., Fu, Y., Woodcock, C.E., Olofsson, P., Vogelmann, J.E., Holden, C., Wang, M., Dai, S., Yu, Y., 2016. Including land cover change in analysis of greenness trends using all available Landsat 5, 7 and 8 images: A case study from Guangzhou, China (2000–2014). Remote Sens. Environ. 185, 243–257. https://doi.org/10.1016/j.rse.2016.03.036.

Zhuo, L., Dai, Q., Hand, D., Chen, N., Zhao, B., Berti, M., 2019. Evaluation of remotely sensed soil moisture for landslide hazard assessment. IEEE J. Sel. Top. Appl. Earth Obs. Remote Sens. 12 (1), 162–173. https://doi.org/10.1109/jstars.2018.2883361.

3.2. Scientific Publication II: Estimation of Soil Organic Carbon Contents in Croplands of Bavaria from SCMaP Soil Reflectance Composites

Reference: Zepp, S., U. Heiden, M. Bachmann, M. Wiesmeier, M. Steininger, B. van Wesemael, 2021. Estimation of Soil Organic Carbon Contents in Croplands of Bavaria from SCMaP Soil Reflectance Composites. Remote Sensing, 2021, 13, 3141.

https://doi.org/10.3390/rs13163141

Status: published

Author`s contribution: **SZ**: Conceptualization, Methodology, Software, Investigation, Data curation, Writing – Original Draft, Visualization. **UH**: Methodology, Writing – review editing, Supervision, Funding Acquisition. **MB**: Methodology, Software, Validation, Writing – review and editing. MW**:** Validation, Writing – review and editing. **MS**: Writing – review and editing. **BvW**: Methodology, Writing – review and editing, Supervision.

Scope of the journal: Remote Sensing is a peer-reviewed, open access journal about the science and application of remote sensing technology, and is published semimonthly online by MDPI. The Remote Sensing Society of Japan (RSSJ) and the Japan Society of Photogrammetry and Remote Sensing (JSPRS) are affiliated with Remote Sensing, and their members receive a discount on the article processing charge.

5-year impact factor: 5.786 (2021)

Article

Estimation of Soil Organic Carbon Contents in Croplands of Bavaria from SCMaP Soil Reflectance Composites

Simone Zepp [a,*], Uta Heiden [b], Martin Bachmann [a], Martin Wiesmeier [c], Michael Steininger [d], Bas van Wesemael [e]

[a] German Aerospace Center (DLR), German Remote Sensing Data Center (DFD), Muenchener Str. 20, 82234 Wessling, Germany

[b] German Aerospace Center (DLR), Remote Sensing Technology Institute (IMF), Muenchener Str. 20, 82234 Wessling, Germany

[c] Bavarian State Research Center for Agriculture, Institute for Organic Farming, Soil and Resource Management, Lange Point 6, 85354 Freising, Germany

[d] Mitteldeutsches Institut für Angewandte Standortkunde und Bodenschutz (MISB), 06114 Halle, Germa

[c] Georges Lemaître Centre for Earth and Climate Research, Earth and Life Institute, Université Catholique de Louvain, 1348 Louvain-la-Neuve, Belgium.

[*] Corresponding author at: German Aerospace Center (DLR), Muenchener Str. 20, 82234 Weßling, Germany

Received: 25 June 2021; Accepted: 5 August 2021; Published: 8 August 2021

Abstract: For food security issues or global climate change, there is a growing need for large-scale knowledge of soil organic carbon (SOC) contents in agricultural soils. To capture and quantify SOC contents at a field scale, Earth Observation (EO) can be a valuable data source for area-wide mapping. The extraction of exposed soils from EO data is challenging due to temporal or permanent vegetation cover, the influence of soil moisture or the condition of the soil surface. Compositing techniques of multitemporal satellite images provide an alternative to retrieve exposed soils and to produce a data source. The repeatable soil composites, containing averaged exposed soil areas over several years, are relatively independent from seasonal soil moisture and surface conditions and provide a new EO-based data source that can be used to estimate SOC contents over large geographical areas with a high spatial resolution. Here, we applied the Soil Composite Mapping Processor (SCMaP) to the Landsat archive between 1984 and 2014 of images covering Bavaria, Germany. Compared to existing SOC modeling approaches based on single scenes, the 30-year SCMaP soil reflectance composite (SRC) with a spatial resolution of 30 m is used. The SRC spectral information is correlated with point soil data using different machine learning algorithms to estimate the SOC contents in cropland topsoils of Bavaria. We developed a pre-processing technique to address the issue of combining point information with EO pixels for the purpose of modeling. We applied different modeling methods often used in EO soil studies to choose the best SOC prediction model. Based on the model accuracies and performances, the Random Forest (RF) showed the best capabilities to predict the SOC contents in Bavaria (R2 = 0.67, RMSE = 1.24%, RPD = 1.77, CCC = 0.78). We further validated the model results with an independent dataset. The comparison between the measured and predicted SOC contents showed a mean difference of 0.11% SOC using the best RF model. The SCMaP SRC is a promising approach to predict the spatial SOC distribution over large geographical extents with a high spatial resolution (30 m).

Keywords: soil reflectance composites, soil modeling, soil organic carbon, Landsat, multispectral

1. Introduction

Precise knowledge about the distribution of soil organic carbon (SOC) contents in agricultural soils is a valuable information for, e.g., food security issues [1] or global climate change [2]. The organic carbon stocks in soils represent one of the largest reservoirs in the global carbon cycle [3,4] and are affected by various drivers [5]. Soils with sufficiently high [6,7] and balanced SOC contents are considered healthy soils [8,9] and are less prone to impacts of climate change [7]. Adequate land management is necessary to preserve soil health and soil quality [10] and enables an increase of agroecosystem resiliency [11].

To capture and quantify SOC contents in agricultural soils for efficient and sustainable land use, data with high spatial resolution is needed in order to understand the impacts of climate change on soil quality [12]. High-resolution surveys at the national to regional scale are urgently required, as detailed spatial patterns in SOC are an important aspect for land management at the farm or even the field scale [13]. For applications with a large geographical extent [14] (national to European-wide), SOC maps are mostly available with a spatial resolution of 250 m to 1 km. The European Soil Data Center (ESDAC) provides several pan-European SOC maps. However, both well-known maps OCTOP: Topsoil Organic Carbon Contents for Europe [15] and the Topsoil Soil Organic Carbon Map based on the LUCAS (Land Use and Coverage Area frame Survey) soil datasets for EU25 [16] are distributed in a coarse 1 km raster format. The maps have, therefore, a limited suitability as a basis for high-resolution analysis at the farm or even the field scale.

Earth Observation (EO) can be a valuable data-source for area-wide mapping with a resolution that allows distinguishing between or even with field patterns [17]. In this context, hyperspectral (e.g., [18–21]) and multispectral images (e.g., [22–24]) are commonly used EO datasets to derive SOC contents. In Table 3.2.1, studies for different European regions are compared regarding their capabilities of SOC modeling. Generally, point soil information was correlated with multi- or hyperspectral pixel values using different machine learning (ML) techniques to derive SOC contents. However, in most studies, the estimation of SOC was restricted to relatively small areas (0.09 to 10.000 km2) in which the soil conditions (bare, smooth and dry soils) were considered to be optimal. This optimization prevented applying the models to cover larger geographical areas, except for a couple of previous efforts [25,26]. Additionally, the use of hyperspectral and multispectral remote sensing data for the estimation of SOC contents and other soil variables is hampered by the need for data that provide bare soil conditions. Mapping of exposed soils and the estimation of soil parameters is challenging due to temporal or permanent vegetation cover [27]. The area of exposed soils on a single remote sensing scene is limited, and often, the periods in which exposed soils dominate are restricted to short time windows [28] when the soil is in seedbed condition. Compositing techniques of multi-temporal satellite image archives provide an alternative and are widely used in the literature [25–34]. The compositing approach allows combining all bare soils of all input scenes, which enables a joint estimation of soil parameters for all exposed soils in the observed time period. For several years, new compositing techniques were developed in the course of opening the Landsat archive [35] that can retrieve exposed soils from multi-temporal satellite image archives [26,28,36,37]. An averaging of exposed soil areas over several years allows producing a new and spatially enhanced data source for soil analyses. Here, the soil spectra are relatively independent from seasonal differences in soil moisture and other soil surface conditions occurring during rain events or longer drought periods. In the resulting new data source, only permanent spatial soil moisture differences such as for the different soil types and texture characteristics remain. However, an in-depth proof of this assumption has not yet been provided.

The operational Soil Composite Mapping Processor (SCMaP) is a multitemporal compositing approach [36], which enables an automated generation of area-wide soil reflectance composites

(SRC) for the estimation of soil parameters using all available multispectral reflectance images for a defined period. So far, SCMaP SRC has not been used as an EO database for the SOC modeling of exposed topsoils in croplands of large geographical extents. Therefore, in this study, the SOC modeling capabilities of the SCMaP SRC are investigated and performed for a large portion of the German federal state of Bavaria and adjacent areas (about 130,000 km2) as solid calibration and validation datasets are available.

Generally, linking point data with EO images (30 m, 20 m pixel resolution) can be considered as a potential source of inaccuracies for soil parameter modeling as not all samples are collected at least 30 m from the field border the sample is related to [38]. In this case, the EO pixel may reflect the signal from adjacent fields with different spectral information, which is related to a single soil sample. New approaches are necessary that can handle the misalignment of the soil database and the spectral pixel information from the EO images for SOC modeling.

The overall purpose is to test the potential of the SCMaP SRC database derived from Landsat images covering 30 years to derive a high-resolution map of SOC contents in Bavarian croplands. For this purpose, the SRC is correlated with point soil measurements to derive spatial SOC contents for an area-wide mapping approach. The objectives of the study are:

1. Develop a spatial/spectral filtering technique to prepare the point dataset of the Bavarian test site for modeling purpose using the novel SCMaP SRC.
2. Apply the 30-year SCMaP SRC to derive SOC contents in Bavaria using different machine learning algorithms.
3. Validate the SOC map using an additional independent external dataset not included in the model calibration and validation

2. Materials and Methods

2.1 Study area

The study area covers most of the Federal State of Bavaria (Figure 3.2.1) and adjacent regions in southeast Germany and was selected regarding the diversity of landscape and soil types. The area south of 48° N was excluded as permanent grassland is the dominating land use in this region, and SCMaP is not able to detect soils covered by permanent vegetation. Moreover, mountainous regions of the Alps in southern Bavaria were also excluded. Due to the frequent cloud coverage in this region, only a small number of cloudless scenes per pixel were available for the compositing process compared to other parts of Bavaria.

The study area comprises about 130,000 km2, in which the elevation ranges between 100 m and 1000 m above sea level. The mean annual temperature lies between 6 ◦C and 10 ◦C, and the precipitation is between 551 mm and 1800 mm. The region is mainly dominated by Cambisols, Luvisols, Stagnosols, Gleysols and Leptosols [49] according to the World Reference Base for Soil Resource [50].

2.2 Soil Organic Carbon Modeling

An overview of the SOC modeling approach is outlined in Figure 3.2.2. Landsat 4–7 collection data from 1984 to 2014 are used to build the SRC based on the SCMaP workflow (Section 2.3). To calibrate an SOC model, SRC reflectance values and spectral indices (Section 2.3) are regressed against topsoil SOC measurements provided by two local authorities and the European LUCAS survey (Section 2.6).

Table 3.2.1: Overview on soil organic carbon (SOC) modeling studies across different regions in Europe.

Study area (size [km²])	**Earth Observation data / soil data: number of samples (samples / km²)**	**SOC range [%]**	**Machine Learning algorithm**	**R^2**	**RMSE [%]**	**RPD**	**Ref.**
Albany Ticket, South Africa (320)	HyMap (hy, A) / 125 (0.39) spectra	0.21 – 5.85	Feature based MLR (1)	0.62	0.43	1.57	[39]
Loam belt, Belgium (BE) (462) / Luxembourg (LUX) (146)	APEX (hy, A) / 84 (1.58) (LUX), 54 (0.12) (BE) spectra / LUCAS spectra	1.69 – 31.8	PLSR (1)	-	field spec: 0.49 (LUX) / 0.15 (BE) LUCAS: 0.49 (LUX) / 0.15 (BE)	field spec: 1.7 (LUX) / 1.4 (BE) LUCAS: 1.7 (LUX) / 1.4 (BE)	[40]
Demmin, Germany (GER) (200) / Loam Belt, BE (426) BE / Gutland-Oesling, LUX (204)	Sentinel-2 (S-2) (ms, A) APEX (hy, A), S-2 resampled (ms, A) / 170 (0.8) (BE) / 194 (0.4) (LUX) / 231 (0.12) (GER) samples	0.6 – 1.6	PLSR / RF (1)	-	PLSR: 0.10 – 0.17 (S-2) / 0.11 – 0.17 (hy) / 0.08 – 0.14 (S-2 res) RF: 0.2 – 1.86 (S-2) / 0.2 – 1.84 (hy) / 0.2 – 1.86 (S-2 res)	PLSR: 1.0 – 1.7 (S-2) / 1.1 – 1.7 (hy) / 1.0 – 1.5 (S-2 res) RF: 1.0 – 1.5 (S-2) / 1.0 – 2.1 (hy) / 1.0 – 2.1 (S-2 res)	[22]
Demmin, GER (10.000)	S-2B (ms, A) / 35 LUCAS spectra	0.5 – 38.4	RF (1)	-	0.68 – 2.67	0.9 – 4.4	[41]
Demmin, GER	S-2 (ms, A), HySpex (hy, A), EnMAP simulated (hy, A) / 181 samples	0.6 – 19.4	RF (1)	-	8.7 – 17.8 (S-2) / 11.0 – 18.8 (EnMAP)	1.2 – 2.5 (S-2) / 1.2 – 2.0 (EnMAP)	[42]
Wallonia, BE (3.630)	Sentinel-2 (ms, B) / 137 (0.038) samples	0.67 – 2.1	PLSR (2)	0.14 ± 0.03 – 0.54 ± 0.12	0.209 ± 0.039 – 0.363 ± 0.036	1.06 ± 0.06 – 1.68 ± 0.45	[43]
4 fields, Czech Republic (CZK) (0.7 – 7.76)	CASI (hy, A), Sentinel-2 (ms, A) / 200 samples)	0.56 – 2.62	support vector machine regression (1)	-	0.12 – 7.95 (hy) / 0.14 – 9.15 (S-2)	1.03 – 2.05 (hy) / 0.89 – 1.92 (S-2)	[44]
4 fields, Lower Rhine Basin (GER) (0.0025 – 0.09)	HyMap (hy, A) / 204 samples	0.8 – 1.85	PLSR (2)	0.34 – 8.83	0.76 – 1.13	1.14 – 2.32	[45]
Europe	Landsat-4, -5, -7, -8 composite (1982-2018) (ms, B) / LUCAS spectra	0.0 – 43.84	gradient boosting trees (1)	0.06 – 0.13	1.52 – 1.68	0.52 – 0.58	[25]
Wulfen, GER (200) GER	HyMap (hy, A) / 73 (0.73) samples	0.7 – 3.85	MLR / PLSR (2)	0 90 (PLSR) / 0.86 (MLR)	0 29 (PLSR) / 0.22 (MLR)	-	[46]
Versailles Plains (VP), (221) / Peyne Valley (PV), France (FRA) (48)	S-2 (ms, A) / 72 (0.33) (VP), 143 (2.98) (PV) samples	0.7 – 3.19 (VP) / 0.4 – 2.18 (PV)	PLSR (2)	0.56 (VP) / 0.02 (PV)	0.123 (VP) / 0.371 (PV)	1.51 (VP) / 1.00 (PV)	[23]

Versailles Plain, FRA (221)	S-2 (ms, A) / 329 (1.49) samples	0.62 – 3.59	PLSR (2)	0.16 – 0.58	0.302 – 0.586	1.0 – 1.5	[47]
Versailles Plain, FRA (221)	S-2 (ms, B) / 329 (1.49) samples	0.62 – 3.59	PLSR (2)	-0.02 – 0.56	0.253 – 0.545	0.99 – 1.53	[37]
Sardice, Czech Republic (1.45)	Sentinel-2 (ms, A), S-2 composite (03/2017 – 05/2019) (ms, B), Landsat-8 (ms, A), CASI (hy, A) (50 (34.5) samples	0.85 – 2.62	RF / PLSR (2)	0.56 – 0.68 (S-2) / 0.81 (S-2 comp) / 0.65 (L-8) / 0.76 (CASI)	0.27 – 0.28 (S-2) / 0.34 (S-2 comp) / 0.28 (L-8) / 0.20 (CASI)	1.4 – 1.52 (S-2) / 1.4 (S-2 comp) / 1.41 (L-8) / 1.81 (CASI)	[48]

(spectral characteristics: ms - multispectral, hy - hyperspectral; scene acquisition: A - single scene, B - multitemporal composite; mapping approach: 1 – spectral model, 2 – digital soil modeling; machine learning algorithms: PLSR – Partial Least Square Regression, MLR – Multiple Linear Regression, RF – Random Forest; accuracy and performance measures: RMSE – Root Mean Square Error, RPD – Ratio of Performance to Deviation; further significance of the regression models are not given in the cited studies, the relationships are likely to be significant given the large number of calibration points in relation to the number of (latent) variables.)

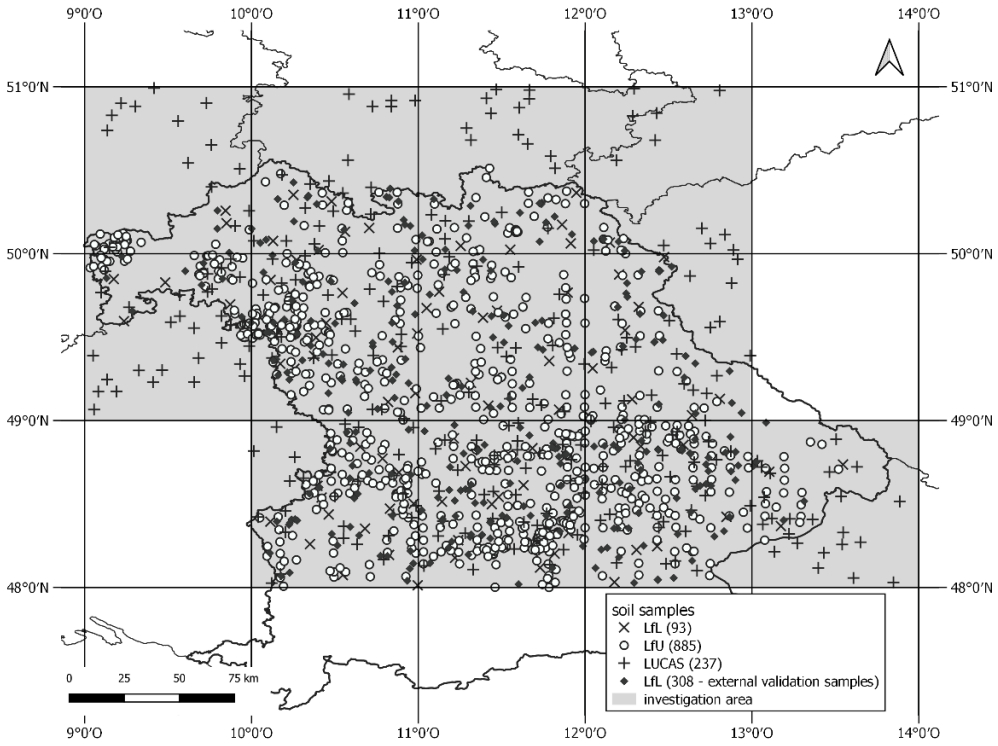

Figure 3.2.1: Overview of the study area in Bavaria and the distribution of the soil dataset (LfU - Bavarian Environmental Agency; LfL - Bavarian State Research Center for Agriculture; LUCAS - Land Use and Coverage Area frame Survey).

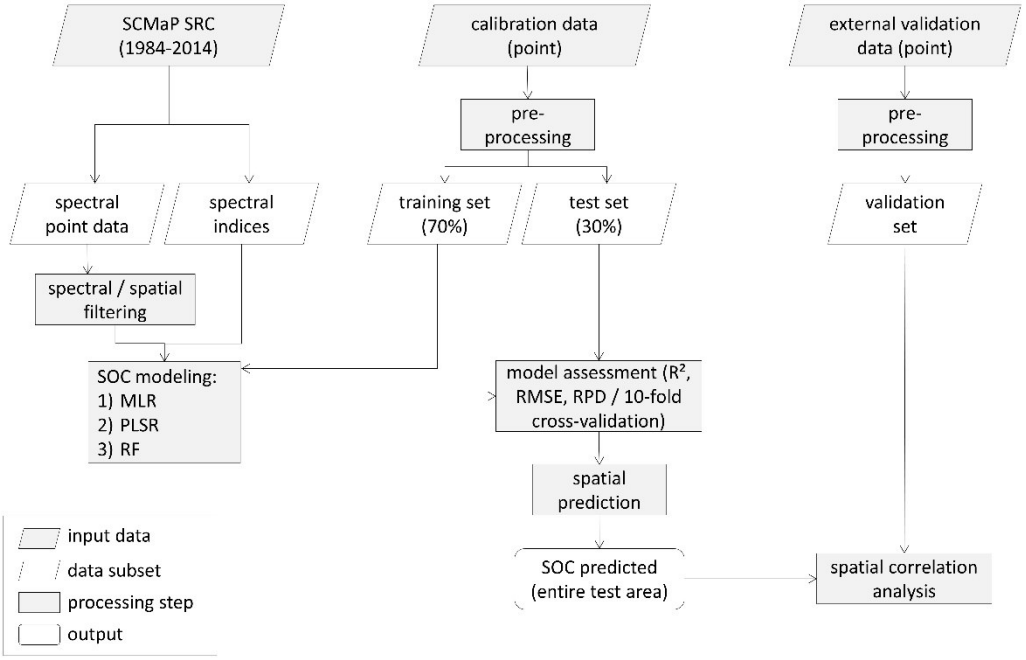

Figure 3.2.2: A flowchart of the SOC modeling approach (SRC - soil reflectance composite; MLR - Multiple Linear Regression; PLSR - Partial Least Square Regression; RF - Random Forest; RMSE - Root Mean Square Error; RPD - Ratio of Performance to Deviation).

Due to the positioning of several measurements at field borders, and thus, the potential integration of disturbances, a new filtering technique was developed and applied to evaluate the quality of calibration samples (Section 2.4). For the regression, three machine learning algorithms

were tested and evaluated (Section 2.5). The models were trained for different datasets combining the reflectances and additional spectral indices.

Per algorithm, the best model is chosen, and the SOC contents are predicted for the entire study area. The prediction results are validated against external, independent SOC point measurements not included in the model calibration by a spatial correlation analysis (Section 2.7).

2.3 SCMaP SRC and Spectral Indices

The SCMaP chain [36] allows the generation of soil reflectance composites for individually determined time periods of different years. Bare soil pixels are selected based on a modified vegetation index (PV) using two thresholds that allow separating predominantly undisturbed soils from all other land cover types such as permanent vegetation and permanent non-vegetation. The derivation of the thresholds is based on an automated technique described in [51]. All selected bare soil pixels are averaged. The operational SCMaP chain can be used to build SRCs containing all pixels in a given time period showing at least once exposed soil.

For the SOC modeling, a period of 30 years (1984–2014) was chosen to provide a smooth spectral database that averages the seasonal variabilities of bare soils. The 30-year period was chosen for several reasons. A high possible soil coverage should be achieved. Using 5-year composites, 31.79% to 34.17% of the entire investigation area are selected as bare soil pixels. Ten-year composites provide 37.54% to 41.21% as exposed soils, and the 30-year composite enables the analysis of 54.53% of the investigation area as uncovered soils. Additionally, a possible large number of soil samples was intended to be used in the modeling dataset. A reduction of the compositing period would have significantly reduced the number of soil samples. For 5-year periods, 112 to 397 soil samples were collected in the respective periods. Based on 10-year composites, 261 to 536 samples are available. For a 30-year compositing range, 1,250 samples can be used for the modeling dataset. Additionally, an average over multiple years enables a reduction of seasonal soil moisture differences and permanent spatial differences remaining in the composite.

The SRC was processed for 228 Landsat-4 TM, 9,990 Landsat-5 ETM and 4,333 Landsat- 7 ETM+ collection scenes [52] available between 1984 and 2014. For all scenes of all sensors, the same pre-processing steps were performed. The FMask algorithm [53,54] was used to detect and remove clouds, cloud shadows and pixels that were covered by snow. Additionally, an atmospheric correction was applied to all scenes using Atmospheric Topographic Correction (ATCOR) software for satellite imagery [55]. The quality of the composites is defined, among other factors, by the number of cloudless scenes per pixel [50]. The consistently large number of cloudless scenes per pixel for the total investigation time is given in Figure A1 in Appendix A.

In addition to the point spectral information of the SCMaP SRC, different indices were selected and computed (Table 3.2.2). Indices are commonly used in remote sensing to parameterize specific spectral features caused by physical and/or chemical properties [56]. Besides established indices, an additional index (SCMaPI) was developed to capture the difference between the green and the SWIRI bands of the SCMaP SRC. The SCMaP shows smaller differences for high SOC content and higher differences for lower SOC content.

2.4 Spectral/Spatial Filtering

Based on Landsat imagery, SCMaP provides soil reflectance information with a pixel resolution of 30 m. The link of a point soil sample to a 30 m pixel can result in inaccuracies if the soil sample

is not collected at least 30 m from the field border. In this case, the SCMaP pixel may combine multiple surfaces with different spectral information, which are related to one soil sample.

Table 3.2.2: Summary of the selected spectral indices.

Spectral Index	Description	Expression	Reference
BI	Brigthness Index	$\frac{\sqrt{(Red \cdot Red) + (Green \cdot Green)}}{2}$	[57]
BI2	Second Brightness Index	$\frac{\sqrt{(Red \cdot Red) + (Green \cdot Green) + (Blue \cdot Blue)}}{3}$	[57]
EVI	Enhanced Vegetation Index	$G \frac{NIR - Red}{NIR + C1 \cdot Red - C2 \cdot Blue + L}$	[58]
NBR2	Normalized Burn Ratio	$\frac{NIR - SWIR\ II}{NIR + SWIR\ II}$	[59]
SCMaPI	SCMaP Index	$\frac{SWIR\ I - Green}{SWIR\ I + Green}$	-
MSAVI2	Modified Soil Adjusted Vegetation Index	$\frac{2 \cdot NIR + 1\sqrt{(2 \cdot NIR + 1)^2 - 8 \cdot (NIR - Red)}}{2}$	[60]
LSWI	Land Surface Water Index	$\frac{NIR - SWIR\ I}{NIR + SWIR\ I}$	[61]
NDSI	Normalized Difference Soil Index	$\frac{SWIR\ I - NIR}{SWIR\ I + NIR}$	[62]
RI	Redness Index	$\frac{Red \cdot Red}{Green \cdot Green \cdot Green}$	[63]
BSI	Bare Soil Index	$\frac{(SWIR\ I + Red) - (NIR + Blue)}{SWIR\ I + Red) + (NIR + Blue)}$	[64]
CI	Color Index	$\frac{Red - Green}{Red + Green}$	[63]
TVI	Transformed Vegetation Index	$(\frac{NIR - Red}{NIR + Red} + 0.5)^{0.5}$	[65]
GRVI	Green-Red-Vegetation Index	$\frac{Green - Red}{NIR + Red}$	[66]
V	Vegetation Index	$\frac{NIR}{Red}$	[67]
GNDVI	Green Normalized Vegetation Index	$\frac{NIR - Green}{NIR + Green}$	[68]
SATVI	Soil Adjusted Total Vegetation Index	$\frac{SWIR\ I - Red}{NIR + Red + 1}(1 + L) - \frac{SWIR\ II}{2}$	[69]
NDVI	Normalized Difference Vegetation Index	$\frac{NIR - Red}{NIR + Red}$	[70]
GSAVI	Green Soil Adjusted Vegetation Index	$\frac{NIR - Green}{NIR + Green + L} \cdot (1 + L)$	[71]
GOSAVI	Green Optimized Soil Adjusted Vegetation Index	$\frac{NIR - Green}{NIR + Green + Y}$	[72]
SAVI	Soil Adjusted Vegetatin Index	$\frac{(\mathrm{NIR} - \mathrm{Red}) \cdot (1 + L)}{(NIR - Red + 0.5)}$	[73]

A proportion of the soil samples (especially the LUCAS points, [38]) are often taken within a few meters from the borders of agricultural fields, e.g., as shown by the photo documentation of the sampling points at the LUCAS viewer online (https://ec.europa.eu/eurostat/statisticalatlas/gis/viewer/?config=LUCAS-2009.json, accessed on 6 August 2021). The disturbance factors primarily exist at the field boundaries. Eliminating all samples that were collected within 30 m of the field border could decrease the number of biased pixels. However, this would drastically decrease the database and was therefore not considered. Instead, a spectral/spatial filtering technique was developed to prepare the soil database and the spectral information from the EO images for SOC modeling.

The filtering technique evaluates the spectral differences between the sample SRC pixel and its eight neighboring pixels. A comparison of the sample spectra to the neighboring pixel spectra allows an estimation if the reflectance spectra of the sample pixel are influenced by any external disturbances or data artefacts (e.g., mixed spectra of soil and a small portion of vegetation, local variation) or if they are comparable to the surrounding spectra. The spectral/spatial filtering aims to detect pixel clusters with deviating spectra to remove this from further processing. For this purpose, all STDs per pixel cluster per band were used to define a threshold to exclude the deviating pixel clusters. Twice, the STD per band of all pixel cluster STDs was selected as the threshold. The threshold was determined and applied per band. The identified pixel cluster containing at least one to several spectral bands above the thresholds was excluded from the dataset.

2.5 Soil Modeling Methods

Three machine learning (ML) algorithms were used and evaluated. A Multiple Linear Regression (MLR), a Partial Least Square Regression (PLSR) [74] and a Random Forest regression (RF) algorithm [75] were applied to model the SOC contents in the topsoils. All three techniques are widely used in soil applications [76–79] and especially for SOC modeling (see Table 3.2.1, [22,23,37,39–49]). The modeling was performed using the Scikitlearn machine learning library for Python [80]. The following parameters were chosen for the RF: n_estimators: 100, max_features: 10, max_depth: 12, min_sample_split: 6, min_samples_leaf: 2 and for the PLSR: n_components: 5.

The calibration dataset was randomly split into a training (70%) and test (30%) subset. The training set was used to train the model, whereas the test subset of the calibration data was used to validate the model. For the model calibration and validation, common accuracy and performance measures, such as the R2 (coefficient of determination, from sklearn.metrics), the root mean square error (RMSE) and the ratio of performance to deviation (RPD), were used to evaluate the model performances and to allow a comparison with the literature (Table 3.2.1). The RPD is an established performance measure that determines the quality of a model [81]. Moreover, the commonly used accuracy and performance measure, the Concordance Correlation Coefficient (CCC) [82], is given to assess the agreement between the predicted and measured SOC contents. Additionally, ten-fold cross-validation (cv) was performed to evaluate the performance of the models. The cv was applied to the training subset of the calibration data. In addition to the established accuracy and performance measures, an analysis of the standardized residuals and the autocorrelation of the residuals for the model calibration samples is given in Figures A2 and A3 in the Appendix A.

Besides the reflectances, additional spectral indices (Table 3.2.2) per spectrally/spatially filtered sampling cluster were calculated and implemented in the modeling framework to investigate the influence of further spectral details. For this purpose, for each algorithm, three

different model setups were prepared to estimate the influence of the spectral indices on the modeling capabilities. The models were trained based on (a) the composite reflectances (R), (b) the composite reflectances and all indices (RI_all) and (c) the composite reflectances and for each algorithm individually selected indices (RI_sel). Besides the reflectances and indices, no other covariates (e.g., clay content of climate variables) were used in the modeling framework.

For each algorithm, a selection of important features (RI_sel) was performed. The identification of the relevant features for the MLR was based on a linear correlation (Pearson's correlation from Python sklearn.metrics). First, the relationship between the reflectances and indices to the modeling variable SOC was evaluated to exclude insignificant features (correlation coefficients (R) > 0.3). All significant feature pairs with correlation coefficients between -0.7 and 0.7 were then selected for the RI_sel dataset. For the PLSR, the variable importance in projection (VIP) per feature was calculated. Features with a VIP higher than 1.0 [22,83] were selected for the RI_sel dataset. For the RF, a calculation of the internal feature importance score (Mean Decrease Impurity (MDI)) was performed. Features with a score higher than 4.0% were selected as relevant features [84,85].

For each algorithm, the best model setup was selected regarding the cross-validation results and the model validation accuracies. For the best performance dataset (RI, RI_all, RI_sel), the models were applied to the 30-year SRC to predict the spatial SOC contents for the entire study area.

2.6 Soil Samples

For point SOC measurements, all available legacy data to cover the highest possible temporal and spatial overlap with the SRC between 1984 and 2014 were used. Kühnel et al. [86] found no significant SOC changes between 1986 and 2015 of Bavarian croplands. The authors analyzed 92 repeatedly measured cropland sites in Bavaria. Therefore, all available sampling points between 1984 and 2014 were combined for the modeling dataset. However, there is a disadvantage of using legacy data, i.e., the sampling schemes are not optimally distributed.

The SOC measurements for the calibration set were provided by the Bavarian Environment Agency (LfU—1071 sampling sites) and the Bavarian State Research Center for Agriculture (LfL—134 sampling sites). Additionally, soil samples (504 sampling sites) collected in the framework of the LUCAS (Land Use and Coverage Area frame Survey) 2009 Topsoil Survey provided by the European Soil Data Centre (ESDAC) [87] were added (Figure 3.2.1). The LfU provided a large database with topsoil samples equally distributed across Bavaria [88]. The sites were each sampled once between 1984 and 2014. The LfL calibration dataset contained data from the permanent soil observation program (BDF) of Bavaria. In contrast to the once sampled LfU sites, these 134 BDFs were sampled multiple times in the observation period. As [86] found no significant change between 1986 and 2015 for the BDF sites across Bavaria, the available samples per BDF between 1984 and 2014 were averaged. Thus, one measurement per sampling location is included in the calibration dataset. The LUCAS soil samples were collected in 2009 from unique spatial positions across the investigation area. SOC contents of the LfU, LfL and LUCAS databases were all determined by dry combustion using elemental analyzers [88,89].

From all data sources, the samples intersecting with the SCMaP SRC and within the investigation period (1984 to 2014) were selected, i.e., 1385 soil samples. Per soil sample, the reflectance spectra and its eight neighboring pixels of the SRC were extracted and averaged to reduce local spatial variability. After the spectral/spatial filtering, 1215 sampling points for model calibration are remaining.

The external validation set was provided by the LfL and included 352 cropland fields with point SOC measurements sampled between 2001 and 2008. For each agricultural field, five sampling locations were randomly selected. At each sampling location (radius = 1.5 m), six soil samples were taken. SOC contents of all six soil samples of all five sampling locations were averaged to one SOC content per field. SOC contents were determined by dry combustions using CN elemental analyzers. For the external validation of the dataset, 308 samples were intersecting with the SCMaP SRC.

The data provided by the LfU contained the highest range of SOC contents (0.26% to 18.30%; Table 3.2.3). The LfL calibration data showed a lower mean SOC content in comparison to the LfU and LUCAS datasets. Overall, the calibration dataset contained locations with higher SOC contents compared to the external validation dataset.

Table 3.2.3: Statistics of the soil organic carbon (SOC) content of the model calibration soil samples and the independent validation soil samples by the different institutions. The number of samples per institute is given based on the spatially/spectrally filtered clusters (LfU – Bavarian Environmental Agency; LfL – Bavarian State Research Center for Agriculture; LUCAS – Land Use and Coverage Area frame Survey; STD – Standard Deviation; IQR – Interquartile Range).

	LfL (93)	**LfU (885)**	**LUCAS (237)**	**LfL (308)**
	(Model Calibration & Validation)			**(Independent Validation)**
minimum SOC content (%)	0.84	0.26	0.57	0.55
maximum SOC content (%)	5.96	18.30	6.81	4.65
mean SOC content (%)	1.74	2.28	2.02	1.58
STD SOC (%)	0.70	2.24	1.06	0.57
median SOC (%)	1.63	1.57	1.71	1.89
IQR (%)	1.74	1.03	1.11	0.72

For the model calibration and validation, the distribution of SOC contents of the training (70%) (Figure 3.2.3a) and test data (30%) (Figure 3.2.3b) were comparable. Both datasets contained samples with high SOC concentrations. The distribution of the SOC percentages of the calibration (cal) and the external independent validation (val) datasets (Figure 3c) showed a similar mean; however, the external validation dataset did not contain as high SOC concentrations.

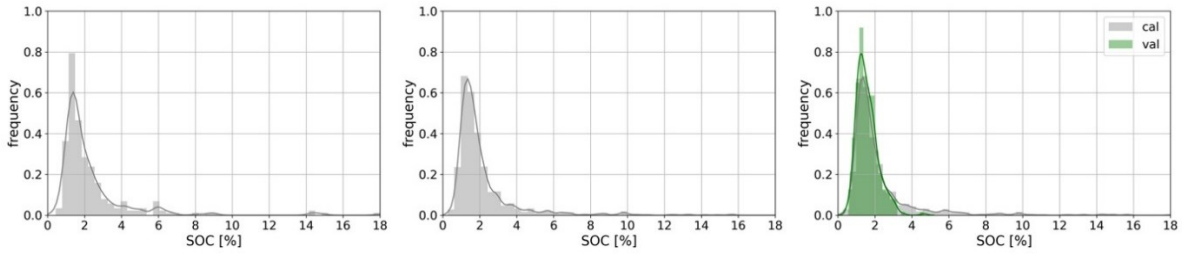

(a) (b) (c)

Figure 3.2.3: Frequency distribution of SOC contents of the (a) training, (b) test portion of the model calibration (cal) dataset and (c) a comparison of the model calibration dataset and the external independent validation (val) dataset.

2.7 External Validation

To evaluate the accuracy of the prediction models more precisely, a further validation was performed using an independent external dataset provided by LfL, which was not included in the training. For each regression algorithm, the best data set up based on the model accuracies and performance was selected and applied to predict the SOC contents for the entire investigation area. The difference for all samples between the predicted and measured SOC contents of the external independent validation dataset were calculated to estimate the averaged difference between the predicted and the measured contents to provide the reliability of predicting SOC for each algorithm.

3. Results

3.1 Spectral/Spatial Filtering

The spectral/spatial filtering was implemented in the model framework to ensure a high-quality calibration database. In order to ensure homogenous pixel clusters, a threshold is necessary to identify the heterogenous pixel clusters. Most of the nine individual pixel spectra per cluster showed homogenous patterns (Figure 3.2.4a). Here, an SOC measurement is linked to valid spectral information. However, a few pixel clusters showed deviating spectra (Figure 3.2.4b). These heterogenous pixel clusters with deviating individual spectra are represented by high standard deviations (STD) and need to be filtered, as here the possibility of any external influence or data artefacts (e.g., mixed spectra of soil and a small portion of vegetation, local variation) impacting the cluster is very high.

Figure 3.2.5 shows six histograms of all STDs per band for all sample clusters of the calibration dataset. As the threshold twice, the STD per band was selected to identify and eliminate the heterogenous clusters with deviating spectra. Overall, 135 pixel clusters (9.7% of the total calibration dataset) were eliminated from the calibration dataset. The preprocessed, spectrally/spatially filtered calibration set accordingly comprises 1250 averaged sampling clusters. As shown in Figure 3.2.5, using the STD as the threshold, a higher number of pixel clusters (674, 48.7%) are identified as heterogeneous clusters. However, a visual analysis showed that too many pixel clusters would be eliminated using the STD as the threshold. It was also tested to set the threshold at three-fold STD (3 STD). Although, this would result in an insufficient selection of heterogenous pixel clusters. A visual analysis has shown that the filtering of 50 pixel clusters (3.6%) selected by the three-fold STD threshold does not filter all heterogenous pixel clusters sufficiently.

The spatial/spectral filtering has a significant positive effect on the model accuracies. The RF was applied to the filtered and unfiltered RI_all datasets. A significant increase of the R^2 (0.64 to 0.67), a decrease of the RMSE (1.38% to 1.26%) and an increase of the RPD (1.46 to 1.56) indicated an improved performance of SOC modeling.

3.2 Feature Selection

For each ML algorithm, a feature selection was performed based on the correlation coefficients for the MLR (Figure 3.2.6), the VIP scores for the PLSR (Figure 3.2.7a) and the feature importance scores for the RF (Figure 3.2.7b). We selected 15 features for the MLR, 14 features for the PLSR, and 10 features for the RF. Overall, similar reflectance bands and indices were identified as important features for the individual RI_sel subsets. For the PLSR and the RF, the Landsat bands two (green), three (red) and four (near infrared—NIR) were selected as important features. For

all three algorithms, the SCMaP and the NDSI were selected, whereas the overlap of selected indices was higher for the PLSR and RF (Figure 3.2.7a,b). However, for the MLR, not all reflectance bands identified as significant features were flagged as independent features showing high R scores (>0.7) in the correlation matrix. This would result in an elimination of most of the reflectance bands. However, they were all included in the TI_sel database as the analysis of the SCMaP SRC reflectances is the focus of this study.

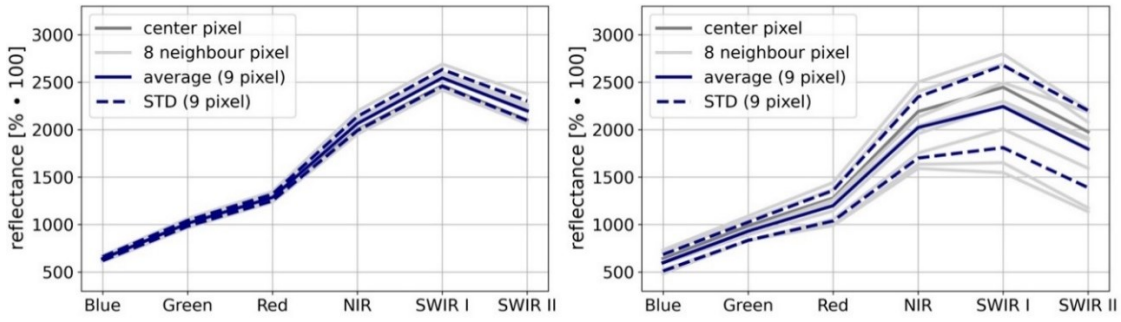

(a) (b)

Figure 3.2.4: SRC reflectances of the center pixel (dark grey), the eight neighboring pixels (grey), the average reflectance (blue solid), the STDs per pixel-cluster (blue dashed) for (a) a homogenous pixel cluster and (b) a heterogenous pixel cluster.

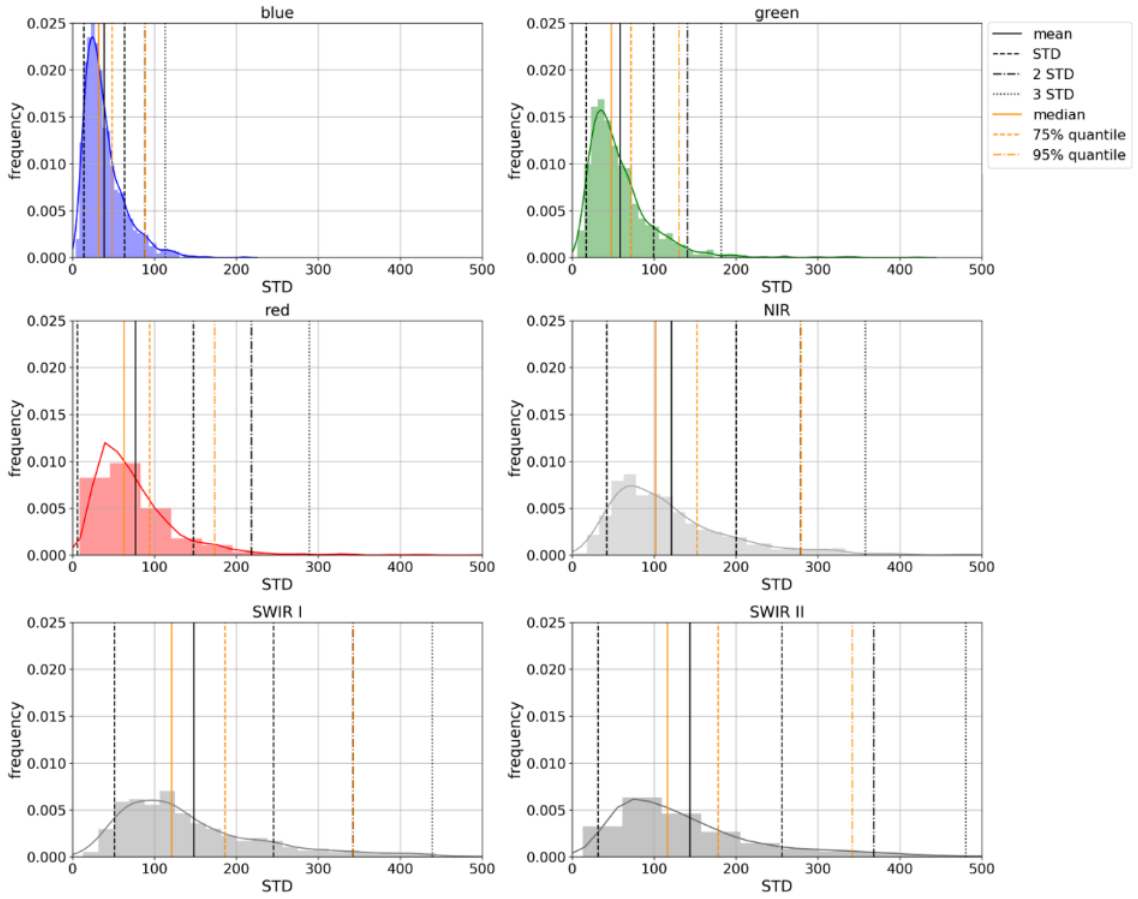

Figure 3.2.5: Frequency distribution of the STDs of all pixel clusters per band. Twice, the STD per band was selected as the threshold for the identification of deviating pixel clusters.

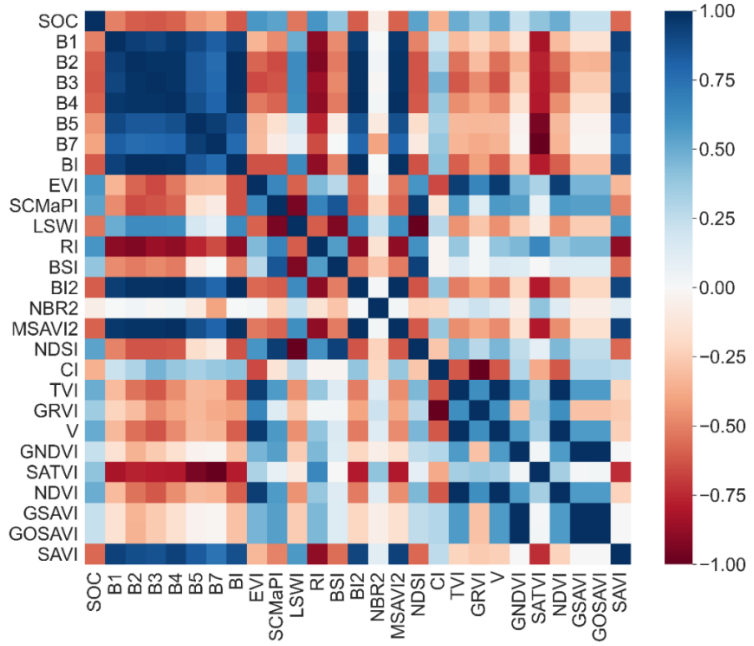

Figure 3.2.6: The correlation matrix (Pearson's correlation) between the reflectances, the indices and the modeling variable SOC. The definition of significant features for SOC modeling and further independent features for the RI_sel dataset are based on the correlations (the hypothesis test by p-values showed for all significant feature combinations a correlation close or equal to zero).

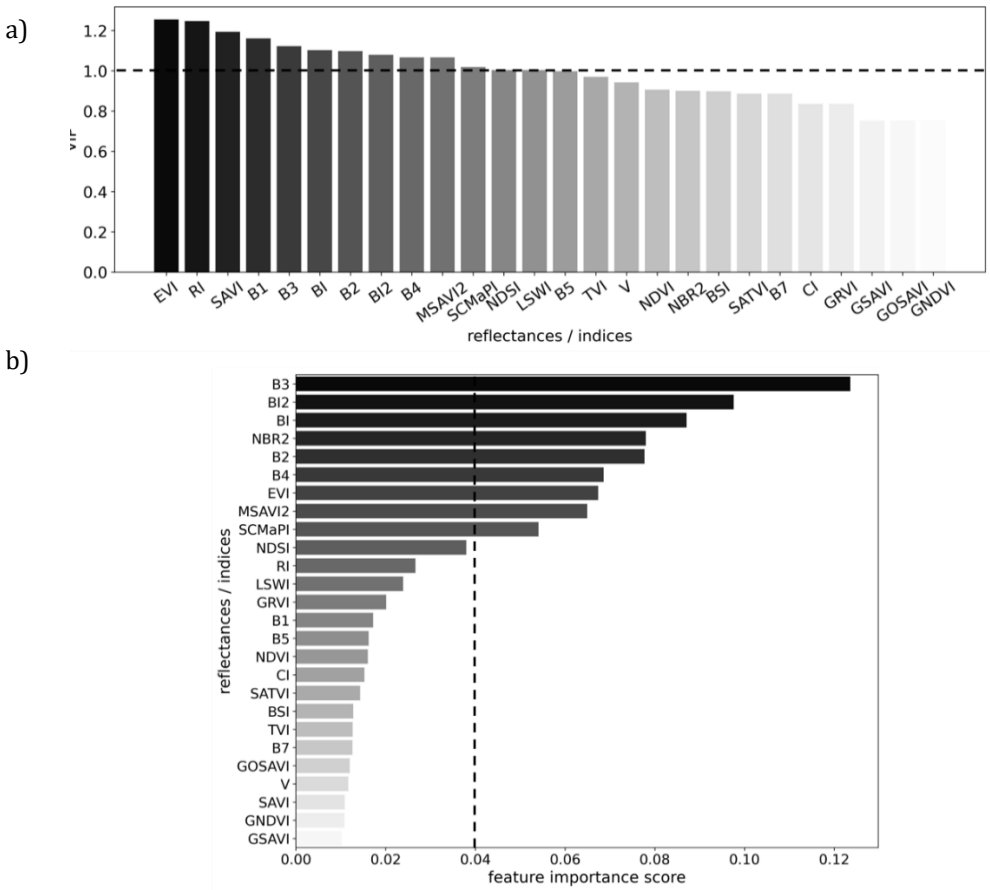

Figure 3.2.7: Feature selection for PLSR and RF. (a) VIP diagram of the PLSR to select the relevant features for the PLSR RI_sel run. Features with a VIP score higher than 1.0 are selected for the RI_sel database. (b) The feature importance score for the RF selection of relevant features. Features with a score higher 0.04 (4%) are selected for the RI_sel database.

3.3 Model Results - Calibration

In order to ensure reliable models not overfitting the data, 10-fold cross-validation (cv) using 70% of the calibration data was additionally conducted to the model calibration using the same portion of data (Table 3.2.4). The remaining 30% of the calibration sampling points excluded from the model training were used for validating the models (Table 3.2.4, Figure 8).

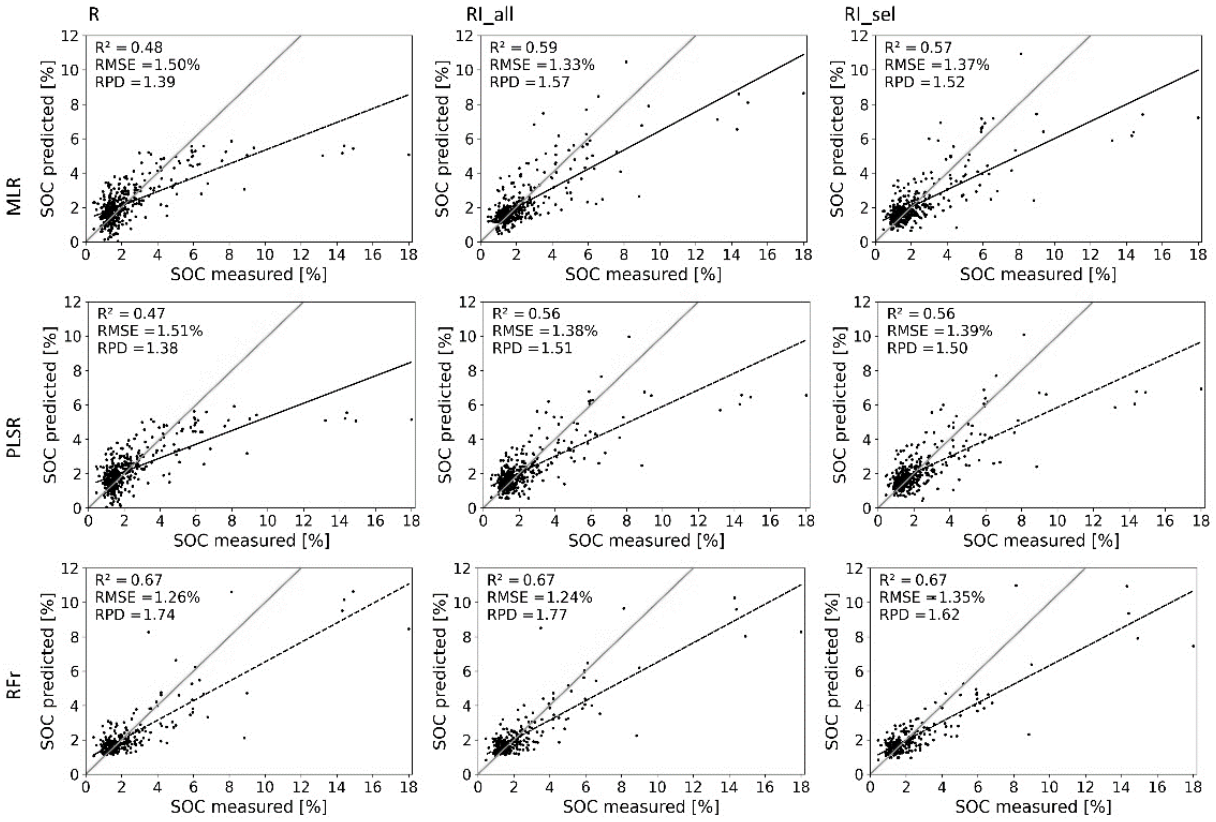

Figure 3.2.8: A comparison of predicted and measured SOC contents using the 30% validation data from LfU, LfL and LUCAS not used for model calibration. Depicted are MLR (upper row), PLSR (middle row) and RF (bottom row) based on reflectances (R), reflectances and all indices (RI_all) and reflectances and per algorithm selected indices (RI_sel). The accuracies (R^2, RPD, RMSE) per algorithm and dataset, the regression (black line) and the 1:1 line (orange) are given.

The model accuracies and performances of the cv in comparison to the calibration results (cal) and validation results (val) are given in Table 3.2.4. Overall, except for minor differences for the RF similar R2, RMSE and RPD values comparing the cal and cv results were detected for all datasets. This indicates that the cal models are valid and did not overfit the data. However, except for MLR and PLSR, based on the R datasets, the cv results are in a similar range compared to the val results. The model val results are in a similar range for the three algorithms. For PLSR and MLR, the use of additional indices is increasing the accuracies significantly. The influence of additional indices on the RF is less visible. Here, the R2 is constant, the RPD is increasing, and the RMSE is decreasing. The RF shows the highest CCC values compared to the MLR and PLSR, whereas the CCC values for PLRS are lower based on the MLR.

Figure 3.2.8 shows the model validation results in detail for all three ML algorithms and for all prepared datasets. Overall, the RF regression performed best, showing the highest R2 (0.67) and RPD scores (1.62 to 1.77) for the different datasets using the 30% validation sampling points of the calibration dataset. Based on RI_all, the best model accuracies comparing all datasets were obtained. The PLSR showed the lowest modeling accuracies with lower R2 and RPDs and a higher RMSE in comparison to the other algorithms. The models based on the RI_all showed higher

accuracies overall than the models based on the R data setup. The indices positively influenced the prediction of SOC. The RI_sel database showed no improvements in the model accuracies for the different ML algorithms. It is worth noting that for high SOC values, all regression approaches and all data set ups (reflectance and/or indices) underestimated the SOC.

Based on the cv and val results, the best set of features for all models was selected. For MLR, PLSR and RF, the model based on RI_all showed the best performances regarding the model validation and is therefore further used in this study. Using the RI_all feature set, the RF showed the best accuracies concerning the model training, cross validation and external validation.

Table 3.2.4: Calibration (cal), cross validation (cv) and first independent validation (val) accuracies for MLR, PLSR and RF using R, RI_all and RI_sel.

Algorithm	Input-datasetup	R^2			RMSE (%)			RPD			CCC
		cal	cv	val	cal	cv	val	cal	cv	val	val
MLR	R	0.40	0.80	0.48	1.48	1.50	1.50	1.27	1.27	1.39	0.61
	RI_all	0.60	0.55	0.59	1.20	1.29	1.44	1.44	1.44	1.57	0.73
	RI_sel	0.52	0.48	0.57	1.32	1.37	1.37	1.39	1.39	1.52	0.70
PLSR	R	0.40	0.38	0.47	1.48	1.50	1.51	1.29	1.27	1.38	0.60
	RI_all	0.52	0.48	0.56	1.34	1.37	1.38	1.43	1.40	1.51	0.69
	RI_sel	0.51	0.48	0.56	1.34	1.37	1.39	1.43	1.39	1.50	0.68
RF	R	0.91	0.53	0.67	0.59	1.31	1.25	3.25	1.46	1.74	0.78
	RI_all	0.86	0.58	0.67	0.71	1.24	1.24	2.67	1.54	1.77	0.78
	RI_sel	0.86	0.58	0.67	0.72	1.23	1.35	2.65	1.55	1.62	0.78

3.4 External Validation

For each ML algorithm, the model based on the best feature subset was selected and applied to the whole investigation area. For each point of the external validation dataset, the predicted SOC contents were compared to the measured SOC values. Figure 3.2.9 shows the differences between the 308 pairs of values of the predicted and measured SOC contents for Figure 3.2.9a MLR (RI_all), Figure 9b PLSR (RI_all) and Figure 3.2.9c RF (RI_all). In total, the average errors were relatively low (0.11% ± 0.56% to 0.21% ± 0.61%) comparing the predicted and the measured values. The comparison of the predicted data based on the RF (RI_all) to the external validation data indicated the lowest mean difference. However, all three histograms showed a Gaussian-like distribution with a small number of outliers and a relatively small bias (mean and median values are close to 0.0 for all cases). The absolute differences ranged between -2.23% to +3.14% for MLR, -1.83% to 2.17% for PLSR and -2.56% to 3.05% for RF.

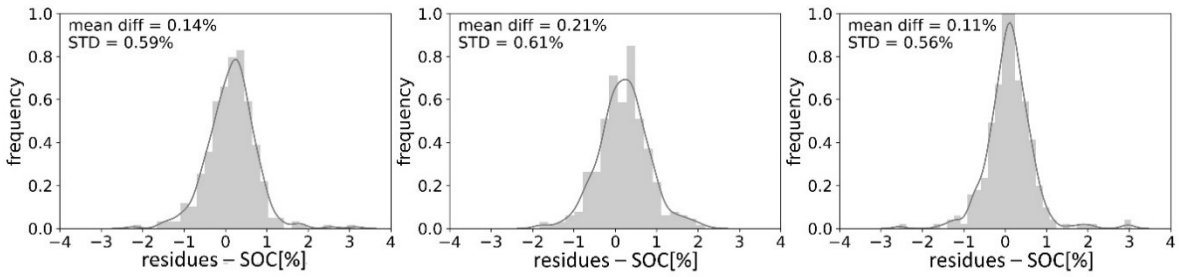

(a) (b) (c)

Figure 3.2.9: Comparison of the difference between the 308 predicted and the measured SOC contents of the external validation dataset using the best set of input data for (a) MLR, (b) PLSR and (c) RF.

3.5 Spatial SOC prediction

Overall, RF using the RI_all dataset provided the best model performance (R2 = 0.67, RPD = 1.77), the highest model accuracy (RMSE = 1.24%) and the lowest mean difference comparing the predicted and the measured SOC contents of the independent external validation dataset (0.11% ± 0.56%). Consequently, the RF based on the RI_all dataset was applied to the whole study area. Figure 3.2.10 shows the spatial prediction results of the RF model.

Most of the study area revealed SOC contents lower than 2.0%, which is comparable to the mean SOC content of the soil datasets (Table 3.2.3). Regions with higher SOC contents (>6.0%) were mainly predicted in the South of Bavaria. Here, several patterns with relatively high SOC contents (>8.0%) are visible. High SOC contents are predicted in the river valleys in the south of the study area and in bogs and marshlands (e.g., Erdinger Moos around the Airport to the northeast of the city Munich or Königsmoos at the northeast of the city Augsburg). This is in line with an SOC map generated for Bavaria using a geostatistical modelling approach that showed the highest SOC stocks in floodplain and bogs [90].

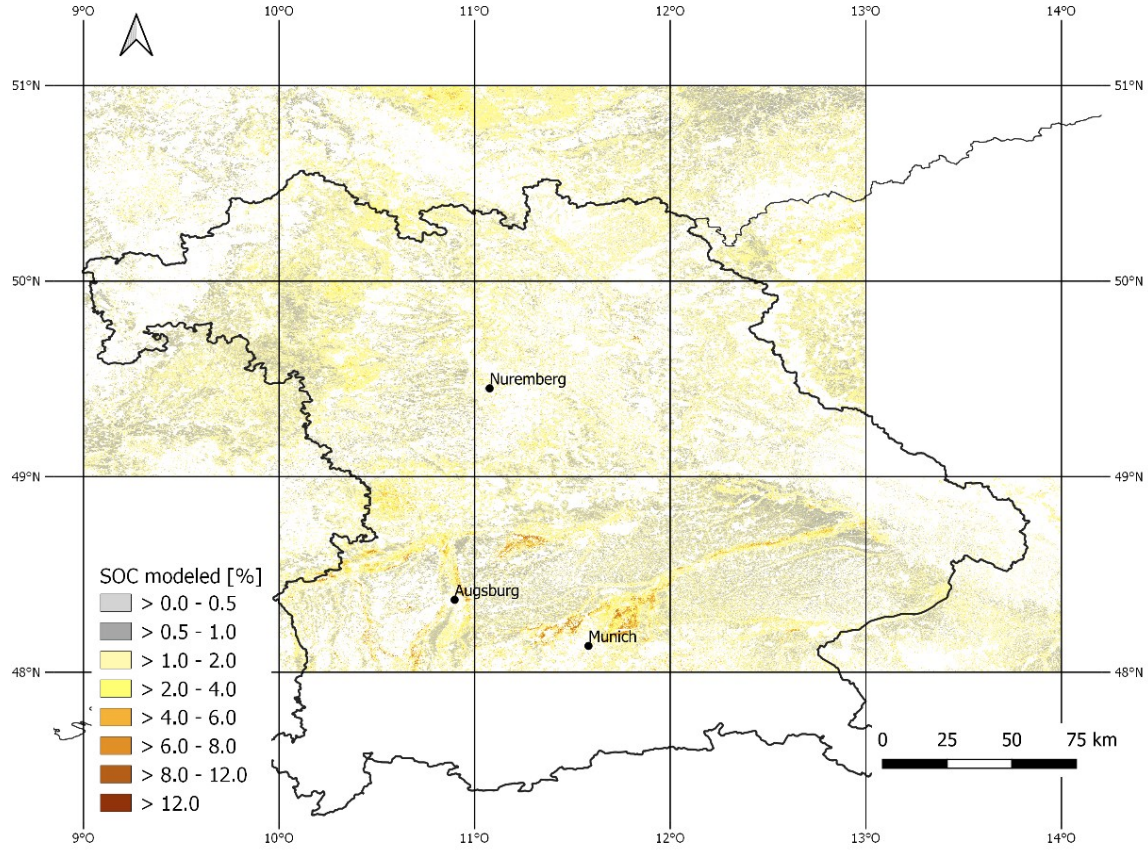

Figure 3.2.10: Spatial prediction of the SOC contents based on the RF (RI_all) model.

4. Discussion

4.1 Spectral/Spatial Filtering

We applied spectral/spatial filtering to enable the link of a 30 m SRC pixel possibly influenced by different spectral information or other artefacts to a single point SOC measurement. The filtering is based on neighborhood relationships by evaluating the spectral information of the

direct neighboring pixel in comparison to the spectral information of the sampling location. It is assumed that the soil sample is representative of the direct surrounding areas.

Due to the analysis of the STDs of all bands of all pixel clusters, all clusters with a heterogenous land cover were identified to be excluded from the input database due to their possible spectral influences. The spatial/spectral filtering has a significant positive effect on the model accuracies.

As shown in Figure 3.2.5, the distribution of the cluster STDs per reflectance band is representing a non-gaussian behavior, which indicates using the median and quantiles is more appropriate. Nevertheless, the selection of the threshold of the 2STD is equal to the 95% quantile for most bands. If the threshold is set using the 95% percentile, additionally six pixel clusters would be excluded and could provide an alternative to the presented method.

In general, the link between EO data with a pixel resolution of several meters and point soil samples provides a challenge for a wide variety of modeling purposes as point information is related to a larger area. The spectral/spatial filtering technique presented can help to identify, in particular, pixels that are not completely within a field boundary and therefore may contain a mixture of several spectral information (e.g., bare soil and vegetation at the edges of fields) for the sample point. As spectral neighborhood relationships of the pixel to which a soil sample is assigned are included in the assessment, the method can also be applied to other areas and is independent of any region or sensor-specific characteristics. The method shown is a simple and robust approach to exclude possibly disturbed pixels from the given data compilation. However, the applicability of the filtering technique has to be evaluated because it might not be best suited for larger or smaller pixel sizes. More suitable approaches that address the issue of linking point information to a pixel with the spatial extent of several meters should be explored.

4.2 Data and Modeling

In contrast to many other studies (Table 3.2.1), we used a bare soil composite consisting of a long time series of spaceborne Landsat imagery. Except for some case studies [25,37,43,48], all other models listed in Table 1 were built for single, cloudless multi- or hyperspectral scenes. In contrast, the SOC contents were predicted for a novel multispectral data source that was based on a large number of input scenes (14,061) for an area of nearly 130,000 km^2. Due to the long compositing period, all variabilities were included, and a stable mean SRC was provided. Small-scale spatial differences due to seasonal soil moisture differences are minimized. Soil moisture differences can have a huge influence on hyperspectral and multispectral remote sensing analysis and are addressed by several authors [91–93]. It hampers the prediction of soil variables from the reflectance spectra [94]. However, the influence of the permanent soil moisture differences regarding the used SRC has to be investigated.

For SOC modeling, three different ML algorithms were used and compared (Table 3.2.4, Figure 3.2.8). Overall, the RF showed the best model performances comparing the R2 (0.62–0.67), RMSE (1.23–1.31), RPD values (1.62–1.77) and CCC results (0.78) for the model validation. However, the results of the RF and PLSR are comparable. Several indices were implemented in order to improve the SOC modeling capabilities. The application of indices is a widely used technique in remote sensing analyses and helps to capture more information, such as band ratios and spectral indices that are, e.g., sensitive to differences in soil properties [44]. As indicated by the model performance (Figure 3.2.8), an improvement can be noted for all three algorithms with the additional use of indices. However, the influence on MLR and PLSR was higher compared to the RF results. In this context, the additionally performed 10-fold cross-validation (Table 3.2.4) showed that a selection of relevant features is not necessarily required for the different ML

algorithms. The PLSR and the RF results using RI_sel showed a small decrease in the model accuracies comparing the RI_all runs.

The model performances (Figure 3.2.8) based on the SCMaP SRC were comparable to the SOC prediction capabilities presented by various authors (Table 3.2.1). However, we covered a distinctly larger area (except for [25]) with a lower soil point density. However, in almost all studies, lower RMSE values were reported for the SOC prediction. The SOC content available for the study area shows a large range (0.26% to 18.3%; Table 3.2.3). A few of the referenced studies were based on a comparable distributed SOC data range. The high RMSEs could be related to the wide range of SOC content in the study area, as indicated by the general underestimation during the calibration stage for high SOC values (Figure 3.2.8). For analyzing the influence of high SOC content, it could be considered to separate organic soils with naturally high SOC contents from mineral soils with lower SOC content. A split of the soil samples regarding their SOC distribution was not considered as there was a small number of soil samples with higher SOC contents (52 samples; SOC content > 6%).

The SOC model performance based on the SCMaP SRC (RPD = 1.24, RMSE = 1.77) was slightly higher compared to the accuracies presented in Table 3.2.1 based on multitemporal Sentinel-2 (RPD = 1.4, RMSE = 0.34 [48], RPD = 1.06–1.68, RMSE = 0.209–0.363 [43], RPD = 0.99–1.53, RMSE = 0.253–0.545 [37]) or Landsat composites (RPD = 0.52–0.58, RMSE = 1.52–1.68 [25], RPD = 1.41, RMSE = 0.28 [48]). However, it must be emphasized that the RMSE's shown are higher compared to the listed studies.

Using a 30-year composite could hamper the mapping of SOC contents if changes occur in the investigation area over time. However, for Bavaria, an analysis of SOC changes of the permanent soil observation sites in Bavaria showed a constant behavior of the SOC contents with relatively low overall changes between 1986 and 2016 [86]. Therefore, the use of a 30-year composite to overcome seasonal soil moisture differences is a reasonable approach to model SOC contents for large geographical areas where SOC changes are limited. Although, further analysis of the compositing technique to overcome seasonal soil moisture differences has to be conducted also with respect to the length of the compositing period. Additionally, for the investigation of SOC changes, the applicability of shorter compositing lengths has to be considered.

4.3 External Validation

In addition to the cross and model validation, we conducted an external validation based on an independent dataset. The predicted and measured SOC contents were compared, and the mean difference was calculated to estimate the accuracy of the modeling. The comparison showed small mean differences for MLR, PLSR and RF (0.11% to 0.21%). However, the SOC distribution of the validation dataset indicated small differences in comparison to the calibration dataset. The calibration dataset stretches between 0.26% and 18.3%, whereas the validation dataset contained samples with SOC contents between 0.55% and 4.65%. Although the majority of the calibration data is represented by the validation samples, very low (0.11% to 0.25%) and very high (4.66% to 18.3%) SOC contents are not included in the validation dataset. The comparison of the predicted SOC contents with the external validation dataset showed a small overestimation of the modeled SOC contents Figure 3.2.9, which has to be considered in the interpretation for the prediction of the entire study area (Figure 3.2.10).

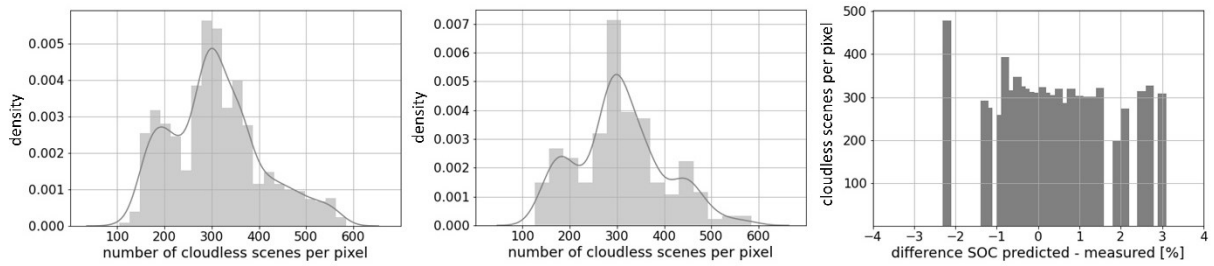

(a) (b) (c)

Figure 3.2.11: The distribution of the number of cloudless scenes per pixel of the calibration (a) and external validation (b) dataset. Plot (c) of the error in prediction (based on the external validation dataset) and measured SOC [%] as a function of cloudless scenes.

To address large-scale SOC predictions (national to European-wide), further standardized validation datasets are needed. However, large-scale SOC maps are mostly available at a lower resolution (250 m to 1 km) and have limited suitability as a basis for validation for the 30 m pixel resolution of the SCMaP SRC database. A different aspect that could be considered for validation is an internal quality measure provided by the number of cloudless scenes per pixel. The usable data availability can be taken into consideration for data validation [51,95]. For the calibration and the validation dataset, an analysis of the number of cloudless observations of all sampling pixels showed a similar distribution (Figure 11a,b). On average, 300 scenes were available for the pixels of the SOC measurements. Both datasets showed a smaller peak on 200 scenes. These pixels are located in areas where the data of one Landsat path row is available. The absolute number of input scenes is smaller there. The smaller peak at 500 scenes per pixel can be related to overlapping areas, where several Landsat path rows are intersecting.

Figure 3.2.11c shows the link between the SOC differences and the distribution of cloudless scenes. The higher differences (< -2% and > 2%) cannot be related to fewer cloudless scenes per pixel as the overall average of 300. These findings indicate that SCMaP captured the exposed soils well at the validation sampling points, and the influence of potentially remaining clouds is minimized and seems not to have any influence.

4.4 SCMaP SRC as Database for Modeling SOC Contents with High Spatial Resolution Covering Large Geographical Areas

In comparison to existing SOC maps (e.g., OCTOP [15], Topsoil Soil Organic Carbon Map based on the LUCAS Soil datasets for EU25 [16] or SoilGrids [96]), SCMaP provides a novel database for the estimation of soil parameters. The compositing approach allows the investigation of all areas which show at least once a bare soil within the observed time period. As the approach was trained using a large database and was successfully validated using independent data, the transferability to large-scale applications is feasible. In addition, high-resolution analysis considering within or between field differences is still possible as the original Landsat pixel size (30 m) is preserved (Figure 12).

As shown in Figures 3.2.10 and 3.2.12, for several areas, relatively high SOC contents were predicted by the RF model. Here, a former peat bog ("Königsmoos") is located, which naturally shows higher SOC contents. Such organic soils naturally contain higher SOC contents (> 18.0%) in comparison to other soils. Most of these peatlands have been drained for agricultural use [97].

A comparison with the soil map 1:200,000 (BUEK200, Federal Institute for Geosciences and Natural Resources, BGR) showed that areas with high predicted SOC contents are mostly fens,

underpinning the correctness of the results. In addition, the qualitative SOC distributions shown in the study area are consistent with the results of SOC mapping in Bavaria shown in [90].

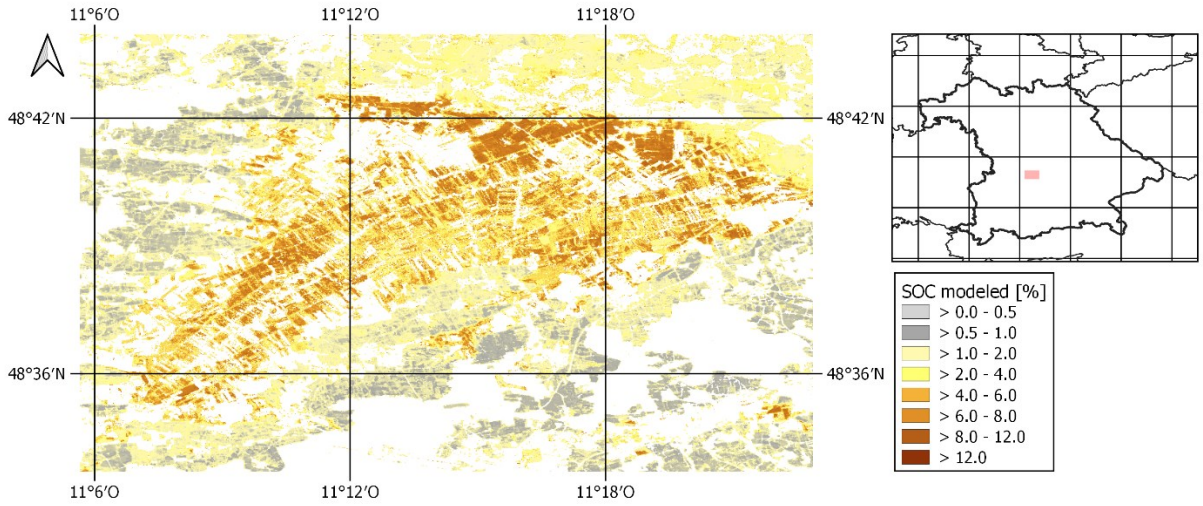

Figure 3.2.12: The spatial distribution of SOC contents for a subset of the investigation data. The prediction possibilities of field scale are visible.

5. Conclusion

The potential of the SCMaP SRC database derived from Landsat images between 1984 and 2014 for large-scale applications with a high spatial resolution was evaluated. We used the SRC to model the spatial SOC distribution of exposed topsoils of croplands in Bavaria. The SRC was correlated with soil point measurements to quantify SOC contents for an area-wide mapping approach. We first developed a spatial/spectral filtering technique to address the challenge of linking a point soil sample to EO data with a pixel resolution of several meters. The results show that a spectral/spatial filtering of heterogenous pixel clusters is improving the SOC modeling.

For SOC quantification, several ML algorithms were applied and compared. The RF showed the highest capabilities to model the SOC content in Bavaria (R2 = 0.67, RMSE = 1.24%, RPD = 1.77). Further, we determined that the use of additional spectral indices compared to the usage of reflectance data alone can improve SOC modeling. In addition to the model validation based on a subset of the data, the best model setups (RI_all) were applied to the entire test area and validated using an external independent dataset (n = 308). The differences between the measured and predicted SOC contents were minor for all three ML algorithms and showed the lowest differences for the RF (0.11% ± 0.56% SOC).

The SCMaP SRC is a promising approach to predict the spatial SOC distribution for mapping a large geographical extent with high resolution at the farm or even the field scale. Nevertheless, for application on a larger scale, a validation approach has to be further developed. Several large-scale SOC products are available, although these maps are distributed on a lower resolution in comparison to the SCMaP capabilities.

Author Contributions: Conceptualization, S.Z. and U.H.; methodology, S.Z., M.B. and B.v.W.; software, S.Z. and M.B.; validation, S.Z., M.B. and M.W.; formal analysis, S.Z.; investigation, S.Z..; data curation, U.H. and S.Z.; writing—original draft preparation, S.Z.; writing—review and editing, S.Z., U.H., M.B., B.v.W., M.W. and M.S.; visualization, S.Z.; supervision, U.H. and B.v.W.; project administration, S.Z.; funding acquisition, U.H. All authors have read and agreed to the published version of the manuscript.

Funding: This research was funded by the German Federal Ministry of Food and Agriculture (BMEL), grant number 281B301816 as part of the Soil-DE Project "Entwicklung von Indikatoren zur Bewertung der Ertragsfähigkeit, Nutzungsintensität und Vulnerabilität landwirtschaftlich genutzter Böden in Deutschland".

Institutional Review Board Statement: Not applicable.

Informed Consent Statement: Not applicable.

Data Availability Statement: Not applicable.

Acknowledgements: We thank the Bavarian agencies, The Bavarian Environment Agency (LfU) and the Bavarian State Research Center for Agriculture (LfL) for providing the soil databases.

Conflicts of Interest: The Authors declare no conflicts of interest.

Appendix A

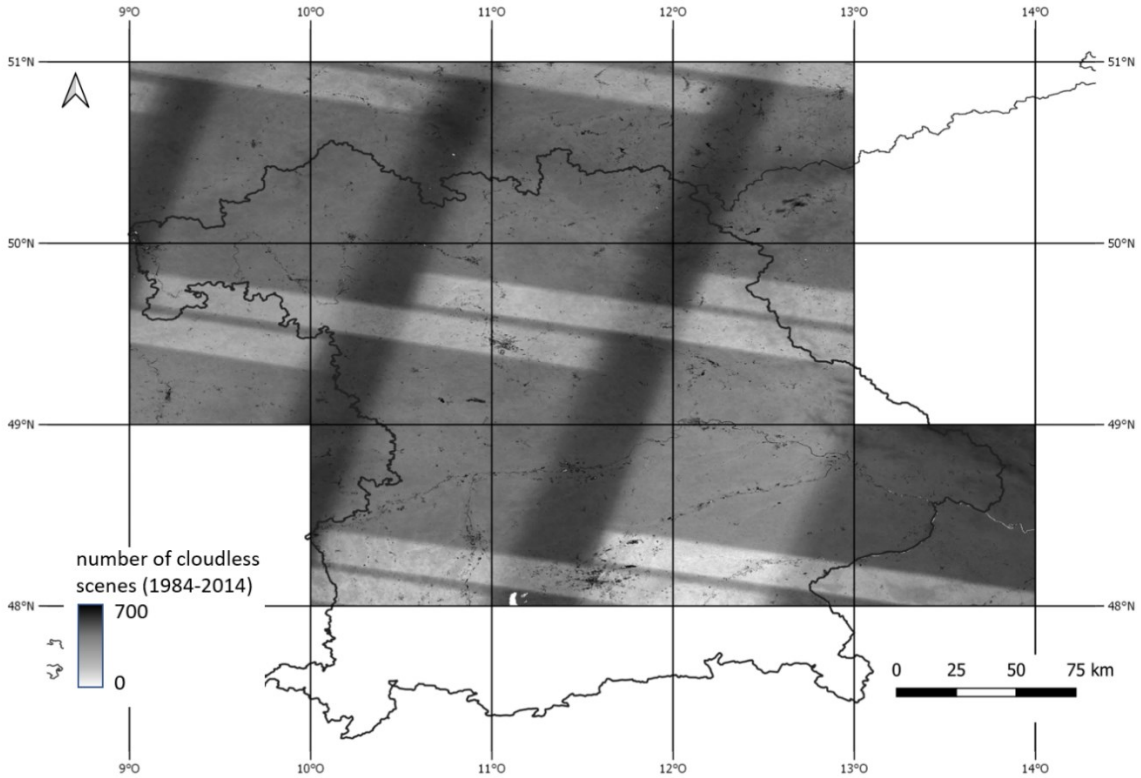

Figure A1: The number of cloudless scenes per pixel for the total composite time (1984-2014) in the investigation area.

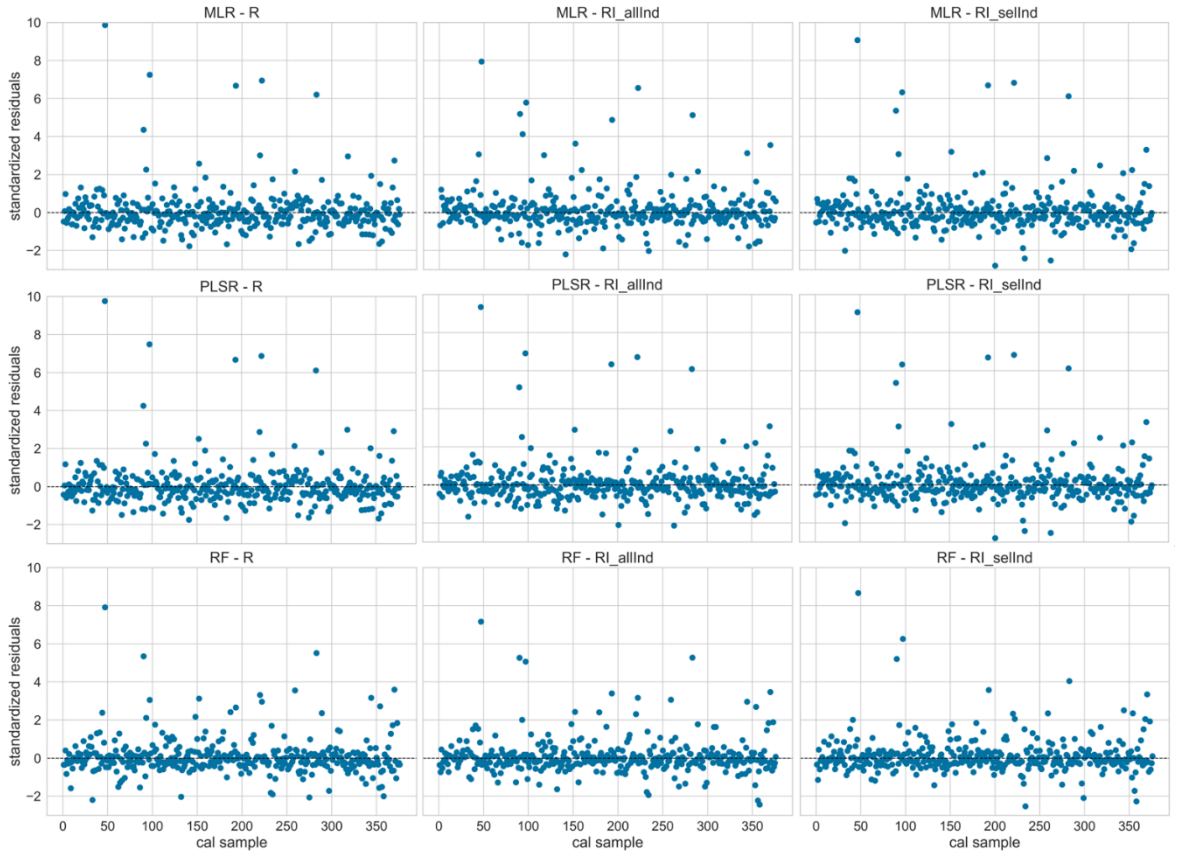

Figure A2: Standardized residuals of the model validation (30% of data points).

Figure A3: Autocorrelation of the prediction residuals of the model validation (30% of data points).

References

1. Lal, R.; Follett, R.F.; Stewart, B.A.; Kimble, J.M. Soil carbon sequestration to mitigate climate change and advance food security. Soil Sci. 2007, 172, 943–956.
2. Lehmann, J.; Hansel, C.M.; Kaiser, C.; Kleber, M.; Maher, K.; Manzoni, S.; Nunan, N.; Reichstein, M.; Schimel, J.P.; Torn, M.S. Persistence of Soil Organic Carbon Caused by Functional Complexity. Nat. Geosci. 2020, 13, 529–534.
3. Jobbágy, E.G.; Jackson, R.B. The vertical distribution of soil organic carbon and its relation to climate and vegetation. Ecol. Appl. 2000, 10, 423–436.
4. Scharlemann, J.P.; Tanner, E.V.; Hiederer, R.; Kapos, V. Global soil carbon: Understanding and managing the largest terrestrial carbon pool. Carbon Manag. 2014, 5, 81–91.
5. Wiesmeier, M.; Urbanski, L.; Hobley, E.; Lang, B.; von Lützow, M.; Marin-Spiotta, E.; van Wesemael, B.; Rabot, E.; Ließ, M.; Garcia-Franco, N. Soil organic carbon storage as a key function of soils—A review of drivers and indicators at various scales. Geoderma 2019, 333, 149–162.
6. Loveland, P.; Webb, J. Is there a critical level of organic mattes in the agricultural soils of temperate regions: A review. Soil Tillage Res. 2003, 70, 1–18.
7. Lal, R. Soil Health and carbon management. Food Energy Secur. 2016, 5, 212–222.
8. Gregorich, E.G.; Carter, M.R.; Angers, D.A.; Monreal, C.M.; Ellert, B. Towards a minimum data set to assess soil organic matter quality in agricultural soils. Can. J. Soil Sci. 1994, 74, 367–385.
9. Lal, R. Digging deeper: A holistic perspective of factors affecting soil organic carbon sequestration in agroecosystems. Glob. Chang. Biol. 2018, 24, 3285–3301.
10. Lorenz, K.; Lal, R.; Ehlers, K. Soil organic carbon stock as an indicator for monitoring land and soil degradation in relation to United Nations' Sustainable Development Goals. Land Degrad. Dev. 2019, 30, 824–838.
11. Gollany, H.T.; Venterea, R.T. Measurements and models to identify agroecosystem practices that enhance soil organic carbon under changing climate. J. Environ. Qual. 2018, 47, 579–587.
12. Paustian, K.; Collier, S.; Baldock, J.; Burgess, R.; Creque, J.; DeLonge, M.; Dungait, J.; Ellert, B.; Frank, S.; Goddard, T.; et al. Quantifying carbon for agricultural soil management: From the current status toward a global soil information system. Carbon Manag. 2019, 10, 567–587.
13. Jandl, R.; Rodeghiero, M.; Martinez, C.; Cotrufo, M.F.; Bampa, F.; van Wesemael, B.; Harrison, R.B.; Guerrini, I.A.; Richter, D.D.; Rustad, L.; et al. Current status, uncertainty and future needs in soil organic carbon monitoring. Sci. Total. Environ. 2014, 468–469, 376–383.
14. Miller, B.A.; Schaetzl, R.J. The historical role of base maps in soil geography. Geoderma 2014,230–231, 329–339.
15. Jones, R.J.A.; Hiederer, R.; Rusco, E.; Montanarella, L. Estimating organic carbon in the soils of Europe for policy support. Eur. J. Soil Sci. 2005, 56, 655–671.
16. de Brogniez, D.; Ballabio, C.; Stevens, A.; Jones, R.J.A.; Montanarella, L.; van Wesemael, B. A Map of the Topsoil Organic Carbon Content of Europe Generated by a Generalized Additive Model. Eur. J. Soil Sci. 2015, 66, 121–134.
17. Crucil, G.; Castaldi, F.; Aldana-Jague, E.; van Wesemael, B.; Macdonald, A.; Van Oost, K. Assessing the performance of UAScompatible multispectral and hyperspectral sensors for soil organic carbon prediction. Sustainability 2019, 11, 1889.
18. Ben-Dor, E.; Chabrillat, S.; Demattê, J.A.M.; Taylor, G.R.; Hill, J.; Whiting, M.L.; Sommer, S. Using imaging spectroscopy to study soil properties. Remote. Sens. Environ. 2009, 113, S38–S55.
19. Bartholomeus, H.; Kooistra, L.; Stevens, A.; van Leeuwen, M.; van Wesemael, B.; Ben-Dor, E.; Tychon, B. Soil organic carbon mapping of partially vegetated agricultural fields with imaging spectroscopy. Int. J. Appl. Earth Obs. Geoinf. 2011, 13, 81–88.
20. Bayer, A.D.; Bachmann, M.; Rogge, D.; Muller, A.; Kaufmann, H. Combining field and imaging spectroscopy to map soil organic carbon in a semiarid environment. IEEE J. Sel. Top. Appl. Earth Obs. Remote. Sens. 2016, 9, 3997–4010.
21. Chabrillat, S.; Ben-Dor, E.; Cierniewski, J.; Gomez, C.; Schmid, T.; van Wesemael, B. Imaging spectroscopy for soil mapping and monitoring. Surv. Geophys. 2019, 40, 361–399. [CrossRef]
22. Castaldi, F.; Hueni, A.; Chabrillat, S.; Ward, K.; Buttafuoco, G.; Bomans, B.; Vreys, K.; Brell, M.; van Wesemael, B. Evaluating the capability of the Sentinel 2 data for soil organic carbon prediction in croplands. ISPRS J. Photogramm. Remote. Sens. 2019, 147, 267–282.
23. Vaudour, E.; Gomez, C.; Fouad, Y.; Lagacherie, P. Sentinel-2 image capacities to predict common topsoil properties of temperate and Mediterranean agroecosystems. Remote. Sens. Environ. 2019, 223, 21–33.
24. Wang, X.; Zhang, Y.; Atkinson, P.M.; Yao, H. Predicting soil organic carbon content in Spain by combining landsat TM and ALOS PALSAR images. Int. J. Appl. Earth Obs. Geoinf. 2020, 92, 102182.

25. Safanelli, J.L.; Chabrillat, S.; Ben-Dor, E.; Demattê, J.A.M. Multispectral models from bare soil composites for mapping topsoil properties over Europe. Remote Sens. 2020, 12, 1369.
26. Diek, S.; Fornallaz, F.; Schaepman, M.E.; De Jong, R. Barest pixel composite for agricultural areas using Landsat time series. Remote Sens. 2017, 9, 1245.
27. Demattê, J.A.M.; Fongaro, C.T.; Rizzo, R.; Safanelli, J.L. Geospatial Soil Sensing System (GEOS3): A powerful data mining procedure to retrieve soil spectral reflectance from satellite images. Remote Sens. Environ. 2018, 212, 161–175.
28. Demattê, J.A.M.; Safanelli, J.L.; Poppiel, R.R.; Rizzo, R.; Silvero, N.E.Q.; de Sousa Mendes, W.; Bonfatti, B.R.; Dotto, A.C.; Salazar, D.F.U.; de Oliveira Mello, F.A.; et al. Bare Earth's surface spectra as a proxy for soil resource monitoring. Sci. Rep. 2020, 10, 4461.
29. Hansen, M.C.; Egorov, A.; Roy, D.P.; Potapov, P.; Ju, J.; Turubanova, S.; Kommareddy, I.; Loveland, T.R. Continuous fields of land cover for the conterminous United States using Landsat data: First results from the Web-Enabled Landsat Data (WELD) project. Remote Sens. Lett. 2011, 2, 279–288.
30. White, J.C.; Wulder, M.A.; Hobart, G.W.; Luther, J.E.; Hermosilla, T.; Griffiths, P.; Coops, N.C.; Hall, R.J.; Hostert, P.; Dyk, A.; et al. Pixel-based image compositing for large-area dense time series applications and science. Can. J. Remote Sens. 2014, 40, 192–212.
31. Hermosilla, T.; Wulder, M.A.; White, J.C.; Coops, N.C.; Hobart, G.W. An integrated Landsat time series protocol for change detection and generation of annual gap-free surface reflectance composites. Remote. Sens. Environ. 2015, 158, 220–234.
32. Griffiths, P.; Nendel, C.; Hostert, P. Intra-annual reflectance composites from Sentinel-2 and Landsat for national-scale crop and land cover mapping. Remote Sens. Environ. 2019, 220, 135–151.
33. Loiseau, T.; Chen, S.; Mulder, V.L.; Dobarco, M.R.; Richer-de-Forges, A.C.; Lehmann, S.; Bourennane, H.; Saby, N.P.; Martin, M.P.; Vaudour, E. Satellite data integration for soil clay content modelling at a national scale. Int. J. Appl. Earth Obs. Geoinf. 2019, 82, 101905.
34. Adams, B.; Iverson, L.; Matthews, S.; Peters, M.; Prasad, A.; Hix, D.M. Mapping forest composition with Landsat time series: An evaluation of seasonal composites and harmonic regression. Remote Sens. 2020, 12, 610. [CrossRef]
35. Wulder, M.A.; White, J.C.; Loveland, T.R.; Woodcock, C.E.; Belward, A.S.; Cohen, W.B.; Fosnight, E.A.; Shaw, J.; Masek, J.G.; Roy, D.P. The global Landsat archive: Status, consolidation, and direction. Remote Sens. Environ. 2016, 185, 271–283. [CrossRef]
36. Rogge, D.; Bauer, A.; Zeidler, J.; Mueller, A.; Esch, T.; Heiden, U. Building an exposed soil composite processor (SCMaP) for mapping spatial and temporal characteristics of soils with Landsat imagery (1984–2014). Remote. Sens. Environ. 2018, 205, 1–17.
37. Vaudour, E.; Fomez, C.; Lagacherie, P.; Loiseau, T.; Baghdadi, N.; Urbina-Salazar, D.; Loubet, B.; Arrouays, D. Temporal mosaicking approaches of Sentinel-2 images for extending organic carbon content mapping in croplands. Int. J. Appl. Earth Obs. Geoinf. 2021, 96, 102277.
38. Weigand, M.; Staab, J.; Wurm, M.; Taubenböck, H. Spatial and semantic effects of LUCAS samples on fully automated land use/land cover classification in high-resolution Sentinel-2 data. Int. J. Appl. Earth Obs. Geoinf. 2020, 88, 102065.
39. Castaldi, F.; Palombi, A.; Santini, F.; Pascucci, S.; Pignatti, S.; Casa, R. Evaludation of the potential of the current and forthcoming multispectral and hyperspectral imagers to estimate soil texture and organic carbon. Remote Sens. Environ. 2016, 179, 54–65.
40. Castaldi, F.; Chabrillat, S.; Jones, A.; Vreys, K.; Bomans, B.; van Wesemael, B. Soil organic carbon estimation in croplands by hyperspectral remote APEX data using the LUCAS topsoil database. Remote Sens. 2018, 10, 153.
41. Castaldi, F.; Chabrillat, S.; Don, A.; van Wesemael, B. Soil organic carbon mapping using LUCAS topsoil database and Sentinel-2 data: An approach to reduce soil moisture and crop residue effects. Remote Sens. 2019, 11, 2121.
42. Castaldi, F.; Chabrillat, S.; van Wesemael, B. Sampling strategies for soil property mapping using multispectral Sentinel-2 and hyperspectral EnMAP satellite data. Remote Sens. 2019, 11, 309.
43. Dvorakova, K.; Heiden, U.; van Wesemael, B. Sentinel-2 exposed soil composite for soil organic carbon prediction. Remote Sens. 2021, 13, 1791.
44. Gholizadeh, A.; Žižala, D.; Saberioon, M.; Bor˚uvka, L. Soil organic carbon and texture retrieving and mapping using proximal, airborne and Sentinel-2 spectral imaging. Remote Sens. Environ. 2018, 218, 89–103.
45. Hbirkou, C.; Pätzold, S.; Mahlein, A.-K.; Welp, G. Airborne hyperspectral imaging of spatial soil organic carbon heterogeneity at the field-scale. Geoderma 2012, 175–176, 21–28.
46. Selige, T.; Böhner, J.; Schmidhalter, U. High resolution topsoil mapping using hyperspectral image and field data in multivariate regression modeling procedures. Geoderma 2006, 136, 235–244.

47. Vaudour, E.; Gomez, C.; Loiseau, T.; Baghdadi, N.; Loubet, B.; Arrouays, D.; Ali, L.; Lagacherie, P. The impact of acquisition date on the prediction performance of topsoil organic carbon from Sentinel-2 for croplands. Remote Sens. 2019, 11, 2143.
48. Žížala, D.; Minaˇrík, R.; Zádorová, T. Soil organic carbon mapping using multispectral remote sensing data: Prediction ability of data with different spatial and spectral resolutions. Remote Sens. 2019, 11, 2947.
49. Wiesmeier, M.; Hübner, R.; Barthold, F.; Spörlein, P.; Geuß, U.; Hangen, E.; Reischl, A.; Schilling, B.; von Lützow, M.; KögelKnabner, I. Amount, distribution and driving factors of soil organic carbon and nitrogen in cropland and grassland soils of Southeast Germany (Bavaria). Agric. Ecosyst. Environ. 2013, 176, 39–52.
50. Wrb, I.W.G. World reference base for soil resources 2015. World Soil Resour. Rep. 2015, 103, 128.
51. Zepp, S.; Jilge, M.; Metz-Marconcini, A.; Heiden, U. The influence of vegetation index thresholding on EO-based assessments of exposed soil masks in Germany between 1984 and 2019. ISPRS J. Photogramm. Remote. Sens. 2021, 178, 366–381.
52. Wulder, M.A.; Loveland, T.R.; Roy, D.P.; Crawford, C.J.; Masek, J.G.; Woodcock, C.E.; Allen, R.G.; Anderson, M.C.; Belward, A.S.; Cohen, W.B.; et al. Current status of Landsat program, science, and applications. Remote Sens. Environ. 2019, 225, 127–147.
53. Zhu, Z.; Woodcock, C.E. Object-based cloud and cloud shadow detection in Landsat imagery. Remote Sens. Environ. 2012, 118, 89–98.
54. Zhu, Z.; Wang, S.; Woodcock, C.E. Improvement and expansion of the Fmask algorithm: Cloud, cloud shadow, and snow detection for Landsat 4-7, 8 and Sentinel-2 images. Remote Sens. Environ. 2015, 159, 269–277.
55. Richter, R.; Schläpfer, D. Atmospheric/Topographic Correction for Satellite Imagery/ATCOR-2/3 User Guide, Version 8.3.1; ReSe Applications Schläpfer Langeggweg: Wil, Switzerland, 2014; Volume 3.
56. Van Deventer, A.P.; Ward, A.D.; Gowda, P.H.; Lyon, J.G. Using thematic mapper data to identify contrasting soil plains and tillage practices. Photogramm. Eng. Remote Sens. 1997, 63, 87–93.
57. Escadafal, R. Remote sensing of arid soil surface color with Landsat thematic mapper. Adv. Space Res. 1989, 9, 159–163.
58. Huete, A.; Didan, K.; Miura, T.; Rodriguez, E.P.; Gao, X.; Ferreira, L.G. Overview of the radiometric and biophysical performance of the MODIS vegetation indices. Remote Sens. Environ. 2002, 83, 195–213.
59. Key, C.H.; Benson, N.C. Landscape Assessment (LA). In FIREMON: Fire Effects Monitoring and Inventory System; Gen. Tech. Rep. RMRS-GTR-164-CD; Lutes, D.C., Keane, R.E., Caratti, J.F., Key, C.H., Benson, N.C., Sutherland, S., Gangi, L.J., Eds.; US Department of Agriculture, Forest Service, Rocky Mountain Research Station: Fort Collins, CO, USA, 2006; p. LA-1-55 2006, 164.
60. Qi, J.; Kerr, Y.; Chehbouni, A. External factor consideration in vegetation index development. Proc. Phys. Meas. Signat. Remote Sens. ISPRS 1994, 723, 730.
61. Xiao, X.; Zhang, Q.; Braswell, B.; Urbanski, S.; Boles, S.; Wofsy, S.; Moore III, B.; Ojima, D. Modeling gross primary production of temperate deciduous broadleaf forest using satellite images and climate data. Remote Sens. Environ. 2004, 91, 256–270.
62. Rogers, A.S.; Kearney, M.S. Reducing signature variability in unmixing coastal marsh thematic mapper scenes using spectral indices. Int. J. Remote. Sens. 2004, 25, 2317–2335.
63. Pouget, M.; Madeira, J.; Le Floch, E.; Kamal, S. Caracteristiques spectrales des surfaces sableuses de la Region Cotiere Nord-Ouest de l'Egypte. Appl. Aux Donnees Satell. SPOT 1990, 4–6.
64. Chen, W.; Liu, L.; Zhang, C.; Wang, J.; Wang, J.; Pan, Y. Monitoring the seasonal bare soil areas in Beijing using multitemporal TM images. In Proceedings of the IGARSS 2004. 2004 IEEE International Geoscience and Remote Sensing Symposium, Anchorage, AK, USA, 20–24 September 2004; Volume 5, pp. 3379–3382.
65. Nellis, M.D.; Briggs, J.M. Transformed vegetation index for measuring spatial variation in drought impacted biomass on Konza Prairie, Kansas. Trans. Kans. Acad. Sci. 1992, 95, 93.
66. Tucker, C.J. Red and photographic infrared linear combinations for monitoring vegetation. Remote Sens. Environ. 1979, 8, 127–150.
67. Jordan, C.F. Derivation of leaf-area index from quality of light on the forest floor. Ecology 1969, 50, 663–666.
68. Gitelson, A.A.; Kaufman, Y.J.; Merzlyak, M.N. Use of a green channel in remote sensing of global vegetation from EOS-MODIS. Remote Sens. Environ. 1996, 58, 289–298.
69. Marsett, R.C.; Qi, J.; Heilman, P.; Biedenbender, S.H.; Watson, M.C.; Amer, S.; Weltz, M.; Goodrich, D.; Marsett, R. Remote sensing for grassland management in the arid southwest. Rangel. Ecol. Manag. 2006, 59, 530–540.
70. Rouse, J.W.; Haas, R.H.; Schell, J.A.; Deering, D.W. Monitoring vegetation systems in the great plains with ERTS proceeding. In Proceedings of the Third Earth Reserves Technology Satellite Symposium, Washington, DC, USA, 10–14 December 1973; Volume 30103017.

71. Tian, Y.; Yan, Z.; Weixing, C. Monitoring soluble sugar, total nitrogen & its ratio in wheat leaves with canopy spectral reflectance. Zuo Wu Xue Bao 2005, 31, 355–360.
72. Rondeaux, G.; Steven, M.; Baret, F. Optimization of soil-adjusted vegetation indices. Remote Sens. Environ. 1996, 55, 95–107.
73. Huete, A.; Huete, A.R. A Soil-Adjusted Vegetation Index (SAVI). Remote Sens. Environ. 1988, 25, 295–309.
74. Wold, S.; Sjöström, M.; Eriksson, L. PLS-Regression: A basic tool of chemometrics. Chemom. Intell. Lab. Syst. 2001, 58, 109–130.
75. Breiman, L. Random forests. Mach. Learn. 2001, 45, 5–32.
76. da Silva Chagas, C.; de Carvalho Junior, W.; Bhering, S.B.; Calderano Filho, B. Spatial prediction of soil surface texture in a semiarid region using random forest and multiple linear regressions. Catena 2016, 139, 232–240.
77. Jiang, Q.; Chen, Y.; Guo, L.; Fei, T.; Qi, K. Estimating soil organic carbon of cropland soil at different levels of soil moisture using VIS-NIR spectroscopy. Remote Sens. 2016, 8, 755.
78. Ward, K.J.; Chabrillat, S.; Neumann, C.; Foerster, S. A remote sensing adapted approach for soil organic carbon prediction based on the spectrally clustered LUCAS soil database. Geoderma 2019, 353, 297–307.
79. Xie, X.; Wu, T.; Zhu, M.; Jiang, G.; Xu, Y.; Wang, X.; Pu, L. Comparison of random forest and multiple linear regression models for estimation of soil extracellular enzyme activities in agricultural reclaimed coastal saline land. Ecol. Indic. 2021, 120, 106925.
80. Pedregosa, F.; Varoquaux, G.; Gramfort, A.; Michel, V.; Thirion, B.; Grisel, O.; Blondel, M.; Prettenhofer, P.; Weiss, R.; Dubourg, V. Scikit-learn: Machine learning in python. J. Mach. Learn. Res. 2011, 12, 2825–2830.
81. Chang, C.-W.; Laird, D.A. Near-infrared reflectance spectroscopic analysis of soil C and N. Soil Sci. 2002, 167, 110–116.
82. Lin, L.I.-K. A Concordance correlation coefficient to evaluate reproducibility. Biometrics 1989, 45, 255–268.
83. Chong, I.-G.; Jun, C.-H. Performance of some variable selection methods when multicollinearity is present. Chemom. Intell. Lab. Syst. 2005, 78, 103–122.
84. Hobley, E.; Wilson, B.; Wilkie, A.; Gray, J.; Koen, T. Drivers of soil organic carbon storage and vertical distribution in Eastern Australie. Plant. Soil 2015, 390, 111–127.
85. Hobley, E.U.; Baldock, J.; Wilson, B. Environmental and human influences on organic carbon fractions down the soil profile. Agric. Ecosyst. Environ. 2016, 223, 152–166.
86. Kühnel, A.; Wiesmeier, M.; Kögel-Knabner, I.; Spörlein, P. Veränderungen der Humusqualität und -Quantität Bayerischer Böden im Klimawandel; Umwelt Spezial; Bayerisches Landesamt für Umwelt: Hof, Germany, 2020.
87. Tóth, G.; Jones, A.; Montanarella, L. LUCAS Topsoil Survey: Methodology, Data and Results; Publications Office: Luxembourg, 2013; ISBN 92-79-32542-6.
88. Wiesmeier, M.; Spörlein, P.; Geuß, U.W.E.; Hangen, E.; Haug, S.; Reischl, A.; Schilling, B.; von Lützow, M.; Kögel-Knabner, I. Soil organic carbon stocks in Southeast Germany (Bavaria) as affected by land use, soil type and sampling depth. Glob. Chang. Biol. 2012, 18, 2233–2245.
89. Origazzi, A.; Ballabio, C.; Panagos, P.; Jones, A.; Fernández-Ugalde, O. LUCAS soil, the largest expandable soil dataset for Europe: A review. Eur. J. Soil Sci. 2018, 69, 140–153.
90. Wiesmeier, M.; Schad, P.; von Lützow, M.; Poeplau, C.; Spörlein, P.; Geuß, U.; Hagen, E.; Reischl, A.; Schilling, B.; Kögel-Knabner, I. Quantification of functional soil organic carbon pools for majow soil units and land uses in southeast Germany (Bavaria). Agric. Ecosyst. Environ. 2014, 185, 208–220.
91. Lobell, D.B.; Asner, G.P. Moisture effects on soil reflectance. Soil Sci. Soc. Am. J. 2002, 66, 722 727.
92. Haubrock, S.-N.; Chabrillat, S.; Lemmnitz, C.; Kaufmann, H. Surface soil moisture quantification models from reflectance data under field conditions. Int. J. Remote. Sens. 2008, 29, 3–29.
93. Nocita, M.; Stevens, A.; Noon, C.; van Wesemael, B. Prediction of soil organic carbon for different levels of soil moisture using vis-NIR spectroscopy. Geoderma 2013, 199, 37–42.
94. Castaldi, F.; Palombo, A.; Pascucci, S.; Pignatti, S.; Santini, F.; Casa, R. Reducing the influence of soil moisture on the estimation of clay from hyperspectral data: A case study using simulated PRISMA data. Remote Sens. 2015, 7, 15561–15582.
95. Mzid, N.; Pignatti, S.; Huang, W.; Casa, R. An analysis of bare soil occurrence in arable croplands for remote sensing topsoil applications. Remote Sens. 2021, 13, 474.
96. Hengl, T.; de Jesus, J.M.; Heuvelink, G.B.M.; Gonzalez, M.R.; Kilibarda, M.; Blagotíc, A.; Shangguan, W.; Wright, M.N.; Geng, X.; Bauer-Marschallinger, B.; et al. SoilGrids250m: Global gridded soil information based on machine learning. PLoS ONE 2017, 12, e0169748.
97. Säurich, A.; Tiemeyer, B.; Don, A.; Fiedler, S.; Bechtold, M.; Amelung, W.; Freibauer, A. Drained organic soils under agriculture —The more degraded the soil the higher the specific basal respiration. Geoderma 2019, 355, 113911.

3.3. Scientific Publication III: Optimized Bare Soil Compositing for Soil Organic Carbon Monitoring of Topsoil Croplands in Bavaria

Reference: Zepp, S., U. Heiden, M. Bachmann, M. Möller, M. Wiesmeier, B. van Wesemael. Optimized Bare Soil Compositing for Soil Organic Carbon Monitoring of Topsoil Croplands in Bavaria using Landsat. ISPRS Journal of Photogrammetry and Remote Sensing, 2023, 202, 287-302.

https://doi.org/10.1016/j.isprsjprs.2023.06.003

Status: published

Author`s contribution: **SZ**: Conceptualization, Methodology, Software, Data curation, Writing – Original Draft, Visualization, Project administration. **UG**: Conceptualization, Writing – Review & Editing, Supervision, Funding acquisition, **MB**: Validating, Writing – Review & Editing. **MM**: Validating, Writing – Review & Editing. **MW**: Validating, Writing – Review & Editing. **BvW**: Validating, Writing – Review & Editing, Supervision.

Scope of the journal: The ISPRS Journal of Photogrammetry and Remote Sensing (P&RS) is the official journal of the International Society for Photogrammetry and Remote Sensing (ISPRS). The Journal provides a channel of communication for scientists and professionals in all countries working in the many disciplines that employ photogrammetry, remote sensing, spatial information systems, computer vision, and related fields. The Journal is designed to serve as a source reference and archive of advancements in these disciplines.

5-year impact factor: 12.7 (2022)

The following chapter contains the manuscript submitted to the journal at the time of thesis submission. The article has in the meantime been accepted and published.

Article

Optimized Bare Soil Compositing for Soil Organic Carbon Monitoring of Topsoil Croplands in Bavaria using Landsat

Simone Zepp [a *], Uta Heiden [b], Marin Bachmann [a], Markus Möller [c], Martin Wiesmeier [d], Bas van Wesemael [e]

[a] German Aerospace Center (DLR), German Remote Sensing Data Center (DFD), Muenchener Str. 20, 82234 Wessling, Germany

[b] German Aerospace Center (DLR), Remote Sensing Technology Institute (IMF), Muenchener Str. 20, 82234 Wessling, Germany

[c] Julius Kühn-Institut (JKI), Federal Research Center for Cultivated Plants, Institute for Crop and Soil Science, Bundesallee 58, 38116 Braunschweig, Germany

[d] Bavarian State Research Center for Agriculture, Institute for Organic Farming, Soil and Resource Management, Lange Point 6, 85354 Freising, Germany

[c] Georges Lemaître Centre for Earth and Climate Research, Earth and Life Institute, Université Catholique de Louvain, 1348 Louvain-la-Neuve, Belgium.

[*] Corresponding author at: German Aerospace Center (DLR), Muenchener Str. 20, 82234 Wessling, Germany

Received: 21. November 2022; Accepted: 10 June 2023; Published: 29 June 2023

Abstract: Soil Organic Carbon (SOC) is an indicator for soil degradation, soil health of croplands and has the potential to mitigate climate change. Induced by recent policy initiatives, awareness for high resolution SOC maps and monitoring of changes is increasing. To quantify SOC contents for area-wide mapping approaches with at least a field resolution, Earth Observation is a valuable data source. Compositing techniques of multi-temporal image archives are widely used to overcome the limitation of vegetation cover of fields during the overpass of the satellite. Comparing current bare soil compositing approaches, two aspects are of particular importance: 1) the index for bare soil selection and 2) the length of the compositing period.

Here, we applied the Soil Composite Mapping Processor (SCMaP) to the Landsat archive data between 2005 and 2019 to optimize parameters for bare soil compositing using images covering Bavaria, Germany. We implemented three spectral indices (PV+BLUE, PV+IR2, and NBR2) for soil reflectance composite (SRC) generation in the SCMaP chain. A validation of the extracted bare soil dates with field observations and phenological information from the crop calendar showed a reliable extraction of bare soil dates for all three indices. Due to the crops in the investigation area spring and autumn months showed the highest proportion of correctly selected bare soil dates. We also analyzed the SOC modeling capabilities of different composed SRCs in combination with available legacy data. In comparison to a seasonal pre-selection of the scenes (spring and autumn months) included in the SRC, the different indices showed a minor influence on SOC modeling. Furthermore, we compared the SOC model capabilities for different SRC compositing lengths (3-, 5-, 7-, 10- and 15-years). Overall, PV+BLUE performed best (R^2: 0.56 – 0.72, RMSE: 1.09 – 1.29%, RPD: 1.51 – 1.91). For PV+BLUE and PV+IR2 longer compositing lengths (from three to 15 years) resulted in an increase of the model accuracies and performances. However, for NBR2 this was not as clear. Based on the results at least a 5-year compositing period is required for SOC monitoring purposes using Landsat data.

Keywords: SOC monitoring, soil reflectance composites, Landsat, soil reflectance, SCMaP, crop phenology, croplands

1. Introduction

The resource soil is at the heart of the sustainability paradigm for human development [Bouma et al. 2019]. In particular, soil organic carbon (SOC) is a crucial soil parameter [Wiesmeier et al. 2019], which can be seen as an indicator for soil degradation [Lorenz et al. 2019], soil health [Lal 2016], and crop yields [Lal 2020]. Equally significant to mention is the fact that the organic carbon stocks in soils are considered as the largest terrestrial reservoirs in the global carbon cycle [Batjes 1996, Jobbgay and Jackson 2000, Denman et al. 2007, Scharlemann et al. 2014] and are an essential parameter for controlling greenhouse gas dynamics [Roy et al. 2022]. Due to its critical role, a high spatiotemporal resolution of SOC distribution and its dynamics in farmlands is decisive for quantifying the role of SOC [Castaldi et al. 2021, Zhou et al. 2021]. In this context, standardized data with a high spatial resolution and a full coverage of large areas are particularly valuable [Jandl et al. 2014], but hardly available [Heuvelink et al. 2021]. In recent years, SOC contents have been intensively studied in croplands mainly using traditional methods based on laboratory analyses of soil samples collected in the field [Nocita et al. 2013]. Existing soil maps such as the Harmonized World Soil Database (1:5,000,000 [Nachtergaele et al. 2009]) or the pan-European SOC maps, provided by the European Soil Data Center (ESDAC [Jones et al. 2005, de Brogniez et al. 2015]), do not yet fulfill the high spatial resolution required for adequate monitoring. In general, the scale is too coarse (250 m to 1 km raster) for analysis at the farm or even the field scale. Several policies, such as the European Green Deal or the EU Soil Strategy for 2030 call for a monitoring program to investigate soil degradation and the general current negative trend of soil health [Montanarella and Panagos 2021]. Monitoring of SOC also in agricultural soils integrating new mapping strategies are addressed. Moreover, the detection of SOC changes requires high temporal resolution in addition to field-scale analysis. However, as Heuvelink et al. [2021] pointed out, there are only a few studies on modelling and mapping temporal variation in SOC. In fact, most maps and databases represent only SOC contents of a single time period.

Earth Observation (EO) is a valuable data source for an area-wide soil mapping to distinguish patterns between or even within fields and is also applicable for monitoring over time. Especially spaceborne multispectral mapping missions (e.g., Landsat and Sentinel-2) allow estimations of SOC changes due to their recurring acquisitions. Several authors used hyperspectral [e.g., Ben-Dor et al. 2009, Bartholomeus et al. 2011, Bayer et al. 2016, Chabrillat et al. 2019] or multispectral datasets to derive SOC contents [e.g., Castaldi et al. 2019 b, Vaudour et al. 2019 b, Wang et al. 2020]. They acquired reflectance values by the remote sensing instrument and correlated these with soil point information using spectral and/or digital soil modeling techniques. Mapping of soils and the subsequent SOC estimation is challenging due to temporal or permanent vegetation as well as crop residue cover [Dematte et al. 2018]. Compositing techniques of multi-temporal image archives are widely used to overcome the limitation of vegetation or residue cover of cropland fields during the overpass of the satellite [e.g., Hansen et al. 2011, White et al. 2014, Hermosilla et al. 2015, Diek et al. 2017, Griffiths et al. 2019, Loiseau et al. 2019, Adams et al. 2020, Dematte et al. 2020, Safanelli et al. 2020, Vaudour et al. 2021]. The spatiotemporal averaging of exposed soil occurrences allows the processing of a spatially enhanced data source for SOC modeling. In recent years several compositing techniques were developed and applied for soil analysis [e.g., Diek et al. 2017, Rogge et al 2018, Dematte et al. 2020, Castaldi et al 2021, Sorenson et al. 2021, Vaudour et al. 2021]. Comparing the available bare soil compositing approaches, two aspects are of particular importance: 1) the index, responsible for the selection of bare soils and 2) the length of the compositing period.

A wide range of indices have been used for bare soil compositing. Vegetation indices such as the Normalized Difference Vegetation Index (NDVI), adapted NDVIs and other spectral indices such as the Normalized Burn Ratio 2 (NBR2) or the Bare Soil Index (BSI) have been applied in different geographical regions and temporal setups. In particular, a combination of the NDVI and the NBR2 is widely used for bare soil detection in different areas based on multispectral Sentinel-2 [e.g., Castaldi et al. 2021, Dvorakova et al. 2021, Vaudour et al. 2021, Mzid et al. 2022] or Landsat imagery [e.g. Dematte et al. 2020, Safanelli et al. 2020, Zepp et al. 2021 b, Mzid et al. 2022]. A pre-selection of valuable scenes is pursued by various approaches, also concerning additional datasets such as soil moisture products [e.g., Vaudour et al. 2019 b, Urbina-Salazar et al. 2021] or the crop phenology [Dvorakova et al. 2021]. According to the efforts made a composite containing the largest number of real and undisturbed exposed soil dates is best suited for SOC modeling. In this context, the question is, if the index (-combination) used, correctly extracts the acquisition dates to be included in the SRC, i.e. fields which are bare, smooth and show dry soils. Furthermore, multispectral images such as Landsat data do not provide a clear spectral separation between bare soils and dry vegetation [Asner and Heidebrecht 2002, Okin 2007, Malec et al. 2015, Dematte et al. 2018]. However, many authors have shown that a strict threshold for compositing allows to minimize this influence [Dematte et al. 2018, Tziolas et al. 2020, Sorenson et al. 2021, Vaudour et al. 2021]. This question will become even more important as the proportion of conservation tillage systems increases [Dang et al. 2020] and the time windows during which the soil is bare become shorter. Additionally, the influence of different indices on the selection of bare soil dates and their effects on SOC modeling are barely investigated. Both aspects are addressed here.

Zepp et al. [2021 b] developed a SOC modeling approach for cropland topsoils of Bavaria using a 30-year SRC (1984-2014) based on the Soil Composite Mapping Processor (SCMaP) approach for bare soil compositing. We showed good modeling accuracies and performances for the test area. However, to determine repeatable SOC contents also for modeling purposes, for instance to address the current political requirements, shorter compositing periods are needed. Especially, to identify SOC dynamics linked to changes in agricultural management. Questions such as which compositing length results in the most accurate modeling of soil parameters or what is the shortest reliable compositing length using Landsat data for SOC modeling have so far only been addressed by a small number of studies. E.g., Castaldi et al. [2021] compared topsoil parameter model capabilities using bare soil composites of one, two and three years based on Sentinel-2 and Landsat 8 data. For long term SOC monitoring, the Sentinel-2 time series do not yet provide a sufficient long database. In this regard, we investigate the potential of different compositing lengths for SOC estimation to determine how the long Landsat time series can be used for long-term SOC quantification purposes and monitoring pursuits.

The overall scope of the paper is to optimize the parameters for SRC generation for recurrent assessments of SOC contents using Landsat data considering the reliability of the selection of exposed soil dates. To address this question the specific objectives of this study are: 1) to compare the exposed soil dates derived by SCMaP to times, when a field is likely to be bare (based on the crop calendar and phenological observations), 2) to investigate the influence of different indices on exposed soil extraction, 3) to analyze the impact of different indices for topsoil SOC prediction in Bavaria, and 4) to evaluate which compositing length and seasons allow the most accurate prediction of SOC contents.

2. Materials and Method

2.1 Study Area

The study area comprises about 130,000 km^2 and covers most of the Federal State of Bavaria and adjacent regions in southeast Germany (Figure 3.3.1). Various landscapes are covered in the study area. The parts south of 48°N were excluded as in this region the mountain range of the Alps is located and permanent grassland is the dominant land use.

The elevation is between 100 m and 1,000 m above sea level. The mean annual temperature ranges between 6°C and 10°C and the precipitation between 551 mm and 1,800 mm per year. Predominant soils are Cambisols, Luvisols, Stagnosols, Gleysols and Leptosols [Wiesmeier et al. 2013, 2014 a, b] according to the World Reference Base for Soil Resources [IUSS Working Group WRB 2015]. The major land use is cropland, where mainly winter crops are cultivated (wheat, barley, and rape) [Bayerisches Landesamt für Statistik 2021]. Further summer crops such as sugar beet, summer wheat or corn are also common.

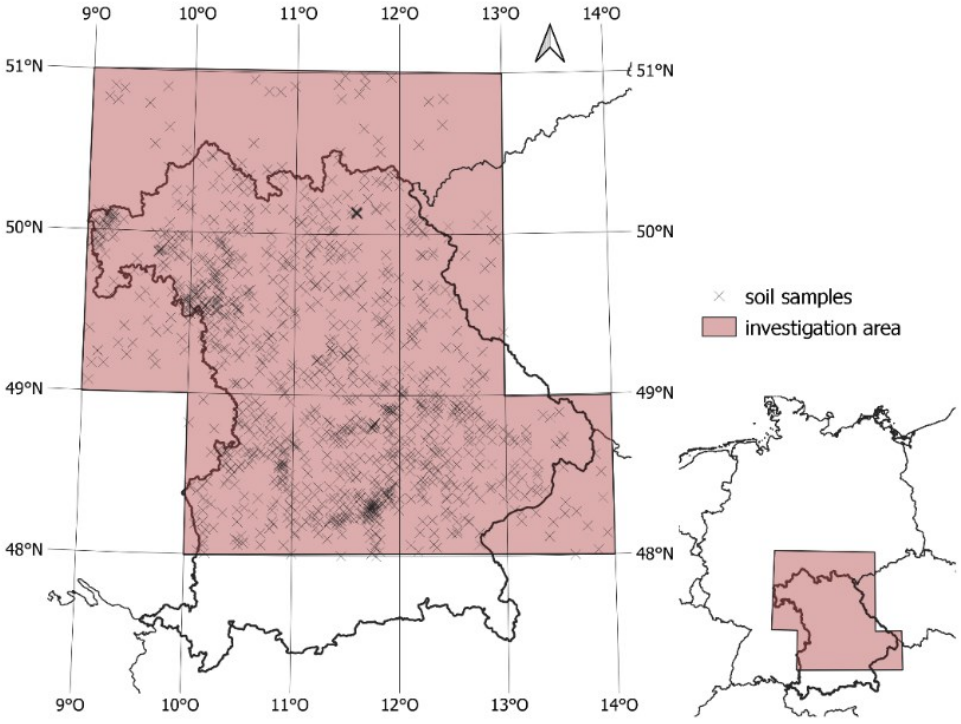

Figure 3.3.1: Study area in southern Germany and location of the soil samples (n = 1,251) for soil organic carbon (SOC) modeling.

2.2 SCMaP SRC

2.2.1 SCMaP approach

The SCMaP (Soil Composite Mapping Processor) processing chain [Rogge et al. 2018] allows the generation of bare soil reflectance composites (SRC) for individually determined time periods covering different years. The operational SCMaP chain can provide SRCs containing all pixels in a given time period showing at least once a bare soil. Per pixel all reflectances of all bare soil occurrences are averaged per band over the compositing period. Here, the SRC as input for SOC modeling was processed using all available Landsat-5 ETM (from 2005 to 2011), Landsat-7 ETM+ (from 2005 to 2019) and Landsat-8 OLI (from 2015 to 2019) Level 1C collection scenes [Wulder et al. 2019] covering the study area. Due to the low solar elevation angle, no scenes for January

and December were used. The same standardized pre-processing steps were applied to all scenes of all sensors. The Atmospheric Topographic Correction (ATCOR) software [Richter and Schläpfer 2014] and the established FMask algorithm [Zhu and Woodcock 2012, Zhu et al. 2015] were used for atmospheric correction and for cloud, cloud shadow, and snow pixel detection. The SCMaP approach requires two thresholds for bare soil selection which are set based on the spatial and temporal behavior of vegetation index composites. The application of the two thresholds allows separating exposed soils from all other land cover types such as permanent vegetation (e.g., grasslands or forests) and permanent non-vegetated land cover types (e.g., urban or water). The derivation of the thresholds is based on an automated technique using constant landcover classes over time (CORINE Land Cover data) and is described in detail by Zepp et al. [2021 a].

2.2.2 Indices

For the SRC generation, bare soil pixels were selected from the multitemporal Landsat database by calculating spectral index values. Originally, SCMaP was developed using an adapted vegetation index (PV+BLUE, equation (1)) extending the NDVI [Rouse et al. 1974]. The blue reflectance band of PV+BLUE was included to minimize the remaining haze effects not filtered adequately by the preprocessing steps [Rogge et al. 2018]. A wide variety of alternative spectral and/or vegetation indices to extract bare soil pixels are discussed in the literature. Here, we implemented two further indices in the SCMaP processing chain to test their influence on bare soil extraction and on the SOC modeling capabilities of the resulting SRCs. Equation (2) describes an alternative, NDVI based index (PV+IR2) [Heiden et al. 2022]. Instead of the blue reflectance band the second reflectance band, of the shortwave infrared wavelength region (SWIR) is used. Especially for soil analysis, the SWIR spectral ranges (1.300 – 2.500 nm) provide several important absorption features as here interactions between soil components and the infrared radiation occur [Ben-Dor and Banin 1995, Ben-Dor et al. 1997, Chabrillat et al. 2002, Bartholomeus et al. 2008, Gomez et al. 2008, Gholizadeh et al. 2021, Mzid et al. 2022]. Additionally, the Normalized Burn Ration II (NBR2, van Deventer et al. 1997) was implemented for SRC generation. The NBR2 (equation 3) is widely used for the derivation of bare soils for single scenes and the derivation of bare soil composites for soil modeling purposes [e.g. Dematte et al. 2018, Castaldi et al. 2019 a, Dvorakova et al. 2020, Safanelli et al. 2020].

The indices are calculated regarding the following equations:

$$PV + BLUE = \frac{\rho_{NIR}-\rho_{Red}}{\rho_{NIR}+\rho_{red}} + \frac{\rho_{NIR}-\rho_{Blue}}{\rho_{NIR}+\rho_{Blue}} \quad (1)$$

$$PV + SWIRII = \frac{\rho_{NIR}-\rho_{Red}}{\rho_{NIR}+\rho_{red}} + \frac{\rho_{NIR}-\rho_{SWIRII}}{\rho_{NIR}+\rho_{SWIRII}} \quad (2)$$

$$NBR2 = \frac{\rho_{SWIRI}-\rho_{SWIRII}}{\rho_{SWIRI}+\rho_{SWIRII}} \quad (3)$$

where ρ is the reflectance [%] of the Blue, Red, NIR (near Infrared) and IR (shortwave infrared) spectral regions (LT04, LT05, LE07: Blue = Landsat Band (B) 1, Red = B3, NIR = B4, IR1 = B5, IR2 = B7; LC08: Blue = B2, Red = B4, NIR = B5, IR1 = B6, IR2 = B7).

For each index, the required set of thresholds for SRC generation was derived following the scheme described by Zepp et al. [2021 a].

2.2.3 Temporal Settings

Different data setups for SRC compositing periods were prepared. First, all available scenes (February to November) for the compositing period 2015-19 (5Y) were used for SRC generation (SRC_{full}). Additionally, a seasonal SRC was processed comprising a combination of spring (March

to May) and autumn scenes (August to October), referred to as $SRC_{spring/autumn}$. The SRC_{full} and the $SRC_{spring/autumn}$ were processed using all three indices (PV+BLUE, PV+IR2 and NBR2). In addition to the 5Y $SRC_{spring/autumn}$, SRCs comprising a varying number of years were processed for the spring/autumn months. A 15-year period covering the years 2005 to 2019 (15Y), a 10-year period covering the years 2010 to 2019 (10Y), a seven-year period covering the years 2013 to 2019 (7Y), and a three-year period covering the years 2017 to 2019 (3Y) were prepared (Table 3.3.1).

Table 3.3.1: Structure of temporal (3 to 15 years) and seasonal (full = February to November, spring/autumn = March to May and August to October) compositing setups per index (PV+BLUE, PV+IR2 and NBR2) for SRC generation.

	full			spring/autumn		
time period	**PV+BLUE**	**PV+IR2**	**NBR2**	**PV+BLUE**	**PV+IR2**	**NBR2**
2005-19 (15Y)				x	x	x
2010-19 (10Y)				x	x	x
2013-19 (7Y)				x	x	x
2015-19 (5Y)	x	x	x	x	x	X
2017-19 (3Y)				x	x	X

The 5Y period was chosen from 2015-19 in line with Zepp et al. [2021 a] as this period was used here for validation of the resulting exposed soil mask to reference datasets for entire Germany. In addition, this period corresponds to the temporal coverage of the available validation data. Starting in 2019, the different composition lengths of three (2017-19), seven (2013-19), ten (2010-19), and 15 years (2005-19) were set backwards.

2.3 Available bare soil dates and validation approach

For the validation of the identified exposed soil dates, two different datasets were available. The Technical University of Munich provided a dataset, referred to as Ref1, containing specific sowing and harvesting dates of adjacent fields in Bavaria for the years 2016, 2017 and 2018. The locations were intersected with the SRC_{full} (2015-19) for identification of the fields covered by the SRC. For the resulting 43 fields, four SRC pixels were selected in each field, ensuring a location completely within the field border. For each field pixel set, bare soil dates were overlapped and all single occurrences were compared to the sowing and harvesting dates of the respective fields. The comparison was performed for all three indices.

A second validation dataset was prepared using the phenological information of the German national meteorological service (Deutscher Wetterdienst, DWD). The DWD is responsible for the provision of meteorological and climatological services [Kaspar et al. 2019] and provides a long history of phenological reports since 1951 [Kaspar et al. 2015]. About 1,600 phenological phases of wild and cultivated plants are captured according to a standardized guideline for entire Germany [Kaspar et al. 2015], are publicly available [Kaspar 2019], and are often used for the extraction of phenological windows for any available year and user-defined region [Möller et al. 2020]. Such kind of standardized information is relevant for a wide range of application in agricultural context [e.g., Gerstmann et al. 2016, Möller et al. 2017, Heupel et al. 2018, Möller et al. 2019, Asam et al. 2022, Buchelli et al. 2022]. For the analysis, the phases sowing, start of growing season (emergence), and harvesting were selected as relevant classes. These phases mark periods when a field is likely to be bare (e.g. seedbed conditions after sowing). Additionally, the ripening was added, as from this point until harvesting non-photosynthetic active vegetation (NPV) is possibly visible from the satellite. For the six main crop types in Bavaria (winter wheat, sugar beet, corn, rape, winter barley and summer barley [Bayerisches Landesamt für Statisik 2021]), the

selected phenological phases of 60 stations equally distributed across the study area were extracted per crop type and year (2015 to 2019). The dates marking the begin and end of the selected phases between 2015 and 2019 of all 60 stations were averaged per crop type and year. Before the phenological phase of sowing and after the phases emergence and harvesting, a buffer of 14 days was empirically added to the periods of exposed conditions, as tillage before sowing and after harvesting create a bare soil. After emergence of the crops, still the majority of soil per pixel is visible from the satellite for a certain period of time.

The above described prepared phenological dates are then used to prepare the validation dataset, referred as to Ref2. For this purpose, 30 fields equally distributed across the study area, were selected. Within the observed 5Y period, the fields have a crop rotation consisting of the six main crops in Bavaria listed above. The information about the crop sequence was derived from the Integrated Administration and Control System (IACS) database. The IACS dataset contains detailed information on the spatial distribution and the main crops grown in each field on a yearly basis. However, no information about cover crops between two consecutive crops was available. Therefore, the time between two crops is treated as likely fallow. However, the bare soil dates obtained during this period must be considered with special care.

For all 30 Ref2 fields, four SRC_{full} (2015-19) pixels were selected ensuring a location completely within the field borders to avoid external influences and mixtures with other field crops or adjacent land covers. All bare soil date occurrences of the selected four pixels per field were intersected. To validate the extracted exposed soil dates, these were compared to the information of Ref2 when a field was likely to be in bare conditions based on the crop calendar. The comparison was comprised for all three indices.

For the 30 Ref2 fields, we additionally investigated the behavior of the index and the derived thresholds responsible for the classification of a pixel as bare soil according to the phenological phases. As described in section 2.2.1 and in detail in Zepp et al [2021 a], within the SCMaP chain two thresholds are defined to select bare soil pixels. The minimum threshold (TH_{min}) selects the bare soil pixels by differentiating between permanently vegetated pixels and pixels showing an alternating vegetation cover. In this regard, we further analyzed the behavior of the index ranges when a field is in bare conditions, covered by vegetation, in the ripening phase, and during the period in which the field is likely to be under fallow conditions (no available phenological information) linked to TH_{min}.

2.4 SOC modeling approach

The SOC modeling approach was described in detail by Zepp et al. [2021 b]. A Random Forest Regression (RF) [Breimann 2001] algorithm was applied to model SOC contents in the cropland topsoils. The RF is a widely used technique in soil analyses [e.g., Wiesmeier et al. 2011, Ward et al. 2019, Dharumarajan and Hegde 2020, Luo et al. 2022] and especially for SOC modeling [Castaldi et al. 2019 b, Vaudour et al. 2019 a, b, Möller et al. 2022, Zepp et al. 2021 b, Sakhaee et al. 2022]. The Scikitlearn machine learning library for Python [Pedregosa et al. 2011] was used. For each SRC period and index a RF was trained and validated and the hyperparameters *n_estimators*, *max_features*, *max_depth*, *min_sample_split*, *min_samples_leaf* and *random_state* were optimized individually.

For SOC modeling, a legacy database of 1.385 soil samples was available. The database comprised soil samples collected between 1984 and 2016 by the Bavarian Environment Agency (LfU) and the Bavarian State Research Center for Agriculture (LfL). Additionally, topsoil cropland samples collected in the Land Use/Land Cover Area Frame Survey (LUCAS) [Fernandez-Ugalde et al. 2022] were used. A detailed description and the pre-processing can be found in Zepp et al.

[2021 b]. Per soil sample, the SRC reflectance and its eight neighboring pixel reflectances were averaged to minimize small scale disturbances. For all pixel clusters, a spectral / spatial filtering [see Zepp et al. 2021 b] was applied to exclude heterogenous pixel clusters as here the possibility of any external influence or data artefacts (e.g., mixed spectra of soil and portion of adjacent land cover) impacting the cluster is high. Filtering is especially important when intersecting EO data, which is characterized by a relatively large pixel size (Landsat = 30 m), with point data. This resulted in a soil database with 1.251 samples (Figure 3.3.1).

The soil dataset was split into a calibration (70%) and a validation subset (30%). Widely used accuracy and performance measures were used to evaluate the model performances and to determine the influence of indices and compositing periods for SRC generation for SOC modeling. For this purpose, the coefficient of determination (R^2, from Python sklearn.metrics), the Root Mean Square Error (RMSE) and the Ratio of Performance to Derivation (RPD) were used. The RPD [Chang and Laird 2002], as a measure to estimate a model's quality, is mainly provided to allow a comparison of the results with those in the literature.

All SRCs (full and spring/autumn) were intersected with the soil database and the overlap of the points was used as input for SOC modeling. In a first step separate SOC models for SRC_{full} and $SRC_{spring/autumn}$ for the three indices (PV+BLUE, PV+IR2 and NBR2) for the 5Y period were trained and validated. Subsequently the capabilities of different time periods for all three indices based on spring and autumn scenes were compared (Table 3.3.1). As described above, besides the 5Y compositing period, 3Y, 7Y, 10Y and 15Y compositing periods were prepared and processed. For each period a separate RF model was trained and validated.

3. Results

3.1 Validation of exposed soil dates

The comparison of bare soil dates with Ref1 is shown in Figure 3.3.2. Here, the periods between sowing and harvesting dates are marked in green. Additionally, the bare soil dates per index are visualized. For PV+BLUE, a total of 190 dates of bare soils were identified. In detail, 67 dates were observed within the period with photosynthetically active vegetation cover between sowing and harvesting. 146 dates were determined before sowing or after harvesting. For PV+IR2, a total of 191 dates of bare soils were captured. Here, 67 dates were in the vegetation period between sowing and harvesting and 145 dates before sowing or after harvesting. For NBR2, in total 118 bare soils dates were observed, which is less than using PV+BLUE and PV+IR2. 45 dates were identified within the growing season between sowing and harvesting and 73 dates before sowing or after harvesting.

Also, the influence of the crop type was investigated. Winter wheat, corn and potato were cultivated on the fields in the available period. For the eleven winter wheat fields, only bare soil dates before sowing and after harvesting were identified. There was no bare soil observation during photosynthetically active vegetation cover. Except for field 1 for no other corn field there was a bare soil observation before the harvesting date. Mainly bare soils were identified before or shortly after the sowing date when the soils are likely bare. However, for field 8, 30 and 32 several bare soil dates between sowing and harvesting were captured, when the fields are likely to be covered by a growing crop and the visibility of bare soil from the satellite is unlikely. For the fields, where corn was cultivated more bare soil dates were identified after harvesting in comparison to the fields, where winter wheat was cultivated. Additionally, more bare soil dates were identified before or within a short period of time after sowing. For the fields 1, 3 and 7, where two consecutive crop periods were available, no bare soil occurrence was determined between a

winter and a summer crop (Figure 3.3.2). The bare soils were detected a few days after harvesting or before sowing when the soil is likely bare.

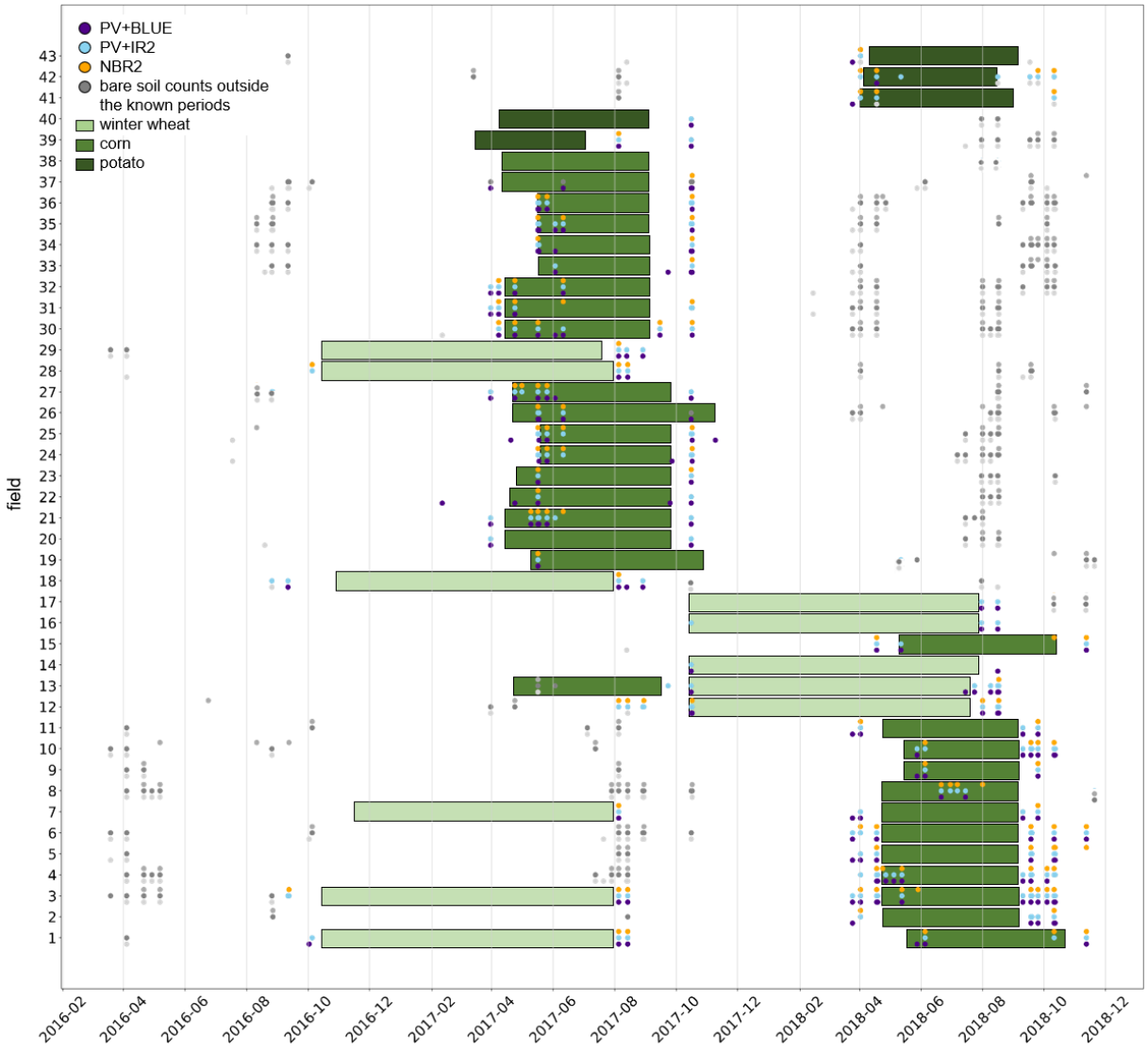

Figure 3.3.2: Bare soil dates based on PV+BLUE, PV+IR2 and NBR2 for 43 sample fields of Ref1. The green bars mark the vegetation periods from sowing to harvesting dates for the cultivated crops winter wheat, corn and potato. The grey dots show the further derived bare soil dates in the observed time range, which are not related to the vegetation periods where sowing and harvesting dates were available.

Table 3.3.2 lists the temporal distribution of the identified bare soil dates before and after sowing and harvesting in detail. For all three indices, a similar number of bare soil dates was selected before and directly after sowing. The majority of bare soil dates was identified after harvesting for all three indices. Within the first 14 days after harvesting, 13.2% of bare soil dates for PV+BLUE, 12.6% for PV+IR2 and 11.0% for NBR2 were observed. 11.6% of the identified bare soil dates for PV+BLUE, 11.5% for PV+IR2 and 11.0% for NBR2 between 15 and 21 days after harvesting. Additionally, more than 22 days after harvesting 21.1% of bare soil dates for PV+BLUE, 20.5% for PV+IR2 and 21.2% for NBR2 were captured. For PV+IR2 and NBR2 no scenes and for PV+BLUE only a small number of scenes was selected directly before harvesting, when the crops are in the ripening phase and the possibility of dry vegetation is high.

Figure 3.3.3 shows the distribution of the predicted bare soil dates between 2016 and 2018. Per month the bare soil dates were summed for all 43 Ref1 test fields. Most of the bare soil dates

were detected in October (PV+BLUE: 38 dates (20.8%), PV+IR2: 43 dates (22.1%), NBR2: 26 dates (22.0%)). Additionally, a large number of bare soil dates was selected in the spring months (April, May and June) and in late summer (August and September). A small number of dates was observed in July and November and no dates were determined in February.

Table 3.3.2: Number of bare soil dates before/after sowing and harvesting for the 43 Ref1 fields shown for all three indices.

phase	index	< 14 days	15 – 21 days	> 22 days
before sowing	PV+BLUE	19	3	15
	PV+IR2	17	4	18
	NBR2	12	3	7
after sowing	PV+BLUE	22	7	22
	PV+IR2	23	8	19
	NBR2	12	5	21
before harvesting	PV+BLUE	3	5	-
	PV+IR2	3	-	14
	NBR2	-	-	7
after harvesting	PV+BLUE	25	22	40
	PV+IR2	24	22	39
	NBR2	13	13	25

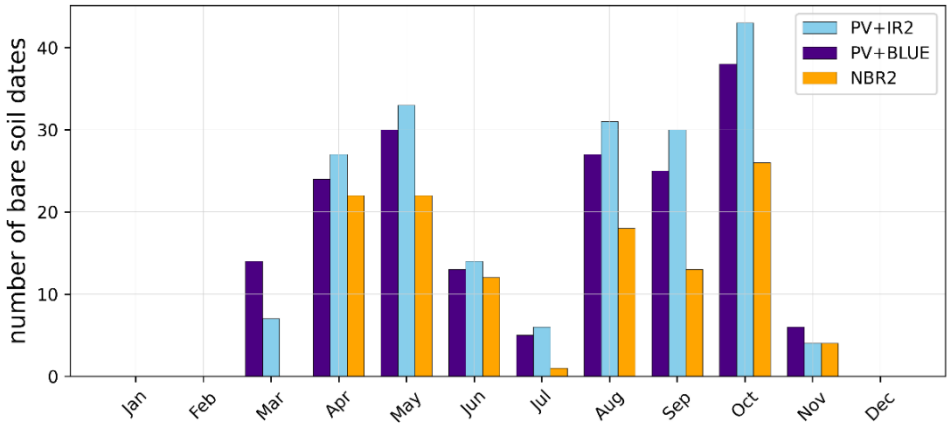

Figure 3.3.3: Summed monthly distribution of exposed soil dates for all 43 Ref1 test fields determined using PV+BLUE, PV+IR2 and NBR2 (no scenes were used for January and December).

Overall, the comparison of extracted bare soil dates between 2015 and 2019 to the selected penological data of Ref2 shows similar patterns (Figure 3.3.4) as the comparison with Ref1 (Figure 3.3.2). The majority of bare soil dates are detected when the field is likely to be in bare conditions and visible from the satellite. Most of the identified dates are at the beginning or end of the crop period, when the field is in seedbed conditions, until a few days after the emergence of the crops or directly after harvesting, when the soils are visible after tillage.

PV+BLUE and PV+IR2 provide a similar number and distribution of extracted bare soil dates. Using NBR2, overall less bare soil dates were extracted. However, the dates based on NBR2 also predominantly correspond to the dates of PV+BLUE and PV+IR2 and were not selected on additional times during the year. Overall, 490 bare soil dates were identified for PV+BLUE, 460 for PV+IR2, and 219 for NBR2 between 2015 and 2019. Due to the crop rotation, fallow land (or cover crops, unfortunately not documented in the census) of several months between winter and

summer crops occurred up to three times in the observed time (Figure 3.3.4). Here, several bare soils were extracted for all three indices.

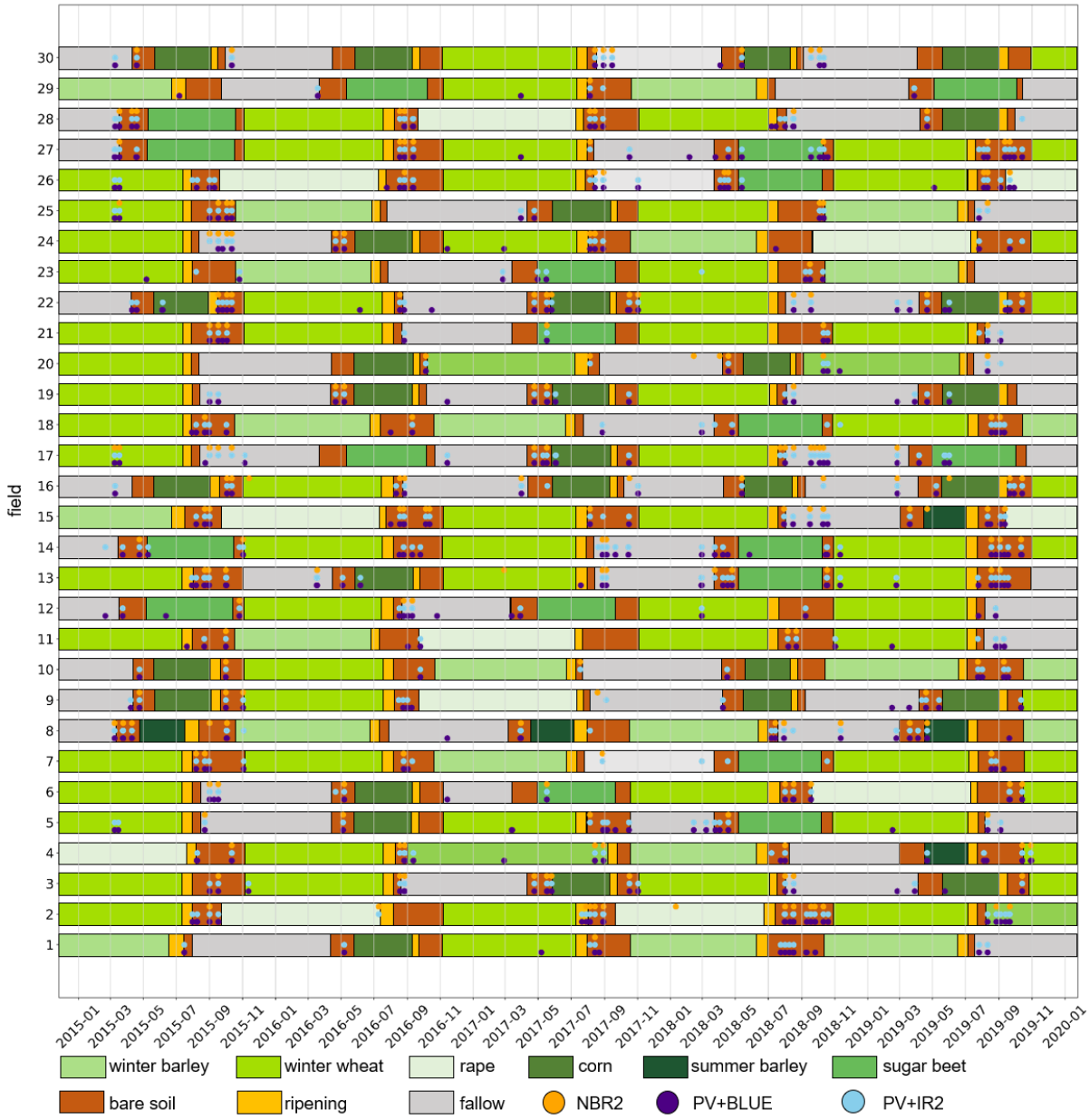

Figure 3.3.4: Bare soil dates based on PV+BLUE (purple), PV+IR2 (light blue) and NBR2 (orange) between 2015 and 2019 in comparison to phenological information of Ref2. The different colored bares mark the time periods the fields are covered by vegetation (green, starting 14 days after emergence until ripening), the stage of ripening (yellow), the field is in bare conditions (brown, 14 days before sowing until 14 days after emergence and from harvesting until 14 days after harvesting) and the stages between two crops (no information about cover crop is given (grey)).

For PV+BLUE 43.1%, for PV+IR2 46.3% and for NBR2 51.1% of the bare soil dates were within the periods the fields are likely uncovered (Figure 3.3.5). More precisely, 34.1% for PV+BLUE, 35.0% for PV+IR2 and 37.0% for NBR2 of the bare soil dates were determined within 14 days before sowing until 14 days after emergence (Figure 3.3.5 – class sowing). 8.9% for PV+BLUE, 11.3% for PV+IR2 and 14.2% for NBR2 of the bare soil dates were selected from harvesting until 14 days after the harvesting date (Figure 3.3.5 – class harvesting). Due to the rotation of winter and summer crops 45.3% for PV+BLUE, 44.6% for PV+IR2 and 43.4% for NBR2 bare soils were identified in the period between two crops (more than 14 days before sowing and more than 14

days after harvesting) (Figure 3.3.5 – class fallow). Some bare soil dates were identified when the field is covered with photosynthetically active vegetation (Figure 3.3.5 – class veg). For PV+BLUE 8.6%, for PV+IR2 6.5% and for NBR2 3.7% of the bare soils within 2015 and 2019 were extracted at least 14 days after emergence. However, none of the identified dates was at the end of the vegetation period, close to the ripening. The phenological phase between ripening and harvesting is a potential source of false positive bare soils as here, due to the multispectral sensor the undetected presence of non-photosynthetic active vegetation may occur, resulting in a misclassification of bare soils. A small percentage of bare soils were detected during the ripening phases. For PV+BLUE 3.1%, for PV+IR2 2.6% and for NBR2 1.8% of the bare soil dates were within the ripening phases before the harvesting date (Figure 3.3.5 – class ripening).

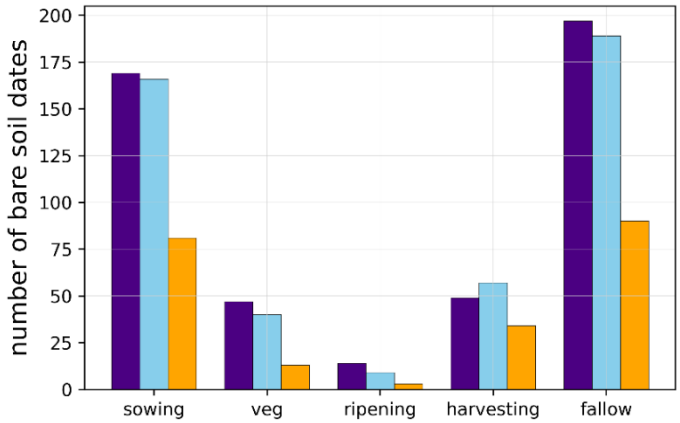

Figure 3.3.5: Cumulated bare soil dates within the summarized phenological phases (sowing, veg = period with photosynthetically active vegetation cover, ripening, harvesting, fallow) of Ref2 for PV+BLUE, PV+IR2 and NBR2.

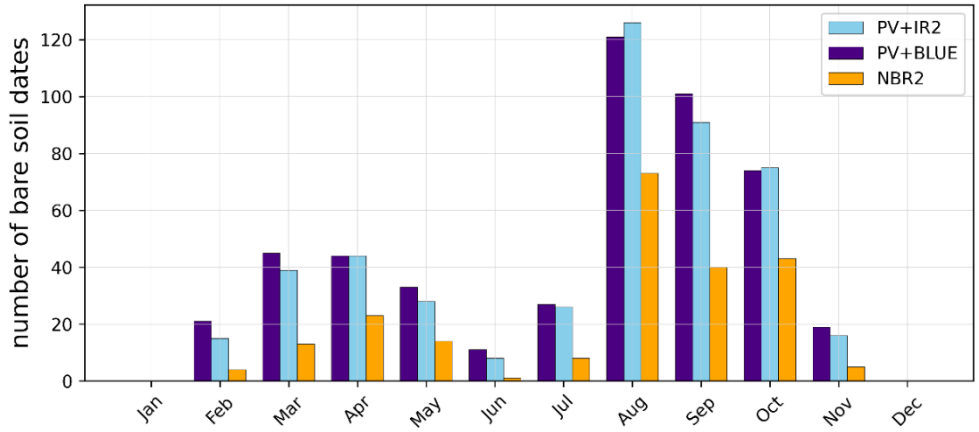

Figure 3.3.6: Summed number of bare soil dates for PV+BLUE, PV+IR2 and NBR2 per month between 2015 and 2019 for the 30 Ref2 test fields (no scenes were downloaded for January and December).

Most of the bare soils between 2015 and 2019 were selected between August and October (August - PV+BLUE: 24.4%, PV+IR2: 26.9%, NBR2: 32.44%; September - PV+BLUE: 20.4%, PV+IR2: 19.4%, NBR2: 17.8%; October - PV+BLUE: 32.4%, PV+IR2: 17.8%, NBR2: 19.1%) (Figure 3.3.6). For all other months less than 10% of bare soil dates were identified per month. The smallest number of scenes were selected for February, June and November (February - PV+BLUE: 4.2%, PV+IR2: 3.2%, NBR2: 1.8%; June - PV+BLUE: 2.2%, PV+IR2: 1.7%, NBR2: 0.4%; November - PV+BLUE: 3.8%, PV+IR2: 3.4%, NBR2: 2.2%). In comparison to the validation of bare soil dates with Ref1 (see Figure 3.3.3) less bare soil dates were determined in the first half of the year compared to the second half of the year for the 30 Ref2 fields. This is related to the fact, that the

Ref2 fields contain more winter crops, while the 43 Ref1 fields are dominated by summer crops (mainly corn).

Figure 3.3.6 shows the range of the indices (PV+BLUE, PV+IR2 and NBR2) of pixels when the fields are likely to be bare (sowing, harvesting), covered by photosynthetically active vegetation (veg), during ripening and under likely fallow conditions (between two crops). The dashed lines show the per index determined TH_{min}, responsible for bare soil selection in the SCMaP chain. All occurrences below the TH_{min} are included as bare soils and are averaged for the respective SRC.

The periods show variable ranges for all three indices. The period with photosynthetic active vegetation cover was dominated by higher indices in comparison to the times when the fields show bare conditions (between sowing and emergence or after harvesting). During ripening, nearly all occurrences were above the TH_{min} and are thus correctly not included into the SRC. A high proportion of dates of the bare periods (sowing, harvesting) fall below the respective TH_{min} for PV+BLUE and PV+IR2. The NBR2 allows less data for the composite processing. However, this indicates that a higher proportion of uncovered soils were not selected as bare soils and were thus not included into the SRC. Even though, a large number of bare soils were detected in between two crops, Figure 3.3.7 indicates a good exclusion of these pixels, as the majority of pixels is not included to the SRC by TH_{min}.

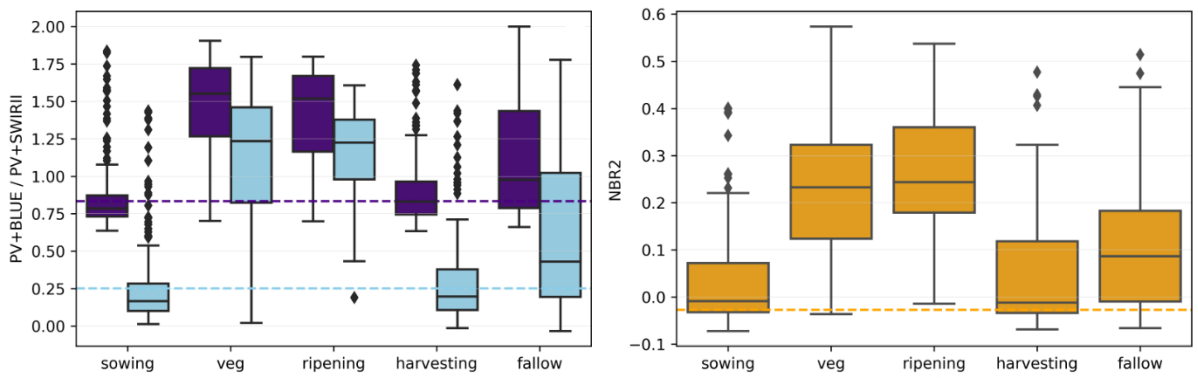

Figure 3.3.7: Index ranges for PV+BLUE (indigo), PV+IR2 (light blue) and NBR2 (orange) for all cloudless scenes within the different summarized phenological phases. Shown are the 30 sample fields of Ref2 dataset. The dashed lines indicate the derived TH_{min} used for bare soil definition of the respective index. All occurrences below TH_{min} are included to the SRC generation.

3.2 Influence of spectral indices and SRC setup on SOC modeling

Although, the number of soil sampling sites between 2015 and 2019 depends on the index and the months included in the SRC, the distribution of the SOC contents were similar (Table 3.3.3). For all three indices the same minimal and maximal SOC contents (0.26% - 18.3%) are observed for SRC_{full} and $SRC_{spring/autumn}$. The mean SOC contents for the different setups varied slightly and ranged from 2.09% (SRC_{full} – PV+BLUE) to 2.21% ($SRC_{spring/autumn}$ – NBR2). All indices and temporal settings provided a large number of intersecting soil samples with the respective SRC (n = 957 – 1,021). The number of available samples for modeling based on $SRC_{spring/autumn}$ was slightly lower in comparison to SRC_{full} for all three indices.

The different indices for SRC generation had a minor influence on the SOC modeling (Table 3.3.3). For all three indices similar R^2 and RPDs were identified. The RMSE varied slightly. Furthermore, the use of $SRC_{spring/autumn}$ provided better model performances, which was indicated by increasing R^2 and RPD for the model validation. However, the model performances for SRC_{full} and $SRC_{spring/autumn}$ were comparable for the three different indices.

Table 3.3.3: Intersecting samples for modeling, SOC statistics and model performances based on SRC_{full} and $SRC_{spring/autumn}$ for the compositing period of 2015-2019 for all three tested indices. Shown are the R^2, RMSE and RPD values of model validation (30% of input data).

2015-19	index	samples	SOC min [%]	SOC max [%]	SOC mean [%]	R^2	RMSE [%]	RPD
SRC_{full}	PV+BLUE	1,021	0.26	18.30	2.09	0.59	1.00	1.57
	PV+IR2	1,018	0.26	18.30	2.15	0.59	1.22	1.57
	NBR2	1,012	0.26	18.30	2.21	0.60	1.28	1.58
$SRC_{spring/autumn}$	PV+BLUE	989	0.26	18.30	2.11	0.67	1.29	1.73
	PV+IR2	957	0.26	18.30	2.14	0.66	1.23	1.71
	NBR2	1,001	0.26	18.30	2.21	0.64	1.05	1.67

3.3 Temporal influence on SOC modeling

Overall, 15Y $SRC_{spring/autumn}$ based on different indices and compositing periods were built for SOC modeling (Table 3.3.4). The 3Y compositing period provided the smallest number of intersecting soil samples (total number of sample points is 932: PV+BLUE, 832: PV+IR2, 884: NBR2) and the 15Y period the largest number of soil samples for SOC modeling (total number of sample points is 1,095: PV+BLUE, 1,070: PV+IR2, 994: NBR2). However, still a valuable amount of soil samples (> 832: PV+IR2) was available for SOC modeling using the shortest compositing period. All periods and indices showed similar SOC distributions and were thus comparable. While the minimum and maximum SOC values were the same for all periods and indices, the mean SOC contents ranged between 2.1% (3Y – PV+IR2) and 2.6% (15Y – PV+BLUE).

Table 3.3.4: Number of samples, SOC statistics and accuracy parameters for SOC modeling based on different compositing lengths using PV+BLUE, PV+IR2 and NBR. The given R^2, RMSE and RPD values represent the model validation based on 30% of the available samples. (In bold the best model per index is given).

time period	index	samples	SOC min [%]	SOC max [%]	SOC mean [%]	R^2	RMSE [%]	RPD
15Y	**PV+BLUE**	**1,095**	**0.26**	**18.30**	**2.63**	**0.72**	**1.16**	**1.91**
	PV+IR2	**1,070**	**0.26**	**18.30**	**2.20**	**0.71**	**1.04**	**1.87**
	NBR2	**994**	**0.26**	**18.30**	**2.18**	**0.68**	**1.12**	**1.76**
10Y	PV+BLUE	1,055	0.26	18.30	2.15	0.69	1.14	1.79
	PV+ IR2	1,033	0.26	18.30	2.17	0.66	1.44	1.73
	NBR2	1,008	0.26	18.30	2.18	0.61	1.34	1.61
7Y	PV+BLUE	995	0.26	18.30	2.14	0.65	1.09	1.68
	PV+ IR2	981	0.26	18.30	2.16	0.61	1.42	1.60
	NBR2	1,005	0.26	18.30	2.18	0.61	1.21	1.60
5Y	PV+BLUE	989	0.26	18.30	2.11	0.67	1.29	1.73
	PV+ IR2	957	0.26	18.30	2.14	0.66	1.23	1.71
	NBR2	1,001	0.26	18.30	2.21	0.64	1.05	1.67
3Y	PV+BLUE	932	0.26	18.30	2.09	0.56	1.19	1.51
	PV+ IR2	832	0.26	18.30	2.05	0.61	1.29	1.60
	NBR2	884	0.26	18.30	2.14	0.66	1.33	1.70

Furthermore, the SOC model performances based on 30% validation data are given. Overall, PV+BLUE and PV+IR2 performed better in comparison to NBR2. Additionally, for PV+BLUE, PV+IR2 and NBR2 a longer compositing period resulted in better model performances. $SRC_{spring/autumn}$ 15Y allowed the most accurate modeling of SRC with the highest R^2 values

(PV+BLUE: 0.72, PV+IR2: 0.71, NBR2: 0.68). From 3Y to 15Y the R^2 and RPD values were mostly increasing with the acquisition period apart from the 7Y for PV+BLUE and PV+IR2.

Using NBR2 for SRC processing showed variable modeling results without a trend of an increase of model performances with increasing length of the compositing period. However, the best model performances for NBR2 were observed for 15Y (R^2: 0.68, RMSE: 1.12%) followed by 3Y (R^2: 0.66, RMSE: 1.33%). Even though, the RMSE for 3Y was relatively high in comparison to the other five longer compositing periods.

4. Discussion

4.1 Validation of exposed soil dates

Most of the selected bare soil dates were located when field observations (Ref1) or the crop calendar (Ref2) show that the soil is likely to be exposed and visible from the satellite (e.g., when the field is in seedbed conditions, directly after sowing or tillage after harvesting). Similar results were obtained for a comparison of 73 fields in total with two different datasets across Bavaria where different crops (summer and winter) were cultivated (Figures 3.3.2, 3.3.3, 3.3.4, and 3.3.6). Furthermore, it was shown that the influence of different vegetation indices for bare soil selection was minor. However, NBR2 extracted less bare soil dates in comparison to PV+BLUE and PV+IR2. The temporal distribution of bare soil dates determined by NBR2 was comparable to the dates observed by PV+BLUE and PV+IR2. For all three indices the same standardized threshold determination was applied. The threshold determination for NBR2 in comparison to the two other tested indices results in a stricter limit for bare soil detection (Figure 3.3.7). The NBR2 threshold resulted in a lower number of exposed soil dates compared to the other indices. Castaldi et al. [2019 b] and Dvorakova et al. [2022] have shown, that the threshold for NBR2 can be a bit more relaxed for bare soil detection. These results can be taken as an indication to adjust the threshold determination for NBR2 in the SCMaP SRC generation process.

Few bare soil dates were determined at the end of the growing season during the ripening phase, where the likelihood to find stubbles or NPV is high (Figure 3.3.5). Especially during the ripening phase, the risk for misclassification of NPV as bare soils is high. As also shown in Figure 3.3.7 the thresholding method required for SRC generation indicates, especially for NBR2, a valid exclusion of scenes within the ripening phase (potentially influenced by NPV and crop residues). However, it has to be considered, that the ripening phase is the shortest phase and the chance for a cloudless Landsat observation is low due to the revisit time of 16 days. For the comparison with Ref1 (where only sowing and harvesting dates were available), a promising result is the fact, that only few bare soil dates were identified at the end of the vegetation period (before the harvesting date), when the possibility for a misclassification of bare soils and crop residues due to mature crops is high (Figure 3.3.2). A significant influence of the spectra of the resulting averaged SRC can thus be excluded.

The comparison of Ref1 information to selected bare soil dates indicate that a separation of summer and winter crops was possible as the months, the bare soils were identified, were varying (Figure 3.3.2). Similar associations were found for the 30 Ref2 fields across Bavaria (Figure 3.3.4). Comparing bare soil dates to crop specific phenological phases, regimes of different crop types can be identified. Beside the clear separation of summer and winter crops, the scheme of the bare soil dates allows a separation e.g., between winter rape and winter wheat or winter barley as for rape the bare soil phase during tillage and seedbed preparation is earlier (Figure 3.3.8). The resulting regimes could be used for further analysis as e.g., crop type classification. However, the analysis also indicates that especially winter wheat is showing systematically misclassified bare soils in the months March to June when the fields are covered by vegetation. A comparison with

the results of other authors is barely feasible, since as i.e., Vaudour et al. [2022] point out, only very few papers provided details about surface condition, date of collection, crop types or crop rotations and management practices. An in-depth analysis of the behavior of bare soil selection has to be conducted in other regions to use the temporal distribution of bare soil dates for further classification.

As shown by Vaudour et al. [2019 and 2021] and Dvorakova et al. [2021], the selection of the acquisition date is a co-determining factor for bare soil products as basis for SOC modeling. [Dvorakova et al. 2021] suggested the selection of scenes for bare soil detection following the greening up approach, when the vegetation index is about to exceed a certain threshold. According to this method, scenes detected immediately before an increase in NDVI are used. At this stage, the fields are in seedbed condition and the bare soils are visible from the satellite without any disturbances. The approach was developed for Sentinel-2 data in Belgium with temperate climate. However, as the revisit time of Sentinel-2 is higher, using Landsat too few scenes are available for this approach for change analysis or modeling purposes over shorter compositing periods. The periods would have to be significantly extended. Regarding the crop regime of the combination of winter and summer crops in Bavaria, scenes in spring and autumn provide the possibility of the mentioned approach. The scenes of the specific seasons potentially offer a high visibility of bare soils under optimal surface conditions, when an eventually occurring soil crust and crop residues have been plowed in and soils are in seedbed condition. Consequently, from March to May and August to September, the largest number of bare soils have been detected (Figures 3.3.3 and 3.3.6). The months are representative for the season when the fields of summer and winter crops are prepared for sowing and the bare soil is likely visible from the satellite.

Based on the above mentioned assumption, we summed the bare soil dates per combined phenological phases for 5Y SRC_{full} (Figure 3.3.9 a) and 5Y $SRC_{spring/autumn}$ (Figure 3.3.9 b) for the 30 Ref2 test fields. Assuming that soils in the period with photosynthetically active vegetation cover (veg) or during the ripening phase are covered and not visible, bare soils selected in these phases are likely to be misclassified. A seasonal pre-selection of input scenes to the SRC reduces these numbers significantly (Figure 3.3.9 b). The amount of bare soil dates before the fields show vegetation cover (sowing) decrease slightly in comparison between SRC_{full} to $SRC_{spring/autumn}$. A pre-selection of scenes indicates a reduction of misclassified bare soil dates during the vegetative stage and ripening.

During the period between a winter and a summer crop, several bare soil dates were selected (Figure 3.3.4). This was especially shown for the 30 Ref2 test fields. The combination of IACS data and large scale available phenological data did not provide a more precise identification of the field conditions in the periods between summer and winter crops. Information about cover crops cultivated between two consecutive crop periods was not provided, but would be a relevant information for the validation of the identified bare soils during the fallow periods. Additionally, information about cover crops is highly valuable and helps to understand the changes in SOC contents. As shown by Seitz et al. [2022], the use of cover crops can increase SOC storage in croplands. The pre-selection of spring and autumn scenes for bare soil identification reduces the bare soil occurrences during the fallow periods (Figure 3.3.9 b). Alternatively, the complete exclusion of the fallow periods based on IACS data for SRC processing is a possibility to reduce the potential misclassifications. It must be considered here, that especially for Landsat an exclusion of the relatively long fallow periods would imply a temporal decrease of potential input scenes for bare soil selection. The decision between too few data points and a good average of bare soil dates has to be analyzed further.

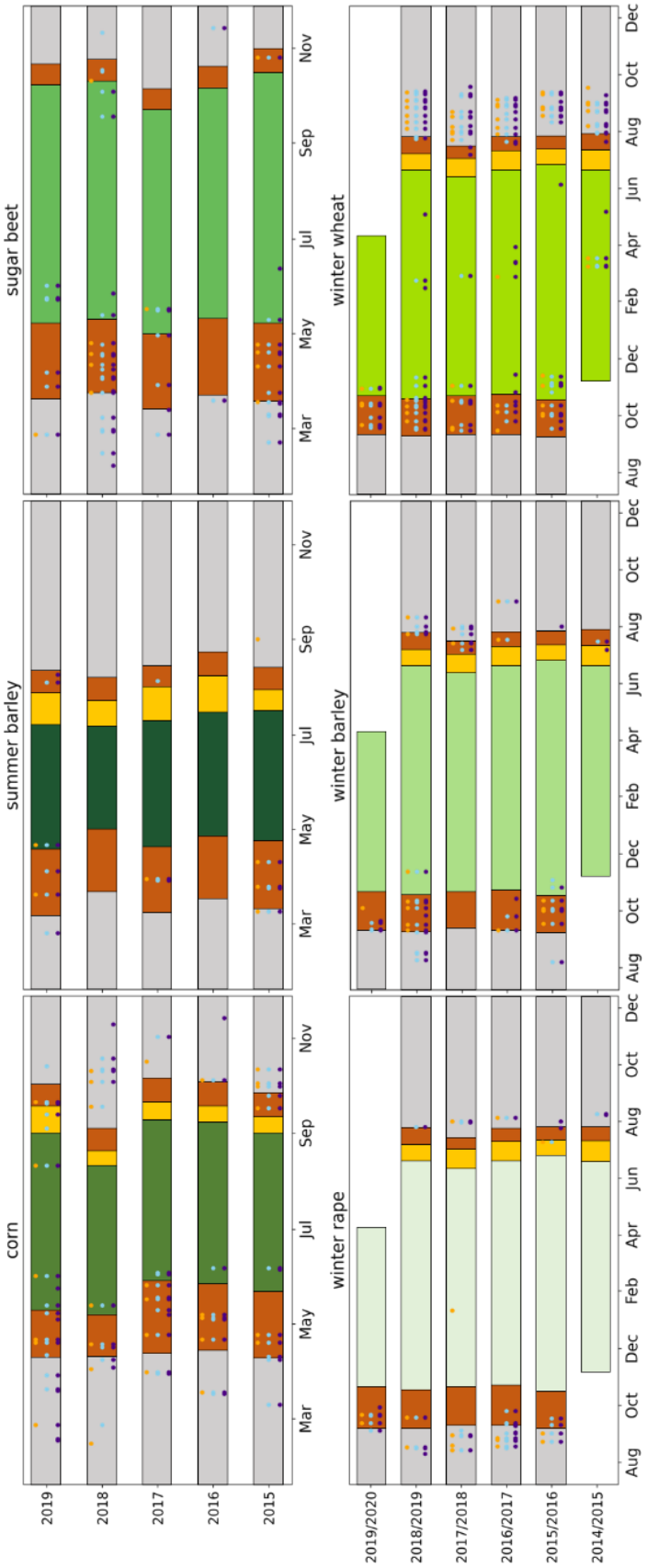

Figure 3.3.8: Bare soil dates based on PV+BLUE (purple), PV+IR2 (light blue) and NBR2 (orange) between 2015 and 2019 in comparison to phenological information of Ref2 for the six main crop types. The colors mark the phenological phases, respectively the summarized periods, when the field shows bare conditions (brown), is covered by vegetation (green), during ripening (yellow) and between two crop periods when the field is likely under fallow conditions (grey).

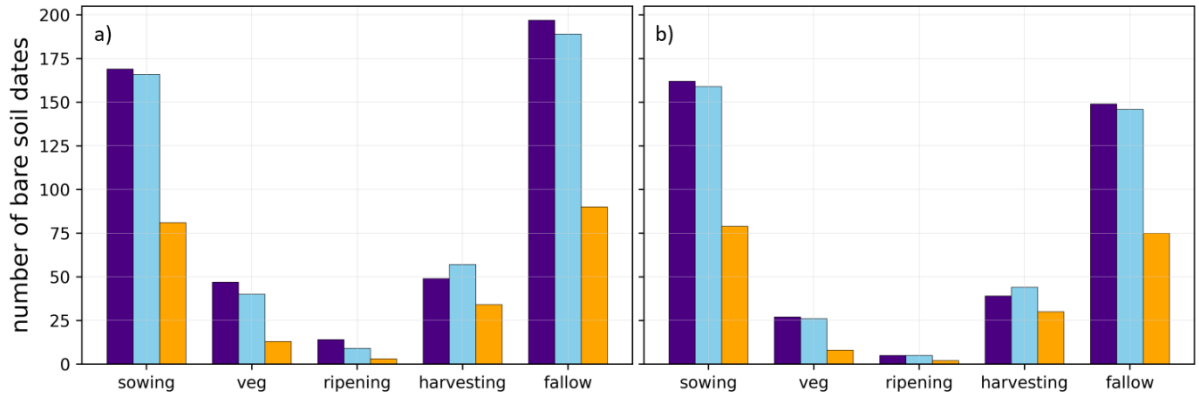

Figure 3.3.9: Bare soil date for the summarized phenological phases (including temporal buffer) using a) all scenes for 5Y SRC generation and b) spring and autumn scenes for 5Y SRC generation for all three indices.

Phenological phases as basis for the selection of time periods which are integrated to the SCMaP chain for SRCs processing can help to reduce the number of dates which are misclassified as bare soil. Here, we tested a pre-selection of seasons integrated to the SRC for the main crops in the study area. To transfer the local approach to different regions, the selection of seasons depending on the locally grown crops is too time consuming. Standardized datasets as input for SCMaP are required. For example, the PhenoWin approach [Möller et al. 2020], which provides spatially averaged phenological information for the common crop types in Germany, could be a valuable input. Per field the specific time periods, the field is showing bare conditions (i.e., visibility from the satellite), can be selected and only these scenes are then integrated to the SCMaP processing chain. However, an information about the spatial distribution of the crop types in the compositing period is mandatory, which is available at least for Sentinel-2 based crop species classifications since 2016 [Preidl et al. 2020, Asam et al. 2022, Blickensdörfer et al. 2022].

4.2 Influence of spectral indices and seasonal SRC set up on SOC modeling

Three indices (PV+BLUE, PV+ IR2 and NBR2) for SRC generation for the purpose of SOC modeling were tested and compared. The SRCs processed with the three indices showed minor influences on the accuracies and performances of the SOC models (Table 3.3.3). However, PV+BLUE showed the best model performances. Generally, for SOC modeling a reliable selection of bare soils integrated to the SRC is required and is controlled by a robust thresholding to separate bare soils from all other land cover classes. The results indicate, that the influence of the index for SRC generation thus influences the SOC modeling less than a valid selection of bare soil dates. As shown in the previous chapters, all indices extracted a similar distribution of bare soil dates integrated to the SRCs. Despite the fact that the NBR2, based on the thresholding strategy developed for SCMaP, more strictly selected bare soil dates, this appears not to be the decisive factor controlling SOC modeling. Also, the distribution of the dates is comparable to the NDVI based indices. However, Castaldi et al. [2019], Dvorakova et al. [2021], and Vaudour et al. [2021] reported better SOC modeling capabilities for stricter set NBR2 thresholds found for the use of Sentinel-2 data [Vaudour et al. 2022].

In line with the findings of other authors, that a pre-selection of scenes (i.e., through the crop calendar, soil moisture related, based on management practices) included in the bare soil detection benefits the SOC modeling, we demonstrated better model performances for $SRC_{spring/autumn}$ for all three indices (Table 3.3.3). In Bavaria due to the presence of summer and winter crops, there are two time periods during the year where the visibility of bare soils from the

satellite is highest. Hence, spring and autumn months are integrated into the SRC. The pre-selection of scenes additionally reduces the processing capabilities, which significantly reduced the processing time for SRC generation. This is of particular value for the processing of multi-year composites with several hundred input scenes for an area-wide mapping approach.

4.3 Influence of time period on SOC modeling

For all three indices the 15Y SRC period provided the best SOC model performances. Overall, for PV+BLUE and PV+IR2 longer time periods provide better SOC predictions compared to shorter compositing periods (Table 3.3.4). In contrast, the NBR2 did not show this behavior. The better model performances might be linked to the number of cloudless scenes integrated to the SRC. For longer compositing periods more cloudless scenes per pixel are available (Table 3.3.5), which might influence the quality of the resulting composite in terms of resulting SOC model performances. Similar associations could already be observed by Dematte et al. [2020] and Zepp et al. [2021 a]. An increase in the number of cloudless scenes results in an increase of the number of bare soil dates per pixel, or in an improvement of the accuracy of the resulting exposed soil mask compared to reference data. Although the number of studies on Sentinel-2 time series is still limited, they all show that about ten bare soil observations are sufficient to stabilize the spectral variability of an SRC pixel [Heiden et al. 2022] and the uncertainty of the SOC prediction [Dvorakova et al. submitted]. Castaldi et al. [2021] showed a correlation between the bare soil count of different compositing lengths between one and three years and the respective SOC predictions. In all studies, the best model performances were obtained for the longest time range i.e., three years for Sentinel 2, for which the largest number of bare soil counts was detected.

Table 3.3.5: Mean number of cloudless scenes for SRC generation for different compositing lengths.

Compositing period	**15Y**	**10Y**	**7Y**	**5Y**	**3Y**
Mean number of cloudless scenes per pixel	127.8	86.4	58.3	53.1	32.8

As Tziolas et al. [2021] point out, soil monitoring at a high spatial resolution over large geographical coverage is urgently needed. In terms of SOC monitoring we obtain, that the 3Y period is not advisable. The SOC prediction performances are not reliable enough (RPD = 1.51, PV+BLUE). However, a 10Y or 15Y compositing period may be too long to adequately detect SOC changes. Cropland soils usually have low and stable SOC contents in comparison to areas covered by permanent vegetation cover [Fließbach et al. 2007]. Changes in management practices can increase the SOC stocks, at least temporarily. E.g. the transition from conventional to organic farming systems has an increasing effect on SOC contents [Gattinger et al. 2012]. Land use changes are responsible for larger increases or decreases of SOC contents [Guillaume et al. 2021]. E.g., the transition from grassland to cropland can result in a significant decrease of SOC contents within a short period of time [Guo and Gifford 2022]. However, it can last several years (~ 20 y) to reach a new equilibrium in temperate zones [Poeplau et al. 2011]. In addition, in Bavaria as in several temperate climate zones, there is a declining trend of SOC in agricultural soils over the last 30 years due to climate change [Guillaume et al. 2021]. The challenge is to define the shortest applicable compositing length to capture SOC changes and at the same time optimizing SOC prediction performances. Hence, the minimal compositing length for monitoring purpose has to contain at least five years (Table 3.3.4). In comparison to the 3Y results the model performances are significantly increasing for 5Y SRC (R^2: 0.56 to 0.66). Expanding the compositing length (i.e. 10Y or 15Y), the increase of the model performances is minor (R^2: 0.69 (10Y), 0.71 (15Y)). However, this behavior has to be confirmed for other regions.

5. Conclusion

The overall scope of the paper was to optimize the parameters for SOC monitoring purposes using Landsat data. We focused on the reliability of the selection of exposed soil dates based on different spectral indices. We first compared the extracted exposed soil dates to times, when a field is likely to be bare. In comparison to the crop calendar all three spectral indices allow a reliable extraction of bare soil dates. Due to the combination of summer and winter crops in the test area, a pre-selection of spring (March to May) and autumn scenes (August to October) allowed a reduction of misclassified bare soil dates. However, the selection depends on the crop types.

We further analyzed the influence of the indices for topsoil SOC prediction in Bavaria using Landsat. Although, PV+BLUE for SRC generation performed almost always best, the indices showed a smaller influence on the model performances in comparison to a pre-selection of periods integrated into the SRC (e.g., built on crop calendar). Based on the results (the correlation of bare soil dates with phenological information), we suggest to use external data sets on phenology for SRC processing. The use of external data sets can enable a more robust selection of bare soil dates, which then correlates with better SOC model performances.

We also evaluated which time period allows the most accurate prediction of SOC contents for monitoring purposes or SOC change analyses using Landsat images. For PV+BLUE and PV+IR2 longer compositing periods (10Y / 15Y) showed better model performances. For NBR2 this was not as clear. For monitoring purpose based on SCMaP Landsat SRCs we propose a compositing length for at least 5Y.

Acknowledgements: We thank the Bavarian agencies, the Bavarian Environment Agency (LfU), the Bavarian State Research Center for Agriculture (LfL) for providing the soil databases. Additionally, we thank the Chair of Organic Agriculture and Agronomy of the Technical University of Munich (TUM) for providing field observations used for building Ref1.

Funding**:** This research was funded by the German Federal Ministry of Food and Agriculture (BMEL), grant number 281B301816" as part of the Soil-DE Project "Entwicklung von Indikatoren zur Bewertung der Ertragsfähigkeit, Nutzungsintensität und Vulnerabilität landwirtschaftlich genutzter Böden in Deutschland"

References

Adams, B., L. Iverson, S. Matthews, M. Peters, A. Prasad, and D. M. Hix. 2020. Mapping forest composition with landsat time series: An evaluation of seasonal composites and harmonic regression. Remote Sensing 12 (4):610.

Asam, S., U. Gessner, R. Almengor González, M. Wenzl, J. Kriese, and C. Kuenzer. 2022. Mapping Crop Types of Germany by Combining Temporal Statistical Metrics of Sentinel-1 and Sentinel-2 Time Series with LPIS Data. Remote Sensing 14 (13):2981.

Asner, G. P., and K. B. Heidebrecht. 2002. Spectral unmixing of vegetation, soil and dry carbon cover in arid regions: comparing multispectral and hyperspectral observations. International Journal of Remote Sensing 23 (19):3939-3958.

Bartholomeus, H., L. Kooistra, A. Stevens, M. van Leeuwen, B. van Wesemael, E. Ben-Dor, and B. Tychon. 2011. Soil organic carbon mapping of partially vegetated agricultural fields with imaging spectroscopy. International Journal of Applied Earth Observation and Geoinformation 13 (1):81-88.

Bartholomeus, H., M. E. Schaepman, L. Kooistra, A. Stevens, W. Hoogmoed, and O. Spaargaren. 2008. Spectral reflectance based indices for soil organic carbon quantification. Geoderma 145 (1-2):28-36.

Batjes, N. H. 1996. Total carbon and nitrogen in the soils of the world. European journal of soil science 47 (2):151-163.

Bayer, A. D., M. Bachmann, D. Rogge, A. Müller, and H. Kaufmann. 2016. Combining field and imaging spectroscopy to map soil organic carbon in a semiarid environment. IEEE Journal of Selected Topics in Applied Earth Observations and Remote Sensing 9 (9):3997-4010.
Bayerisches Landesamt für Statistik 2021. Ernte der Feldfrüchte und des Grünlandes in Bayern 2020 - Totalerhebung. In Statistische Berichte.
Ben-Dor, E., and A. Banin. 1995. Near-infrared analysis as a rapid method to simultaneously evaluate several soil properties. Soil Science Society of America Journal 59 (2):364-372.
Ben-Dor, E., S. Chabrillat, J. A. M. Demattê, G. Taylor, J. Hill, M. Whiting, and S. Sommer. 2009. Using imaging spectroscopy to study soil properties. Remote Sensing of Environment 113:S38-S55.
Ben-Dor, E., Y. Inbar, and Y. Chen. 1997. The reflectance spectra of organic matter in the visible near-infrared and short wave infrared region (400–2500 nm) during a controlled decomposition process. Remote Sensing of Environment 61 (1):1-15.
Blickensdörfer, L., M. Schwieder, D. Pflugmacher, C. Nendel, S. Erasmi, and P. Hostert. 2022. Mapping of crop types and crop sequences with combined time series of Sentinel-1, Sentinel-2 and Landsat 8 data for Germany. Remote Sensing of Environment 269:112831.
Bouma, J., L. Montanarella, and G. Evanylo. 2019. The challenge for the soil science community to contribute to the implementation of the UN Sustainable Development Goals. Soil Use and Management 35 (4):538-546.
Breiman, L. 2001. Random forests. Machine learning 45 (1):5-32.
Bucheli, J., T. Dalhaus, and R. Finger. 2022. Temperature effects on crop yields in heat index insurance. Food Policy 107:102214.
Castaldi, F. 2021. Sentinel-2 and Landsat-8 Multi-Temporal Series to Estimate Topsoil Properties on Croplands. Remote Sensing 13 (17):3345.
Castaldi, F., S. Chabrillat, A. Don, and B. van Wesemael. 2019 a. Soil organic carbon mapping using LUCAS topsoil database and Sentinel-2 data: An approach to reduce soil moisture and crop residue effects. Remote Sensing 11 (18):2121.
Castaldi, F., A. Hueni, S. Chabrillat, K. Ward, G. Buttafuoco, B. Bomans, K. Vreys, M. Brell, and B. van Wesemael. 2019 b. Evaluating the capability of the Sentinel 2 data for soil organic carbon prediction in croplands. ISPRS Journal of Photogrammetry and Remote Sensing 147:267-282.
Chabrillat, S., E. Ben-Dor, J. Cierniewski, C. Gomez, T. Schmid, and B. van Wesemael. 2019. Imaging spectroscopy for soil mapping and monitoring. Surveys in Geophysics 40 (3):361-399.
Chabrillat, S., A. F. Goetz, L. Krosley, and H. W. Olsen. 2002. Use of hyperspectral images in the identification and mapping of expansive clay soils and the role of spatial resolution. Remote Sensing of Environment 82 (2-3):431-445.
Chang, C.-W., and D. A. Laird. 2002. Near-infrared reflectance spectroscopic analysis of soil C and N. Soil science 167 (2):110-116.
Dang, Y. P., R. C. Dalal, and N. W. Menzies. 2020. No-till farming systems for sustainable agriculture: challenges and opportunities: Springer.
de Brogniez, D., C. Ballabio, A. Stevens, R. Jones, L. Montanarella, and B. van Wesemael. 2015. A map of the topsoil organic carbon content of Europe generated by a generalized additive model. European journal of soil science 66 (1):121-134.
Demattê, J. A., J. L. Safanelli, R. R. Poppiel, R. Rizzo, N. E. Q. Silvero, W. d. S. Mendes, B. R. Bonfatti, A. C. Dotto, D. F. U. Salazar, and F. A. d. O. Mello. 2020. Bare earth's surface spectra as a proxy for soil resource monitoring. Scientific reports 10 (1):1-11.
Demattê, J. A. M., C. T. Fongaro, R. Rizzo, and J. L. Safanelli. 2018. Geospatial Soil Sensing System (GEOS3): A powerful data mining procedure to retrieve soil spectral reflectance from satellite images. Remote Sensing of Environment 212:161-175.
Denman, K. L., G. Brasseur, A. Chidthaisong, P. Ciais, P.M. Cox, R.E. Dickinson, D. Hauglustaine, C. Heinze, E. Holland, D. Jacob, U., and S. R. Lohmann, P.L. da Silva Dias, S.C. Wofsy and X. Zhang. 2007. Couplings between changes in the climate system and biogeochemistry. Climate change:499587.
Dharumarajan, S., and R. Hegde. 2022. Digital mapping of soil texture classes using Random Forest classification algorithm. Soil Use and Management 38 (1):135-149.
Diek, S., F. Fornallaz, M. E. Schaepman, and R. De Jong. 2017. Barest pixel composite for agricultural areas using landsat time series. Remote Sensing 9 (12):1245.
Dvorakova, K., U. Heiden, K. Pepers, G. van Os, G. Staats, and B. van Wesemael. Improving Soil Organic Carbon Predictions from Sentinel-2 Soil Composites by Assessing Surface Conditions and Uncertainties. Available at SSRN 4056879.
Dvorakova, K., U. Heiden, and B. van Wesemael. 2021. Sentinel-2 exposed soil composite for soil organic carbon prediction. Remote Sensing 13 (9):1791.

Dvorakova, K., P. Shi, Q. Limbourg, and B. van Wesemael. 2020. Soil organic carbon mapping from remote sensing: the effect of crop residues. Remote Sensing 12 (12):1913.
Fernandez-Ugalde, O., S. Scarpa, A. Orgiazzi, P. Panagos, M. Van Liedekerke, A. Marechal, and A. Jones. 2022. LUCAS 2018 Soil Module.
Fliessbach, A., H.-R. Oberholzer, L. Gunst, and P. Mäder 2006. Soil organic matter and biological soil quality indicators after 21 years of organic and conventional farming. Agriculture, Ecosystems and Environment 118:273-284.
Gattinger, A., A. Muller, M. Haeni,C. Skinner, A. Fliessbach, N. Buchmann, P. Mäder, M. Stolze, P. Smith, N.E.-H. Scialabba, and U. Niggli 2012. Enhanced top soil carbon stocks underorganic farming, Proceedings of the National Academy of Sciences 109.44. 18226-18231.
Gerstmann, H., D. Doktor, C. Gläßer, and M. Möller. 2016. PHASE: a geostatistical model for the Kriging-based spatial prediction of crop phenology using public phenological and climatological observations. Computers and Electronics in Agriculture 127:726-738.
Gholizadeh, A., C. Neumann, S. Chabrillat, B. van Wesemael, F. Castaldi, L. Borůvka, J. Sanderman, A. Klement, and C. Hohmann. 2021. Soil organic carbon estimation using VNIR–SWIR spectroscopy: The effect of multiple sensors and scanning conditions. Soil and Tillage Research 211:105017.
Gomez, C., R. A. V. Rossel, and A. B. McBratney. 2008. Soil organic carbon prediction by hyperspectral remote sensing and field vis-NIR spectroscopy: An Australian case study. Geoderma 146 (3-4):403-411.
Guillaume, T., L. Bragazza, C. Levasseur, Z. Libohova, and S. Sinaj 2021. Long-term soil organic carbon dynamics in temperate cropland-grassland systems. Agriculture, Ecosystems and Environment 305:107184.
Guo, L.B., and R.M. Gifford 2002. Soil carbon stocks and land use change: a meta analysis. Global Change Biology 8, 345-360.
Griffiths, P., C. Nendel, and P. Hostert. 2019. Intra-annual reflectance composites from Sentinel-2 and Landsat for national-scale crop and land cover mapping. Remote Sensing of Environment 220:135-151.
Hansen, M. C., A. Egorov, D. P. Roy, P. Potapov, J. Ju, S. Turubanova, I. Kommareddy, and T. R. Loveland. 2011. Continuous fields of land cover for the conterminous United States using Landsat data: First results from the Web-Enabled Landsat Data (WELD) project. Remote Sensing Letters 2 (4):279-288.
Heiden, U., P. d'Angelo, P. Schwind, P. Karlshöfer, R. Müller, S. Zepp, M. Wiesmeier, and P. Reinartz 2022. Soil Reflectance Composites – Improved Thresholding and Performance Evaluation. Remote Sensing 14:4526.
Hermosilla, T., M. A. Wulder, J. C. White, N. C. Coops, and G. W. Hobart. 2015. An integrated Landsat time series protocol for change detection and generation of annual gap-free surface reflectance composites. Remote Sensing of Environment 158:220-234.
Heupel, K., D. Spengler, and S. Itzerott. 2018. A progressive crop-type classification using multitemporal remote sensing data and phenological information. PFG–Journal of Photogrammetry, Remote Sensing and Geoinformation Science 86 (2):53-69.
Heuvelink, G. B., M. E. Angelini, L. Poggio, Z. Bai, N. H. Batjes, R. van den Bosch, D. Bossio, S. Estella, J. Lehmann, and G. F. Olmedo. 2021. Machine learning in space and time for modelling soil organic carbon change. European journal of soil science 72 (4):1607-1623.
Jandl, R., M. Rodeghiero, C. Martinez, M. F. Cotrufo, F. Bampa, B. Van Wesemael, R. B. Harrison, I. A. Guerrini, D. d. Richter Jr, and L. Rustad. 2014. Current status, uncertainty and future needs in soil organic carbon monitoring. Science of the total environment 468:376-383.
Jobbágy, E. G., and R. B. Jackson. 2000. The vertical distribution of soil organic carbon and its relation to climate and vegetation. Ecological applications 10 (2):423-436.
Jones, R. J., R. Hiederer, E. Rusco, and L. Montanarella. 2005. Estimating organic carbon in the soils of Europe for policy support. European journal of soil science 56 (5):655-671.
Kaspar, F., F. Kratzenstein, and A. K. Kaiser-Weiss. 2019. Interactive open access to climate observations from Germany. Advances in Science and Research 16:75-83.
Kaspar, F., K. Zimmermann, and C. Polte-Rudolf. 2015. An overview of the phenological observation network and the phenological database of Germany's national meteorological service (Deutscher Wetterdienst). Advances in Science and Research 11 (1):93-99.
Lal, R. 2016. Soil health and carbon management. Food and Energy Security 5 (4):212-222 - 2020. Soil organic matter content and crop yield. Journal of Soil and Water Conservation 75 (2):27A-32A.
Lal, R. 2020. Soil organic matter content and crop yiels. Journal of soil and water conservation 75:2, 27A-32A.
Loiseau, T., S. Chen, V. L. Mulder, M. R. Dobarco, A. C. Richer-de-Forges, S. Lehmann, H. Bourennane, N. P. Saby, M. P. Martin, and E. Vaudour. 2019. Satellite data integration for soil clay content modelling at a national scale. International Journal of Applied Earth Observation and Geoinformation 82:101905.

Lorenz, K., R. Lal, and K. Ehlers. 2019. Soil organic carbon stock as an indicator for monitoring land and soil degradation in relation to U nited N ations' S ustainable D evelopment G oals. Land Degradation & Development 30 (7):824-838.
Luo, C., Y. Wang, X. Zhang, W. Zhang, and H. Liu. 2022. Spatial prediction of soil organic matter content using multiyear synthetic images and partitioning algorithms. CATENA 211:106023.
Malec, S., D. Rogge, U. Heiden, A. Sanchez-Azofeifa, M. Bachmann, and M. Wegmann. 2015. Capability of spaceborne hyperspectral EnMAP mission for mapping fractional cover for soil erosion modeling. Remote Sensing 7 (9):11776-11800.
Möller, M., L. Boutarfa, and J. Strassemeyer. 2020. PhenoWin–An R Shiny application for visualization and extraction of phenological windows in Germany. Computers and Electronics in Agriculture 175:105534.
Möller, M., J. Doms, H. Gerstmann, and T. Feike. 2019. A framework for standardized calculation of weather indices in Germany. Theoretical and Applied Climatology 136 (1):377-390.
Möller, M., H. Gerstmann, F. Gao, T. C. Dahms, and M. Förster. 2017. Coupling of phenological information and simulated vegetation index time series: Limitations and potentials for the assessment and monitoring of soil erosion risk. CATENA 150:192-205.
Möller, M., S. Zepp, M. Wiesmeier, H. Gerighausen, and U. Heiden. 2022. Scale-Specific Prediction of Topsoil Organic Carbon Contents Using Terrain Attributes and SCMaP Soil Reflectance Composites. Remote Sensing 14 (10):2295.
Montanarella, L., and P. Panagos. 2021. The relevance of sustainable soil management within the European Green Deal. Land use policy 100:104950.
Mzid, N., F. Castaldi, M. Tolomio, S. Pascucci, R. Casa, and S. Pignatti. 2022. Evaluation of Agricultural Bare Soil Properties Retrieval from Landsat 8, Sentinel-2 and PRISMA Satellite Data. Remote Sensing 14 (3):714.
Nachtergaele, F., H. Velthuizen, L. Verelst, and D. Wiberg. 2009. Harmonized World Soil Database (HWSD). Food and Agriculture Organization of the United Nations, Rome.
Nocita, M., A. Stevens, C. Noon, and B. van Wesemael. 2013. Prediction of soil organic carbon for different levels of soil moisture using Vis-NIR spectroscopy. Geoderma 199:37-42.
Okin, G. S. 2007. Relative spectral mixture analysis—A multitemporal index of total vegetation cover. Remote Sensing of Environment 106 (4):467-479.
Pedregosa, F., G. Varoquaux, A. Gramfort, V. Michel, B. Thirion, O. Grisel, M. Blondel, P. Prettenhofer, R. Weiss, and V. Dubourg. 2011. Scikit-learn: Machine learning in Python. the Journal of machine Learning research 12:2825-2830.
Popleau, C., A. Don, L. Vesterdal, J. Leifeld, B. van Wesemael, J. Schumacher, and A. Gensior 2011. Temporal dynamics of soil organic carbon after land-use change in the temperate zone – carbon response functions as a model approach. Global Change Biology 17:2415-2427.
Preidl, S., M. Lange, and D. Doktor. 2020. Introducing APiC for regionalised land cover mapping on the national scale using Sentinel-2A imagery. Remote Sensing of Environment 240:111673.
Richter, R., and D. Schläpfer. 2014. Atmospheric/Topographic Correction for Airborne Imagery, ATCOR-4 User Guide, Version 6.2. 1. DLR-IB 565-02/08. Deutsches Zentrum für Luft-und Raumfahrt (DLR): Weßling, Germany:225.
Rogge, D., A. Bauer, J. Zeidler, A. Mueller, T. Esch, and U. Heiden. 2018. Building an exposed soil composite processor (SCMaP) for mapping spatial and temporal characteristics of soils with Landsat imagery (1984–2014). Remote Sensing of Environment 205:1-17.
Rouse Jr, J. W., R. H. Haas, J. Schell, and D. Deering. 1973. Monitoring the vernal advancement and retrogradation (green wave effect) of natural vegetation.
Roy, A., K. Bag, P. Tigga, P. Kumar, and R. K. Didawat. 2022. Estimation of Soil Organic Carbon by Remote Sensing. Chief Editor Dr. Neeraj Kumar:79.
Safanelli, J. L., S. Chabrillat, E. Ben-Dor, and J. A. Demattê. 2020. Multispectral models from bare soil composites for mapping topsoil properties over Europe. Remote Sensing 12 (9):1369.
Sakhaee, A., A. Gebauer, M. Ließ, and A. Don. 2022. Spatial prediction of organic carbon in German agricultural topsoil using machine learning algorithms. SOIL 8 (2):587-604.
Scharlemann, J. P., E. V. Tanner, R. Hiederer, and V. Kapos. 2014. Global soil carbon: understanding and managing the largest terrestrial carbon pool. Carbon Management 5 (1):81-91.
Seitz, D., L. M. Fischer, R. Dechow, M. Wiesmeier, and A. Don. 2022. The potential of cover crops to increase soil organic carbon storage in German croplands. Plant and soil:1-17.
Sorenson, P., S. Shirtliffe, and A. Bedard-Haughn. 2021. Predictive soil mapping using historic bare soil composite imagery and legacy soil survey data. Geoderma 401:115316.
Tziolas, N., N. Tsakiridis, E. Ben-Dor, J. Theocharis, and G. Zalidis. 2020. Employing a multi-input deep convolutional neural network to derive soil clay content from a synergy of multi-temporal optical and radar imagery data. Remote Sensing 12 (9):1389.

Tziolas, N., N. Tsakiridis, S. Chabrillat, J. A. Demattê, E. Ben-Dor, A. Gholizadeh, G. Zalidis, and B. Van Wesemael. 2021. Earth observation data-driven cropland soil monitoring: A review. Remote Sensing 13 (21):4439.

Urbina-Salazar, D., E. Vaudour, N. Baghdadi, E. Ceschia, A. C. Richer-De-Forges, S. Lehmann, and D. Arrouays. 2021. Using Sentinel-2 Images for Soil Organic Carbon Content Mapping in Croplands of Southwestern France. The Usefulness of Sentinel-1/2 Derived Moisture Maps and Mismatches between Sentinel Images and Sampling Dates. Remote Sensing 13 (24):5115.

Van Deventer, A., A. Ward, P. Gowda, and J. Lyon. 1997. Using thematic mapper data to identify contrasting soil plains and tillage practices. Photogrammetric engineering and remote sensing 63:87-93.

Vaudour, E., A. Gholizadeh, F. Castaldi, M. Saberioon, L. Borůvka, D. Urbina-Salazar, Y. Fouad, D. Arrouays, A. C. Richer-de-Forges, and J. Biney. 2022. Satellite Imagery to Map Topsoil Organic Carbon Content over Cultivated Areas: An Overview. Remote Sensing 14 (12):2917.

Vaudour, E., C. Gomez, Y. Fouad, and P. Lagacherie. 2019 a. Sentinel-2 image capacities to predict common topsoil properties of temperate and Mediterranean agroecosystems. Remote Sensing of Environment 223:21-33.

Vaudour, E., C. Gomez, P. Lagacherie, T. Loiseau, N. Baghdadi, D. Urbina-Salazar, B. Loubet, and D. Arrouays. 2021. Temporal mosaicking approaches of Sentinel-2 images for extending topsoil organic carbon content mapping in croplands. International Journal of Applied Earth Observation and Geoinformation 96:102277.

Vaudour, E., C. Gomez, T. Loiseau, N. Baghdadi, B. Loubet, D. Arrouays, L. Ali, and P. Lagacherie. 2019 b. The impact of acquisition date on the prediction performance of topsoil organic carbon from Sentinel-2 for croplands. Remote Sensing 11 (18):2143.

Wang, X., Y. Zhang, P. M. Atkinson, and H. Yao. 2020. Predicting soil organic carbon content in Spain by combining Landsat TM and ALOS PALSAR images. International Journal of Applied Earth Observation and Geoinformation 92:102182.

Ward, K. J., S. Chabrillat, C. Neumann, and S. Foerster. 2019. A remote sensing adapted approach for soil organic carbon prediction based on the spectrally clustered LUCAS soil database. Geoderma 353:297-307.

White, J. C., M. Wulder, G. Hobart, J. Luther, T. Hermosilla, P. Griffiths, N. Coops, R. Hall, P. Hostert, and A. Dyk. 2014 a. Pixel-based image compositing for large-area dense time series applications and science. Canadian Journal of Remote Sensing 40 (3):192-212.

Wiesmeier, M., F. Barthold, B. Blank, and I. Kögel-Knabner. 2011. Digital mapping of soil organic matter stocks using Random Forest modeling in a semi-arid steppe ecosystem. Plant and soil 340 (1):7-24.

Wiesmeier, M., F. Barthold, P. Spörlein, U. Geuß, E. Hangen, A. Reischl, B. Schilling, G. Angst, M. von Lützow, and I. Kögel-Knabner. 2014. Estimation of total organic carbon storage and its driving factors in soils of Bavaria (southeast Germany). Geoderma Regional 1:67-78.

Wiesmeier, M., R. Hübner, F. Barthold, P. Spörlein, U. Geuß, E. Hangen, A. Reischl, B. Schilling, M. von Lützow, and I. Kögel-Knabner. 2013. Amount, distribution and driving factors of soil organic carbon and nitrogen in cropland and grassland soils of southeast Germany (Bavaria). Agriculture, ecosystems & environment 176:39-52.

Wiesmeier, M., P. Schad, M. von Lützow, C. Poeplau, P. Spörlein, U. Geuß, E. Hangen, A. Reischl, B. Schilling, and I. Kögel-Knabner. 2014 b. Quantification of functional soil organic carbon pools for major soil units and land uses in southeast Germany (Bavaria). Agriculture, ecosystems & environment 185:208-220.

Wiesmeier, M., L. Urbanski, E. Hobley, B. Lang, M. von Lützow, E. Marin-Spiotta, B. van Wesemael, E. Rabot, M. Ließ, and N. Garcia-Franco. 2019. Soil organic carbon storage as a key function of soils-A review of drivers and indicators at various scales. Geoderma 333:149-162.

WRB, I. W. G. 2006. World reference base for soil resources.

Wulder, M. A., T. R. Loveland, D. P. Roy, C. J. Crawford, J. G. Masek, C. E. Woodcock, R. G. Allen, M. C. Anderson, A. S. Belward, and W. B. Cohen. 2019. Current status of Landsat program, science, and applications. Remote Sensing of Environment 225:127-147.

Zepp, S., U. Heiden, M. Bachmann, M. Wiesmeier, M. Steininger, and B. van Wesemael. 2021 b. Estimation of Soil Organic Carbon Contents in Croplands of Bavaria from SCMaP Soil Reflectance Composites. Remote Sensing 13 (16):3141.

Zepp, S., M. Jilge, A. Metz-Marconcini, and U. Heiden. 2021 a. The influence of vegetation index thresholding on EO-based assessments of exposed soil masks in Germany between 1984 and 2019. ISPRS Journal of Photogrammetry and Remote Sensing 178:366-381.

Zhou, T., Y. Geng, C. Ji, X. Xu, H. Wang, J. Pan, J. Bumberger, D. Haase, and A. Lausch. 2021. Prediction of soil organic carbon and the C: N ratio on a national scale using machine learning and satellite data: A comparison between Sentinel-2, Sentinel-3 and Landsat-8 images. Science of the total environment 755:142661.

Zhu, Z., S. Wang, and C. E. Woodcock. 2015. Improvement and expansion of the Fmask algorithm: Cloud, cloud shadow, and snow detection for Landsats 4–7, 8, and Sentinel 2 images. Remote Sensing of Environment 159:269-277.
Zhu, Z., and C. E. Woodcock. 2012. Object-based cloud and cloud shadow detection in Landsat imagery. Remote Sensing of Environment 118:83-94.

4. Conclusion & Outlook

The following chapter summarizes the main findings of this thesis. Furthermore, a synthesis and recommendations are given, how the Landsat SCMaP SRCs can be used for SOC estimation and (retrospective) monitoring purposes to enhance the spatial and/or temporal limitation/s of current soil maps, databases and monitoring approaches.

4.1. Summary

The aim of this thesis was to explore the capabilities of Landsat SRC for SOC estimation and (retrospective) monitoring of topsoil croplands in Bavaria, Germany. The three publications (chapter 3) present the analyses performed, the challenges that raised, the final results and their critical discussion. In the following, the key findings of the three publications are summarized in order to answer the ROs stated in chapter 2.

RO1: Derivation and Validation of masks that contain exposed soil pixels from multi-year Landsat data stacks for Germany from 1984 to 2019.

Publication 1 (chapter 3.1) focused on the complexity of methodological improvements of the index thresholding, which is a fundamental part of the SCMaP workflow, and on the validation of the spatial and temporal distribution of exposed soil pixels. A new automated sampling strategy for thresholding required for an area-wide application of the SCMaP methodology was developed to substitute the manual selection approach. Here, a random sampling of stable CLC pixels for the threshold definition and to separate exposed soils from all other LC classes in the SCMaP processing chain built the baseline. The newly developed sampling is a reliable workflow for the identification of the spatial and temporal distribution of exposed soils. We have chosen TA_{min} of 0.831 and TA_{max} of 1.697 for the generation of the exposed soil masks. In particular the high correlation results (R^2 = 0.79 to 0.90) of exposed soil areas in comparison to two different reference datasets (Destatis and CORINE Land Cover) containing the spatial cropland distribution per federal state and on county level across time, prove the applicability of the new threshold definition. However, the presented results have shown the large dependencies of the vegetation index approach on environmental conditions (i.e., northwestern Germany). Thus, a regionalization of the parameter settings for, e.g., bio-geographical regions instead of counties or countries is recommended. The validation with two independent reference datasets confirmed the need for a regional differentiation of the thresholds (i.e., lower correlation accuracies for Lower Saxony). Additionally, the applied fixed percentile rule for the determination of TH_{max} had to be adapted from 0.995 to 0.900. However, the results also indicate replacing the percentile rule by a more suitable and robust method according to the sampling scheme. Furthermore, the analyses have shown the importance of a reliable number of cloudless scenes per compositing period for the extraction of exposed soils. Time periods (2000-04 and 2005-09) composed of more

than 55 cloudless scenes per pixel enabled higher correlation coefficients ($R^2 > 0.87$). In contrast, weaker correlation coefficients ($R^2 < 0.82$) were identified for periods containing less than 45 cloudless scenes per pixel. In summary, the exposed soil pixels derived from SCMaP based on the new automated and random sampling of landcover class pixels for the determination of thresholds is a reliable workflow and enables the identification of the distribution of exposed soils. Thus, it can be used as a temporally and spatially enhanced database, which also can be a valuable data source for land cover analysis in the future.

RO2: Estimating the potential of the SCMaP SRC generated from Landsat images covering 30 years to derive a high-resolution map of SOC contents in Bavarian croplands.

The 30-year SCMaP SRC was successfully used to model the spatial SOC distribution of exposed topsoils of croplands in Bavaria in publication 2 (chapter 3.2). For this purpose, the 30-year SRC was correlated with legacy soil point measurements to quantify SOC contents for an area-wide mapping approach to separate within field patterns. The analyses have shown, that a spatial/spectral filtering of the database, to exclude heterogenous pixel clusters, is a valuable approach linking soil samples to EO data with a pixel resolution of several meters (e.g., Landsat: 30 m). Twice the standard deviation (STD) per band was selected as threshold. However, as the distribution of the cluster STDs per reflectance band is representing a non-gaussian behavior, this indicates using the median and quantiles for threshold determination is more appropriate for further investigations. The spatial/spectral filtering should also be considered for an implementation of higher temporal resolution data (e.g., Sentinel-2) or higher spectral resolution data (e.g., EnMAP) with similar spatial pixel size in the future.

The results, highlight the successful use of a Random Forest Machine Learning approach to predict the spatial SOC distribution for an area-wide mapping. The reflectances in combination with spectral indices showed the highest performances and accuracies of the model validation using 30% of the input sample data base ($R^2 = 0.67$, RMSE = 1.24%, RPD = 1.77). The findings were confirmed by an external validation based on field data not included in the model calibration and validation process. The comparison between the measured and predicted SOC contents showed a mean difference of 0.11% SOC using the Random Forest model and the best data setup (reflectances and indices). The SCMaP SRC is a promising approach to predict the spatial SOC distribution over large geographical extents with a high spatial resolution (30 m). However, the long compositing range of 30 years should only be used in areas, where no SOC changes are documented or expected. For monitoring purpose or regions with a dynamic behavior of SOC contents, shorter compositing periods are required.

RO3: Optimization of parameters for SRC generation for recurrent assessments of SOC contents using Landsat data, considering the reliability of the selection of exposed soil dates.

In order to address the third objective, exposed soil dates integrated into the SRCs were validated and the influence of different parameters (i.e., vegetation indices, composition of compositing periods, and lengths) on SOC modeling were evaluated in publication 3 (chapter 3.3). First, the bare soil dates identified using different indices were compared to times when the field is likely to be bare. For this purpose, field observations and information based on the crop calendar were intersected with the bare soil dates. The analyses have shown that there is a reliable correlation between the SCMaP bare soil dates in comparison to reference data. This was proven

for all three implemented indices. Due to the typical combination of summer and winter crops in the investigation area, a pre-selection of spring (March to May) and autumn scenes (August to October) is recommended. Based on the pre-selection misclassified soils are reduced, during times when the fields are likely to be covered with vegetation or crop residues. Pursuing to transfer the approach to other climatic regions, the pre-selection should depend on regional crop types in the investigation area.

Further, the influences of the vegetation indices for bare soil extraction, the pre-selection of months integrated into the SRC and the compositing length on SOC predictions were investigated. Although, the PV+BLUE index for SRC generation performed best for Landsat data (R^2: 0.56 – 0.72, RMSE: 1.09% – 1.29%, RPD: 1.51 – 1.91), the indices indicated smaller impacts for SOC prediction in comparison to a crop type-based pre-selection of scenes for SRC generation. In general, the findings indicate that the use of external data sets on phenology to select input scenes integrated for SRC processing, provides a more robust selection of bare soil dates. This results in better SOC prediction performances (SRC_{full}: R^2: 0.59 – 0.60, RMSE: 1.00% – 1.28%, RDP: 1.57 – 1.58 / $SRC_{spring/autumn}$: R^2: 0.64 – 0.67, RMSE: 1.05% – 1.29%, RDP: 1.67 – 1.73). As large-scale field observations are barely available statistical datasets with phenological information, as provided by the Germany's National Meteorological Service (Deutscher Wetterdienst - DWD), can represent a suitable option for area-wide mapping.

For monitoring purpose or SOC change analyses using Landsat images longer compositing periods (10 years / 15 years) showed better SOC prediction performances. However, such compositing lengths could be too long for monitoring purposes. Based on the findings, a compositing length of at least 5 years is purposed using SCMaP Landsat SRCs for analyzing (retrospective) SOC changes of topsoil croplands.

Overall, the findings presented in the publications (chapters 3.1, 3.2, 3.3) demonstrated, that SCMaP SRCs generated with the updated index thresholding based on bio-geographical regions can be utilized for SOC predictions and (retrospective) change analyses. The use of SCMaP in combination with the newly standardized random selection of land cover pixels for threshold derivation enabled an area wide extraction of exposed soil areas and thus the processing of SRCs for SOC mapping within field patterns of topsoil croplands in Bavaria, Germany. In this context, the Random Forest regression approach to combine composite reflectances, derived spectral indices and SOC field measurements are a valuable approach for SOC estimation. A spatial/spectral filtering of heterogenous pixel clusters significantly increased the model capabilities. For monitoring purposes to capture SOC changes, compositing lengths of at least 5-years are recommended for that purpose. Thereby, the pre-selection of scenes for SRC generation effected the SOC model performances more than in comparison different of spectral indices used for SRC processing. The knowledge obtained is highly relevant for fulfilling the rising requirements and needs proposed by the policy for high spatial and temporal SOC mapping and (retrospective) monitoring purposes of SOC developments as introduced in chapter 1.2.

4.2. Outlook

Due to the application of the Landsat SCMaP SRCs for SOC prediction, exemplarily for a test area in Germany and adjacent regions, the work successfully provided an operational approach for SOC estimation and retrospective monitoring of cropland topsoils not permanently covered

by vegetation. The human impacts on cropland soils were huge in the past and SOC as a key element for healthy and productive soils will also be an essential future research aspect. The developed methods indicate the potential to improve the understanding and knowledge of SOC developments and give an answer to the different political inquiries raised. SCMaP in combination with the developed automated index thresholding approach is a valuable method for SRC processing as input for cropland SOC predictions. With this work, some central aspects controlling the SOC modeling based on Landsat data were answered. However, during the analyses several assumptions were made requiring an in-depth proof. Additionally, further questions (se Figure 2.1) emerged, which have to be investigated in the future.

For further improvements, the spectral behavior of the SRCs should be investigated. So far, there was no validation of the SRC spectra and field measurements. A comparison of the temporal development of the SRC spectra of consecutive 5-year SRCs between 1984 and 2019 indicated a spectral stability. However, a comparison of the averaged SRC spectra with field spectroscopy data (e.g., airborne or field hyperspectral measurements) could enlarge the understanding for soil parameter modeling and minimize uncertainties. In this context, it has to be considered, that the comparison of a single field spectra to the averaged situation of several years could be biased by temporal differences in soil moisture or temporal tillage conditions. The validation data need to be carefully selected. Laboratory spectra as the reflectance measurements from the LUCAS dataset for validation are not suitable, as the samples are often prepared (i.e., dried and sieved) and measured under optimal conditions (i.e., illumination, vertical measurement). A potential validation approach could be enabled by comparing all bare soil pixel spectra, identified by the thresholds (before averaging to the SRC) to field spectra, representing different conditions (e.g., soil moisture, tillage). Here, the position of the field spectra whether these are within or outside the pixel spectral range can give more insights about the uncertainties.

The model performances based on the SCMaP SRC were comparable to the SOC prediction capabilities presented by various authors (see chapter 3.2, publication 2, Table 3.2.1). However, in almost all studies, lower RMSE values were reported for the SOC prediction. The results provided showed relatively high model uncertainties in the investigation area (RMSE 1.24% for 30-year SRC). However, here a high range of SOC contents occurs (0.26% - 18.3%). For analyzing the influence of such a high SOC variability, it could be considered to separate mineral and organic soils as the latter ones have naturally higher SOC contents. However, for this analysis a division was not considered due to the low amount of organic soil samples. Another step forward would be to transfer the modeling method to other soil parameters (e.g., soil texture distribution, iron content, pH). Several authors have already shown the feasibility of mapping e.g., clay (e.g., Diek et al. 2017, Sorenson et al. 2021), texture distributions (e.g., Safanelli et al. 2020, Mzid et al. 2022, Zhou et al. 2022), or other physico-chemical properties as Calcium Carbonate ($CaCO_3$) (e.g., Safanelli et al. 2020, Castaldi et al. 2021) or pH (e.g., Ghazali et al. 2020, Safanelli et al. 2020) in different temperate regions using compositing approaches. Landsat SCMaP SRCs provide a reliable data source for topsoil content estimation and monitoring. The interaction of different soil parameters can enlarge the knowledge of the geosphere soil and provide more insights for a sustainable use of the resource.

The most critical point using the presented compositing approach based on multispectral satellite imagery is related to the fact, that a clear separation of bare soils and dry vegetation (i.e., crop residues) is not unambiguous possible (Asner and Heidebrecht, 2002; Okin, 2007; Dematté et al., 2018). This issue was discussed in all three publications, as it could be a potential source of uncertainties in the model results. With regard to other publications, the successful separation of

NPV and soils represents one of the biggest challenges using multispectral EO data for soil parameter modeling. However, findings presented by other authors have shown, that a robust index thresholding is enabling a separation of NPV and soils. The findings of the third publication (chapter 3.3) can indicate a robust separation of bare soils and dry vegetation using the developed index thresholding approach. As shown, a small number of exposed soil dates was selected when the field is likely be covered with crop residues or at the end of the vegetative active phase, when the chance for drying vegetation is high (based on the crop calendar). At this point it must be brought up for discussion, that the methodological design of the operational SCMaP processor and the use of the resulting SRCs for soil parameter modeling are developed for an area-wide mapping approach covering the national or even broader spatial scales. This also includes the design of the index thresholding. The data-driven approach is dedicated to large-scale applications. However, a separation of NPV and soils is strongly affected by regional dependencies. A compromise between a reliable separation of soils and NPV and the applicability as an operational processor must be considered. In general, a spectral validation of the SRC data, mentioned above, would enable an in-depth proof of a successful separation. The recently launched hyperspectral spaceborne EnMAP (Environmental Mapping Analysis Program - Guanter et al. 2015) satellite could provide a valuable addition here. However, it has to be considered, that due to the mission architecture local limited areas can be observed for a small number of dates per year. The fusion of Landsat and EnMAP data can enable an in-depth analysis of the successful separation of NPV and soils and additionally benefit significantly the analyses. Hotspots identified with large-scale data-based approaches (Landsat) in combination with the high potential for hyperspectral in-depth analysis is a promising sensor combination for a more accurate understanding of SOC developments in the future.

The proposed methods in this thesis contribute to a spatiotemporal enlarged knowledge about soils and an enhanced understanding of SOC predictions in view of monitoring purposes. Especially, the long history of Landsat imagery is a valuable database for SOC prediction and (retrospective) monitoring. It enables a comprehensive understanding, which is essential for future needs.

References

Adams, B., L. Iverson, S. Matthews, M. Peters, A. Prasad, and D. M. Hix. 2020. Mapping forest composition with landsat time series: An evaluation of seasonal composites and harmonic regression. Remote Sensing 12 (4):610.

Adhikari, K., and A. E. Hartemink. 2016. Linking soils to ecosystem services—A global review. Geoderma 262:101-111.

Asner, G. P., and K. B. Heidebrecht. 2002. Spectral unmixing of vegetation, soil and dry carbon cover in arid regions: comparing multispectral and hyperspectral observations. International Journal of Remote Sensing 23 (19):3939-3958.

Bartholomeus, H., L. Kooistra, A. Stevens, M. van Leeuwen, B. van Wesemael, E. Ben-Dor, and B. Tychon. 2011. Soil organic carbon mapping of partially vegetated agricultural fields with imaging spectroscopy. International Journal of Applied Earth Observation and Geoinformation 13 (1):81-88.

Bayer, A. D., M. Bachmann, D. Rogge, A. Müller, and H. Kaufmann. 2016. Combining field and imaging spectroscopy to map soil organic carbon in a semiarid environment. IEEE Journal of Selected Topics in Applied Earth Observations and Remote Sensing 9 (9):3997-4010.

Ben-Dor, E., S. Chabrillat, J. A. M. Demattê, G. Taylor, J. Hill, M. Whiting, and S. Sommer. 2009. Using imaging spectroscopy to study soil properties. Remote Sensing of Environment 113:S38-S55.

Blouin, M., M. E. Hodson, E. A. Delgado, G. Baker, L. Brussaard, K. R. Butt, J. Dai, L. Dendooven, G. Pérès, and J. Tondoh. 2013. A review of earthworm impact on soil function and ecosystem services. European journal of soil science 64 (2):161-182.

Blume, H.-P., G. W. Brümmer, R. Horn, E. Kandeler, I. Kögel-Knabner, R. Kretzschmar, K. Stahr, B.-M. Wilke, S. Thiele-Bruhn, and G. Welp. 2010. Lehrbuch der bodenkunde: Springer.

Bouma, J., L. Montanarella, and G. Evanylo. 2019. The challenge for the soil science community to contribute to the implementation of the UN Sustainable Development Goals. Soil Use and Management 35 (4):538-546.

Castaldi, F. 2021. Sentinel-2 and Landsat-8 Multi-Temporal Series to Estimate Topsoil Properties on Croplands. Remote Sensing 13 (17):3345.

Castaldi, F., S. Chabrillat, A. Don, and B. van Wesemael. 2019. Soil organic carbon mapping using LUCAS topsoil database and Sentinel-2 data: An approach to reduce soil moisture and crop residue effects. Remote Sensing 11 (18):2121.

Chabrillat, S., E. Ben-Dor, J. Cierniewski, C. Gomez, T. Schmid, and B. van Wesemael. 2019. Imaging spectroscopy for soil mapping and monitoring. Surveys in Geophysics 40 (3):361-399.

Ciais, P., M. Wattenbach, N. Vuichard, P. Smith, S. Piao, A. Don, S. Luyssaert, I. Janssens, A. Bondeau, and R. Dechow. 2010. The European carbon balance. Part 2: croplands. Global Change Biology 16 (5):1409-1428.

Collier, S. M., S. M. Green, A. Inman, D. W. Hopkins, H. Kendall, M. M. Jahn, and J. A. Dungait. 2021. Effect of farm management on topsoil organic carbon and aggregate stability in water: A case study from Southwest England, UK. Soil Use and Management 37 (1):49-62.

COM, E. 2006. Communication from the Commission to the Council, the European Parliament, the European Economic and Social Committee and the Committee of the Regions-Thematic Strategy for Soil Protection [SEC (2006) 620][SEC (2006) 1165]: COM/2006/0231 Final.

COM, E. 2011. 571 final, Communication from the Commission to the European Parliament, the Council, the European Economic and Social Committee and the Committee of the Regions. Roadmap to a Resource Efficient Europe.

Conant, R. T., S. M. Ogle, E. A. Paul, and K. Paustian. 2011. Measuring and monitoring soil organic carbon stocks in agricultural lands for climate mitigation. Frontiers in Ecology and the Environment 9 (3):169-173.

Daughtry, C. S., P. Doraiswamy, E. Hunt Jr, A. Stern, J. McMurtrey Iii, and J. Prueger. 2006. Remote sensing of crop residue cover and soil tillage intensity. Soil and Tillage Research 91 (1-2):101-108.

de Brogniez, D., C. Ballabio, A. Stevens, R. Jones, L. Montanarella, and B. van Wesemael. 2015. A map of the topsoil organic carbon content of Europe generated by a generalized additive model. European journal of soil science 66 (1):121-134.

Demattê, J. A., J. L. Safanelli, R. R. Poppiel, R. Rizzo, N. E. Q. Silvero, W. d. S. Mendes, B. R. Bonfatti, A. C. Dotto, D. F. U. Salazar, and F. A. d. O. Mello. 2020. Bare earth's surface spectra as a proxy for soil resource monitoring. Scientific reports 10 (1):1-11.

Demattê, J. A. M., C. T. Fongaro, R. Rizzo, and J. L. Safanelli. 2018. Geospatial Soil Sensing System (GEOS3): A powerful data mining procedure to retrieve soil spectral reflectance from satellite images. Remote Sensing of Environment 212:161-175.

Diek, S., F. Fornallaz, M. E. Schaepman, and R. De Jong. 2017. Barest pixel composite for agricultural areas using landsat time series. Remote Sensing 9 (12):1245.

Diek, S., M. E. Schaepman, and R. De Jong. 2016. Creating multi-temporal composites of airborne imaging spectroscopy data in support of digital soil mapping. Remote Sensing 8 (11):906.

Dvorakova, K., U. Heiden, and B. van Wesemael. 2021. Sentinel-2 exposed soil composite for soil organic carbon prediction. Remote Sensing 13 (9):1791.

Dwyer, J. L., D. P. Roy, B. Sauer, C. B. Jenkerson, H. K. Zhang, and L. Lymburner. 2018. Analysis ready data: enabling analysis of the Landsat archive. Remote Sensing 10 (9):1363.

EJP SOIL. 2022. Sustainable environment, Soil Health, Ecosystem services & Biodiversity [cited. Available from https://ejpsoil.eu/sustainable-environment-soil-health-ecosystem-services-biodiversity, last access 02.11.2022].

FAO. 2015. Healthy soils are the basis for healthy food production: FAO.

FAO ITPS. 2018. Global Soil Organic Carbon Map (GSOCmap) - Technical Report, 162.

Flood, N. 2013. Seasonal composite Landsat TM/ETM+ images using the medoid (a multi-domensional median). Remote Sensing 5 (12):6481-6500.

Francaviglia, R., C. Di Bene, R. Farina, L. Salvati, and J. L. Vicente-Vicente. 2019. Assessing "4 per 1000" soil organic carbon storage rates under Mediterranean climate: a comprehensive data analysis. Mitigation and Adaptation Strategies for Global Change 24 (5):795-818.

Gallo, B. C., J. A. Demattê, R. Rizzo, J. L. Safanelli, W. d. S. Mendes, I. F. Lepsch, M. V. Sato, D. J. Romero, and M. P. Lacerda. 2018. Multi-temporal satellite images on topsoil attribute quantification and the relationship with soil classes and geology. Remote Sensing 10 (10):1571.

Ghazali, M. F., K. Wikantika, A. B. Harto, and A. Kondoh. 2020. Generating soil salinity, soil moisture, soil pH from satellite imagery and its analysis. Information Processing in Agriculture 7 (2):294-306.

Gholizadeh, A., C. Neumann, S. Chabrillat, B. van Wesemael, F. Castaldi, L. Borůvka, J. Sanderman, A. Klement, and C. Hohmann. 2021. Soil organic carbon estimation using VNIR–SWIR spectroscopy: The effect of multiple sensors and scanning conditions. Soil and Tillage Research 211:105017.

Giuliani, G., P. Mazzetti, M. Santoro, S. Nativi, J. Van Bemmelen, G. Colangeli, and A. Lehmann. 2020. Knowledge generation using satellite earth observations to support sustainable development goals (SDG): A use case on Land degradation. International Journal of Applied Earth Observation and Geoinformation 88:102068.

Griffiths, P., C. Nendel, and P. Hostert. 2019. Intra-annual reflectance composites from Sentinel-2 and Landsat for national-scale crop and land cover mapping. Remote Sensing of Environment 220:135-151.

Guanter, L., H. Kaufmann, K. Segl, S. Foerster, C. Rogass, S. Chabrillat, T. Kuester, A. Hollstein, G. Rossner, and C. Chlebek. 2015. The EnMAP spaceborne imaging spectroscopy mission for earth observation. Remote Sensing 7 (7):8830-8857.

Guillaume, T., L. Bragazza, C. Levasseur, Z. Libohova, and S. Sinaj. 2021. Long-term soil organic carbon dynamics in temperate cropland-grassland systems. Agriculture, ecosystems & environment 305:107184.

Hansen, M. C., A. Egorov, D. P. Roy, P. Potapov, J. Ju, S. Turubanova, I. Kommareddy, and T. R. Loveland. 2011. Continuous fields of land cover for the conterminous United States using Landsat data: First results from the Web-Enabled Landsat Data (WELD) project. Remote Sensing Letters 2 (4):279-288.

Heiden, U., P. d'Angelo, P. Schwind, P. Karlshöfer, R. Müller, S. Zepp, M. Wiesmeier, and P. Reinartz. 2022. Soil Reflectance Composites—Improved Thresholding and Performance Evaluation. Remote Sensing 14 (18):4526.

Hengl, T., J. Mendes de Jesus, G. B. Heuvelink, M. Ruiperez Gonzalez, M. Kilibarda, A. Blagotić, W. Shangguan, M. N. Wright, X. Geng, and B. Bauer-Marschallinger. 2017. SoilGrids250m: Global gridded soil information based on machine learning. PloS one 12 (2):e0169748.

Hermosilla, T., M. A. Wulder, J. C. White, N. C. Coops, and G. W. Hobart. 2015. An integrated Landsat time series protocol for change detection and generation of annual gap-free surface reflectance composites. Remote Sensing of Environment 158:220-234.

Heuvelink, G. B., M. E. Angelini, L. Poggio, Z. Bai, N. H. Batjes, R. van den Bosch, D. Bossio, S. Estella, J. Lehmann, and G. F. Olmedo. 2021. Machine learning in space and time for modelling soil organic carbon change. European journal of soil science 72 (4):1607-1623.

Hiederer, R., M. Köchy. 2011. Global soil organic carbon estimates and the harmonized world soil database EUR 79 (25225):10.2788.

Holben, B. N. 1986. Characteristics of maximum-value composite images from temporal AVHRR data. International Journal of Remote Sensing 7 (11):1417-1434.
Jandl, R., M. Rodeghiero, C. Martinez, M. F. Cotrufo, F. Bampa, B. Van Wesemael, R. B. Harrison, I. A. Guerrini, D. d. Richter Jr, and L. Rustad. 2014. Current status, uncertainty and future needs in soil organic carbon monitoring. Science of the total environment 468:376-383.
Jobbágy, E. G., and R. B. Jackson. 2000. The vertical distribution of soil organic carbon and its relation to climate and vegetation. Ecological applications 10 (2):423-436.
Jones, R. J., R. Hiederer, E. Rusco, and L. Montanarella. 2005. Estimating organic carbon in the soils of Europe for policy support. European journal of soil science 56 (5):655-671.
Kumar, R., S. Pandey, and A. Pandey. 2006. Plant roots and carbon sequestration. Current Science:885-890.
Lal, R. 2004. Soil carbon sequestration impacts on global climate change and food security. science 304 (5677):1623-1627.
Lal, R. 2006. Enhancing crop yields in the developing countries through restoration of the soil organic carbon pool in agricultural lands. Land Degradation & Development 17 (2):197-209.
Lal, R., R. F. Follett, B. A. Stewart, and J. M. Kimble. 2007. Soil carbon sequestration to mitigate climate change and advance food security. Soil science 172 (12):943-956.
Lal, R. 2014. Societal value of soil carbon. Journal of Soil and Water Conservation 69 (6):186A-192A.
Lal, R. 2016. Soil health and carbon management. Food and Energy Security 5 (4):212-222.
Lal, R. 2018. Digging deeper: A holistic perspective of factors affecting soil organic carbon sequestration in agroecosystems. Global Change Biology 24 (8):3285-3301.
Lehmann, J., D.A. Bossio, I. Kögel-Knabner, M.C. Rilig. 2020 The concept of future prospects of soil health. Nature Reviews Earth & Environment 1 (10):544-553.
Lin, C., A.-X. Zhu, Z. Wang, X. Wang, and R. Ma. 2020. The refined spatiotemporal representation of soil organic matter based on remote images fusion of Sentinel-2 and Sentinel-3. International Journal of Applied Earth Observation and Geoinformation 89:102094.
Loiseau, T., S. Chen, V. L. Mulder, M. R. Dobarco, A. C. Richer-de-Forges, S. Lehmann, H. Bourennane, N. P. Saby, M. P. Martin, and E. Vaudour. 2019. Satellite data integration for soil clay content modelling at a national scale. International Journal of Applied Earth Observation and Geoinformation 82:101905.
Loizzo, R., M. Daraio, R. Guarini, F. Longo, R. Lorusso, L. Dini, and E. Lopinto. 2019. Prisma mission status and perspective. Paper read at IGARSS 2019-2019 IEEE International Geoscience and Remote Sensing Symposium.
Lorenz, K., R. Lal, and K. Ehlers. 2019. Soil organic carbon stock as an indicator for monitoring land and soil degradation in relation to U nited N ations' S ustainable D evelopment G oals. Land Degradation & Development 30 (7):824-838.
Loveland, P., and J. Webb. 2003. Is there a critical level of organic matter in the agricultural soils of temperate regions: a review. Soil and Tillage Research 70 (1):1-18.
Malec, S., D. Rogge, U. Heiden, A. Sanchez-Azofeifa, M. Bachmann, and M. Wegmann. 2015. Capability of spaceborne hyperspectral EnMAP mission for mapping fractional cover for soil erosion modeling. Remote Sensing 7 (9):11776-11800.
McBratney, A. B., U. Stockmann, D. A. Angers, B. Minasny, and D. J. Field. 2014. Challenges for soil organic carbon research. In Soil carbon, 3-16: Springer.
Meersmans, J., D. Arrouays, A. J. Van Rompaey, C. Pagé, S. De Baets, and T. A. Quine. 2016. Future C loss in mid-latitude mineral soils: Climate change exceeds land use mitigation potential in France. Scientific reports 6 (1):1-11.
Möller, M., S. Zepp, M. Wiesmeier, H. Gerighausen, and U. Heiden. 2022. Scale-Specific Prediction of Topsoil Organic Carbon Contents Using Terrain Attributes and SCMaP Soil Reflectance Composites. Remote Sensing 14 (10):2295.
Montanarella, L., and P. Panagos. 2021. The relevance of sustainable soil management within the European Green Deal. Land use policy 100:104950.
Musinguzi, P., J. S. Tenywa, P. Ebanyat, M. M. Tenywa, D. N. Mubiru, T. A. Basamba, and A. Leip. 2013. Soil organic carbon thresholds and nitrogen management in tropical agroecosystems: concepts and prospects.
Mzid, N., F. Castaldi, M. Tolomio, S. Pascucci, R. Casa, and S. Pignatti. 2022. Evaluation of Agricultural Bare Soil Properties Retrieval from Landsat 8, Sentinel-2 and PRISMA Satellite Data. Remote Sensing 14 (3):714.
Mzid, N., S. Pignatti, W. Huang, and R. Casa. 2021. An analysis of bare soil occurrence in arable croplands for remote sensing topsoil applications. Remote Sensing 13 (3):474.
Nachtergaele, F., H. van Velthuizen, L. Verelst, N. Batjes, K. Dijkshoorn, V. van Engelen, G. Fischer, A. Jones, and L. Montanarela. 2010. The harmonized world soil database. Paper read at Proceedings of the 19th World Congress of Soil Science, Soil Solutions for a Changing World, Brisbane, Australia, 1-6 August 2010.

Okin, G. S. 2007. Relative spectral mixture analysis—A multitemporal index of total vegetation cover. Remote Sensing of Environment 106 (4):467-479.
Orgiazzi, A., C. Ballabio, P. Panagos, A. Jones, and O. Fernández-Ugalde. 2018. LUCAS Soil, the largest expandable soil dataset for Europe: a review. European journal of soil science 69 (1):140-153.
Panagos, P., C. Ballabio, Y. Yigini, and M. B. Dunbar. 2013. Estimating the soil organic carbon content for European NUTS2 regions based on LUCAS data collection. Science of the total environment 442:235-246.
Panagos, P., and L. Montanarella. 2018. Soil Thematic Strategy: An important contribution to policy support, research, data development and raising the awareness. Current Opinion in Environmental Science & Health 5:38-41.
Panagos, P., M. Van Liedekerke, P. Borrelli, J. Köninger, C. Ballabio, A. Orgiazzi, E. Lugato, L. Liakos, J. Hervas, A. Jones, and L. Montanarella. European Soil Data Centre 2.0: Soil data and knowledge in support of the EU policies. European journal of soil science n/a (n/a):e13315.
Phiri, D., M. Simwanda, S. Salekin, V. R. Nyirenda, Y. Murayama, and M. Ranagalage. 2020. Sentinel-2 data for land cover/use mapping: a review. Remote Sensing 12 (14):2291.
Poeplau, C., A. Jacobs, A. Don, C. Vos, F. Schneider, M. Wittnebel, B. Tiemeyer, A. Heidkamp, R. Prietz, and H. Flessa. 2020. Stocks of organic carbon in German agricultural soils—Key results of the first comprehensive inventory. Journal of Plant Nutrition and Soil Science 183 (6):665-681.
Post, W. M., and K. C. Kwon. 2000. Soil carbon sequestration and land-use change: processes and potential. Global Change Biology 6 (3):317-327.
Poulton, P., J. Johnston, A. Macdonald, R. White, and D. Powlson. 2018. Major limitations to achieving "4 per 1000" increases in soil organic carbon stock in temperate regions: Evidence from long-term experiments at Rothamsted Research, United Kingdom. Global Change Biology 24 (6):2563-2584.
Ren, W., K. Banger, B. Tao, J. Yang, Y. Huang, and H. Tian. 2020. Global pattern and change of cropland soil organic carbon during 1901-2010: Roles of climate, atmospheric chemistry, land use and management. Geography and Sustainability 1 (1):59-69.
Richter, R., and D. Schläpfer. 2013. Atmospheric/topographic correction for satellite imagery (ATCOR-2/3 User Guide, Version 8.3. 1, February 2014). ReSe Applications Schläpfer, Langeggweg 3.
Rogge, D., A. Bauer, J. Zeidler, A. Mueller, T. Esch, and U. Heiden. 2018. Building an exposed soil composite processor (SCMaP) for mapping spatial and temporal characteristics of soils with Landsat imagery (1984–2014). Remote Sensing of Environment 205:1-17.
Rouse Jr, J. W., R. H. Haas, J. Schell, and D. Deering. 1973. Monitoring the vernal advancement and retrogradation (green wave effect) of natural vegetation.
Safanelli, J. L., S. Chabrillat, E. Ben-Dor, and J. A. Demattê. 2020. Multispectral models from bare soil composites for mapping topsoil properties over Europe. Remote Sensing 12 (9):1369.
Scharlemann, J. P., E. V. Tanner, R. Hiederer, and V. Kapos. 2014. Global soil carbon: understanding and managing the largest terrestrial carbon pool. Carbon Management 5 (1):81-91.
Schjønning, P., L. de Jonge, P. Moldrup, B. Christensen, and J. Olesen. 2010. Searching the critical soil organic carbon threshold for satisfactory tilth conditions–test of the Dexter clay: carbon hypothesis. Paper read at Proceedings of the 1st international conference and exploratory workshop on soil architecture and physico-chemical functions" Cesar".
Seitz, D., L. M. Fischer, R. Dechow, M. Wiesmeier, and A. Don. 2022. The potential of cover crops to increase soil organic carbon storage in German croplands. Plant and soil:1-17.
Šeremešić, S., D. Milošev, I. Đalović, T. Zeremski, and J. Ninkov. 2011. Management of soil organic carbon in maintaining soil productivity and yield stability of winter wheat. Plant Soil & Environment 57 (5):216-221.
Sims, N. C., J. R. England, G. J. Newnham, S. Alexander, C. Green, S. Minelli, and A. Held. 2019. Developing good practice guidance for estimating land degradation in the context of the United Nations Sustainable Development Goals. Environmental Science & Policy 92:349-355.
Sleutel, S., S. De Neve, and G. Hofman. 2007. Assessing causes of recent organic carbon losses from cropland soils by means of regional-scaled input balances for the case of Flanders (Belgium). Nutrient Cycling in Agroecosystems 78 (3):265-278.
Sorenson, P., S. Shirtliffe, and A. Bedard-Haughn. 2021. Predictive soil mapping using historic bare soil composite imagery and legacy soil survey data. Geoderma 401:115316.
Soussana, J.-F., S. Lutfalla, F. Ehrhardt, T. Rosenstock, C. Lamanna, P. Havlík, M. Richards, J.-L. Chotte, E. Torquebiau, and P. Ciais. 2019. Matching policy and science: Rationale for the '4 per 1000-soils for food security and climate'initiative. Soil and Tillage Research 188:3-15.
Stevens, A., M. Nocita, G. Tóth, L. Montanarella, and B. van Wesemael. 2013. Prediction of soil organic carbon at the European scale by visible and near infrared reflectance spectroscopy. PloS one 8 (6):e66409.

Stocker, B. D., R. Roth, F. Joos, R. Spahni, M. Steinacher, S. Zaehle, L. Bouwman, and I. C. Prentice. 2013. Multiple greenhouse-gas feedbacks from the land biosphere under future climate change scenarios. Nature Climate Change 3 (7):666-672.

Todd-Brown, K.E., J.T. Randersin, W.M. Post, F.M. Hoffman, C. Tarnocai, E.A. Schuur, S.D. Allison. 2013. Causes of variation in soil carbon simulations from CMIP5 Earth system models and comparison with observations. Biogeosciences 10(3):1717-1736.

Tóth, G., T. Hermann, M. R. da Silva, and L. Montanarella. 2018. Monitoring soil for sustainable development and land degradation neutrality. Environmental Monitoring and Assessment 190 (2):1-4.

Tziolas, N., N. Tsakiridis, E. Ben-Dor, J. Theocharis, and G. Zalidis. 2020. Employing a multi-input deep convolutional neural network to derive soil clay content from a synergy of multi-temporal optical and radar imagery data. Remote Sensing 12 (9):1389.

Tziolas, N., N. Tsakiridis, S. Chabrillat, J. A. Demattê, E. Ben-Dor, A. Gholizadeh, G. Zalidis, and B. Van Wesemael. 2021. Earth observation data-driven cropland soil monitoring: A review. Remote Sensing 13 (21):4439.

Urbina-Salazar, D., E. Vaudour, N. Baghdadi, E. Ceschia, A. C. Richer-De-Forges, S. Lehmann, and D. Arrouays. 2021. Using Sentinel-2 Images for Soil Organic Carbon Content Mapping in Croplands of Southwestern France. The Usefulness of Sentinel-1/2 Derived Moisture Maps and Mismatches between Sentinel Images and Sampling Dates. Remote Sensing 13 (24):5115.

Van Groenigen, J. W., C. Van Kessel, B. A. Hungate, O. Oenema, D. S. Powlson, and K. J. Van Groenigen. 2017. Sequestering soil organic carbon: a nitrogen dilemma: ACS Publications.

Vaudour, E., C. Gomez, Y. Fouad, and P. Lagacherie. 2019. Sentinel-2 image capacities to predict common topsoil properties of temperate and Mediterranean agroecosystems. Remote Sensing of Environment 223:21-33.

Vaudour, E., C. Gomez, P. Lagacherie, T. Loiseau, N. Baghdadi, D. Urbina-Salazar, B. Loubet, and D. Arrouays. 2021. Temporal mosaicking approaches of Sentinel-2 images for extending topsoil organic carbon content mapping in croplands. International Journal of Applied Earth Observation and Geoinformation 96:102277.

Wang, X., Y. Zhang, P. M. Atkinson, and H. Yao. 2020. Predicting soil organic carbon content in Spain by combining Landsat TM and ALOS PALSAR images. International Journal of Applied Earth Observation and Geoinformation 92:102182.

Ward, K. J., S. Chabrillat, C. Neumann, and S. Foerster. 2019. A remote sensing adapted approach for soil organic carbon prediction based on the spectrally clustered LUCAS soil database. Geoderma 353:297-307.

Watson, R. T., I. R. Noble, B. Bolin, N. Ravindranath, D. J. Verardo, and D. J. Dokken. 2000. Land use, land-use change and forestry: a special report of the Intergovernmental Panel on Climate Change: Cambridge University Press.

White, J. C., M. Wulder, G. Hobart, J. Luther, T. Hermosilla, P. Griffiths, N. Coops, R. Hall, P. Hostert, and A. Dyk. 2014. Pixel-based image compositing for large-area dense time series applications and science. Canadian Journal of Remote Sensing 40 (3):192-212.

Wiesmeier, M., C. Poeplau, C. A. Sierra, H. Maier, C. Frühauf, R. Hübner, A. Kühnel, P. Spörlein, U. Geuß, and E. Hangen. 2016. Projected loss of soil organic carbon in temperate agricultural soils in the 21st century: effects of climate change and carbon input trends. Scientific reports 6 (1):1-17.

Zepp, S., U. Heiden, M. Bachmann, M. Wiesmeier, M. Steininger, and B. van Wesemael. 2021. Estimation of Soil Organic Carbon Contents in Croplands of Bavaria from SCMaP Soil Reflectance Composites. Remote Sensing 13 (16):3141.

Zepp, S., M. Jilge, A. Metz-Marconcini, and U. Heiden. 2021. The influence of vegetation index thresholding on EO-based assessments of exposed soil masks in Germany between 1984 and 2019. ISPRS Journal of Photogrammetry and Remote Sensing 178:366-381.

Zhou, Y., W. Wu, and H. Liu. 2022. Exploring the Influencing Factors in Identifying Soil Texture Classes Using Multitemporal Landsat-8 and Sentinel-2 Data. Remote Sensing 14 (21):5571.

Zhu, Z., S. Wang, and C. E. Woodcock. 2015. Improvement and expansion of the Fmask algorithm: Cloud, cloud shadow, and snow detection for Landsats 4–7, 8, and Sentinel 2 images. Remote Sensing of Environment 159:269-277.

Žížala, D., R. Minařík, and T. Zádorová. 2019. Soil organic carbon mapping using multispectral remote sensing data: Prediction ability of data with different spatial and spectral resolutions. Remote Sensing 11 (24):2947.